

Technical Analysis of Drum Lid Ejections- ARP V

December 2018

Technical Analysis of Drum Lid Ejections-ARP V

December 2018

**Idaho Cleanup Project Core
Idaho Falls, Idaho 83402**

**Prepared for the
U.S. Department of Energy
Assistant Secretary for Environmental Management
Under DOE Idaho Operations Office
Contract DE-EM0004083**

Technical Analysis of Drum Lid Ejections-ARP V

RPT-1662

December 2018

Prepared by

<hr/> Signature on File, see DRF 361251	<hr/> 12/3/2018
Rod E. Arbon, Ph.D Chemist, TRU Programs	Date
<hr/> Signature on File, see DRF 361251	<hr/> 12/3/2018
Gary S. Groenewold, Ph.D Chemical Sciences	Date
<hr/> Signature on File, see DRF 361251	<hr/> 12/3/2018
Greg S. Sprenger Engineering	Date

Concurrence by

<u>Signature on File, see DRF 361251</u>	<u>12/3/2018</u>
Bill Reed, P.E. Engineering Manager	Date

<u>Signature on File, see DRF 361251</u>	<u>12/3/2018</u>
John McCoy RH/CH TRU Waste Program Manager	Date

<u>Signature on File, see DRF 361251</u>	<u>12/3/2018</u>
Brad Eldredge, Ph.D, P.E. Chemical Engineering	Date

<u>Signature on File, see DRF 361251</u>	<u>12/3/2018</u>
Jason Chapple Operations Manager	Date

<u>Signature on File, see DRF 361251</u>	<u>12/3/2018</u>
Lee Fife Cause Analyst	Date

Approved by

<u>Signature on File, see DRF 361251</u>	<u>12/3/2018</u>
Joe Giebel Chief Engineering	Date

ABSTRACT

In April 2018, Fluor Idaho LLC had four drums containing transuranic waste over-pressurize, resulting in lid ejection and expulsion of waste material (approximately 50%). The parent drums were part of a retrieval effort in the mid-1970s and were exhumed from a portion of the Subsurface Disposal Area Pits 11 and 12, beginning in 1974 and ending in 1978. The drums were later retrieved from the cargo containers and sent to characterization (real time radiography and nondestructive assay), opened, contents visually inspected, and contents repackaged into new “daughter” drums within the Accelerated Retrieval Project V facility. Lid ejection and waste expulsion occurred within 5-12 hours after repackaging.

The lid ejections were accompanied with significant heat generation. Empirical evidence of heat generation was observed in each reacted daughter 55-gallon drum. The heat generated was sufficient to warp the high-density polyethylene liner (~ 122°C to 137°C) in three of the drums and char paper labels (~230°C) and the drum paint (~400°C) on one drum.

To determine the potential reactant(s), a comprehensive chemical analysis was performed by two independent laboratories, Southwest Research Institute, and Savannah River National Laboratory, on the reacted drum contents, ejected drum material, and related drums. A comprehensive chemical compatibility analysis was performed on the analytical results and the most likely reactant(s) identified. The oxidation of depleted uranium (DU) was the source of the heat generation. The chemical behavior of DU (reactive properties and lack of visual indicators during packaging) is consistent with the event.

The heat generated was sufficient to initiate secondary chemical reactions leading to significant gas formation sufficient to generate pressures in excess of those needed (25 psi) to eject the lid and contents. These reactions fall into two categories:

1. Simple volatilization of organics and water (H₂O) present in the drum
2. Chemical reactions that generate gaseous products, principally methane (CH₄).

Both reactions are driven by the heat generated by the uranium oxidation that was initiated when the parent drum contents were exposed to the atmosphere.

Reactions that produce gaseous products focus on CH₄, which is by far the largest contributor to the increasing head-space gases, and to the increased drum pressure. Specifically, the hydrolysis of beryllium carbide (Be₂C) has been identified as the source of methane production.

CONTENTS

ABSTRACT.....	iii
ACRONYMS.....	xiii
1. EVENT OVERVIEW.....	1
1.1 Technical Team Objectives.....	1
1.2 Event Description.....	1
1.2.1 Process Overview-Sludge Repack Process.....	1
1.2.2 Drums Involved in Lid Ejection.....	3
1.2.3 Processing Sequence, Lid Ejection, and Key Observations.....	3
1.2.4 Post-Event Observations.....	5
1.3 Event Drums Origin.....	12
1.3.1 Item Description Code SD-176.....	12
1.4 Working Hypothesis.....	15
2. EVENT CHARACTERIZATION.....	16
2.1 Objectives and Summary.....	16
2.1.1 Analytical Laboratory Selection.....	16
2.1.2 Target Analyte and Methodology Selection.....	16
2.2 Sampling Efforts.....	17
2.2.1 Sample Management.....	17
2.2.2 Sampling Approach.....	18
2.2.3 Ejected Material.....	18
2.2.4 Reacted Drum Samples.....	21
2.2.5 Large Particle Samples.....	21
2.2.6 Sorting Table.....	21
2.2.7 Tray 299.....	21
2.2.8 Mechanistic Sample Selection.....	23
3. EVENT CHARACTERIZATION RESULTS.....	26
3.1 Objectives and Summary.....	26
3.2 Chemical Characterization.....	26
3.2.1 Quality Assurance Flags.....	26
3.2.2 Radio-isotopes.....	27
3.2.3 Metals.....	27
3.2.4 Organics – Volatile Organics, Semi-Volatile Organics, and Polychlorinated Bi-phenols.....	32
3.2.5 Anions.....	32

3.2.6	Metal Turnings	36
3.2.7	Mechanistic Sample Results.....	37
3.3	Additional Lines of Inquiry	48
3.3.1	Hydrogen and Methane	48
3.3.2	Humidity Stability	48
3.3.3	Bulk Density.....	49
3.3.4	pH.....	49
3.4	Laboratory and Analytical Data Comparison.....	51
4.	EVENT INVESTIGATION AND INTERPRETATION.....	52
4.1	Objective and Summary	52
4.2	Chemical Compatibility.....	52
4.2.1	Chemical Compatibility Summary.....	52
4.2.2	Empirical Evidence Supporting Uranium as an Energy Source for the Drum Rupture.....	53
4.3	Depleted Uranium as the Event Initiator	54
4.3.1	Un-oxidized Uranium.....	54
4.3.2	Slowly Accelerating, Exothermic Oxidation.....	55
4.3.3	Uranium Oxidation by O ₂ Can Be Accelerating	55
4.3.4	Uranium Oxidation Rates by O ₂ Sharply Increase with Increasing Temperature	55
4.3.5	Humid Air Oxidation is Faster than O ₂ Oxidation	55
4.3.6	The Size of Uranium Material in the Waste Can Affect Oxidation Rates and Ignition Temperatures	55
4.4	Heat Build-Up and Thermodynamic Modeling of Uranium Oxidation Reactions.....	56
4.4.1	Waste Temperature as a Function of Mass.	58
4.4.2	Localized Heating	58
5.	SECONDARY REACTIONS DUE TO HEAT GENERATION	59
5.1	Volatilization of Organics and Water.....	59
5.2	Reactions that Produce Methane	61
5.3	Selection of Beryllium Carbide as the Most Probable Contributor to CH ₄ Generation	64
5.4	Bench Test Demonstrating Methane Production and Pressure Generation.....	64
5.4.1	Pressure and CH ₄ Production: Comparison of Ejected vs. Drum Material	65
5.4.2	Effect of Pre-Evacuation, H ₂ O on Gas Production	67
5.4.3	Evaluation of the Effect of Regal Oil: DCM Extraction and Mineral Oil Addition.....	68
5.4.4	CH ₄ Production Differentiated by Waste Sample Density.....	70

5.4.5	Impact of Acid/Base.....	79
5.4.6	Reaction Temperature Dependence	87
5.4.7	Estimating the Amount of Beryllium Carbide	91
5.4.8	Elimination of Be metal as a potential source of gas pressure	93
5.5	Evaluating the Thermodynamic Favorability of Beryllium Carbide Hydrolysis	93
6.	COMPARISON WITH WASTE FROM DRUMS LOCATED PROXIMATE TO THE EVENT DRUM, THE SORTING TABLE, TRANSFER TRAY, AND A HISTORICALLY HIGH CH ₄ DRUM	95
6.1	Composition and Speciation in Un-Ruptured Drums.....	95
7.	LID EJECTION PRESSURES.....	100
7.1	Objective and Summary	100
7.2	Fluor Idaho Mechanical Pressurization Testing	100
7.2.1	Empirical Lid Ejection Pressures	100
7.2.2	Waste Mass needed to Eject Drum Lid.....	102
7.3	Combustion versus Over-pressurization.....	102
7.3.1	Bulging Lids.....	102
7.3.2	Combustion and Limiting Oxygen Concentration	102
7.3.3	Sympathetic Deflagration.....	103
8.	ACCEPTABLE KNOWLEDGE EVALUATION OF BERYLLIUM CARBIDE AND DEPLETED URANIUM.....	104
8.1	Beryllium Carbide	104
8.2	Depleted Uranium-Building 444	104
8.2.1	Trough Processing/Mixing.....	104
9.	CONCLUSION	105
9.1	Reaction Summary	105
10.	RECOMMENDATIONS	107
11.	REFERENCES.....	108
	Appendix A—Chemical Compatibility	A-1
	Appendix B—Literature Review of Uranium Oxidation.....	B-1
	Appendix C—Radiolysis Incident Timeframe	C-1
	Appendix D—Parameter Investigations Supporting the Pressure, Temperature vs. Time Experiments.....	D-1
	Appendix E—SwRI Particle Size Distribution Data Sheets	E-1
	Appendix F—Pneumatic Rupture Test.....	F-1

FIGURES

1.	Typical SRP waste drum configuration	2
2.	Ejected waste material on lids and floor	7
3.	Ejected drum lid that appears inverted.....	7
4.	Drum 10648033 post-event exterior	8
5.	Drum 10648033 post-event interior.....	9
6.	Metal coupon color changes due to heat.....	9
7.	Drum 10647918 post-event exterior	10
8.	Drum 10647918 post-event interior.....	10
9.	Drum 10648030 post-event interior.....	11
10.	Drum 10647931 post-event exterior	11
11.	Drum 10647931 post-event interior.....	12
12.	Sampling locations for ejected and drum materials	22
13.	Parent-daughter drum relations.....	24
14.	Graphical representation of the metals measured in the samples collected after the drum rupture event	31
15.	Carbon steel	36
16.	Stainless steel.....	36
17.	Aluminum alloy	36
18.	Beryllium metal	36
19.	Leaded brass	36
20.	High chrome stainless steel.....	36
21.	Copper alloy.....	37
22.	Temperature of Drum Waste as a Function of Waste Mass.....	58
23.	EDS of a metallic sample shown to be principally beryllium.....	62
24.	Pressure vessel used for pressure vs. temperature profiles of samples of waste materials	65
25.	Pressure vs. temperature profile for ejected sample 1013, compared with samples collected from the drum	66
26.	CH ₄ concentrations (volume %) in the head-space of the pressure vs. temperature experiments.....	67
27.	Pressure vs. temperature (set value) for ejected sample 1013, 1g. atmosphere, pretreatment and H ₂ O availability compared	68

28.	Pressure vs. set temperature profiles of extracted samples 1013 and 6013	69
29.	Pressure vs. temperature traces for 2 g aliquots of ejected sample 1013, unmodified, and amended with a small quantity of mineral oil	70
30.	Schematic diagram for serial density separation using diiodomethane, then dibromomethane	71
31.	EDS spectral data for heavy fraction of sample SWR005013A	72
32.	Uranium (left) and carbon (right) elemental maps of the heavy faction of Sample SWR005013A	73
33.	Energy dispersive X-ray spectroscopy analyses of density separated fractions of ejected sample 5013	74
34.	X-ray diffraction (XRD) analyses of density separated fractions of ejected sample 5013	75
35.	Pressure vs. temperature (set point) profiles for light and heavy fractions of ejected sample 5013	76
36.	Pressure, temperature vs. time plots	78
37.	Pressure, temperature vs. time plots for ejected sample 1023	80
38.	Pressure, temperature vs. time plots for ejected sample 1013	82
39.	Pressure, temperature vs. time plots for H ₂ SO ₄ addition to density-separated fractions of ejected sample 5013.	84
40.	Pressure, temperature vs. time plots for KOH addition to density-separated fractions of ejected sample 5013 All experiments were externally heated to 90°C	86
41.	Serial pressure, temperature vs. time plots for ejected sample 1013. The initial headspace atmosphere was Ar, and the heating rate was 1°C/m in all experiments	88
42.	Serial pressure, temperature vs. time plots for ejected sample 1013	90
43.	Serial pressure, temperature vs. time plots for ejected sample 1013	92
44.	Pressure, temperature vs. time experiments for samples of Be metal powder	94
45.	Metal concentrations measured by ICP	96
46.	XRD spectra of waste samples from un-ruptured drums that were proximate to the event drum	97
47.	Pressure, temperature vs. time experiments conducted for waste samples from un-ruptured drums processed on April 10	98
48.	Pressure, temperature vs. time experiment conducted for a 3 g sample of the first un-ruptured drum sampled April 10 (sample from Drum 10648022), subsequent to addition of 50 µL H ₂ O	99
49.	ARP V drum event reaction summary	106
B-1.	Oxidation rates plotted v time (H), modeled using Epstein’s equation (2)	B-3
B-2.	Plot of extent of uranium oxidation by O ₂ measured as the oxide thickness, versus time	B-5

B-3.	Parabolic – linear kinetic model for oxidation of metal surfaces, developed by Haycock ¹⁶ , and applied by Ritchie ²⁸ to the uranium oxidation of Loriers.....	B-6
B-4.	Oxidation rates vs. temperature, from Arrhenius expressions of Ritchie	B-7
B-5.	Oxidation rate versus temperature modeled using the semi-empirical rate law developed by McGillivray.....	B-9
B-6.	Overall oxidation rates modeled at varying H ₂ O partial pressures, using the expression of McGillivray.....	B-9
B-7.	Rate constant for U + H ₂ O modeled at 25°C, 50°C, 75°C and 100°C, versus fractional relative humidity	B-10
B-8.	Comparison of rates versus temperature, using phenomenological models of Ritchie	B-11
B-9.	Relationship between ignition temperature and surface area reported by Schnizlein in 1959	B-12
B-10.	Ignition temperature of uranium vs. log material surface area	B-13
D-1.	Pressure vs. temperature profiles for floor (ejected) samples 1013 and 6013, acquired at heating rates of 1°C/min and 10°C/min, respectively.....	D-3
D-2.	Left, pressure vs. set temperature profiles for varying sample sizes of ejected sample 1013.....	D-4
D-3.	Pressure v temperature profiles. Left, sample 1013 (ejected material), 1 g, heated in air and Ar	D-5

TABLES

1.	Identified parent and event drums.....	3
2.	Key event drum observations.....	4
3.	Post-event drum observations.....	6
4.	Limitations and validations reports.....	19
5.	Correlation between sampling location and analytical sample identification.....	20
6.	Potential target drums for sampling and characterization.....	25
7.	SwRI data qualifier flags	26
8.	Validator data qualifier tags.....	27
9.	Radio-isotopes in the ejected material and reacted drums	28
10.	Metals in the ejected material and reacted drums	29
11.	Volatile organic compounds in ejected material and drum contents	33
12.	Semi-volatile organic compounds in ejected material and drum contents.....	34
13.	PCBs in ejected material and drum contents	35

14.	Anion concentrations in the ejected material and drum contents	35
15.	Radio-isotope results.....	38
16.	Metals in the mechanistic samples.....	39
17.	Volatile organic compounds in the mechanistic samples	42
18.	Semi-volatile organic compounds in the mechanistic samples.....	43
19.	Head-space gas composition from the mechanistic sample drums	45
20.	Analytical data from the target drums.....	47
21.	Composition of gas released from ejected material at 22°C and 50°C.....	48
22.	Composition of gas released from drum samples at 22°C and 50°C.....	48
23.	Moisture stability test results	49
24.	Bulk Density of the event materials.....	50
25.	pH of the event materials	50
26.	Input and output of thermodynamic modeling conducted using the HSC Chemistry code.....	57
27.	Concentrations of volatile and semi-volatile organic compounds, PCBs and anions in samples collected from within the event drum, and from material that was ejected during the event	60
28.	Empirical drum pressure temperature results.....	101
29.	Estimated kilograms of waste needed to eject drum lid.....	102
30.	Measured beryllium and DU.....	107
A-1.	Chemicals/Materials of Concern.....	A-5
A-2.	EPA Hazardous Waste Compatibility Chart.....	A-23
A-3.	Reactivity Group Number Compatibility Evaluation	A-24

ACRONYMS

AEC	Atomic Energy Commission
AK	acceptable knowledge
AMWTP	Advanced Mixed Waste Treatment Project
ANL-W	Argonne National Laboratory-West
ARP	Accelerated Retrieval Project
Be ₂ C	beryllium carbide
CBFO	Carlsbad Field Office
CH ₄	methane
DPS	drum packaging station
DOE	Department of Energy
DOT	Department of Transportation
DU	depleted uranium
EDS	energy dispersive x-ray spectroscopy
EO	equipment operator
EPA	Environmental Protection Agency
EWR	early waste retrieval
FGE	fissile gram equivalent
FID	flame ionization detector
H ₂ O	water
HDPE	high density polyethylene
HSG	head-space gas
ICP-AES	inductively coupled plasma-atomic emission spectroscopy
ICPP	Idaho Chemical Processing Plant
ICP-MS	inductively coupled plasma – mass spectroscopy
ID	identification
IDC	Item Description Code
IDR	initial drum retrieval
INL	Idaho National Laboratory
INTEC	Idaho Nuclear Technology and Engineering Complex
L&V	limitations and validations
MFC	Materials and Fuels Complex
NCR	non-conforming condition
NDA	non-destructive assay

NRF	Naval Reactors Facility
O ₂	oxygen
PCB	polychlorinated biphenyl
PPE	personal protective equipment
ppb	parts per billion
ppm	parts per million
ppt	parts per trillion
psig	pounds per square inch gauge
PVC	polyvinyl chloride
QA/QC	quality assurance/quality control
RA	Retrieval Area
RFP	Rocky Flats Plant
RGN	reactivity group numbers
RPD	relative percent difference
RTR	real time radiography
RWMC	Radioactive Waste Management Complex
SAM	Sample and Analysis Management Office
SDA	Subsurface Disposal Area
SDG	sample delivery group
SEM	scanning electron microscopy
SME	subject matter expert
SPM	Site Project Manager
SPR	sampling procedure
SRNL	Savannah River National Laboratory
SRP	Sludge Repackaging Project
STP	standard temperature pressure
SVOC	semi-volatile organic compounds
SwRI	Southwest Research Institute
TAN	Test Area North
TGA	thermogravimetric analysis
TI	thermal imaging
TIC	tentatively identified compounds
TOS	task order statement of work
TRU	transuranic
TRA	Test Reactor Area

TSA-RE	Transuranic Storage Area-Retrieval Enclosure
U ⁰	zero valent uranium
UC	uranium carbide
VE	Visual Examination
VOA	volatile organic analyses
VOC	volatile organic compounds
WIPP	Waste Isolation Pilot Plant
WMF	Waste Management Facility
WTS	Waste Tracking System
XRD	x-ray diffraction analysis

Technical Analysis of Drum Lid Ejections-ARP V

1. EVENT OVERVIEW

On April 11, 2018, four newly-repackaged drums had been processed through the Accelerated Retrieval Project (ARP) V (WMF-1617) as part of the Sludge Repackaging Project (SRP) and were staged in an airlock awaiting transfer. Late in the evening, the drums over-pressurized, ejecting their lids and approximately 50% of the drum contents, which were dispersed throughout the airlock. The event activated the facility fire detection system initiating an emergency response from the Idaho National Laboratory (INL) Site fire department, Radiation Protection, and Operations. Significant contamination in the airlock occurred, but no contamination was released outside the airlock.

1.1 Technical Team Objectives

Multiple efforts were undertaken to understand and recover from this event. One action involved the commissioning of a technical investigation by the Fluor Idaho Program Manager. The objectives of the technical team investigation were twofold:

1. Determining the reactive components/mechanism resulting in the ejection of the drum lids at ARP V.
2. Document the sampling/analysis and technical evaluation to support future processing, characterization, and waste disposition decisions for similar waste.

This report details the technical investigation. This report does not address the programmatic cause of this event nor does it describe the significant operational efforts undertaken to decontaminate both the horizontal and vertical surfaces of the airlock.

1.2 Event Description

1.2.1 Process Overview-Sludge Repack Process

The ARP SRP process remediates waste containers identified as requiring treatment due to the potential presence of WIPP-prohibited items (e.g. sealed inner containers, liquids, and other items such as aerosol cans). The processing of containers at ARP V begins with the staging of drums in the ARP V airlock for entry into the Retrieval Area (RA). From the airlock, the drums are taken into the RA where they are opened with a telehandler or excavator. The waste is emptied onto a carbon steel sorting table where the waste is manipulated with the bucket of the excavator. When liquids are present Oil-Dri® Premium Absorbent is added (no free liquids were associated with the event drums). Once mixing is complete and no free liquid is observed, the waste is transferred into a lined waste tray that is staged at the edge of the sorting table for transfer to a drum packaging station (DPS).

In the DPS, gloveboxes are open to the RA on one end where the trays are introduced. Operations personnel access the waste through glovebox ports and rake through the waste (using hand tools), verifying no liquids are present and no prohibited items exist. Visual Examination (VE) personnel oversee the waste processing in the DPSs and document the visual waste descriptions, verifying that no prohibited items remain in the waste and that the waste meets the VE criteria for WIPP. The waste is transferred to a new drum as part of the DPS process, and the new drum is assigned a new drum container identification (ID). The visual examination events are documented in the Waste Tracking System (WTS). As shown in Figure 1, the drum packaging consists of a polyvinyl chloride (PVC) bag which encompasses a high-density polyethylene (HDPE) drum liner into which the waste is loaded. Finally, after waste loading, the tray liner is bundled and placed on top along with any secondary debris waste created in the process of packaging in the DPS. The PVC bag, which also contains filtered vents, is sealed, and the vented drum lid installed. The drums are moved to Waste Management Facility (WMF)-610 to undergo nondestructive assay (NDA) and are then staged for future processing or disposal. The vents are designed to prevent the accumulation of flammable levels of radiolytically-generated hydrogen yet retain radioactive particulates. The vents have no performance specifications regarding gases other than hydrogen.

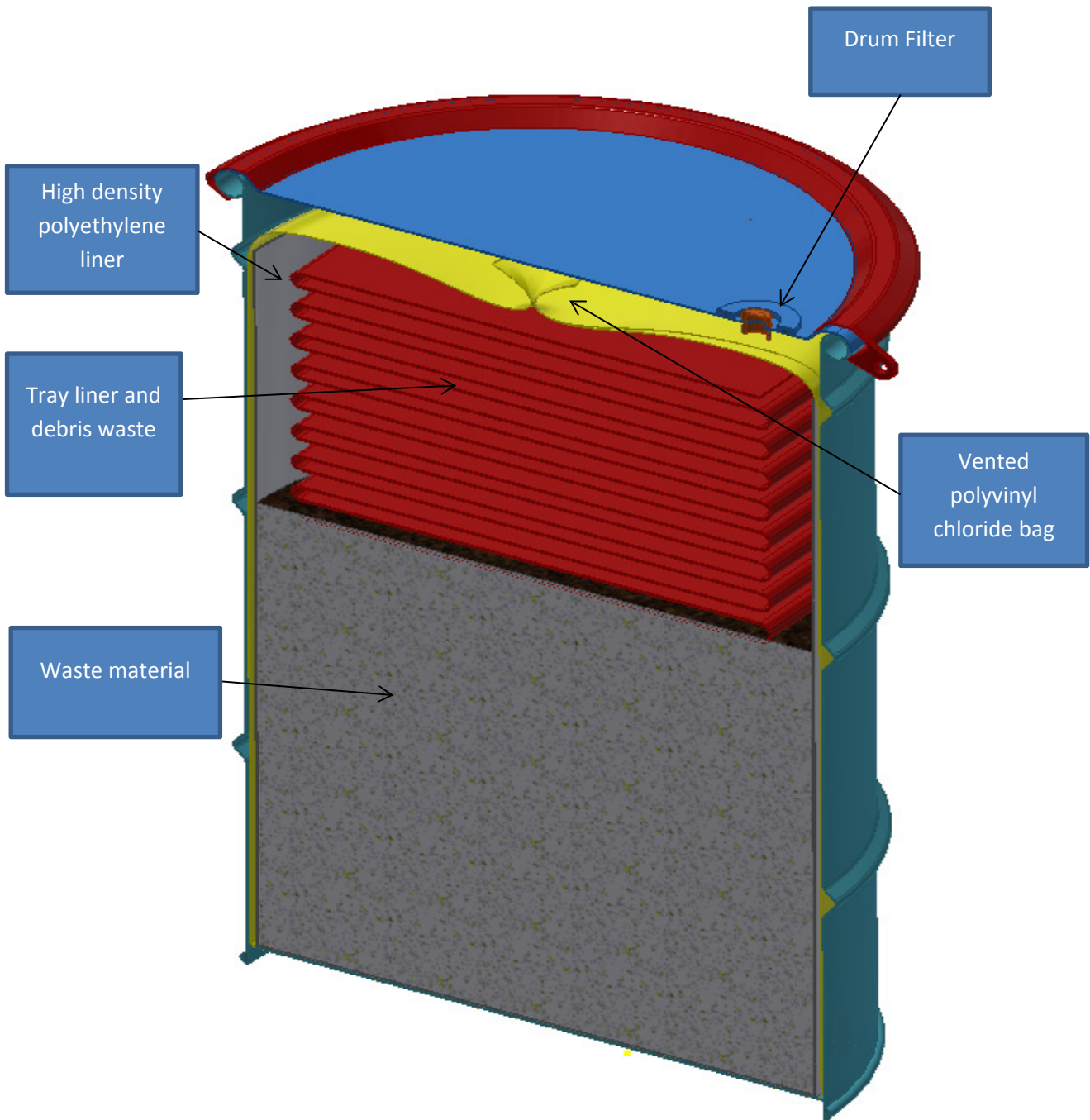


Figure 1. Typical SRP waste drum configuration.

1.2.2 Drums Involved in Lid Ejection

There were four drums that experienced lid ejection and expulsion of waste material. These drums, identified as repackaged daughter event drums, as well as the identified parent drums are given in Table 1 below. Table 1 also provides the parent radionuclide assay results, visual examination description of the repackaged daughter drums contents taken from the Waste Tracking System (WTS), and the WTS reported net weight.

Table 1. Identified parent and event drums.

Identified Parent Drum Numbers	Identified Parent Description	Summary Radionuclide Assay of Identified Parent	Repackaged Daughter Drum Numbers	Current Daughter Drum Status	Visual Examination Description of Daughter Drum
10595963	55-gal inner drum, bagged with horsetail, homogenous solid with black specks throughout. Appears to be floor sweepings. Net weight 367.15 pounds.	11.9 kg DU (U-238), 23.8 g U-235, 0.032 g U-234	SRP34398 10647931	Event drum	Remaining waste is inorganic matrix consisting of moderate gray crumbly sludge. Net weight 179.7 pounds. 43.5% fill height homogenous solid
			SRP34402 10648033	Event drum	Remaining waste is organic matrix consisting of gray powdery sludge. Net weight 181.2 pounds. 43.9% fill height homogenous solid
10630243	55-gal inner drum, homogeneous solid, empty polyethylene bottle at bottom. Appears to contain sludge. Net weight 532.9 pounds.	TRU = 5,940 nCi/g, 0.274 g Am-241, 0.0214 g Np-237, 5.96 g total Pu	SRP34384 10647909	No reaction	Remaining waste is inorganic matrix consisting of light brown crumbly sludge. Net weight 191.2 pounds. 46.4% fill height homogenous solid
			SRP34405 10648030	Event drum	Remaining waste is inorganic matrix consisting of gray powdery sludge. Net weight 227.7 pounds. 55.2% fill height homogenous solid
10630238	Chunky sludge, no poly bottles. Appears to contain sludge. Net weight 470.25 pounds.	TRU = 251 nCi/g, 0.0156 g Am-241, 0.00112 g Np-237, 0.172 g U-235	SRP34415 10647918	Event drum	Remaining waste is inorganic matrix consisting of reddish brown crumbly sludge. Net weight 167.2 pounds. 40.5% fill height homogenous solid
			Array 2, Grid I-10	Not packaged	Currently no visual record

The identified parent drums were selected based on processing time. Three identified parent drums contributed to the contents of the daughter drums. Section 8.2.1 of this report discusses the parent-daughter drum relationship based on the analytical results.

1.2.3 Processing Sequence, Lid Ejection, and Key Observations

Based on the visual record and interviews with operators packaging the waste, there were no visible reactions such as sparking, smoke, or incandescent glowing observed at the time of packaging. Table 2 provides the event drums' closure times, estimated lid ejection times, and key observations made by the first responders. The closure times are recorded in a log book immediately after closing. The elapsed time between lid closure and lid ejection is an approximation.

Table 2. Key event drum observations.

Drum Number	Lid Closure/ Torqueing Time	Elapsed Time to Lid Ejection	Key Observations
10648033 SRP34402	14:51	7 hours 44 minutes	<p>Fire Department reported a missing lid on Drum 10648033 at 22:57. Smoke alarm received at 22:35. Lid ejection estimated to occur at 22:35</p> <ul style="list-style-type: none"> • Entry Team Reported ruptured drum. • 190°F (87°C) reading on Thermal Imaging (TI) camera. • White HDPE drum liner described as caving in. • First responders described the matrix as “boiling sand”. • Attempted to pull back material with a shovel so Metal X (NaCl and Saran) could be applied. • TI camera reading 264°F (129°C). • Entry team reports Metal X ineffective began backing out. • 23:14 RCTs have not arrived drum temperature reported at 215°F. • Event drum moved away TI camera 284°F (140°C) prior to moving and 298°F (148°C) after moving. • Upon exiting it was noted that an additional drum lid was bulging.
10647918 SRP34415	15:17	9 hours 7 mins to 11 hours and 43 minutes	<p>00:24 a second event was described/heard. At 03:00 drum number three was heard. The fourth event/drum time is not known. However, personnel were present after 03:00 and never heard another noise from the building. Given that, all drums were believed to have lost their lids by 03:00.</p> <p>The exact time of lid ejection is not known.</p>
10648030 SRP34405	14:43	9 hours 41 mins to 12 hours and 17 minutes	<p>00:24 a second event was described/heard. At 03:00 drum number three was heard. The fourth event/drum time is not known. However, personnel were present after 03:00 and never heard another noise from the building. Given that, all drums were believed to have lost their lids by 03:00.</p> <p>The exact time of lid ejection is not known.</p>
10647931 SRP34398	14:36	9 hours 48 minutes to 12 hours and 24 minutes	<p>00:24 a second event was described/heard. At 03:00 drum number three was heard. The fourth event/drum time is not known. However, personnel were present after 03:00 and never heard another noise from the building. Given that, all drums were believed to have lost their lids by 03:00.</p> <p>The exact time of lid ejection is not known.</p>

The timeframe from lid closure to lid ejection for all four drums occurred within approximately 5-12 hours. This compact timeframe supports the working hypothesis, provided in Section 1.4 of this report, that each drum experienced a common reaction or reactions.

The investigation detailed in this report confirms all of the key first responder observations which are bulleted below. Sub bullets, which discuss the ramifications of the first responder observations, are provided. Each observation and its implications are addressed in this report.

- Only one drum was observed to have ejected its lid.
 - Ultimately, three additional drums were discovered to have lost their lids for a total of four drums. All lid ejections occurred within approximately 5-12 hours.
- Upon entry, the drum with the ejected lid was 190°F (87°C) based on TI camera reading.
 - The drum was experiencing a thermal event.
 - Prior to an exterior reading of 190°F (87°C), the drum lid was already ejected.
- The HDPE drum liner was described as caving in.
 - The waste temperature adjacent to the HDPE was approaching the yield/melting point for HDPE.
- First responders described the matrix as “boiling sand”.
 - Significant gas generation was occurring.
- The first responders pulled back the waste material with a shovel so Metal X could be applied.
 - This mixing/oxygenation impacted the extent of the drum reaction.
- Drum 10648033 was physically pulled away from the adjacent drums. The TI camera measured 284°F (140°C) prior to moving and 298°F (148°C) after moving.
 - The thermal event continued after mixing and appeared to be accelerating.
- Upon exiting it was noted that an additional drum lid was bulging.

1.2.4 Post-Event Observations

Table 3 contains a post-event description of the drum contents and condition after ejection of the drum lid. It was visually obvious that the four event drums experienced different thermal conditions during the event. All of the drums originally contained rigid liner and PVC bags. In three drums, the rigid liners were slightly deformed, but relatively intact. Additionally, the PVC bags were torn during the depressurization event and showed some signs of thermal exposure on their exposed edges. Drum 10648033, stirred by firefighters, experienced a significant thermal event which resulted in the consumption of the HDPE liner and PVC bag as well as charring of the exterior paint and paper labels of the drum.

Table 3. Post-event drum observations.

Drum Number	Drum Percent Full	Matrix Description	HDPE Liner and PVC Packaging	Drum Condition	Estimated Drum Temperature
10648033	~25 %	Gray waste material. Appears to be melted material within the drum adjacent to the drum wall. Black charring on the drum wall.	Absent.	Paint above the waste matrix is charred and black. Bottom of the drum is slightly bulged. Mouth of the drum appears round. See Figures 4 and 6.	Due to the charring of the paper label and the paint the drum experienced a temperature of ~230°C to 400°C Uneven paint charring.
10647918	~25 %	Gray waste material.	HDPE rigid liner is present and slightly warped.	Paint is white and in good shape. Bottom of the drum is bulged. Mouth of the drum appears round. See Figures 7 and 8.	Drum contents were heated sufficient to warp the high-density polyethylene liner (~ 122 to 137°C). Indications of uneven heating.
10648030	~25 %	Gray waste material.	HDPE rigid liner is present and warped.	Paint is white and in good shape. Bottom of the drum is bulged. See Figure 9.	Drum contents were heated sufficient to warp the high-density polyethylene liner (~122 to 137°C). Indications of uneven heating.
10647931	~25 %	Gray waste material.	HDPE rigid liner is present and slightly warped. Red packaging lapped over the edge of the drum.	Paint is white and in good shape. Bottom of the drum is bulged. See Figures 10 and 11.	Drum contents were heated sufficient to warp the high-density polyethylene liner (~ 122 to 137°C). Indications of uneven heating.

1.2.4.1 Ejected Waste Material. As shown in Figure 2, significant waste material was ejected into the ARP V facility. The material was distributed across the entire facility but with deeper amounts adjacent to the drums. The gray color of the ejected material was consistent across the facility floor. Torn tray liner material was also present.



Figure 2. Ejected waste material on lids and floor.

1.2.4.2 Ejected Drum Lid. As shown in Figure 3, the ejected lids were bent and as shown appeared inverted. This inverted drum lid supports the conclusion that the torquing used at ARP V was sufficient to prevent loss of pressure due to lid deformation prior to “popping open”.

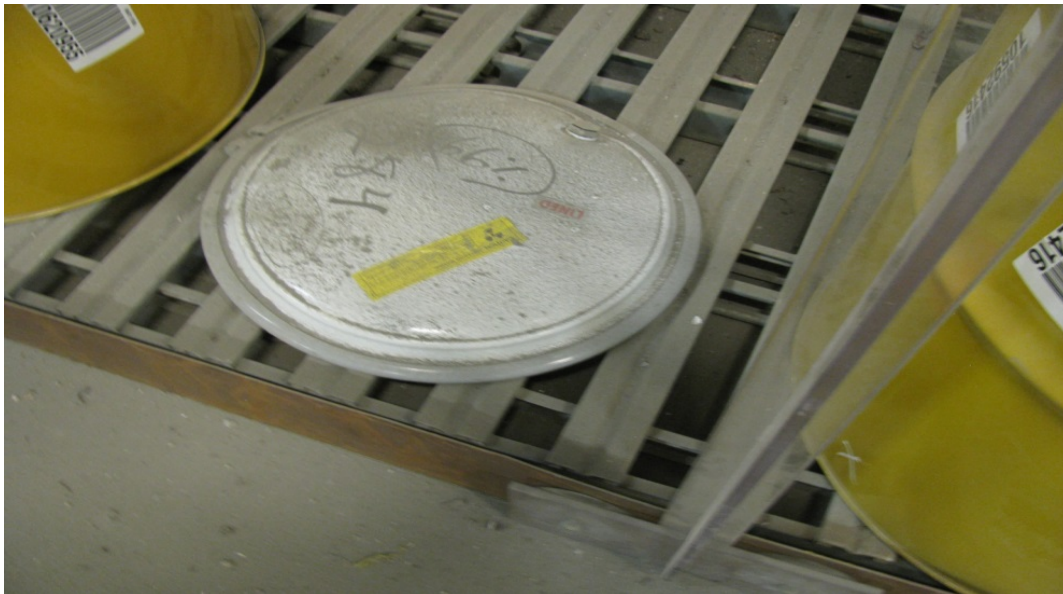


Figure 3. Ejected drum lid that appears inverted.

1.2.4.3 Drum 10648033 Post-Event Observations. Drum 10648033 was stirred by the fire fighters in an attempt to extinguish the heat source. As shown in figures 4 and 5, Drum 10648033 showed signs of significant thermal exposure. The paint on the exterior of the drum was charred above the level of the remaining material. Further, the rigid liner and the PVC bag no longer existed; they were consumed during the event. Drum 10648033 experienced significant thermal heating. As shown in Figure 4, the paint charring was significant. The Carlsbad Field Office (CBFO) performed paint and heating tests. Based on this work, the drum experienced temperatures around 230 to 400°C (The lower temperature is based on the charred labels). It is interesting to note that the base of the drum was only discolored. Apparently, the waste matrix insulated the metal from the heat. Also, the charring was not even, indicating uneven heating.

Thermal modeling was performed by the Waste Isolation Pilot Plant (WIPP) technical assessment team that investigated the February 14, 2014, radiological release event at WIPP. Coupons were cut from a pristine drum obtained from Los Alamos. Samples were approximately 2 inches square. The coupons were heated in air using several ovens. Exposure temperatures included 100°C, 200°C, 300°C, 400°C, 500°C, and 700°C. The heating experiments were used to:

- Determine temperature required to turn paint from white to black
- Establish general kinetics for color change
- Bound upper temperature exposure for drum.

The results are given in Figure 6.

When compared to the remainder of the drums, the difference in the heat generated appears to be due to the mixing/oxygenation of Drum 10648033 contents which occurred by the actions of the first responders.



Figure 4. Drum 10648033 post-event exterior.

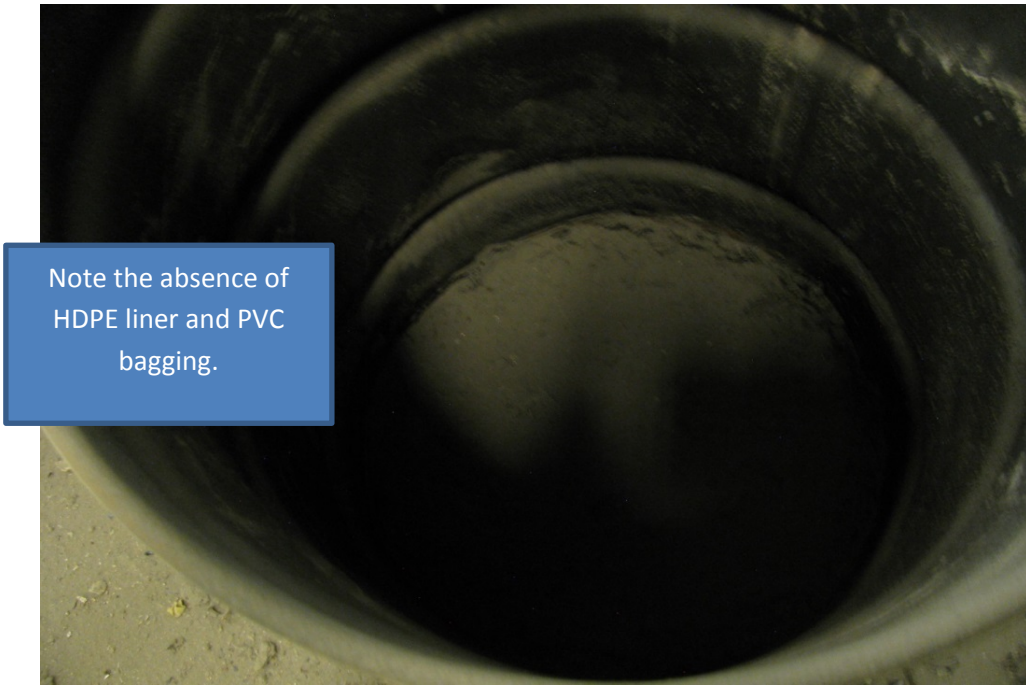


Figure 5. Drum 10648033 post-event interior.

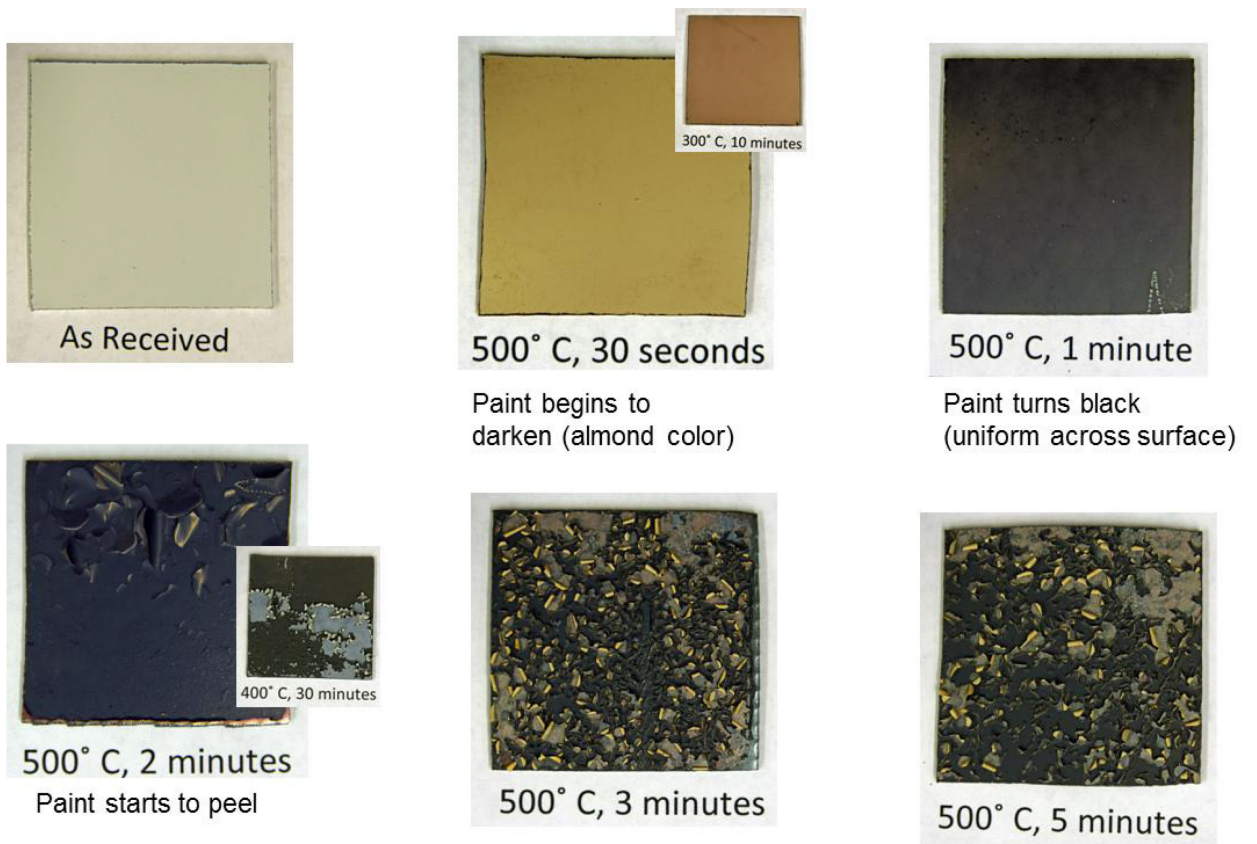


Figure 6. Metal coupon color changes due to heat.

1.2.4.4 Drum 10647918 Post-Event Observations. Figures 7 and 8 show the exterior and interior condition of drum 10647918 post-event.

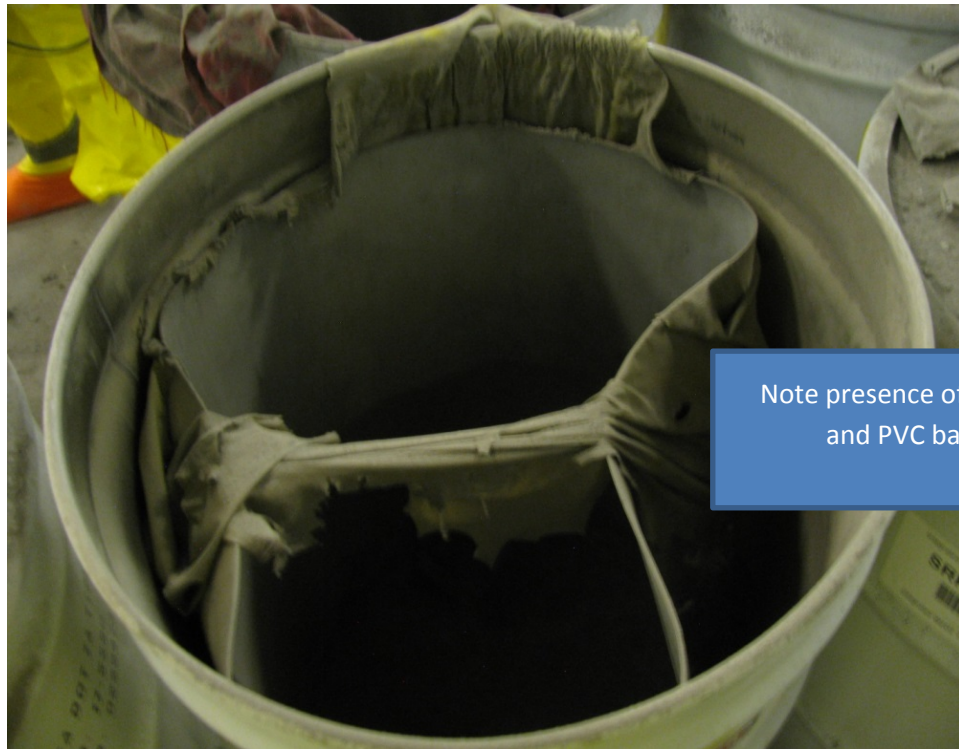


Figure 7. Drum 10647918 post-event exterior.



Figure 8. Drum 10647918 post-event interior.

1.2.4.5 Drum 10648030. Figures 9 and 10 show the interior and exterior condition of drum 10648030 post-event.



Note presence of HDPE liner and PVC bagging.

Figure 9. Drum 10648030 post-event interior.

1.2.4.6 Drum 10647931. Figures 10 and 11 show the interior and exterior condition of drum 10647931 post-event.

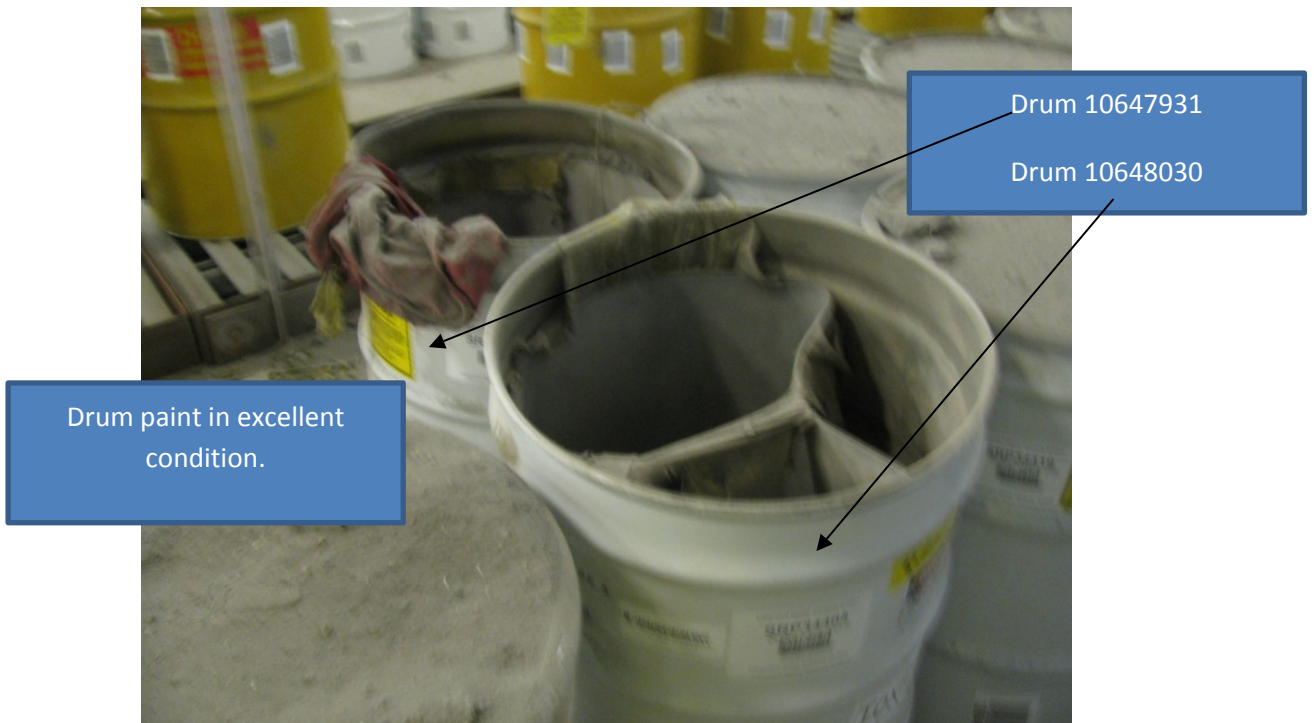


Figure 10. Drum 10647931 post-event exterior.

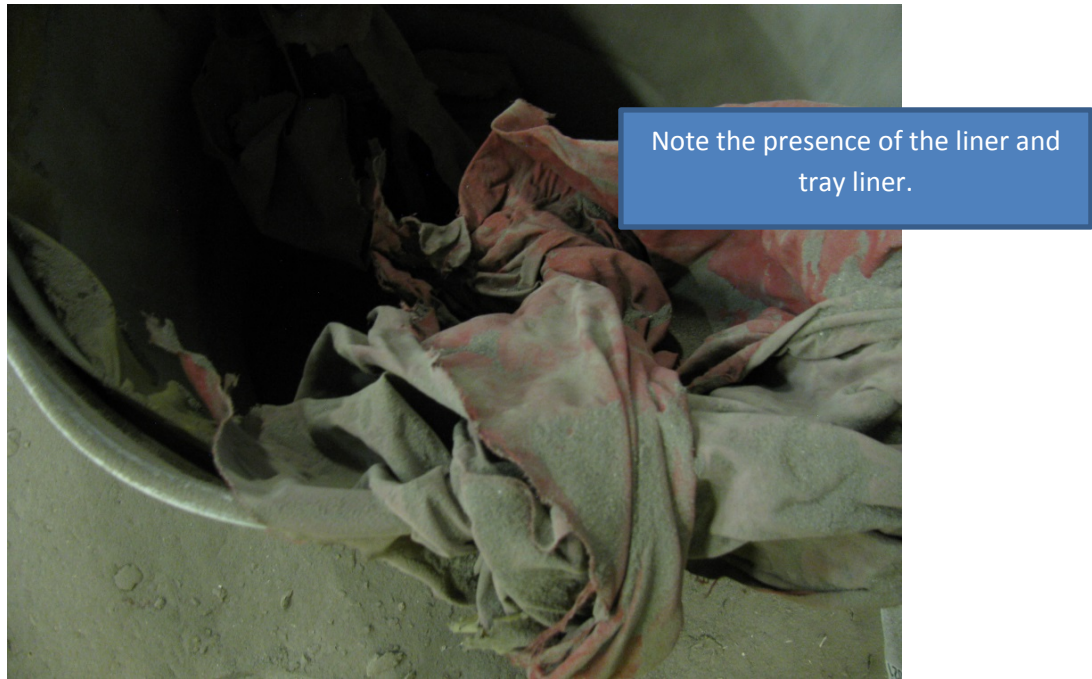


Figure 11. Drum 10647931 post-event interior.

1.3 Event Drums Origin

1.3.1 Item Description Code SD-176

The parent drums had been assigned an item description code (IDC) of SD-176 and had been retrieved from the Radioactive Waste Management Complex (RWMC) subsurface disposal area (SDA). The RWMC SDA is a historical landfill at the INL. The SDA landfill was established in 1952 and covers an area of approximately 97 acres. From 1952 to 1972, radioactive waste, including transuranic (TRU) waste, was buried in INL SDA pits, trenches, and soil vault rows. During the period of operation, the Rocky Flats Plant (RFP), the INL, and various off-site waste generators disposed of waste into the SDA.

In the mid-1970s, the IDR (Initial Drum Retrieval) and EWR (Early Waste Retrieval) projects, exhumed various types of waste and waste containers from the SDA. The IDR and EWR projects exhumed both 55-gallon and 30-gallon containers. Secondary wastes (e.g., personal protective equipment [PPE], tools, etc.) identified as TRU were containerized into 55-gallon drums or Tri-Wall containers (cardboard) and overpacked. The exhumed wastes were overpacked into cargo containers, fiberglass boxes, M-III bins (DOT 7A steel bins), and 83/85-gallon drums. The cargo containers, bins, and other waste containers were transferred to the INL Transuranic Storage Area-Retrieval Enclosure (TSA-RE) and placed into retrievable storage.

The INL RWMC IDR Project exhumed waste from a portion of the SDA Pits 11 and 12, beginning in 1974 and ending in 1978. An estimated 20,262 drums were exhumed. 91.5% of the drums had good integrity and were intact. These were placed into cargo containers and bins.

The INL RWMC EWR Project examined and/or exhumed waste from a portion of Pits 1 and 2 and Trenches 5, 7, 8, 9, and 10 beginning in 1976 and ending in 1978. Approximately 820 containers were exhumed. Most of the EWR exhumed waste containers were in poor condition and the waste was bagged and repackaged into 55-gallon drums or Tri-Wall containers. The 55-gallon drums or Tri-Wall containers were overpacked into M-III bins or fiberglass boxes.

- Pit 1 opened on November 1, 1957 and closed on October 1, 1959

- Pit 2 was opened on October 1, 1959 and closed on July 1, 1963
- Trench 5 was opened on November 4, 1955 and closed on March 29, 1956
- Pit 6 was opened on May 18, 1967 and closed on October 22, 1968
- Trench 7 was opened on August 14, 1956 and closed on December 20, 1956
- Trench 8 was opened on December 13, 1956 and closed on May 7, 1957
- Trench 9 was opened on January 17, 1957 and closed on September 6, 1957
- Trench 10 was opened on July 19, 1957 and closed on February 7, 1958
- Pit 11 was opened on April 14, 1970 and closed on October 16, 1970
- Pit 12 was opened on July 2, 1970 and closed on September 12, 1972.

The RFP, the INL, and various off-site waste generators disposed of waste into the SDA. The primary contributor of TRU waste to the SDA was the RFP. Other generators that had waste that was transhipped through the RFP contributing a minor portion of waste to the SDA include:

- Coors Porcelain Company
- Colorado School of Mines
- Denver Research Institute
- United States Geological Survey
- U.S. Food and Drug Administration
- U.S. Department of Interior
- GE Sandia
- Bureau of Land Management
- U.S. Fish and Wildlife Commission
- Rocky Mountain Arsenal
- VA Hospital.

The following five areas contributed most of the INL waste to the SDA.

- The ICPP (now the Idaho Nuclear Technology and Engineering Center; INTEC)
- The Naval Reactors Facility (NRF)
- Test Area North (TAN)
- The Test Reactor Area (TRA; now the Reactor Technology Complex)
- Argonne National Laboratory-West (ANL-W) (now the Materials and Fuels Complex; MFC).

Other generators contributed minor volumes of material as noted in RPT-TRUW-91, *Acceptable Knowledge Document for Pre-1980 INL Exhumed Waste*.¹

Following transfer of the overpacks to the TSA-RE, the containers were stored above ground on asphalt pads. Storage of transuranic containers (drums, boxes, bins, cargos, etc.) at TSA-RE began in 1970, as required by the Atomic Energy Commission (AEC). Storage was initially uncovered, but as the pads filled they were covered with wood, plastic, geofabric, and soil. The bins and cargos were not covered. In 1993 a roof enclosure was built around TSA-RE, covering the soil stacks, bins and cargo.

In 2002, retrieval operations in TSA-RE began. Operations were limited to removing the soil overburden, and unstacking drums and covered boxes. In 2009, unpack of IDR and EWR generated cargo and bin containers began. Cargo and bin unpack included:

- Opening overpack box in controlled conditions
- Removing one drum at a time
- Assigning a container ID
- Recording historical information, if available, in WTS
- Overpacking as necessary
- Sending the drum for vent, NDA and Real Time Radiography (RTR)
- Storing in an enclosed building pending validation of characterization data and remediation or disposal.

When historic information was available, this information was linked with the container ID in WTS and the unpacked container would be associated with a generator, generation process, generator assigned waste form, etc. This information was then used to assign an IDC to the container linking the waste to its historic lineage, and the waste form was then confirmed during characterization.

However, if historical information was not available, the containers unpacked from cargos and bins would be temporarily assigned an IDC of SD-179 (Pre-1980 INL-Exhumed SDA Waste Retrieval Containers). During characterization, the waste form would be determined and an IDC of SD-176 (Pre-1980 INL-Exhumed SDA Homogeneous Solids), SD-177 (Pre-1980 INL-Exhumed SDA Heterogeneous Debris) or SD-178 (Pre-1980 INL-Exhumed SDA Soil) would then be assigned with acceptable knowledge (AK) concurrence.

Following IDC assignment, containers of sludge waste that are identified for potential SRP processing (after 2015) undergo review and screening. AK review is performed for appropriate IDC assignment and review of historical information if available. NDA subject matter expert (SME) review is performed for potential pyrophoric (roaster oxide or high U-238), nitrate salt, and fissile gram equivalent (FGE) assignment. RTR information, including recordings if necessary, is reviewed. Site Project Manager (SPM) reviews of non-conforming conditions (NCRs) and other information (RTR SME review, weights, inner container information, etc.) are performed.

Following these reviews, containers requiring SRP remediation that are deemed acceptable are approved for this processing. Containers that are unacceptable for SRP processing are rejected. Rejected containers may undergo additional review, may require IDC change, may require additional processing, etc.

Containers approved for SRP processing are sent to SRP for remediation on approved shipments or loads. Each campaign is limited to waste of the same IDC with the exception of waste having IDCs RF-001, RF-002, RF-741, RF-742, RF-003, and RF-743, according to RPT-TRUW-05, *Waste Matrix Code Reference Manual*². SRP limits processing to one unique IDC, with the exception of those listed above; processing of these can be done together. When processing waste with a new IDC is initiated, all waste from the previous IDC is removed from the building to minimize cross contamination between IDCs.

The output of this process is assigned an IDC of CW-216 and the location of the CW-216 containers is tracked in WTS. If this process does not yield sufficient information for shipping and disposal, additional investigations are conducted as needed. The above information was summarized from RPT-TRUW-91.

1.4 Working Hypothesis

Based upon the event observations, parent assay results, and prior operational experience, the following working hypothesis was developed:

A reactive metal-initiated heating resulted in secondary reactions (volatile pressurization) and lid ejection.

This working hypothesis assisted in developing the target analyte list, analytical laboratory selection, and analytical testing approaches.

2. EVENT CHARACTERIZATION

2.1 Objectives and Summary

The objective of the event characterization was to acquire a detailed set of chemical, physical, and radiological data required to test the working hypothesis. To achieve this objective a series of sampling and analytical activities were completed as described in sampling procedure SPR-252, *Sampling and Analysis Protocol for Investigation of the ARP V Drum Incident*³. The sampling lines of inquiry were refined as analytical and testing results were received and reviewed. Sufficient data was collected to identify the reactive components responsible for drum over-pressurization.

2.1.1 Analytical Laboratory Selection

To support the characterization and investigation effort, two independent laboratories were selected to perform the analytical measurements. These laboratories were Southwest Research Institute Laboratories (SwRI), located in San Antonio, Texas, and the Savannah River National Laboratory (SRNL), located near Aiken, South Carolina. These laboratories were selected because they:

- Offer a broad range of analytical capability and consulting services
- Are permitted to handle radiologically-contaminated materials
- Are recognized throughout the Department of Energy (DOE) complex for good performance
- Have a good track record for providing high-quality services to INL
- Are certified DOE laboratories
- Are on the Idaho National Laboratory Qualified Suppliers List
- Participate in blind sample submittals
- Participate successfully in round-robin performance evaluations.

Additionally, two analytical laboratories provide the opportunity to compare independently-generated results and ensure the highest quality in the data.

2.1.2 Target Analyte and Methodology Selection

Given the wide range of chemicals used at both RFP and INL, the potential list of reactants is large (thousands of compounds). A comprehensive list of analytes was developed to encompass the most likely reactive components involved in the ARP V drum lid ejection events and therefore the most likely generator processes at RFP and INL. SPR-252 contains a comprehensive list of the target analytes.

The following techniques were utilized to characterize the sample material:

- Gamma Spectroscopy
- Alpha Spectroscopy
- Metals, Totals and Tentatively Identified Compounds (TICs)
- Anions
- Volatile Organic Compounds and TICs
- Semi-Volatile Organic Compounds and TICs
- Dioxins and Furans

- Polychlorinated Biphenyls
- Ignitability
- Thermogravimetric Analysis
- Scanning Electron Microscopy
- X-Ray Powder Diffraction.

2.2 Sampling Efforts

2.2.1 Sample Management

The Fluor Idaho Sample and Analysis Management Office (SAM) provided support to the sampling, analysis, and data management activities throughout the technical investigation. The mission of the SAM is to establish and maintain effective value-added processes for procurement and delivery of defensible analytical data and information of known quality and usability to the customer.

To initiate the analytical and characterization effort, SAM representatives assisted selecting qualified analytical service providers. The representative prepared requisite contracts and task order statements of work (TOS) for the analytical laboratories. The TOS referenced the appropriate analytical methods, typically Environmental Protection Agency methods, and Quality Assurance/Quality Control (QA/QC) protocols to ensure the data met Fluor Idaho's requirements.

During the sampling activities, a representative from the SAM guided collection and packaging of the samples. The SAM provided necessary sampling tools, containers, labels, and chain of custody forms for the sampling activities. The SAM also coordinated packaging for shipment and arranged for appropriate transportation to the analytical laboratories.

Preservation requirements and maximum sample holding times are obtained from the SAM representative; holding times are defined from the date of sample collection to the date of sample preparation or analysis, unless otherwise specified. A SAM representative coordinated analyses per SPR-252 with the off-site laboratories to achieve programmatic and quality requirements.

Sample labeling ensured samples were individually identifiable and tracked. A label identifying the unique field sample number was affixed to each sample bottle. Uniqueness was required to maintain consistency and prevent the same identification code from being assigned to more than one sample. Additionally, SAM personnel managed information that correlated the samples, characterization requirements, and results for complete fidelity in the analytical effort.

Chain of custody documentation was maintained by the SAM representative for all samples throughout the collection and shipment process.

All data packages were reviewed to ensure they are contractually compliant and include quality control and technical components needed to complete a data validation if appropriate. Data packages are validated by the generator and internally validated.

Data validation is a systematic process that applies a defined set of performance-based criteria to a body of data that can result in the qualification of data. The product of data validation is a Limitations and Validations (L&V) report for each data package. The L&V report contains an overall assessment of the quality and usability of the radio-analytical data. The L&V report typically contains the assessment of data quality and the laboratory's QA/QC performance, a summary of the results data for each analysis type, a listing of the data qualifier flags assigned to each individual analytical result, and an explanation of the flags assigned. The L&V report contains a detailed review of each parameter evaluated indicating

whether the frequency requirements were met and whether the results obtained were acceptable. The report contains a description of any nonconformance or deficiencies identified, and qualification of the affected data. The L&V report is designed to give data users a resource to help them make informed decisions regarding data usability.

Unique graphs, pressure tests, and visual examinations are validated during the generation and interpretation of the data to ensure these data meet contractual requirements and technical expectations.

As results were generated and transmitted by the laboratories, the SAM received and archived the data in an organized and retrievable manner. Data was electronically filed for access by the technical investigation team. The SAM tracked the data to ensure all requests made through the contract TOS were fulfilled.

Table 4 lists the L&V reports generated for this effort. The table provides a crosswalk between the sample delivery groups (SDG) and the associated L&V reports. The data packages and the L&V reports are stored at the Fluor Idaho office in an electronic information management database and are available on request.

Table 5 contains a crosswalk of all of the samples collected and unique identifiers.

2.2.2 Sampling Approach

The sampling approach and methods are fully described in SPR-252. Samples were collected by trained and qualified operations personnel under the support and guidance of a representative from the SAM office. The SAM representative provided necessary sampling tools, containers, labels, and chain of custody forms for the sampling activities.

It is worthwhile to note that the sampling was based on directed sampling. It was not intended to give each sample location an equal chance of selection (e.g. random selection of a grid). Grab samples were collected using a new disposable sampling scoop for each sample from the specified locations. The collected material was composited in 250 mL bottles, then sealed. Three bottles were filled at each sampling location. One bottle was sent to each of the analytical laboratories for characterization and the third was retained as an archive.

2.2.3 Ejected Material

The first sampling event focused on the ejected material that was dispersed throughout the airlock. The objective of gathering samples of this material was to characterize the event material. It was recognized that these samples would represent a composite blend of the material from the drums. Since the overall sampling plan was not yet finalized, an interim plan was prepared and documented in EPF-MISC-1386, *ARP-V Drum Incident Bulk Sampling, Transportation and Analysis Plan*.⁴

Material ejected from the event drums was dispersed throughout the Airlock of WMF-1617. The depth of this material decreased radially from the event drums. After reviewing photographs of the area taken during the initial assessment entries, sampling was directed using engineering and scientific judgment to locations and waste forms believed to best support the identification of the reactive material. Figure 12 shows the locations from which directed samples of the ejected material were collected and are shown with the oval bubbles. Samples were obtained from the floor and from the tops of unreacted drums near the open event drums. Due to the volume of material on the floor near Drum 10647918, a field duplicate sample was obtained from this location.

Table 4. Limitations and validations reports.

Analysis	Initial Entry SDG #	L&V Letter #	Ejected Material SDG #	L&V Letter #	Drum Contents SDG #	L&V Letter #	Large Particle SDG #	L&V Letter #	Headspace Gas SDG #	L&V Letter #	Mechanistic Sample SDG #	L&V Letter #
Americium-241	103139-01	JSL-269-18	SWR005013A	JSL-270-18	SWR013013A	JSL-317-18					108999-01	JSL-320-18
Plutonium Isotopic	103139-01	JSL-269-18	SWR005013A	JSL-270-18	SWR013013A	JSL-317-18					108999-01	JSL-320-18
Uranium Isotopic	103139-01	JSL-269-18	SWR005013A	JSL-270-18	SWR013013A	JSL-317-18					108999-01	JSL-320-18
Dioxins/Furans			SWR003013A	JSL-156-18	SWR011013A	JSL-160-18						
Gamma	103139-01	JSL-269-18	SWR005013A	JSL-270-18	SWR013013A	JSL-317-18					108999-01	JSL-320-18
Strontium-90			SWR005013A		SWR011013A							
Total Metals Standard TAL* (plus TICs) ICP and ICP-MS	103132-01	JSL-213-18	SWR001023A	JSL-208-18	SWR010013A	JSL-214-18					109000-01	JSL-320-18
Carbonates (TIC-TOC)			SWR001013A	JSL-207-18	SWR010013A	JSL-228-18					108997-01	JSL-314-18
Anions			SWR001013A	JSL-207-18	SWR010013A	JSL-228-18					108997-01	JSL-314-18
Anions (Citrate)			SWR001013A	JSL-207-18	SWR010013A	JSL-228-18					108997-01	JSL-314-18
Polychlorinated Biphenyls			SWR006013A	JSL-163-18	SWR011013A	JSL-164-18						
SVOC Priority Pollutant TAL (plus TICs)			SWR00203A	JSL-155-18	SWR011013A	JSL-159-18					108996-01	JSL-302-18
VOCs Priority Pollutant TAL (plus TICs)			SWR004013A	JSL-157-18	SWR011013A	JSL-166-18			108341-01 and 108343-01	JSL-297-18 and JSL-299- 18	108996-01	JSL-302-18
Uranium by ICP-MS	103123-01	JSL-210-18	SWR001023A	JSL-211-18	SWR011013A	JSL-212-18					109000-01	JSL-318-18
SEM and SEM-XRF	103132-01	N/A	SWR001013A	JSL-207-18	SWR010013A	JSL-228-18	8ARW00301R5	N/A			108997-01	N/A
XRD		N/A	SWR001013A	JSL-207-18	SWR010013A	JSL-228-18	8ARW00301R5	N/A			108997-01	N/A
Thermogravimetric			SWR001013A	JSL-207-18	SWR010013A	JSL-228-18					108997-01	N/A
Mass Screen	103132-01	N/A	SWR001013A	N/A	SWR011013A	N/A					109000-01	N/A
ICP-MS scan and TICs	103132-01	JSL-213-18	SWR001013A	JSL-208-18	SWR011013A	JSL-214-18					108996-01	JSL-319-18
SW-846 Method 1050 C			SWR001013A	JSL-207-18	SWR010013A	JSL-228-18					108997-01	N/A
Gross Alpha/Beta	103139-01	JSL-269-18										
DSC			SWR001013A	JSL-207-18	SWR011013A	JSL-228-18					108997-01	N/A
Gas Analysis			SWR001013A	N/A	SWR011013A	N/A			108341-01 and 108343-01	JSL-294-18 and JSL-295- 18	108996-01	N/A
Bulk Density			SWR001013A	JSL-207-18	SWR011013A	JSL-228-18					108997-01	JSL-314-18
Humidity Study			SWR001013A	N/A	SWR011013A	N/A					108996-01	N/A
Pressure/Heat			SWR006013A	N/A	SWR0110013A	N/A					108996-01	N/A
Hygroscopic Testing												
Gases Generation											108997-01	N/A
Thermal Conductivity											108996-01	N/A
pH			631472	JSL-301-18	631472	JSL-301-18					108997-01	JSL-314-18
Infrared Spectroscopy or Fourier Transform Infrared Spectroscopy												

Table 5. Correlation between sampling location and analytical sample identification.

Sampling			Sample Identifiers						
Category	Location	Description	Site-Wide Overpack Drum Number	Site-Wide Drum Number	SRP/ARP Drum Number	Sample Number	SWRI SOLID Sample Number	SWRI GAS Sample Number	SRNL SOLID Sample Number
Ejected Material	1	SRP-34415	NA	NA	NA	001013A	SWR001013A	NA	SRN001013A
Ejected Material	2	SRP-34415, Duplicate	NA	NA	NA	001023A	SWR001023A	NA	SRN001023A
Ejected Material	3	SRP-34415	NA	NA	NA	002013A	SWR002013A	NA	SRN002013A
Ejected Material	4	SRP-34402	NA	NA	NA	003013A	SWR003013A	NA	SRN003013A
Ejected Material	5	SRP-34402	NA	NA	NA	004013A	SWR004013A	NA	SRN004013A
Ejected Material	6	SRP-34418	NA	NA	NA	005013A	SWR005013A	NA	SRN005013A
Ejected Material	7	SRP-34390	NA	NA	NA	006013A	SWR006013A	NA	SRN006013A
Ejected Material	8	SRP-34419	NA	NA	NA	007013A	SWR007013A	NA	SRN007013A
Event Drum Contents	1	SRP-34415	NA	10647918	SRP34415	010013A	SWR010013A	NA	SRN010013A
Event Drum Contents	2	SRP-34402 (Burnt Drum)	NA	10648033	SRP34402	011013A	SWR011013A	NA	SRN011013A
Event Drum Contents	4	SRP-34398	NA	10647931	SRP34398	013013A	SWR013013A	NA	SRN013013A
Event Drum Contents	5	SRP-34405	NA	10648030	SRP34405	014013A	SWR014013A	NA	SRN014013A
Mechanistic Sample	NA	Historic High Methane	NA	10560041	ARP82996	NA	109343-01, 109344-01	108350-01	NA
Mechanistic Sample	NA	ARP V Daughter Drums Processed 4-10-18	10653846	10648022	SRP34419	NA	109331-01, 109332-01	108343-01	NA
Mechanistic Sample	NA	ARP V Daughter Drums Processed 4-10-18	10653845	10647908	SRP34385	NA	109334-01, 109335-01	108347-01	NA
Mechanistic Sample	NA	ARP V Daughter Drums Processed 4-10-18	NA	10647902	SRP34399	NA	NA	108341-01	NA
Mechanistic Sample	NA	ARP V Daughter Drums Processed 4-10-18	NA	10647928	SRP34393	NA	109337-01, 109338-01	108342-01	NA
Mechanistic Sample	NA	ARP V Daughter Drums Processed 4-11-18	10652979	10647909	SRP34384	NA	109340-01, 109341-01	108348-01	NA
Mechanistic Sample	NA	Table	NA	NA	NA	NA	108996-01, 108997-01	NA	NA
Mechanistic Sample	NA	Tray	NA	NA	NA	NA	108999-01, 109000-01	NA	NA
Mechanistic Sample	NA	Smear	NA	NA	NA	NA	109446-01, 109447-01	NA	NA

2.2.4 Reacted Drum Samples

The next phase of sampling focused on material that remained in the four event drums. The objective with this sampling was to chemically and radiologically characterize the material that remained in the event drums. Sampling and analysis of the materials from these four drums was conducted per guidance in SPR-252. This was accomplished using disposable scoops fitted with long handles, which allowed the operator to remain outside the volume of the event drum. Grab samples were collected from the full depth of the drums and therefore represents a composite of the drum's contents.

Again, Figure 12 shows the locations from which the event drums material was collected, designated with the circle bubbles.

2.2.5 Large Particle Samples

During cleanup operations, personnel noticed that two of the larger particles produced small sparks when moved across the floor. This effect was consistent with the behavior of breaching the oxide layer on DU. These larger materials were collected by the operations team and placed in an open stainless-steel pan for examination and sampling. The objective was to identify the reactive material involved in the event. Sampling and analysis of this material was controlled by EPF-MISC-1388, *ARP-V Drum Incident Cleanup Monitoring Plan*.⁵ This material was assayed via gram estimation. Sub-samples of the material were sent to SwRI for testing. Archive samples were retained.

2.2.6 Sorting Table

During the SRP operation, the contents of a drum are dumped onto a sorting table by heavy equipment operators (EO) in the RA. After an initial inspection for prohibited items, the EO used the excavator bucket to scrape the waste from the table into a lined tray for transfer to the drum packaging station. After this operation, the table is considered "Operationally Clean," meaning a small amount of waste material can remain on the table. This material was targeted for sampling to estimate the potential for cross-contamination during the operation.

During a sampling activity, operations personnel used hand tools to scrape, brush, and remove agglomerated material from the surface of the table. This material was collected and blended before three 250 mL sub-samples were obtained. Two of the 250 mL containers were shipped to SwRI for analysis. An archive sample was retained.

2.2.7 Tray 299

During the repackaging operation, several trays can be staged with waste material in preparation for introduction to the DPS. Tray 299 was filled with material during operations on the day of the event. However, as the shift ended, the tray was placed in a storage area in anticipation of continued processing the following day. The parent-daughter chart, Figure 13, shows the relation of Tray 299 to the other drums processed the day of the event.

Due to the temporal proximity, and possibility it contained event material, this material was sampled and transferred to SwRI for characterization. The material was collected and blended before three 250 mL sub-samples were obtained. Two of the 250 mL containers were shipped to SwRI for analysis. An archive sample was retained.

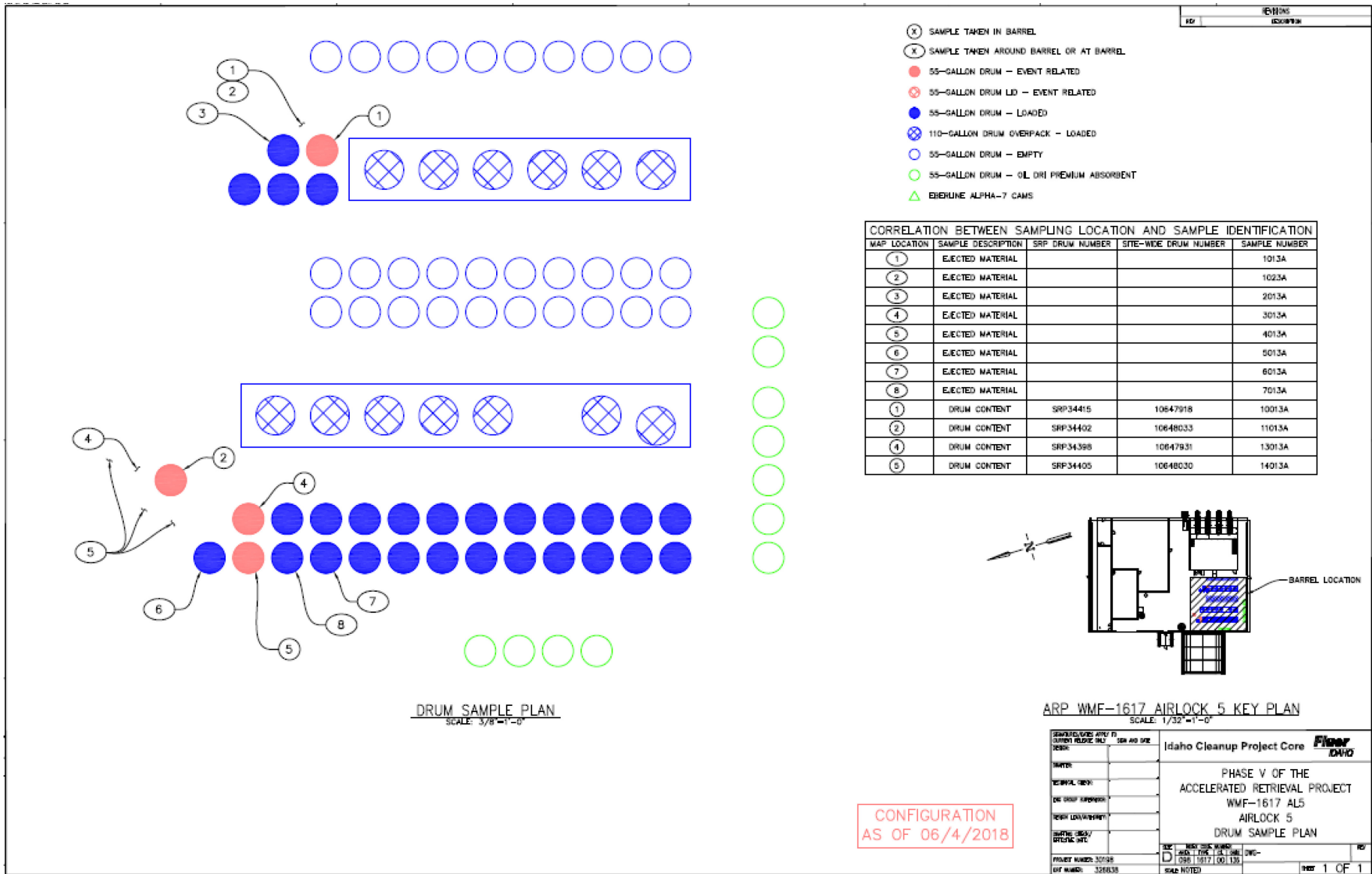


Figure 12. Sampling locations for ejected and drum materials.

2.2.8 Mechanistic Sample Selection

To support the determination of the reaction mechanism additional drum samples were obtained. Methane had been detected in the reacted event drum samples. Determining the source of this methane was believed to support the cause of the lid ejections. In addition, in 2016 several drums were discovered at Advanced Mixed Waste Treatment Project (AMWTP) that produced significant quantities of methane, beyond the allowable limit for shipment and disposal at WIPP. These drums were the source of samples referred to as ‘historic high methane’ and were evaluated for sampling. Finally, drums processed the same day and the day prior to the event drums were also evaluated.

To facilitate drum identification, a headspace screen for methane was performed. Drums processed on April 10 and 11 were evaluated for methane. Drums containing high and low methane were selected for solid sampling. One historically high methane drum was also selected. The selections summarized above are discussed in the following sections.

2.2.8.1 Unreacted Daughter Drums As shown in Figure 13, material processed near the time of the event was contained in several output or daughter drums that were identified as potential target drums, including drums from the day of the event and the day before. The potential target drums are listed in Table 6. To identify additional target drums, flammable gas screening was conducted. This was accomplished via syringe sampling through the septum port on the drum vent filters then analyzing the gas by a Flammable Gas Analyzer. Methane concentrations (see Table 20) in the samples were used to identify the remaining target drums for sampling selection. To ensure the likelihood of finding the analyte(s) that could be correlated with methane production in the event waste material, samples with both high and low methane concentrations were selected as targets for sample collection.

Drum 10647909 was closely related to the event drums. As shown in the parent-daughter relation diagram, Figure 13, the material in this drum had similar origin as the event drums and should have similar composition. This drum was selected as a high-value target for sampling and analysis.

The selected mechanistic drums are identified in red font in Table 6.

Once mechanistic drums were identified, head-space gas (HSG) samples were drawn (using evacuated summa canisters provided by the analytical laboratory) through the septum port of the drum vent filter. The HSG and the solid sub-samples were shipped to SwRI for analysis.

Samples of the solid contents were also obtained by moving the selected drums into the RA of WMF-1617. The drums were then opened by the equipment operator using a telehandler. The drum’s contents were dumped onto the sorting table and blended by the EO using the telehandler. The blended material is then placed into a liner tray where the sample was collected. Archive samples were retained.

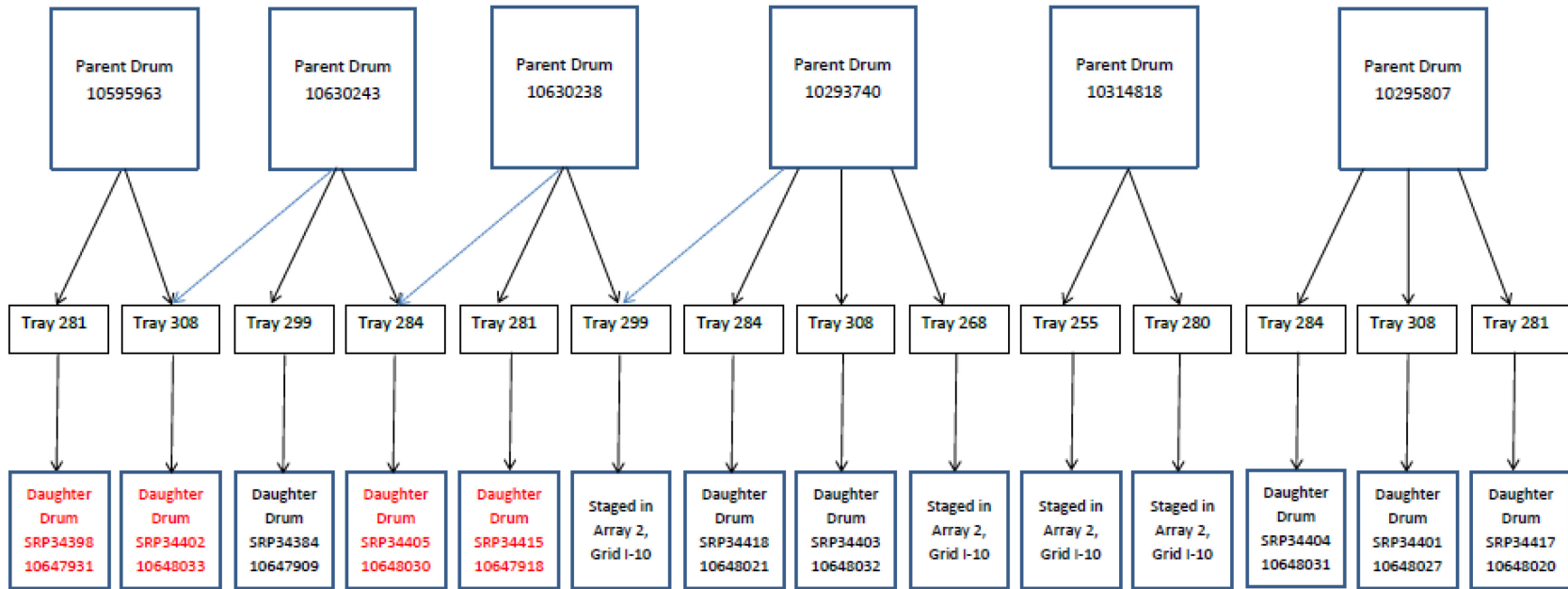
This activity is described in SPR-252.

2.2.8.2 Historically High Methane Producing Drums. As discussed, methane production was observed in several drums from ARP as early as September 2010. These containers were suspected to have characteristics similar to the event material. By visual inspection, these drums appear similar to the ARP V event waste, and a population of these drums was considered as mechanistic samples. This population was also screened for methane. Based on the high methane concentration, Drum 10560041 was selected for solid sampling. A HSG sample was drawn and a solid sample was obtained. This activity is described in SPR-252. The HSG and the solid sub-sample were shipped to SwRI for analysis. Archive samples were retained.

**4-11-2018 SRP Event – Parent Daughter Relationship,
Rev. 1**

Updated on 4/30/2018 to include daughter IWTS & WTS barcode numbers for correlation to VE data.

24



-----> Indicates that, based on the chronological tray filling order, material from subsequent drums being added to the tray prior to being sent to the DPS to fill the designated daughter drum.

Event Drums

Figure 13. Parent-daughter drum relations.

Table 6. Potential target drums for sampling and characterization.

Category	Drum Number	Process Drum Number	Methane Screening (ppm)
Historic High Methane	10555533	ARP72091	<MDL
	10545888	ARP81996	2790
	10545889	ARP82171	2182
	10545891	ARP82207	1499
	10545920	ARP82215	4347
	10545890	ARP82216	2058
	10545924	ARP82150	2438
	10560041	ARP82996	23398
	Unknown	ARP60110	NA
	Unknown	ARP60112	NA
ARP V Daughter Drums Processed 4-10-18	10647913	SRP34380	<MDL
	10647159	SRP34248	<MDL
	10648022	SRP34419	33341
	10647487	SRP34337	<MDL
	10648035	SRP34400	<MDL
	10647924	SRP34386	<MDL
	10647908	SRP34385	<MDL
	10647902	SRP34399	NA
	10647928	SRP34393	NA
	ARP V Daughter Drums Processed 4-11-18	10647909	SRP34384
10648032		SRP34403	1342

3. EVENT CHARACTERIZATION RESULTS

3.1 Objectives and Summary

This chapter presents the results of the compositional characterization conducted on event materials and mechanistic samples (material associated with the event material). This information supports the objective of this report as stated in Section 1.1. The results indicate significant amounts of uranium, beryllium, and zirconium in the event materials. Further, a variety of metal turnings were observed in the samples. The compositional data for the mechanistic samples show a strong correlation between beryllium in the material and methane concentrations in the drum's head-space gas.

3.2 Chemical Characterization

The following sections present the analytical data.

3.2.1 Quality Assurance Flags

The analytical data presented in the following sections have been assigned flags to describe the quality of the value. Data qualifiers are assigned by SwRI according to their QA Program. The INL SAM data validator independently reviews the data and assigns flags according to the INL procedures. The flags assigned by SwRI and the INL SAM Data Validator are defined in Tables 7 and 8.

Table 7. SwRI data qualifier flags.

SwRI		
Inorganic - Wet Chem and Metals		
U		Result is less than the SwRI Reporting Limit (RL)
N		Matrix Spike and/or matrix spike duplicate criteria was not met
X		Analytical spike criteria was not met
E		Result is estimated due to interferences
D		Result is reported from dilution
*		Duplicate criteria was not met
Inorganic - ICP Masses		
U		Undetected
	•	Relative percent difference (RPD) greater than 20%
Organic - VOC and SVOC		
B		Analyte is found in the blank as well as the sample
D		Concentration value is from dilution
E		Concentration exceeded calibration range
J		Estimated value
U		Analyzed for, but not detected
Organic - PCB		
P		RPD exceeds 40%
D		Reported at a secondary dilution
E		Concentration exceeded calibration range
J		Estimated value
U		Analyzed for, but not detected

Table 8. Validator data qualifier tags.

VALIDATOR		
Inorganic		
O		In control limits
M		Outside control limits Would require UJ or J flag, but not R flag
Z		Outside control limits Would require R flag
N/A		Not applicable
NP		Assessment required, but not performed
X		Contractual and/or technical issues noted, but data nor adversely affected.
I		Contractual and/or technical issues noted, data adversely affected Would require UJ, J, or R flag
G		Units reported did not correlate with the method
Organic		
U		Analyzed for, but not detected
J		Estimated value
N		Tentative Identification
NJ		Tentative Identification and estimated value
UJ		Not detected However, the quantitation limit is approximate may be inadequate
Radiological		
U		Analyzed for, but not detected
UJ		Analysis performed, but result is questionable
J		Analysis performed, and radioactivity detected However, value is estimate only
R		Result was rejected

3.2.2 Radio-isotopes

The radionuclide concentrations in the ejected material and the reacted drums are presented in Table 9. Radionuclides were measured using a gas proportional counter, alpha spectrometry, and gamma analysis, as appropriate.

3.2.3 Metals

Metal concentrations in the material were measured by Inductively Coupled Plasma-Atomic Emission Spectroscopy (ICP-AES), using Environmental Protection Agency (EPA) Method 6010. The results for the ejected material the reacted drums are presented in Table 10 with results reported in parts per million (ppm) (equivalent to mg/kg). These results do not indicate oxidation states of the metals, only the total metal content, regardless of oxidation state.

Table 9. Radio-isotopes in the ejected material and reacted drums.

Sample ID	Units	Floor Samples														Drum Samples									
		1013A		1023A		2013A		3013A		4013A		5013A		06013A		7013A		10013A		11013A		13013A		14013A	
Analyte		Result	Q	Result	Q	Result	Q	Result	Q	Result	Q	Result	Q	Result	Q	Result	Q	Result	Q	Result	Q	Result	Q	Result	Q
Uranium-233	mg/kg	1.04E-03	D	7.34E-04	D	9.45E-04	D	6.22E-04	D	5.16E-04	D	4.54E-04	D	4.34E-04	D	8.79E-04	D	6.98E-04	D	4.47E-04	D	6.44E-04	D	5.44E-04	D
Uranium-234	mg/kg	1.10E-01	D	2.40E-01	D	1.81E-01	D	1.62E-01	D	1.37E-01	D	1.73E-01	D	1.50E-01	D	1.87E-01	D	2.47E-01	*DJ	1.36E-01	*DJ	4.02E-02	*DJ	9.93E-02	*DJ
Uranium-235	mg/kg	2.77E+01	D	5.25E+01	D	4.82E+01	D	4.86E+01	D	4.07E+01	D	5.25E+01	D	4.02E+01	D	5.39E+01	D	6.44E+01	*DJ	4.29E+01	*DJ	1.16E+01	*DJ	3.13E+01	*DJ
Uranium-236	mg/kg	6.56E-01	D	9.80E-01	D	1.13E+00	D	1.07E+00	D	9.30E-01	D	1.05E+00	D	8.77E-01	D	1.11E+00	D	1.47E+00	*DJ	9.27E-01	*DJ	2.81E-01	*DJ	6.29E-01	*DJ
Uranium-238	mg/kg	1.64E+04	D	3.03E+04	D	3.11E+04	D	2.78E+04	D	2.22E+04	D	2.98E+04	D	2.51E+04	D	3.33E+04	D	3.61E+04	*DJ	2.57E+04	*DJ	6.50E+03	*DJ	1.79E+04	*DJ
Total U	mg/kg	1.64E+04	DJ	3.04E+04	DJ	3.11E+04	DJ	2.78E+04	DJ	2.22E+04	DJ	2.99E+04	DJ	2.51E+04	DJ	3.34E+04	DJ	3.62E+04	*DJ	2.57E+04	*DJ	6.51E+03	*DJ	1.79E+04	*DJ
%U235	wt%	0.169%		0.173%		0.155%		0.175%		0.183%		0.176%		0.160%		0.162%		0.178%		0.167%		0.178%		0.175%	
Pu-238	pCi/g	4.21E+04		4.58E+04		5.21E+04		8.73E+04		9.43E+04		6.30E+04		6.08E+04		7.85E+04		6.89E+04	J	6.10E+04	J	5.89E+04	J	4.81E+04	UJ
Pu-239/240	pCi/g	1.67E+06		1.49E+06		2.74E+06		3.43E+06		3.52E+06		2.96E+06		3.02E+06		3.91E+06		2.40E+06		2.39E+06		3.87E+06		2.29E+06	
Pu-239	pCi/g	1.36E+06	U	1.20E+06	U	2.23E+06		2.80E+06		2.84E+06	UJ	2.39E+06		2.45E+06		3.17E+06		1.99E+06	U	1.95E+06	U	3.17E+06	UJ	1.85E+06	
Pu-240	pCi/g	3.14E+05		2.88E+05		5.08E+05		6.35E+05		6.77E+05		5.68E+05		5.74E+05		7.44E+05		4.12E+05		4.35E+05		7.00E+05		4.36E+05	
Pu-242	pCi/g	3.72E+03	UU	4.95E+03	UU	3.55E+03	UUJ	8.73E+03	UUJ	2.30E+03	UU	5.48E+02	UU	3.65E+03	UU	3.57E+03	UU	1.97E+03	UU	5.38E+03	UU	7.07E+03	UU	5.35E+03	UU
Pu-244	pCi/g	1.24E+03	UU	0.00E+00	UU	5.92E+02	UU	1.45E+03	UU	1.15E+03	UU	0.00E+00	UU	1.22E+03	UU	1.19E+03	UU	1.97E+03	UU	0.00+03	UU	0.00E+00	UU	3.56E+03	UU
Am-241	pCi/g	3.40E+06		3.23E+06		5.70E+06		6.39E+06		6.45E+06		5.38E+06		5.62E+06		7.36E+06		4.40E+06		5.04E+06		6.63E+06		6.13E+06	

The percentage of U-235 ranged from 0.16% to 0.18%.

Table 10. (continued).

Sample ID Units	Floor Samples														Drum Samples									
	1013A mg/kg		1023A mg/kg		2013A mg/kg		3013A mg/kg		4013A mg/kg		5013A mg/kg		6013A mg/kg		7013A mg/kg		10013A mg/kg		11013A mg/kg		13013A mg/kg		14013A mg/kg	
Analyte	Result	Q	Result	Q	Result	Q	Result	Q	Result	Q	Result	Q	Result	Q	Result	Q	Result	Q	Result	Q	Result	Q	Result	Q
nickel	469	J	239	J	555	J	592	J	1200	J	660	J	649	J	844	J	1,810	*J	414	*J	283	*J	348	*J
niobium	942	J	1,050	J	1,570	J	315	J	934	J	2,030	J	1,390	J	989	J	1,850	*J	1,550	*J	92.1	*J	987	*J
palladium	22.7	UN UJ	23.3	UN UJ	22.2	UN UJ	24.9	UN UJ	21.6	UN UJ	21.4	UN UJ	23.1	UN UJ	23	UN UJ	19.4	U	18.9	U	21.9	U	19.6	U
phosphorus	1,680	J	1,130	J	1,040	J	619	J	433	J	291	J	309	J	345	J	3,060	*J	9,580	*J	250	*J	409	*J
platinum	2.93		2.2		3.7		1.85	J	1.87		2.3		2.46		2.01		2.03		1.53		0.588		1.27	
potassium	15,200		9,320		17,800		30,300		27,500		24,700		27,400		27,300		17,000		24,100		35,600		29,000	
praseodymium	1.32	JJ	0.96	JJ	1.73	JJ	1.63	JJ	1.43	JJ	1.64	JJ	1.4	JJ	1.48	JJ	0.898	JJ	0.946	JJ	0.914	JJ	1.26	JJ
rhenium	0.909	U UJ	0.932	U UJ	0.888	U UJ	0.996	U UJ	0.865	U UJ	0.857	U UJ	0.924	U UJ	0.921	U UJ	0.0777	U UJ	0.0755	U UJ	0.0878	U UJ	0.0784	U UJ
rhodium	0.239		0.236		0.204		0.294		0.368		0.285		0.419		0.233		0.512	*	0.232	*	0.285	*	0.488	*
rubidium	8.6		8.87		7.93		11.9		11.2		9.79		10.9		11.2		8.13		13.7		14.8		16.5	
ruthenium	0.909	UN UJ	0.932	UN UJ	0.888	UN UJ	0.996	UN UJ	0.865	UN UJ	0.857	UN UJ	0.924	UN UJ	0.921	UN UJ	0.777	UN UJ	0.755	UN UJ	0.878	UN UJ	0.784	UN UJ
samarium	1.05	J	0.656	J	1.37		1.12	J	1.35	J	0.943		1.05	J	1.16	J	0.711		0.852		0.693		0.979	
scandium	6.42	J	4.95	J	9	J	5.75	J	4.76	J	6.43	J	6.08	J	5.14	J	6.57		5.01		2.3		4.54	
selenium	22.7	U	23.3	U	22.2	U	24.9	U	21.6	U	21.4	U	23.1	U	23	U	19.4	U	18.9	U	21.9	U	19.6	U
silicon	84,300		77,800		78,200		111,000		110,000		105,000		104,000		89,900		93,600		77,600		99,100		112,000	
silver	9.09	U	9.32	U	8.88	U	9.96	U	8.65	U	8.57	U	9.24	U	9.21	U	9.33	UN	9.06	UN	10.5	UN	9.41	UN
sodium	37,200		22,100		62,800		85,500		80,300		64,100		68,800		85,500		54,400		137,000		86,900		72,200	
strontium	205		123		131		123		154		74.4		69.4		80.9		306	*	82.7	*	107	*	159	*
sulfur	1,540		760		1,680		1,700		1,860		1,690		1,580		1,550		1,860	J	3,170	J	1,410	J	2,010	J
tantalum	15.2	J	9.32	J	19.7	J	1.66	J	11.4	J	21.1	J	17.9	J	11.9	J	22.1	*J	20.8	*J	1.92	*J	19.8	*J
tellurium	0.312	JN XJ	0.26	JN XJ	0.318	JN XJ	0.199	UN XU	0.173	JN XJ	0.443	JN XJ	0.185	UN XU	0.208	JN XJ	0.27	J	0.394		0.176	U	0.157	U
terbium	0.233		0.208		0.298		0.248		0.233		0.253		0.394		0.254		0.183		0.22		0.125	J	0.202	
thallium	0.668	*	0.695	*	0.774	*	1.25	*	1.69	*	1.18	*	1.78	*	0.847	*	2.38	*J	0.913	*J	0.564	*J	1.4	*J
thorium	5.19		4.69		6.99		5.03		4.36		5.82		5.16		4.83		5.66		4.68		2.58		4.78	
thulium	0.403		0.346		0.544		0.342		0.26		0.361		0.341		0.29		0.331		0.293		0.154	J	0.255	
tin	213		144		57.2		113		39.8		163		178		169		436	*J	38.7	*J	373	*J	75	*J
titanium	523	J	320	J	786	J	833	J	820	J	830	J	802	J	828	J	675	J	744	J	519	J	812	J
tungsten	116	*J	49.5	*J	105	*J	197	*J	53.4	*J	197	*J	132	*J	75.4	*J	93.4	*J	111	*J	18.1	*J	115	*J
uranium	16,300	J	23,500	J	30,400	J	30,100	J	23,600	J	30,300	J	25,600	J	32,900	J	37,500	*J	24,900	*J	6,520	*J	17,100	*J
vanadium	28.4	*J	12.2	*J	27	*J	29.5	*J	34.7	*J	25.1	*J	25.8	*J	28.4	*J	30.2	*J	24	*J	29.4	*J	45.7	*J
ytterbium	3.58		2.46		5.01		3.4		2.39		3.7		3.4		2.54		3		2.39		1.03		2.33	
Yttrium	20.8	NJ	13.8	NJ	29.9	NJ	29.7	NJ	30.1	NJ	27.8	NJ	82.5	NJ	35.6	NJ	20.6		20.8		9.67		16.5	
zinc	2,440	*J	696	*J	570	XJ	677	XJ	1,470	XJ	603	XJ	748	XJ	925	XJ	809	*J	5,000	*J	790	*J	576	*J
zirconium	11,300		6,530		16,200		9,200		7,330		10,900		10,300		7,670		10,700		8,160		2,650		7,040	

3.2.3.1 Metals expressed as a mole/kg. Results are represented in a column plot to facilitate visual comparisons (Figure 14, top). The quantity of beryllium is substantial in that it averages 103,000 ppm by weight. When the weight concentrations are normalized by dividing by the respective atomic weights, what is seen is that on a molar basis, Be is by far the most abundant metal (Figure 14, bottom).

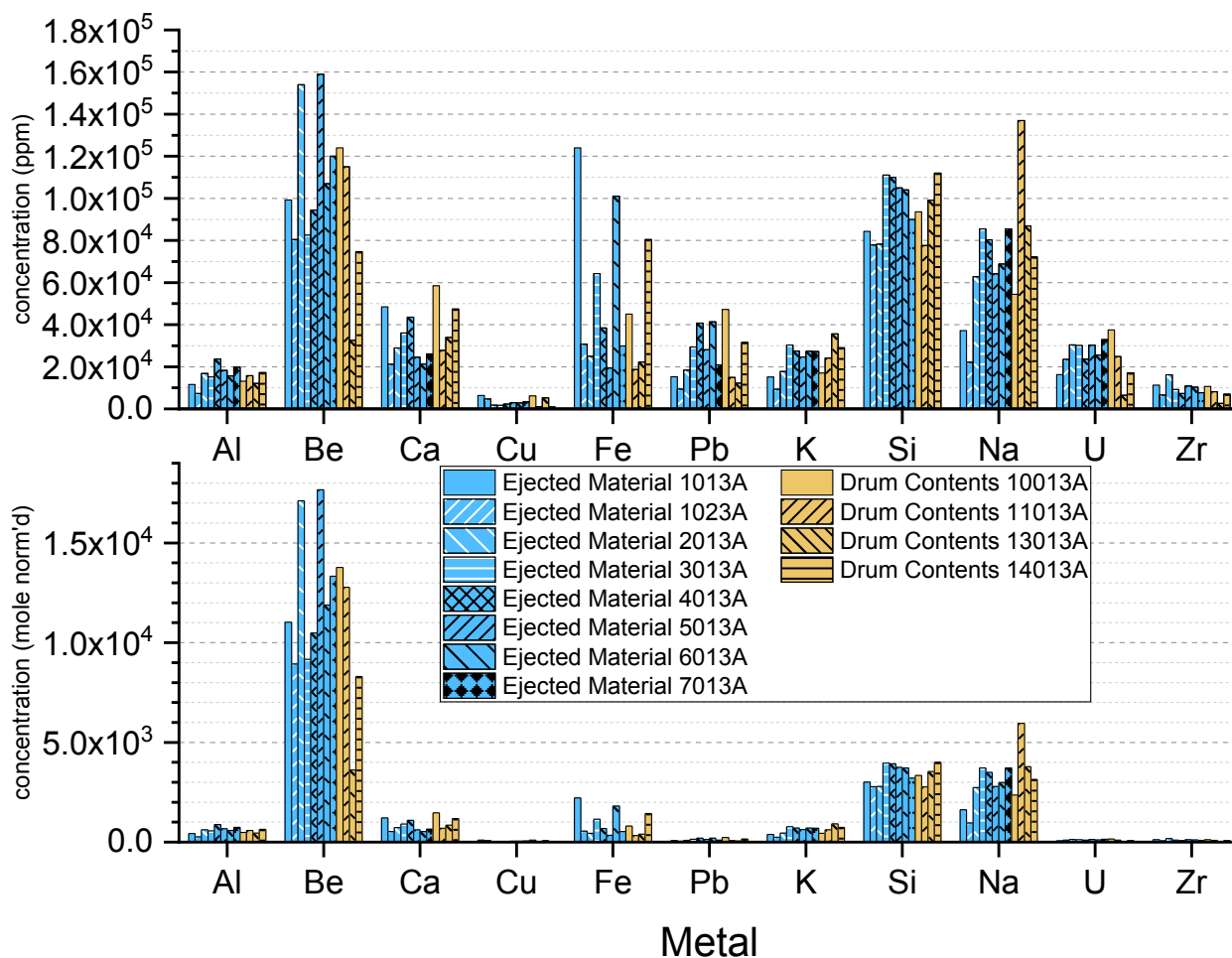


Figure 14. Graphical representation of the metals measured in the samples collected after the drum rupture event. Samples of ejected material are colored using gold tones, while samples of material from the drums use blue tones. Top, metal concentrations as measured on a mass/mass basis (e.g., mg/kg). Bottom, concentrations on a molar basis, after normalizing to the atomic weights (e.g., millimole/kg).

3.2.4 Organics – Volatile Organics, Semi-Volatile Organics, and Polychlorinated Bi-phenols

To determine the potential contribution from organic compounds in the waste material, a variety of organic analyses were performed on the ejected and reacted drum materials. This included characterization of volatile organics (VOCs), semi-volatile organics (SVOCs), and polychlorinated biphenols (PCBs) These constituents were measured using gas chromatography-mass spectroscopy following EPA SW-846 methods 8260, 8270, and 8082, respectively. The results for the ejected and reacted drums materials are presented in Tables 11, 12, and 13.

Dioxins and furans were measured in part per trillion (ppt) levels. Due to the low concentrations, it was assumed that these constituents did not contribute to the event and are not reported here.

Significant reduction in concentration of the organic constituents is shown between the ejected material and the reacted drum material. This is due to continued thermal exposure experience by the material remaining in the drum after the lid was displaced and the contents were partially ejected.

3.2.5 Anions

Anion concentrations were measured to identify constituents that potentially caused or contributed to the event. Anions were measured in the ejected and reacted drum materials using ion chromatography per EPA method E300. The results for the ejected and reacted drum material are presented in Table 14.

Fluoride was found in concentrations between 1.3 to 5.2 ppm. Significant amounts of nitrate and nitrite were measured and could have contributed as an oxidizer in the reaction. The chloride concentration in the reacted drum sample 11013A was elevated due to the addition of Met-L-X (a sodium chloride based dry powder extinguishing agent) during the fire fighters' response to the event.

Table 11. Volatile organic compounds in ejected material and drum contents. Many samples were diluted.

Sample ID Concentration unit	Floor Samples																Drum Samples							
	1013A µg/kg		1023A µg/kg		2013A µg/kg		3013A µg/kg		4013A µg/kg		5013A µg/kg		6013A µg/kg		7013A µg/kg		10013A µg/kg		11013A µg/kg		13013A µg/kg		14013A µg/kg	
Compound	Result	Q	Result	Q	Result	Q	Result	Q	Result	Q	Result	Q	Result	Q	Result	Q	Result	Q	Result	Q	Result	Q	Result	Q
carbon disulfide	25	J	29	J	16	J	5.3	J	4.8	U	8.6	J	4.8	J	4.8	J	87	U	80	U	87	U	99	U
acetone	3,000	D	2,300	D	2,400	D	2,200	D	2,900	D	3,500	D	3,800		5,000	D	340		390		370		210	
trans-1,2-dichloroethene	4.8	U	5.0	U	4.8	U	4.9	U	4.8	U	4.9	U	11	J	8.8	J	87	U	80	U	87	U	99	U
chloroform	1,100	J	390	J	690	J	440	J	420	J	550	D	440	J	420	J	87	U	80	U	87	U	99	U
carbon tetrachloride	110	J	170	J	4.8	U	4.9	U	4.8	U	7.9	J	4.6	U	5.7	J	87	U	80	U	87	U	99	U
2-butanone	330	J	330	J	430	DJ	440	DJ	370	J	660	E	890	E	600	E	170	U	180		210		170	JJ
benzene	68	J	60	J	170	J	210	J	220	J	180	J	220	J	190	J	250		130		87	U	99	U
trichloroethene	18,000	J	17,000		28,000		17,000		18,000		33,000	J	22,000	J	30,000	J	87	U	960		860		230	
<i>n</i> -butyl alcohol	48	U	50	U	48	U	49	U	48	U	49	U	46	U	35	U	870	U	800	U	870	U	990	U
methyl methacrylate	48	R	50	R	48	R	49	R	48	R	49	R	46	R	35	R	870	R	800	R	870	R	990	R
methacrylate	48	U	67	J	9,100		4,000		4,100		7,500		6,600		8,000		87	U	80	U	1000		99	U
toluene	160	J	120	J	810		550		410		640		410		400		87	U	250		87	U	99	U
tetrachloroethene	200	J	190	J	8,700		4,500		5,100		7,300		5,600		5,300		87	U	210		470		99	U
4-methyl-2-pentanone	72	J	53	J	77	J	90	J	84	J	82	J	90	J	60	J	170	U	160	U	170	U	200	U
ethylbenzene	27	J	21	J	50	J	56	J	60	J	52	J	62	J	51	J	87	U	80	U	87	U	99	U
m/p-xylene	42	J	32	J	80	J	85	J	110	J	85	J	93	J	81	J	170	U	160	U	170	U	200	U
o-xylene	20	J	16	J	36	J	40	J	46	J	37	J	43	J	34	J	87	U	80	U	87	U	99	U
xylene (Total)	62	J	48	J	120	J	130	J	160	J	120	J	140	J	120	J	260	U	240	U	260	U	300	U
1,2-dibromo-3-chloropropane	14	J	62	J	40	J	4.9	U	23	J	54	J	4.6	U	18	J	87	U	80	U	87	U	99	U

Table 12. Semi-volatile organic compounds in ejected material and drum contents.

Sample ID Concentration unit	Floor Samples														Drum Samples									
	1013A µg/kg		1023A µg/kg		2013A µg/kg		3013A µg/kg		4013A µg/kg		5013A µg/kg		6013A µg/kg		7013A µg/kg		10013A µg/kg		11013A µg/kg		13013A µg/kg		14013A µg/kg	
Compound	Result	Q	Result	Q	Result	Q	Result	Q	Result	Q	Result	Q	Result	Q	Result	Q	Result	Q	Result	Q	Result	Q	Result	Q
phenol	16,000		14,700		17,900		7,790		6,490		15,800		6,950		8,470		2,810		2,010	U	2,480		2,750	
2-methylphenol (<i>o</i> -cresol)	567	J J	2,000	U	860	J J	723	J J	513	J J	862	J J	506	J J	532	J J	1,940	U	2,010	U	1,950	U	1,960	U
3&4-methylphenol (<i>m</i> -cresol & <i>p</i> -cresol)	1470	J J	1,190	J J	2,060	J J	1,680	J J	1,170	J J	2,240		1,110	J J	1,390	J J	1,940	U	2,010	U	1,950	U	1,960	U
2,4-dimethylphenol	1,960	U	2,000	U	2,070	U	649	J J	1,920	U	687	J J	1,830	U	1,790	U	1,940	U	2,010	U	1,950	U	1,960	U
benzoic acid	1,960	U	2,000	U	2,070	U	1,970	U	1,920	U	3,310	J J	1,830	U	1,790	U	1,940	U	2,010	U	1,950	U	1,960	U
diethylphthalate	3,390	B U	3,900	B U	4,250	B U	4,290	B U	3,590	B U	4,110	B U	3,970	B U	2,790	B U	1,940	U	2,010	U	1,950	U	1,960	U
pentachlorophenol	1,960	U	2,000	U	2,070	U	1,970	U	1,920	U	1,990	U	1,830	U	1,790	U	1,940	U	2,010	U	2,640		1,960	U
phenanthrene	497	J J	2,000	U	654	J J	845	J J	575	J J	630	J J	628	J J	625	J J	1,940	U	2,010	U	1,950	U	1,960	U
di- <i>n</i> -butylphthalate	1,960	U	2,000	U	549	J J	1,970	U	1,920	U	548	J J	1,830	U	511	J J	1,940	U	2,010	U	1,950	U	1,960	U
fluoranthene	1,960	U	2,000	U	2,070	U	575	J J	1,920	U	1,990	U	470	J J	474	J	1,940	U	2,010	U	1,950	U	1,960	U
pyrene	1,960	U	2,000	U	2,070	U	540	J J	1,920	U	1,990	U	1,830	U	1,790	U	1,940	U	2,010	U	1,950	U	1,960	U
butylbenzylphthalate	1,960	U	542	J J	661	J J	1,970	U	1,920	U	745	J J	1,830	U	1,120	J J	1,940	U	2,010	U	1,950	U	1,960	U
bis(2-ethylhexyl)phthalate	25,700		27,600		35,000	D	19,000		13,000		29,600		14,900		27,300		1,320	J J	2,010	U	6,180		2,290	
di- <i>n</i> -octylphthalate	7,280		8,790		12,100		5,830		4,110		9,370		5,560		8,690		1,940	U	2,010	U	1,860	J J	1,960	U
acetophenone	1,380	J J	1,410	J J	1,540	J J	995	J J	751	J J	1,780	J J	867	J J	1,170	J J	1,940	U	2,010	U	1,950	U	1,960	U

Table 13. PCBs in ejected material and drum contents.

Sample ID	Floor Samples												Drum Samples											
	1013A		1023A		2013A		SWR00		4013A		5013A		6013A		7013A		10013A		11013A		13013A		14013A	
Units	µg/kg		µg/kg		µg/kg		µg/kg		µg/kg		µg/kg		µg/kg		µg/kg		µg/kg		µg/kg		µg/kg		µg/kg	
Compound	Result	Q	Result	Q	Result	Q	Result	Q	Result	Q	Result	Q	Result	Q	Result	Q	Result	Q	Result	Q	Result	Q	Result	Q
Aroclor-1254	40,100		20,100		45,000		58,000		48,500		48,700		48,900		50,000		5,900		1,500	E J	41,400		7,400	J
Aroclor-1260	8,510		4,940	J J	10,000		10,400		9,100		10,300		9,550		10,100		1,340		429	J J	6,600		1,450	J

Table 14. Anion concentrations in the ejected material and drum contents.

Sample ID	Floor Samples												Drum Samples											
	1013A		1023A		2013A		3013A		4013A		5013A		6013A		7013A		10013A		11013A		13013A		14013A	
Units	mg/Kg		mg/Kg		mg/Kg		mg/Kg		mg/Kg		mg/Kg		mg/Kg		mg/Kg		mg/Kg		mg/Kg		mg/Kg		mg/Kg	
Anion	Result	Q	Result	Q	Result	Q	Result	Q	Result	Q	Result	Q	Result	Q	Result	Q	Result	Q	Result	Q	Result	Q	Result	Q
bromide	27.5	J	27.7	J	23.8	J	12.6	J	14.2	J	24.0	J	19.7	J	14.8	J	58.5		75.6		3.34	U	39.8	
chloride	4,940	D	4,340	D	3,380	D	9,720	D	6,700	D	3,810	D	4,980	D	4,370	D	5,810	D	105,000		5,840	D	6,510	D
fluoride	13,000	D	14,200	D	24,300	D	46,700	D	43,300	D	31,800	D	42,600	D	39,900	D	25,500	*D	21,000	*D	52,300	*D	48,900	*D
nitrate-N*	8,760	D	6,090	D	6,200	D	6,650	D	7,270	D	6,670	D	7,010	D	6,330	D	3,160	D	1,520	D	13,700	D	6,350	D
nitrite-N*	491	D	395	D	469	D	787	D	727	D	589	D	697	D	666	D	141	DJ	54.7	DJ	1,010	DJ	324	DJ
phosphate-P*	38.3	UD	3.73	U	3.52	U	32.6		3.85		3.56	U	3.70	U	3.35	U	3.66	*NJ	3.81	U*N UJ	3.34	U*N UJ	3.47	U*N UJ
sulfate	1,840	D	1,520	D	1,520	D	2,450	D	2,320	D	1,920	D	2,290	D	2,010	D	3,550		6,570	D	2,540	D	3,790	D
citrate	0.100	UN UJ	0.100	UN UJ	0.100	UN UJ	0.160	N	0.198	N	0.225	N	0.594	N	0.242	N	3.48	UN UJ	3.81	UN UJ	3.34	UN UJ	6.95	NJ

3.2.6 Metal Turnings

Visual examination of the ejected and drum material identified the presences of a variety of metal turnings. These turnings were removed from the samples and examined by optical microscopy and elemental compositions were determined by energy dispersive x-ray spectroscopy (EDS). These analyses identified carbon steel, stainless steel, aluminum alloy, beryllium metal, leaded brass, high chrome stainless steel, and copper alloy. This variety of turnings indicates that portions of the event material originated in a metal manufacturing facility. Typical/representative microscopic images are provided in Figures 15 through 21.

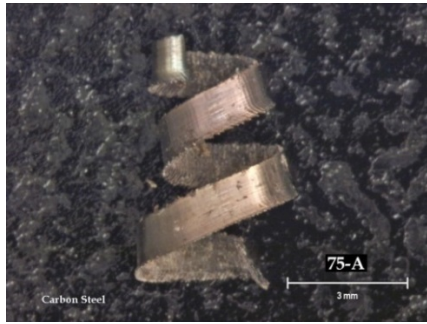


Figure 15. Carbon steel.

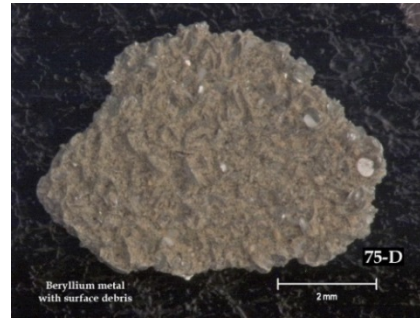


Figure 18. Beryllium metal.

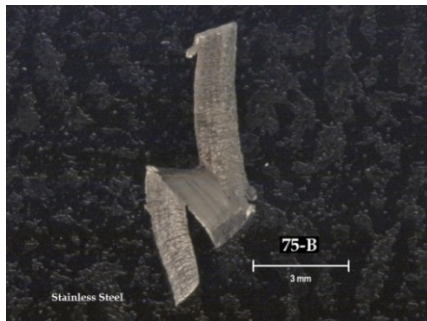


Figure 16. Stainless steel.

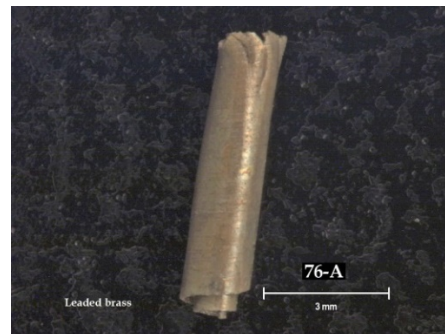


Figure 19. Leaded brass.

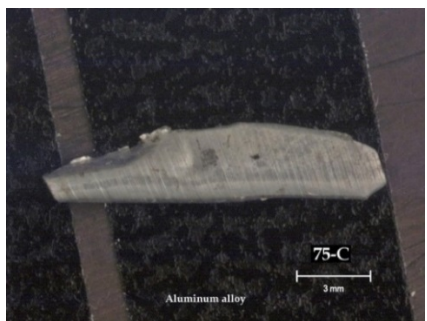


Figure 17. Aluminum alloy.

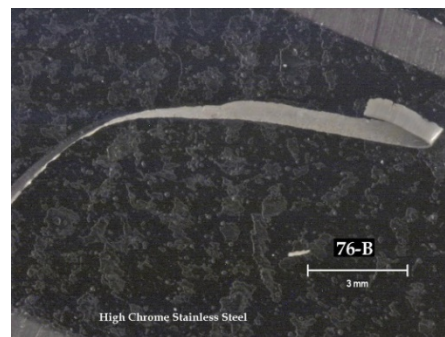


Figure 20. High chrome stainless steel.

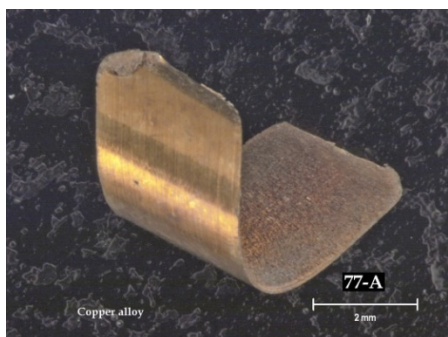


Figure 21. Copper alloy.

3.2.7 Mechanistic Sample Results

To support the determination of the reaction mechanism, additional drums and sample materials were selected. This section includes the historical high methane drums that were sampled and analyzed for comparison with the composition of the ARP V event drums. The results are provided below (refer to tables 5 and 6 for correlation).

3.2.7.1 Radio-isotopes. Radio-isotopes were measured, and results are presented in Table 15.

3.2.7.2 Metals. Table 16 contains the metals measured in the mechanistic samples (sample taken to elucidate the reaction mechanism).

3.2.7.3 Organics – Volatile Organics and Semi-Volatile Organics. Tables 17 and 18 contain the volatile and semi-volatile results, respectively. Due to the low informational value, PCBs were not measured in the mechanistic sample.

Table 15. Radio-isotope results.

Sample ID		Table		Tray		SRP34419		SRP34385		SRP34393		SRP34384		ARP82996	
Isotope	Units	Result	Q	Result	Q	Result	Q	Result	Q	Result	Q	Result	Q	Result	Q
Pu-238	pCi/g	3.85E+05		7.48E+04		2.96E+03		4.62E+04		6.24E+04	U	7.95E+03		9.25E+03	
Pu-239/240	pCi/g	1.98E+07		1.27E+06		1.18E+05		1.76E+06		2.49E+06		3.13E+05		2.21E+05	
Pu-244	pCi/g	2.00E+04	UU	2.20E+03	UU	1.64E+02	UU	0.00E+00	UU	0.00E+00	UU	3.79E+02	UU	9.73E+02	UU
Am-241	pCi/g	2.07E+07		1.55E+06		1.91E+05		4.36E+06		1.41E+07		2.96E+05		9.10E+05	
U-234	pCi/g	1.85E+03		4.11E+02		2.99E+03		1.86E+02		1.01E+03		2.06E+02		1.03E+02	
U-235	pCi/g	2.40E+02	UUJ	2.14E+01	UJ	5.31E+02	UU	1.65E+01	UUJ	4.72E+01	UU	6.71E+00		4.02E+00	
U-236	pCi/g	0.00E+01	UU	3.25E+01		3.20E+02	UU	2.21E+00	UU	1.27E+01	UU	2.70E+00		1.88E+00	UUJ
U-238	pCi/g	3.67E+03		3.12E+02		2.02E+04		2.33E+02		1.14E+02		3.38E+01		1.57E+02	

Table 16. Metals in the mechanistic samples. All samples were diluted, thus the “D” qualifier applies throughout.

Sample ID Units	Table mg/kg		Tray mg/kg		SRP34419 mg/kg		SRP34385 mg/kg		SRP34393 mg/kg		SRP34384 mg/kg		ARP82996 mg/kg	
	Result	Q	Result	Q	Result	Q	Result	Q	Result	Q	Result	Q	Result	Q
aluminum	14600		6840		22100		8130		6980		19000		38800	
antimony	21.4	J	20.9	U	44.1	J	24.1	U	24.3	J	19.9	U	23.8	U
arsenic	9.46	*	5.69	*	8.25	*	2.41	U*	2.22	U*	5.53	*	9.93	*
barium	266		75.8		85.5		54.6		70.4		195		496	
beryllium	31100		3390		302000		318		158		118		27700	
bismuth	33.2	U	33.5	U	36.3	U	38.6	U	35.5	U	31.8	U	38.0	U
boron	882	U	969	U	602	U	484	U	539	U	496	U	810	U
cadmium	100		13.0		19.1		41.7		148		46.3		22.7	
calcium	67300		132000		5620		34400		26400		59900		32500	
cerium	25.4		8.40		25.2		17.3		40.6		13.7		49.6	
cesium	20.9		3.62		19.9		6.74		30.2		3.12		4.06	
chromium	2000	*NJ	147	*NJ	2640	*NJ	79.3	*NJ	219	*NJ	71.5	*NJ	76.1	*NJ
cobalt	24.4		6.96		34.8		3.51		7.60		2.93		7.50	
copper	335		71.4		9890		36.7		89.0		32.6		79.8	
dysprosium	1.31	*	0.556	*	4.28	*	0.496	*	0.502	*	1.07	*	2.50	*
erbium	1.20	*	0.373	*	3.40	*	0.290	*	0.299	*	0.581	*	1.34	*
europium	0.228		0.136	J	0.186		0.125	J	0.118	J	0.276		0.705	
gadolinium	1.27		0.687		2.61		0.684		0.802		1.33		3.51	
gallium	41.0	J	66.3	J	6.71	J	12.8	J	33.4	J	13.0	J	11.0	J
germanium	0.119	JNJ	0.300	NJ	0.311	NJ	0.0966	UN UJ	0.0886	UN UJ	0.394	NJ	0.497	NJ
gold	0.829	UN UJ	0.837	UN UJ	0.907	UN UJ	0.966	UN UJ	0.886	UN UJ	0.795	UN UJ	0.951	UN UJ
hafnium	77.5	*J	1.55	*J	583	*J	1.18	*J	1.44	*J	0.991	*J	1.65	*J
holmium	0.314		0.118	J	0.747		0.0966	U	0.103	J	0.204		0.441	
indium	0.0829	U	0.0837	U	0.0907	U	0.0966	U	0.0886	U	0.0795	U	0.0951	U
iridium	0.0829	U	0.0837	U	0.0907	U	0.0966	U	0.0886	U	0.0795	U	0.0951	U

Table 16. (continued)

Sample ID Units	Table mg/kg		Tray mg/kg		SRP34419 mg/kg		SRP34385 mg/kg		SRP34393 mg/kg		SRP34384 mg/kg		ARP82996 mg/kg	
	Result	Q	Result	Q	Result	Q	Result	Q	Result	Q	Result	Q	Result	Q
iron	76400	*	68300	*	42500	*	27100	*	25800	*	34400	*	38400	*
lanthanum	12.4	U	12.6	U	13.6	U	14.5	U	13.3	U	11.9	U	21.2	U
lead	5270	J	944	J	73300	J	2190	J	5600	J	68.7	J	16.5	J
lithium	46.3		10.0	J	27.4		9.66	U	8.86	U	10.5	J	18.3	J
lutetium	0.336		0.0837	U	1.29		0.0966	U	0.0886	U	0.0803	J	0.188	J
magnesium	12100		12800		4150		6780		8890		8620		9340	
manganese	623		514		445		198		210		172		326	
molybdenum	34.3	*NJ	8.37	U*N	131	*N	9.66	U*N	8.86	U*N	21.9	*NJ	15.9	J*N J
neodymium	5.40	*	3.31	*	5.32	*	3.10	*	3.32	*	5.90	*	18.6	*
nickel	1120	*	84.4	*	1490	*	58.6	*	161	*	40.4	*	66.3	*
niobium	119	*NJ	19.2	*NJ	3040	J*N J	5.66	*NJ	1.68	J*NJ	4.92	*NJ	18.4	*NJ
palladium	20.7	UN	20.9	UN	22.7	UN	24.1	UN	22.2	UN	19.9	UN	23.8	UN
phosphorus	1600	J	5380	J	255	J	370	J	402	J	1070	J	877	J
platinum	1.46	*	0.0837	U*	4.12	*	0.0966	U*	0.0950	J*	0.0795	U*	0.0951	U*
potassium	30600		8620		2200		8000		21700		6770		11600	
praseodymium	1.44	J	0.866	J	1.35	J	0.820	J	0.918	J	1.55	J	5.00	J
rhenium	0.829	U	0.837	U	0.907	U	0.966	U	0.886	U	0.795	U	0.951	U
rhodium	0.0829	U	0.0837	U	0.482		0.0966	U	0.0886	U	0.0795	U	0.0951	U
rubidium	18.7		12.7		4.94		9.80		12.9		25.7		56.9	
ruthenium	0.829	UN UJ	0.837	UN UJ	0.907	UNJ	0.966	UNJ	0.886	UNJ	0.795	UNJ	0.951	UNJ
samarium	1.09		0.633		1.05		0.583		0.675		1.15		3.38	
scandium	2.38		0.973		5.18		1.18		1.07		2.60		5.45	
selenium	20.7	U	20.9	U	22.7	U	24.1	U	22.2	U	19.9	U	23.8	U
silicon	116000		87200		33700		93200		100000		132000		196000	
silver	19.1	NJ	8.37	UNJ	9.07	UN	9.66	UN	8.86	UN	128	NJ	9.51	UN

Table 16. (continued)

Sample ID Units	Table mg/kg		Tray mg/kg		SRP34419 mg/kg		SRP34385 mg/kg		SRP34393 mg/kg		SRP34384 mg/kg		ARP82996 mg/kg	
	Result	Q	Result	Q	Result	Q	Result	Q	Result	Q	Result	Q	Result	Q
sodium	61800	*J	28900	*J	3120	*J	11900	*J	31100	*J	8680	*J	10200	*J
strontium	252		607		41.3		35.2		68.4		135		189	
sulfur	3390		2150		1970		620		1470		4080		2050	
tantalum	2.48		3.69		35.3		4.48		0.659		9.68		1.79	
tellurium	0.166	UNUJ	0.167	UN UJ	0.481	NJ	0.193	UNJ	0.177	UNJ	0.159	UNJ	0.190	UNJ
terbium	0.194		0.0922	J	0.300		0.0966	U	0.0915	J	0.174		0.425	
thallium	0.330	J	0.0837	U	1.95	J	0.184	JJ	0.325	J	0.207	J	0.414	J
thorium	4.25		1.36		11.1		1.05		1.09		3.02		7.16	
thulium	0.207		0.0837	U	0.593		0.0966	U	0.0886	U	0.0887		0.196	
tin	41.3	NJ	17.9	JNJ	597	NJ	19.3	UN	17.9	JNJ	15.9	UN	19.0	UN
titanium	814	J	508	J	933	J	395	J	405	J	967	J	1950	J
tungsten	47.2	*J	13.5	*J	206	*J	5.13	*J	12.2	*J	2.87	*J	6.10	*J
uranium	12500		1120		67300		751		340		116		476	
vanadium	37.4		23.7		16.7		26.7		26.8		50.1		77.3	
ytterbium	1.38	*	0.364	*	4.29	*	0.288	*	0.307	*	0.535	*	1.24	*
yttrium	12.3		4.45		41.8		4.36		6.39		8.03		14.0	
zinc	686	J	310	J	449	J	255	J	642	J	90.2	J	107	J
zirconium	3660	*J	185	*J	25800	*J	44.8	*J	102	*J	34.9	*J	56.1	*J

Table 17. Volatile organic compounds in the mechanistic samples.

Sample ID	Table		Tray		SRP34419		SRP34385		SRP34393		SRP34384		ARP82996	
Concentration Unit:	µg/kg		µg/kg		µg/kg		µg/kg		µg/kg		µg/kg		µg/kg	
Compound	Result	Q	Result	Q	Result	Q	Result	Q	Result	Q	Result	Q	Result	Q
chloromethane	99	U	96	U	97	U	100	U UJ	160	U	93	U	95	U
vinyl chloride	99	U	96	U	97	U	100	U UJ	160	U	93	U	95	U
bromomethane	99	U	96	U	97	U	100	U UJ	160	U	93	U	95	U
chloroethane	99	U	96	U	97	U	100	U UJ	160	U	93	U	95	U
1,1-dichloroethene	99	U	96	U	97	U	220	J	69	J J	93	U	46	J J
acrolein	490	U	480	U	490	U	510	U UJ	810	U	460	U	480	U
methylene chloride	99	U	96	U	32	J J	100	J J	60	J J	93	U	95	U
<i>trans</i> -1,2-dichloroethene	99	U	96	U	97	U	160	J	160	U	93	U	95	U
1,1-dichloroethane	99	U	96	U	97	U	100	U UJ	160	U	93	U	95	U
acrylonitrile	99	U	96	U	97	U	100	U UJ	160	U	93	U	95	U
chloroform	54	J J	96	U	190		150000	D	43000	D	93	U	360	
carbon tetrachloride	42	J J	96	U	90	J J	1000000	D	430000	D	39	J J	1500	
1,1,1-trichloroethane	99	U	96	U	97	U	550	J	170		93	U	95	U
benzene	99	U	96	U	97	U	110	J	160	U	93	U	95	U
1,2-dichloroethane	99	U	96	U	97	U	100	U UJ	160	U	93	U	95	U
trichloroethene	3,500		32	J J	4200	D	1100000	D	540000	D	370		1200	
1,2-dichloropropane	99	U	96	U	97	U	640	J	100	J J	93	U	95	U
bromodichloromethane	99	U	96	U	97	U	36	J J	160	U	93	U	95	U
2-chloroethyl vinyl ether	200	U	190	U	200	U	200	U UJ	320	U	190	U	190	U
<i>cis</i> -1,3-dichloropropene	99	U	96	U	97	U	100	U UJ	160	U	93	U	95	U
toluene	310		110		190		2500	J	1400		330		56	J J
tetrachloroethene	830		96	U	2800		10000000	D	7700000	D	410		2200	D
1,1,2-trichloroethane	99	U	96	U	97	U	600	J	160	U	93	U	95	U
dibromochloromethane	99	U	96	U	97	U	100	U UJ	160	U	93	U	95	U
chlorobenzene	99	U	96	U	97	U	230	J	63	J J	93	U	95	U
ethylbenzene	99	U	96	U	97	U	35000	E J	7900		93	U	95	U
bromoform	99	U	96	U	97	U	100	U UJ	160	U	93	U	95	U
1,1,2,2-tetrachloroethane	99	U	96	U	97	U	1800	J	160	U	93	U	95	U

Table 18. Semi-volatile organic compounds in the mechanistic samples.

Sample ID	Table		Tray		SRP34419		SRP34385		SRP34393		SRP34384		ARP82996	
Concentration unit:	µg/kg		µg/kg		µg/kg		µg/kg		µg/kg		µg/kg		µg/kg	
Compound	Result	Q	Result	Q	Result	Q	Result	Q	Result	Q	Result	Q	Result	Q
bis(2-chloroethyl)ether	2,020	U	1,850	U	1,450	U	7,160		494	JJ	1,910		1,760	
phenol	3,590		517	JJ	46,400	D	2,190	JJ	654	JJ	1,910	U	989	JJ
benzyl alcohol	2,020	U	558	JJ	1,450	U	8,970		4,000		1,910	U	1,760	U
<i>o</i> -cresol	2,020	U	1,850	U	1,070	JJ	7,160	U	1,870	U	1,910	U	1,760	U
hexachloroethane	2,020	U	1,850		1,450	U	146,000		53,400	D	1,910	U	46,300	D
<i>m</i> -cresol & <i>p</i> -cresol	1,070	JJ	1,850	U	4,240		3,960	JJ	1,870	U	1,910	U	1,760	U
naphthalene	2,020	U	1,850	U	894	JJ	5,000	JJ	1,760	JJ	1,910	U	846	JJ
benzoic acid	2,020	U	1,850	U	1,450	U	7,160	U	1,870	U	1,910	U	1,760	U
hexachlorobutadiene	2,020	U	1,850	U	1,450	U	45,300		15,500		1,910	U	42,600	D
2-methylnaphthalene	2,020	U	1,850	U	1,450	U	9,160		2,880		539	JJ	2,720	
diethylphthalate	2,020	U	1,850	U	481	JJ	7,160	U	1,870	U	1,910	U	1,760	U
pentachlorophenol	1,150	JJ	968	JJ	1,450	U	7,160	U	1,840	JJ	1,910	U	1,230	JJ
phenanthrene	1,010	JJ	1,850	U	501	JJ	6,680	JJ	2,810		495	JJ	795	JJ
di- <i>n</i> -butylphthalate	1,220	JJ	1,850	U	1,020	JJ	14,500		4,430		1,910	U	681	JJ
fluoranthene	2,020	U	1,850	U	1,450	U	7,160	U	899	JJ	1,910	U	1,760	U
Pyrene	2,020	U	1,850	U	1,450	U	7,160	U	1,470	JJ	1,910	U	1,760	U
Butylbenzylphthalate	4,150		1,850	U	1,370	JJ	125,000	D	29,100		1,910	U	1,760	U
bis(2-ethylhexyl)phthalate	28,100		2,760		81,800	D	358,000	D	114,000	D	2,040		11,800	
di- <i>n</i> -octylphthalate	2,950		1,850	U	25,900	D	7,160	U	1,870	U	1,910	U	1,760	U
2,3,4,6-tetrachlorophenol	848	JJ	1,850	U	1,450	U	4,940	JJ	1,830	JJ	1,910	U	1,720	JJ
acetophenone	1,850	JJ	1,850	U	3,910		7,160	U	1,870	U	1,910	U	1,760	U

3.2.7.4 Summa Canisters. Head-space gas samples were gathered from the drums within the Mechanistic Sample population. These samples were gathered using summa canisters (evacuated and delivered by SwRI) The HSG was analyzed for volatile organic compounds (VOC), methane, hydrogen, carbon monoxide, carbon dioxide, oxygen, and nitrogen. The results of these analyses are presented in Table 19. Results for methane, hydrogen, carbon monoxide, and carbon dioxide are presented in Table 20.

Table 19. Head-space gas composition from the mechanistic sample drums.

	Sample ID	SRP 34393		SRP 34419		SRP 34385		SRP 34384		SRP 34399		ARP 82996	
CAS	Compound	Result	Q	Result	Q	Result	Q	Result	Q	Result	Q	Result	Q
TO-15 COMPOUNDS PPB (V/V)													
71-55-6	1,1,1-trichloroethane	1500	U	140	U	3500	U	83		1400	U	7	
76-13-1	1,1,2-trichlorotrifluoroethane	1600		140	U	3500	U	200		1400		6.8	U
75-35-4	1,1-dichloroethene	1700		1200		3500	U	68	U	1700		310	
67-64-1	acetone	8600		140	U	25000		210		13000		6.8	U
71-43-2	benzene	1500	U	140	U	3500	U	68	U	4500		6.8	U
75-15-0	carbon disulfide	3800		390		3500	U	68	U	3500		6.8	U
56-23-5	carbon tetrachloride	950000	D	2300		2900000	D	23000	D	900000	D	71	
75-00-3	chloroethane	1500	U	140	U	3500	U	68	U	1400	U	11	
67-66-3	chloroform	250000	D	2100		820000	D	490		260000	D	290	
74-87-3	chloromethane	1500	U	140	U	3500	U	68	U	1400	U	17	
156-59-2	<i>cis</i> -1,2-Dichloroethene	1500	J J	140	U	5700		110		1400	U	6.8	U
64-17-5	ethanol	5500		830		3500	U	68	U	8600		35	
100-41-4	ethylbenzene	1500	U	140	U	3500	U	120		1400	U	6.8	U
142-82-5	hepatene	1500	U	140	U	3500	U	390		1400	U	6.8	U
87-68-3	hexachlorobutadiene	1500	U	140	U	3500	U	68	U	1400	U	34	
179601-23-1	<i>m/p</i> -xylene	1500	U	140	U	6500	J J	190		2800	U	14	U
80-62-6	methyl methacrylate	25000		2600		6900		68	U	23000		6.8	U
75-09-2	methylene chloride	4400		140	U	12000		68	U	3800		6.8	U
91-20-3	naphthalene	7400		140	U	3500	U	68	U	1400	U	6.8	U
95-47-6	<i>o</i> -xylene	1500	U	140	U	3500	U	160		1400	U	6.8	U

Table 19. (continued)

	Sample ID	SRP 34393		SRP 34419		SRP 34385		SRP 34384		SRP 34399		ARP 82996	
CAS	Compound	Result	Q	Result	Q	Result	Q	Result	Q	Result	Q	Result	Q
TO-15 COMPOUNDS PPB (V/V)													
127-18-4	tetrachloroethene	810000	D	15000	D J	2800000	D J	58000	D	570000	D	300	
108-88-3	tolulene	1500	U	2400		3500	U	1100		1600		24	
79-01-6	trichloroethene	370000	D	64000	D	1200000	D	400000	D	320000	D	120	
FIXED GASES, PPMV (OR %)													
74-82-8	methane	144	U	13700	D	139	U	134	U	160	U	1170	
1333-74-0	hydrogen	288	U	268	U	278	U	268	U	320	U	312	U
124-38-9	carbon dioxide	294		526		570		514		426		744	
630-08-0	carbon monoxide	144	U	134	U	139	U	134	U	160	U	156	U
7782-44-7	oxygen %	18.8%		16.1%		18.0%		16.4%		18.7%		20.6%	
7727-37-9	nitrogen %	73.2%		64.0%		74.0%		76.0%		70.8%		76.0%	
7440-37-1	argon %	0.99%		1.10%		1.10%		1.10%		1.60%		1.30%	
WATER AND CORROSIVE GASES, PPMV													
7647-01-0	hydrochloric acid	15.2		12.3	U	13.1	U	12.5	U	14.4	U	14.6	U
7782-50-5	chlorine	10.5		6.14	U	6.56	U	6.25	U	6.94		7.29	U
7732-18-5	water	15200	J J	2460	J J	13900	J J	20500	J J	14000	J J	6950	J J

3.2.7.5 Mechanistic Sample Compositional Correlations. The drums processed on April 10 and 11 were selected for additional solid sampling based on methane screening results as described in Section 2.2.6. Drums containing high and low methane concentration were selected. Analytical data from the selected drums is presented in Table 20 along with methane concentrations, uranium and beryllium concentrations, and volatile organic data.

Table 20. Analytical data from the target drums.

Category	Process Drum Number	Methane Screening (ppmv)	Solid Sample	Summa Sample	
			Mg/kg	Gas (ppmv)	VOC (ppb) (v/v)
Historic High Methane	ARP82996	23398	U = 476 Be = 27,700	CH ₄ = 1170 H ₂ = <MDL CO ₂ = 744 CO = <MDL O ₂ = 20.6% N ₂ = 76.0%	chloroform = 290 carbon tetrachloride = 71 trichloroethene = 120 methyl methacrylate = <MDL tetrachloroethene = 300
ARP V Daughter Drums Processed 4-10-18	SRP34419	33341	U = 67,300 Be = 302,000	CH ₄ = 13,700 H ₂ = <MDL CO ₂ = 526 CO = <MDL O ₂ = 16.1% N ₂ = 64.0%	chloroform = 2100 carbon tetrachloride = 2300 trichloroethene = 64,000 methyl methacrylate = 2600 tetrachloroethene = 15,000
	SRP34385	<MDL	U = 751 Be = 318	CH ₄ = <MDL H ₂ = <MDL CO ₂ = 570 CO ₂ DUP = 485 CO = <MDL O ₂ = 18.0% N ₂ = 74.0%	chloroform = 820,000 carbon tetrachloride = 2,900,000 trichloroethene = 1,200,000 methyl methacrylate = 6900 tetrachloroethene = 2,800,000
	SRP34399	Not Sampled	Not Sampled	CH ₄ = <MDL H ₂ = <MDL CO ₂ = 426 CO ₂ DUP = 466 CO = <MDL O ₂ = 18.7% N ₂ = 70.8%	chloroform = 260,000 carbon tetrachloride = 900,000 trichloroethene = 320,000 methyl methacrylate = 23,000 tetrachloroethene = 570,000
	SRP34393	Not Sampled	U = 340 Be = 158	CH ₄ = <MDL H ₂ = <MDL CO ₂ = 294 CO = <MDL O ₂ = 18.8% N ₂ = 73.2%	chloroform = 250,000 carbon tetrachloride = 950,000 trichloroethene = 370,000 methyl methacrylate = 25,000 tetrachloroethene = 810,000
ARP V Daughter Drums Processed 4-11-18	SRP34384	<MDL	U = 116 Be = 118	CH ₄ = <MDL H ₂ = <MDL CO ₂ = 514 CO = <MDL O ₂ = 16.4% N ₂ = 76.0%	chloroform = 490 carbon tetrachloride = 23,000 trichloroethene = 400,000 methyl methacrylate = <MDL tetrachloroethene = 58,000

High beryllium concentration in the solid material is associated with high methane in the head-space.

3.3 Additional Lines of Inquiry

3.3.1 Hydrogen and Methane

A simple experiment to evaluate for gaseous oxidation products such as carbon dioxide (CO₂), nitrous oxide (N₂O), and hydrogen (H₂) was performed to determine if there were ongoing chemical oxidation reactions occurring. Methane (CH₄) was also included as an analyte. A little over 1 gram of sample was placed into two 40 mL glass VOA vials and purged with argon (or other desired gas). One vial was equilibrated at room temperature and the other was equilibrated at 50°C until the desired sampling time was reached. A minimum of two days was allowed for equilibration. After 48-72 hours, a portion of the headspace gas was then pulled and analyzed for CH₄, H₂, and CO₂. The analysis of CH₄ was performed by using a flame ionization detector (FID) equipped with a Haysep D stainless steel column. The analysis of H₂ and CO₂ were performed by using a pulsed discharge helium ionization detector (PDHID) equipped with a 60/80 Carboxen-1000 stainless steel column. The results of the tests on the ejected material and the drum samples are presented in tables 21 and 22, respectively.

Table 21. Composition of gas released from ejected material at 22°C and 50°C.

Conditions	Ejected Material					
	48 hours at 22°C			48 hours at 50°C		
Sample ID	2013A	5013A	5013A DUP	2013A	5013A	5013A DUP
Units	ppmv	ppmv	ppmv	ppmv	ppmv	ppmv
Analyte	Result	Result	Result	Result	Result	Result
methane	3,119	3,590	3,917	46,071	46,540	54,999
hydrogen	<MDL	<MDL	<MDL	<MDL	<MDL	<MDL
carbon dioxide	<MDL	<MDL	<MDL	<MDL	<MDL	<MDL

Table 22. Composition of gas released from drum samples at 22°C and 50°C.

Conditions	Drum Samples									
	72 hours at 22°C					48 hours at 50°C				
Sample ID	10013A	10013A DUP	11013A	13013A	14013A	10013A	10013A DUP	11013A	13013A	14013A
Units	ppmv	ppmv	ppmv	ppmv	ppmv	ppmv	ppmv	ppmv	ppmv	ppmv
Analyte	Result	Result	Result	Result	Result	Result	Result	Result	Result	Result
methane	195	270	1,580	432	540	2,798	3,883	18,071	2,982	6,859
hydrogen	<MDL	107	278	<MDL	<MDL	<MDL	<MDL	<MDL	<MDL	<MDL
carbon dioxide	<MDL	<MDL	<MDL	<MDL	<MDL	<MDL	<MDL	<MDL	<MDL	<MDL

3.3.2 Humidity Stability

Tests were conducted to determine the hygroscopic tendency of the event material. Humidity levels were controlled using saturated salt solutions in an enclosed chamber, specifically, saturated MgCl₂·6H₂O = 33%, saturated NaBr·2H₂O = 58%, and saturated BaCl₂·2H₂O = 90%. The samples were introduced into the chamber and percent weight gained was measured. The results of these tests are presented in Table 23.

Table 23. Moisture stability test results.

	2013A (Ejected)	6013A (Ejected)	10013A (Drum)	14013A (Drum)	Control (Blank Vial)
Humidity Level (%)	% Wt Gain	% Wt Gain	% Wt Gain	% Wt Gain	% Wt Gain
33%	0.210%	0.115%	-0.259%	0.033%	0.172%
58%	0.469%	0.413%	0.139%	0.305%	0.064%
90%	0.885%	0.806%	0.715%	0.664%	0.080%

3.3.3 Bulk Density

The bulk density was determined for each of the event material was measured using ASTM method 5057. The results of these tests are presented in Table 24.

3.3.4 pH

All test samples were initially dry, with no free liquids, so a direct pH measurement could not be acquired. The pH of the event materials was measured using EPA SW-846 Method 9045. The results of these tests are presented in Table 25. The materials, when mixed with water, were basic.

Table 24. Bulk Density of the event materials.

	Ejected Material								Drum Contents			
Sample ID	1013A	1023A	2013A	3013A	4013A	5013A	6013A	7013A	10013A	11013A	13013A	14013A
Bulk Density (g/mL)	0.884	0.905	0.868	0.882	0.866	0.945	0.951	1.03	0.787	0.89	1.03	0.868

Table 25. pH of the event materials.

	Ejected Material								Drum Contents			
Sample ID	1013A	1023A	2013A	3013A	4013A	5013A	6013A	7013A	10013A	11013A	13013A	14013A
pH	10.73	10.67	10.52	10.66	10.76	10.59	10.75	10.66	11.2	9.14	11.36	11.07

3.4 Laboratory and Analytical Data Comparison

The analyte concentrations were determined following approved laboratory protocols at SwRI and substantiated by SRNL. This approach allowed comparison of analyte concentration data between the two laboratories and between different techniques. The results from the laboratories were comparable. Additionally, the results from multiple techniques, e.g. total metals and Inductively Coupled Plasma – Mass Spectrometry (ICP-MS), were comparable.

4. EVENT INVESTIGATION AND INTERPRETATION

4.1 Objective and Summary

The objective of Section 4 is to identify the most likely cause of the lid ejections. A summary of Section 4 is as follows:

- Perform a chemical compatibility evaluation (binary chemical evaluation) and determine the most likely cause or causes of the event.
 - DU was identified as the most likely cause (Section 4.2 and Appendix A)
- Evaluate the empirical evidence supporting DU
 - All of the empirical evidence supports DU as the initiator (Section 4.3 and 4.4).
- Thermodynamically evaluate the measured amount of DU and the heat generated.
 - Modeling supports the generation of localized heat between 300 to 700°C (see Section 4.4.1).

4.2 Chemical Compatibility

Chemical compatibility was performed by evaluating the analytical data from the chemical and radiological analysis of the drums involved in ejecting their lids and applying the EPA document “A Method for Determining the Compatibility of Hazardous Wastes,” EPA-600/2-80-076⁶ protocol. Constituents were assigned reactivity group numbers (RGN) and when the EPA method did not provide an RGN for the waste component the judgement of a chemist was used. This chemical compatibility evaluation is specific to the drums involved in the ARP V incident. The compatibility evaluation was intended to refine the identification of the most likely reactive constituents. The detailed chemical compatibility evaluation is given in Appendix A. A summary is provided in Section 4.2.1.

4.2.1 Chemical Compatibility Summary

The first conclusion is that water reactive substances were not a concern in the waste because the visual examination of the waste before packaging indicated no free liquids or breached containerized liquids. The identified parent containers were reported as containing light, fluffy, flowing material, not clumpy or damp sludge. The absence of liquid precludes aqueous fluid from being a source of an incompatible reaction.

The exception to this conclusion is uranium when it exists in the waste in the metallic form. When metallic uranium is exposed to the ambient atmosphere, its surface will immediately oxidize to form a thin layer of UO_2 that is protective against further oxidation. However, over the course of time when sealed in bagging, for example, uranium will continue to slowly oxidize, forming hypervalent oxide UO_{2+x} depleting O_2 and H_2O in the process. Hypervalent UO_{2+x} is a form of uranium that is significantly more susceptible to H_2O oxidation when subsequently exposed to the ambient atmosphere with a relative humidity $> 2\%$ (See Section 4.3 of this report). Prior studies have indicated that the reaction of H_2O with oxygen anions at the surface of the UO_{2+x} lattice will form OH^- which is capable of diffusing through the oxide layer to the underlying uranium metal, where it exothermically reacts to form UO_2 and H_2 , the latter subsequently reacting with additional metal to form UH_3 . If the heat generated by these reactions cannot be dissipated, the temperature will increase, which will further speed the diffusion of OH^- (and also the more slowly diffusing O_2^-) through the oxide layer to the metal surface, and increase the rate of the oxidation reaction, releasing more heat, and further increasing the temperature.

The pyrophoric nature of uranium hydride is well documented. If present, it would have reacted during repackaging.

After evaluating the data, multiple incompatible chemical reaction possibilities can be discounted. Even though the results were post incident, many compounds may remain and can be detected. The evidence indicates most volatile and semi-volatile compounds were not present or at concentrations that could have participated in an incompatible reaction. The exception is methane. Heating the residue from the WMF-1617 (ARP V) drum incident liberated large quantities of methane (See Section 5). Methane could cause pressurization, fire, and an explosion – although this did not occur (See Section 6). Along with the methane, carbon dioxide was also liberated. Carbon dioxide may not pose the same potential chemical risks as methane, but it could contribute to a pressurization event.

Alkali and alkaline earth metals (RGN 21) are not a concern in the waste because they would have been oxidized during the course of their intended reactions or were never present as an unreacted (zero-valent) metal. For example, potassium metal was not used in Rocky Flats processes, but was present as potassium hydroxide.

Most metals listed in the analysis could not have participated in an incompatible reaction. Either the metals were previously reacted, would not have survived storage, or were not in the proper configuration (fine powder).

From the analysis results, the reducing agents (RGN 105) are represented by sodium and phosphorus. Sodium metal was not used as a reagent because of the difficulty of storage and use. Also, the storage requirements for sodium metal would prevent it from persisting in the waste. The source of sodium in the waste is from other reagents that contain the sodium counter ion. In this instance, the situation with phosphorus is very similar. Elemental phosphorus was not used in the processes that generated the waste. The phosphorus contribution to the waste is due to reagents that contained the phosphorus. Sodium and phosphorus will not be available for further chemical reactions in the waste form.

Most metals that are pyrophoric only exhibit pyrophoricity as fine powder or fines (RGNs 22 and 101). The fines need to be stored under an inert atmosphere to prevent spontaneous ignition. Since storage conditions were not under an inert atmosphere, pyrophoric fines would not have persisted.

The metals that could have participated in oxidation reactions generating heat are plutonium and uranium. Plutonium is not considered because it was recovered up to the economic discard limit. This prevents the plutonium from being in the waste in an amount that is reactive. Uranium, especially DU did end up as a waste product. Uranium metal does not have to be in the form of fines to ignite, and the larger particle sizes (coarse fines) can survive in the waste, particularly in anoxic conditions, for long periods of time. Re-introduction of oxidants, i.e. oxygen (O₂) and H₂O, can re-start the uranium oxidation reactions, which are exothermic and hence can drive other secondary reactions.

4.2.2 Empirical Evidence Supporting Uranium as an Energy Source for the Drum Rupture

The identification of DU as the reactive component is well supported by consideration of the historical origin of the parent drum, observations, and analyses of samples from the event site:

- Generator descriptions of Building 444 (Section 8.2), supports the oxidation state of the DU i.e. un-oxidized
- DU was identified in each drum with an ejected lid
- Sparking of the waste material during clean-up is consistent with the behavior of DU and has been observed multiple times at AMWTP
- The chemical behavior of DU (i.e. tendency to undergo exothermic oxidation and lack of visual indicators) is consistent with the conditions encountered during packaging

- Thermogravimetric analysis (TGA) results indicating that the involved metals were not completely oxidized
- The sparking phenomenon is consistent with the presence of un-oxidized, zero-valent uranium metal. At Rocky Flats, DU waste was roasted to convert uranium metal to oxide, to prevent exothermic oxidation from occurring within the waste drums. However, it is well known that the roasting process periodically generated incompletely oxidized uranium, which can survive in that form for long periods of time
- Oxidation of uranium is exothermic
- The characteristics of uranium oxidation are consistent, with the latency period observed between the initial exposure of the parent drum waste to atmosphere and the rupture of the daughter drum. While uranium-IV oxide (UO₂) can provide a passivating layer for underlying uranium metal, continued oxidation results in a spalling black oxide coat which would permit diffusion of oxygen and H₂O from the headspace atmosphere to the underlying uranium metal. Once in contact with O₂ and H₂O, uranium metal will resume oxidation, with concomitant generation of heat. Rates of reaction would be expected to be slow at first; however, rates of diffusion and oxidation will increase with increasing temperature, accounting for the initiation time between opening the parent and the rupture event.

4.3 Depleted Uranium as the Event Initiator

As noted above, the properties of metallic uranium, specifically the tendency to undergo exothermic oxidation, are consistent with the generation of heat in the event drums. These properties have been the subject of a significant number of scientific studies over the course of the past 70 years, many of which are available in the open scientific literature. A review of these studies, detailed in the following section, has shown reactivity of zero-valent uranium (U⁰) with O₂ and H₂O, and further that the evolution of the oxide layer can lead to a destabilization of the U⁰/U oxide system, resulting in faster oxidation rates at lower temperatures.

As discussed in the chemical compatibility evaluation uranium was identified as the most likely event initiator consistent with the events in ARP V. This conclusion draws support from the following considerations:

1. DU has the ability to undergo slowly-accelerating, exothermic oxidation once exposed to oxidizing gases in the atmosphere
2. The particle size of the uranium material may be responsible for faster-than-expected oxidation rates
3. The heat generated by the uranium oxidation is capable of initiating and accelerating secondary reactions which can produce gaseous products.

These considerations that support the role played by uranium as the event initiator are discussed in the subsequent sections and discussed in detail in Appendix B.

4.3.1 Un-oxidized Uranium

The parent drums to the event drums were originally disposed of in Pits 11 and 12 in 1970. Therefore, the waste was approximately 48 years old. Age of the waste does not ensure that the material has been oxidized. The fact that DU can remain in drum for 40 + years has been demonstrated by multiple contractors who retrieved pit disposed waste in Idaho and encountered un-oxidized uranium that reacts visibly generating flame and sparks when a drum/bag is breached. For the event drums, the DU oxidation was not visible when the waste was repackaged but the repackaging process did begin an oxidation reaction. Un-oxidized uranium was packaged and shipped to Idaho for disposal. The waste may have had a protective

coating, e.g. cutting oils, or was sealed in bagging to prevent the intrusion of air. Once bagged, oxidation is limited to the oxygen or water vapor available within the waste bag. Eventually, all the O₂ and H₂O in the waste bags were consumed, at which point the oxidation stopped. This occurred before all of the U⁰ was oxidized. When the 1970-packages were opened, the U⁰, incompletely passivated by uranium oxide, was exposed to O₂ and H₂O, which re-initiated the oxidation process

4.3.2 Slowly Accelerating, Exothermic Oxidation

The hypotheses that the initiation of the drum rupture event was caused by heat from a slowly accelerating uranium oxidation motivated a review of available literature, to determine whether such an explanation might have precedent. There are numerous reports in the literature that describe uranium oxidation, including ignition events, that are strongly exothermic and have sharp temperature dependencies, characteristics that are consistent with the drum rupture event. This section provides an overview of the behavior of uranium oxidation with a detailed synopsis of the literature provided in Appendix B.

4.3.3 Uranium Oxidation by O₂ Can Be Accelerating

Even under isothermal conditions, U oxidation rates have been observed to increase with time.⁷⁻¹⁰ The acceleration is thought to be due to the modification to the oxide layer which occurs as the reaction progresses. The initial oxidation reaction will form UO₂, which can effectively passivate the underlying U metal. However, UO₂ will continue to react to the more thermodynamically favored UO₃, and as this reaction continues, a more disordered UO_{2+x} layer is formed which is more permeable to O₂⁻ and OH⁻ (from O₂ and H₂O, respectively).²⁷ The UO_{2+x} layer is also less mechanically stable, and will undergo cracking and spalling, which result in exposure of uranium metal to the head-space atmosphere.

4.3.4 Uranium Oxidation Rates by O₂ Sharply Increase with Increasing Temperature

Isothermal experiments conducted at different temperatures also showed that reaction rate profiles sharply increased with increasing temperature,^{9,11} up to a point: at high temperatures, reaction rates can slow, which is thought to be due to rapid formation of a thick oxide layer that slows diffusion to the metal.¹² Other models indicate increasing oxidation rates from 270 K to 670 K, although the rate of increase does slow as temperature increases.^{9,13} For example, in a humid atmosphere, the oxidation rate increases by a factor of about 20,000 as the temperature increases from ~ 27°C to ~ 127°C.^{9,13}

4.3.5 Humid Air Oxidation is Faster than O₂ Oxidation

Multiple studies indicate that oxidation is significantly faster by H₂O than by O₂. Comparing rates at 127°C, oxidation in humid air is ~ 500 times faster compared to pure O₂.^{9,13} Other comparisons quoted H₂O oxidation rates to be faster than O₂ by a factor of 5,000¹⁴. Thus, the presence of humidity in the headspace atmosphere will exert a disproportionate effect in speeding up the oxidation reaction and rate of heat generation. It is worthwhile noting that the presence of O₂ in a H₂O vapor atmosphere has the opposite effect, O₂ actually slowed the rate of oxidation; the observation led to the suggestion that hazards of run-away uranium oxidation can be mitigated by allowing uranium to oxidize in dry air rather than ambient air. This observation is in accord with those previously made by Solbrig and coworkers.³⁰

4.3.6 The Size of Uranium Material in the Waste Can Affect Oxidation Rates and Ignition Temperatures

The surface area of the uranium materials present in the waste likely exerts a large effect on the rate of oxidation and on the ignition temperature. Multiple reports have stated that uranium present as small particles or sheets with high surface areas have low ignition temperatures, ranging from 240 - 450°C.^{5,7,10,11} These temperatures are much lower than the ignition temperature of cubes of U, which are in the 650 - 700°C range.¹⁰ This is potentially significant because it has been noted that small uranium particles that ignite at abnormally low temperatures can in turn cause ignition of larger objects, which by themselves would not ignite. The situation for particulate uranium is even worse: particles in the ~ 900 μm size range ignited between 320 and 400°C, while drums with 100 μm particles may ignite at ambient

temperatures.¹² If the particles are at all insulated, then phenomenological ignition temperatures may be lowered further. This could be the case if the uranium particles were existing at some depth in a non-heat-conducting matrix,^{1,11} like uranium oxide, or diatomaceous earth (Micro-Cel E, which is the waste form matrix).

While the majority of object- and particle-size studies have examined the effect on ignition, surface area must necessarily affect oxidation rates in the same fashion, i.e., higher surface areas will correlate with faster oxidation rates, raising temperatures which further increases subsequent oxidation rates, and may cause ignition temperatures to be exceeded. Waste particle size was measured for the drums reported in this report (See Appendix E). For the ejected samples, ~ 70% of the material was < 707 μm , maximizing with about 25% of the mass in the 250 – 354 μm size category. Particles in the < 250 μm size category accounted for about 15% of the material. The drum samples tend to be larger, with only ~ 60% of the material < 707 μm , and about 75% of the material in the drum samples was > 500 μm . The smaller particle size categories are ~ 10% or less – significantly smaller fractions compared to the ejected samples for these size categories. Particles in the < 250 μm size category accounted for only ~ 5% of the mass of the drum samples. While specific sizes of the uranium-containing particles are not determined by the particle size distribution measurements, it is possible that a fraction of the uranium does exist in the form of smaller particles, which would exhibit faster oxidation rates, and perhaps lower ignition temperatures.

4.4 Heat Build-Up and Thermodynamic Modeling of Uranium Oxidation Reactions

The oxidation of uranium by O_2 , and H_2O is exothermic. If heat generated cannot be dissipated, then temperature will increase, resulting in a much faster rate of oxidation, as shown above. The fact that the oxide layer is insulating will slow heat dissipation, and so as the oxide layer thickens, the rate of heat dissipation decreases, and the temperature will increase. Sites of heating have also been correlated to metal irregularities that can become sites of accelerated oxidation or ignition if the rate of liberation of heat due to metal oxidation is greater than the rate of heat loss.⁷

To determine the equilibrium concentrations of the DU as well as the empirical concentrations of key active components HSC (enthalpy [H], entropy [S] and heat capacity [C] data) Chemistry database was utilized. HSC Chemistry contains an extensive thermochemical database, more than 25,000 chemical compounds, yielding a powerful calculation method for studying the effects of different variables on the chemical system at equilibrium. The major advantage of using HSC Chemistry to perform the reaction balance calculation is that the software includes a database of thermochemical properties (ΔH_f , ΔS_f , C_p , molecular weight, density, etc.) as a function of temperature. Hence the calculation of enthalpies, equilibrium amounts, and heats of reaction at the specified temperatures is greatly simplified. HSC Chemistry also keeps track of the component and elemental balances to ensure that the mass balance is achieved. HSC does not take into account the kinetics (rates) of chemical reactions. However, it is a very useful tool in obtaining the reaction conditions and yields for comparison to experimental/empirical observations.

HSC calculation results for 600 g of DU (the lowest DU mass observed in event drums) as a function of base matrix mass (Micro-Cel E [CaSiO_3]) reacted with air, sodium nitrate and some water are shown in Table 26. The products are primarily UO_3 , with a small quantity of uranyl hydroxide, indicating that the thermodynamically favored products are uranium in the +6-oxidation state (Table 26). The oxidants are O_2 , H_2O , which are completely consumed, and nitrate, which was partially consumed. The complete oxidation of uranium to U+6 species is not what occurs in the event drum, because the model cannot take into account passivating effects of the initially formed UO_2 . However, the model does indicate that uranium present as U^0 , UO_2 , and UO_{2+x} retains its thermodynamic potential to undergo further reduction. The calculation also predicts that complete oxidation would result in a temperature of 453°C under adiabatic conditions (no heat losses to the surroundings).

Table 26. Input and output of thermodynamic modeling conducted using the HSC Chemistry code.

INPUT SPECIES (1) Formula	Temperature, C	Amount kmol	Amount kg			
N ₂ (g)	25.000	0.004	0.109			
O ₂ (g)	25.000	0.001	0.033			
H ₂ O(g)	25.000	5.51E-05	0.001			
NO ₃ (g)	25.000	0.000	0.000			
NO ₂ (g)	25.000	0.000	0.000			
NaNO ₃	25.000	0.008	0.680			
Na ₂ O	25.000	0.000	0.000			
U	25.000	0.003	0.600			
UO ₃	25.000	0.000	0.000			
U ₃ O ₈	25.000	0.000	0.000			
UO ₃ •H ₂ O	25.000	0.000	0.000			
UO ₃ •0.9H ₂ O	25.000	0.000	0.000			
UO ₂ (OH) ₂	25.000	0.000	0.000			
CaSiO ₃	25.000	0.041	4.801			
OUTPUT SPECIES (1) Formula	Temperature, C	Amount kmol	Amount kg			
N ₂ (g)	25.000	0.005	0.138			
O ₂ (g)	25.000	2.65E-29	0.000			
H ₂ O(g)	25.000	4.51E-10	0.000			
NO ₃ (g)	25.000	5.10E-32	0.000			
NO ₂ (g)	25.000	1.49E-38	0.000			
NaNO ₃	25.000	0.006	0.501			
Na ₂ O	25.000	0.001	0.065			
U	25.000	7.19E-174	0.000			
UO ₃	25.000	0.002	0.495			
U ₃ O ₈	25.000	0.000	0.206			
UO ₃ •H ₂ O	25.000	2.58E-05	0.008			
UO ₃ •0.9H ₂ O	25.000	2.36E-05	0.007			
UO ₂ (OH) ₂	25.000	8.08E-06	0.002			
CaSiO ₃	25.000	0.041	4.801			
Balance:		Kmol	Kg			
		-1.58E-03	0			
Material Balance Element	Input kmol	Output kmol	Balance kmol	Input kg	Output kg	Balance kg
Ca	0.041	0.041	0.000	1.656	1.656	0.000
H	0.000	0.000	0.000	0.000	0.000	0.000
N	0.016	0.016	0.000	0.221	0.221	0.000
Na	0.008	0.008	0.000	0.184	0.184	0.000
O	0.150	0.150	0.000	2.401	2.401	0.000
Si	0.041	0.041	0.000	1.161	1.161	0.000
U	0.003	0.003	0.000	0.600	0.600	0.000
Temperature of Products + 453.395 degrees C				When Heat Balance = 0		

4.4.1 Waste Temperature as a Function of Mass.

As can be seen in Figure 22, the adiabatic temperature ranges from 700°C to 288°C, depending on the mass of the CaSiO_3 present together with the 600 g of uranium. This temperature range is consistent with the first responder drum surface temperatures observed. In addition, as discussed in Sections 5 and 6 of this report the modeled temperature exceeds that temperature required to result in lid ejection.

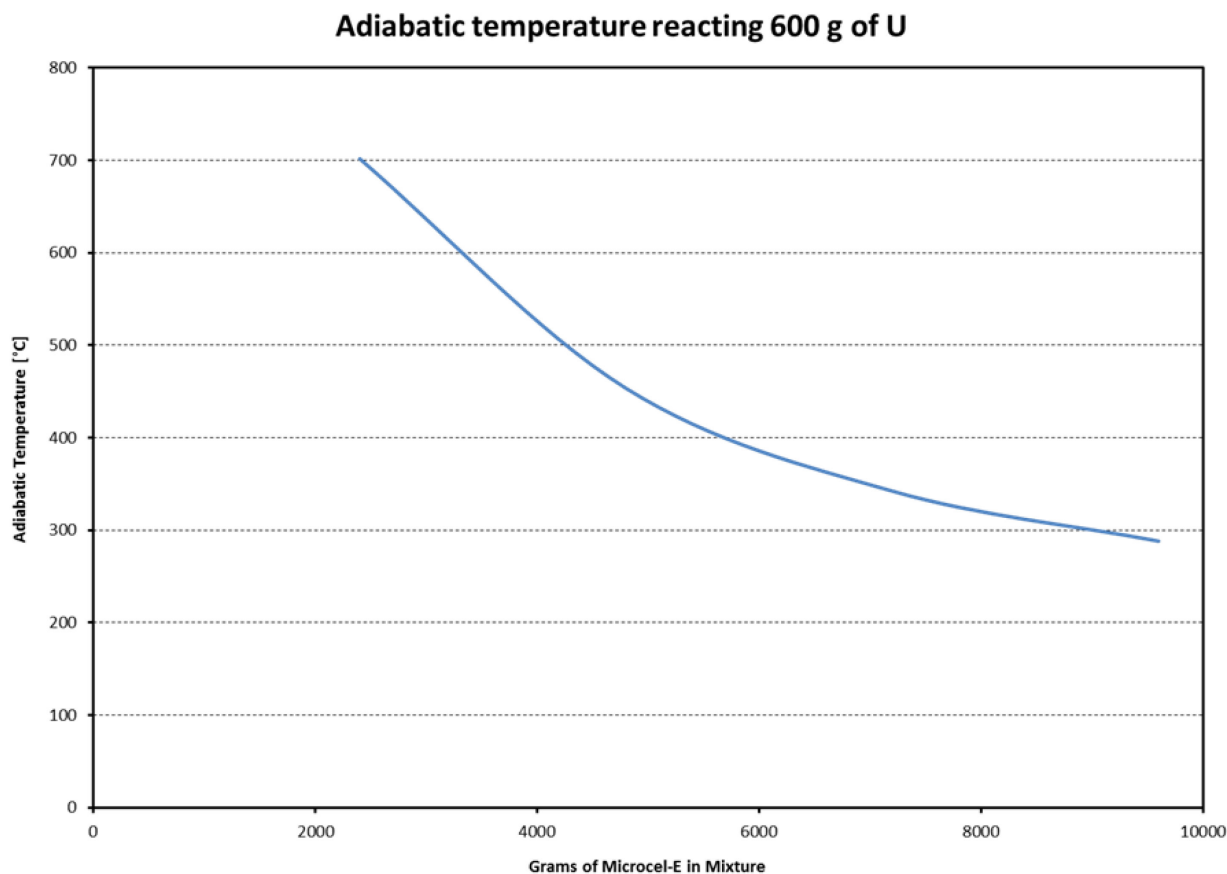


Figure 22. Temperature of Drum Waste as a Function of Waste Mass.

4.4.2 Localized Heating

During waste processing operations the waste matrix was spread out and sufficiently oxygenated on the tray to initiate the reaction, but no heat accumulated sufficient to be measured. Once the waste was transferred to the daughter drums the low thermal conductivity of the matrix provided insulation which retained heat, thereby increasing reaction rates. Reiterating, both diffusion of oxygen through the uranium oxide layer, and uranium oxidation reaction rates increase with increasing temperature, which would result in an initially slow exothermic reaction that progressively becomes faster, thus accounting for the induction time between opening the parent and the rupture event.

However, the uranium was not uniformly distributed within the daughter drums. Once the drum ruptured, a fraction of the uranium-bearing waste was ejected, while the remainder was retained within the drum. First responder personnel mixed the remainder within the drum, which increased availability of oxygen and accelerated the oxidation reaction in the main event drum. It is certain that the event drum achieved much higher temperatures subsequent to this action, as evidenced by significant charring after oxygenation by stirring, blackening the exterior paint, and consuming the high-density polyethylene liner and PVC bag.

5. SECONDARY REACTIONS DUE TO HEAT GENERATION

A key aspect of the drum rupture involves secondary reactions that produce gaseous products which increase the pressure in the head-space inside the drum. These reactions fall into two categories:

1. Simple volatilization of organics and H₂O present in the drum
2. Chemical reactions that generate gaseous products, principally CH₄.

Both volatilization and chemical reactions are driven by the heat generated by the uranium oxidation that was initiated when the parent drum contents were exposed to the atmosphere.

5.1 Volatilization of Organics and Water

The notion that the heat generated by the reaction in the drum volatilized organics and H₂O was supported by a comparison of analytical measurements of waste samples that were ejected, with those that remained in the drum (Table 27). The samples that remained in the drum were exposed to higher temperatures, and contained much lower concentrations of organic compounds, including PCBs, which is a result of losses by volatilization. The fact that the PCBs were lower in concentration in the drum samples was surprising because they have high boiling points, and volatilization would require high temperatures. The organic concentrations in the samples that were ejected from the drum were much higher, consistent with the idea that these samples were not exposed to high temperatures. While some of the results could be explained by heterogeneity of the constituents in the original waste container, overall the results are consistent with volatilization of constituents due to heating, with the most volatilization occurring for materials that remained in the drums.

It is important to note that the rapid volatilization of organics and water due to heat is sufficient to eject drum lids (pressure needed to eject a lid was empirical determined to be ~ 49 psi; see Appendix F for details). To illustrate, Section 5.4.8 of this report investigated, in part, the addition of a small amount of water to a lab sample of Be metal. In this experiment, 50 μ L H₂O was added to 0.24 g of Be powder and heated as described in Section 5.4.8. The H₂O volatilized, resulting in a steady pressure increase to a maximum of 56 psig at 250°C, which exceeds the empirical pressure needed to eject the drum lid. Upon cooling to 46°C, the water condensed and the pressure dropped to a residual P_{final} = 4 psig (see Section 5.4.8 for additional details). This simple experiment demonstrates that the heating of water is enough to generate sufficient pressure to eject a drum lid.

Table 27. Concentrations of volatile and semi-volatile organic compounds, PCBs and anions in samples collected from within the event drum, and from material that was ejected during the event.

			DU: 37500 mg/kg	Burnt Drum DU: 24900 mg/kg	DU: 6520 mg/kg	DU: 17100 mg/kg
			SWR010013A	SWR011013A	SWR013013A	SWR014013A
Chemical Class	Compound	Average Ejected Concentration (mg/kg)	632268 (mg/kg)	632269 (mg/kg)	632270 (mg/kg)	632271 (mg/kg)
Volatile Organics	Acetone	2,390	340	390	370	220
	Trichloroethene	23,166	0	960	860	230
	Methyl Methacrylate	5,857	0	0	1,000	0
Semivolatiles	Phenol	10,316	2,810	0	2,480	2,760
	Bis(2-Ethylhexyl)phthalate	23,133	1,320	0	6,180	2,290
	Acetophenone	1,160	0	0	0	0
PCBs	Aroclor-1254	48,500	5,900	1,500	41,400	7,400
Anions	Nitrate	6,184	3,160	1,520	13,700	6,350
	Nitrite	582	141	55	1,010	324
	Fluoride	36,300	25,500	21,000	52,300	48,900

5.2 Reactions that Produce Methane

Reactions that produce gaseous products focused on CH₄, which is the biggest contributor to the accumulated head-space gases, and to the increased drum pressure. As noted previously, CH₄ was measured in the event drum samples after the rupture. And historically, there are drums within the ARP inventory that have shown the propensity for CH₄ generation. To test these observations, equilibrium experiments were conducted in which samples of ejected waste, and waste remaining in the event drum were placed in a chamber, heated, and then analyzed for head-space composition. The measurements showed that ejected samples generated increased CH₄ concentrations in their head-space at higher temperatures. Methane was also generated by the drum samples, however the quantity produced was lower compared with the ejected samples, an observation consistent with the higher temperatures experienced by the drum samples; which could have depleted the capacity for generating CH₄.

A second type of experiment involved placing samples of the drum contents and ejected waste material in a sealed chamber, and then heating the chamber using a linear temperature ramp. The ejected waste samples displayed significant pressure increases of 200 – 400 psig in the 140 – 220°C range, and analysis of the head-space showed that the majority of the gas was CH₄. The samples collected from within the event drum also showed pressure increases due to CH₄, however the pressure increase was about an order of magnitude lower, again consistent with depletion of methane sourced by exposure to higher temperatures during the event.

The origin of the CH₄ that was produced points toward rapid hydrolysis of Be₂C. Examination of historical records of drum contents showed a correlation between high Be concentrations and high CH₄ concentrations in the head-space.

Energy dispersive X-ray analysis showed high carbon content in mm-sized objects for which Be was the principle metal (Figure 23), and the Be was the most prevalent metal measured in the elemental analysis of the samples, as high as 30 % by weight. Subsequent EDS and X-ray diffraction (XRD) analyses of a low-density fraction of samples accentuated the carbide signature, and also supported the presence of abundant Be₂C, BeO, and Be metal.

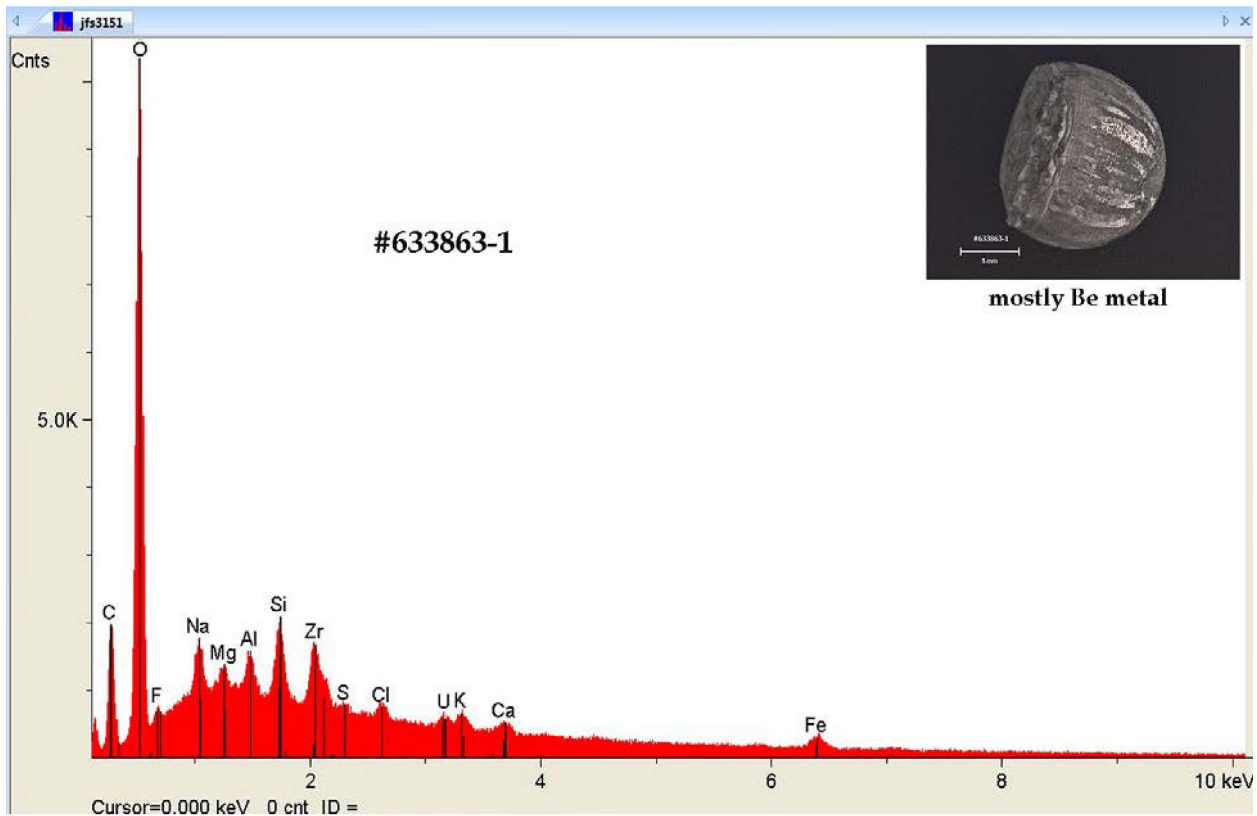
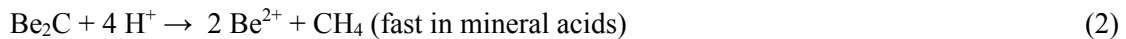


Figure 23. EDS of a metallic sample shown to be principally beryllium

Beryllium carbide undergoes hydrolysis reactions in water, acid and base, according to the reactions 1-3 below. Thus, it is likely that if significant quantities of Be_2C were present in the waste, exposure to atmospheric H_2O , or H_2O volatilized from the solid, would cause hydrolysis either by direct reaction with Be_2C , or by hydrolysis forming acid or base on the surface of the solid. The reaction with H_2O at ambient temperature is reported to be slow but will certainly be accelerated at elevated temperatures. The rate of CH_4 production is also accelerated by the presence of aqueous acid or base (see Section 5.5.4).



Aside from Be₂C, four other hypotheses have been considered to explain CH₄ generation. These are judged to be significantly less likely to be responsible for the production of CH₄, however they are discussed below in order to provide a more complete view of the logic supporting the selection of Be₂C as the most likely source of CH₄:

1. Catalytic cracking of paraffinic regal oil over diatomaceous earth. This explanation draws support from the fact that Regal oil is present in the samples, as demonstrated by the analysis of the volatile organics. The analysis showed a broad peak that was multiple minutes wide eluting at long GC retention times, consistent with the presence of a large hydrocarbon mixture. Further, diatomaceous earth catalysts have historically been used for catalytic cracking of paraffins. However, it is noted that while CH₄ is produced, it tends to be the least favored product, and should be accompanied by other small organics that are present in abundance. Strong evidence for other, abundant small organics was not observed.

Several bench-scale experiments were performed in which the waste samples were exposed to mineral oil, and some augmentation of CH₄ generation was observed. However, this is likely due to the heat transfer properties of the oil, so in sum the evidence in favor of Regal oil as a source of the CH₄ is not as strong as for Be₂C.

2. Hydrolysis of uranium carbide (UC). Based on XRD and scanning electron microscopy (SEM) data, the waste material from Rocky Flats contains quantities of UC, present as a result of molding fabrication operations that utilized graphite molds. UC has ceramic properties, and is stable at high temperatures, and has been considered as a possible material for use as nuclear fuel. It will react exothermically with O₂ at high temperatures, 600 – 800K.^{36,37} More recent studies have reported the pyrophoric character of UC – 5 μm particles have been reported to ignite at room temperature,³⁷ however ignition of similarly sized particles was reported ~ 200°C.^{38,39}

The pyrophoricity is strongly linked to prior history of the UC³¹. The hydrolysis reaction to produce CH₄ is well known³³:



In addition to methane, smaller amounts of other gaseous products are realized as well as inorganic uranium oxide. High-purity uranium monocarbide, when allowed to react with water at temperatures between 25 and 99°C, yielded a gelatinous, hydrous, tetravalent uranium oxide and a gas (93 mL [STP] per gram of UC hydrolyzed) consisting of 86 vol. % methane, 11 vol. % hydrogen, 1.8 vol. % ethane, and small quantities of saturated C3- to C6- hydrocarbons. The gaseous products contained all the carbon originally present in the carbide. Hydrolysis, at 80°C, of monocarbide specimens containing dispersed uranium metal yielded the expected gaseous products and an additional 2 moles of hydrogen per mole of uranium metal.

The reports of methane generation from UC suggest that this is a potential contributor to the gas generation phenomenon, and indeed the ratio of H₂ to CO₂ initially observed in heating samples of ejected material seemed consistent with the UC hydrolysis products reported in the literature. This was further bolstered by the X-ray Dispersive Fluorescence element mapping which showed the uranium and carbon were coincident in some of the particulate samples (see Figure 24). However, it is difficult to reconcile the very large emission of CH₄ needed to rupture a drum, with the small number of moles of uranium present in the waste. Furthermore, the heavy fraction produced from the density separation of the waste samples did not display a dramatic production of CH₄ when it was tested using the pressure vs. temperature experiment. Finally, commercial samples of UC when tested under similar conditions, produced methane fairly lethargically under base hydrolysis, and produced nearly equimolar quantities of H₂ and CH₄ during water hydrolysis (46 vol% H₂, 54 vol% CH₄) With acidic hydrolysis the UC produced predominately hydrogen (95%) under the same test conditions that produced predominantly methane from the ejected samples. So, when present,

the UC may contribute a small quantity of methane, but is not the predominant source of the high volumes of methane observed. In most cases it is likely that the UC from Rocky Flats was destroyed before the material became waste.

3. Anaerobic microbial metabolism is ruled out. In systems where CH_4 is produced, microbial action can frequently be identified as the source, particularly if there is a carbon source. While there is a carbon source in the form of Regal oil, the very rapid production of CH_4 in the pressure vs. temperature experiments strongly indicates a chemical origin, not biological.
4. Finally, radiolytic production of CH_4 is ruled out. Radiolysis can produce both methane and hydrogen. Radiolytic production of methane and or hydrogen as source of flammable gas in the reaction timeframe was evaluated in Appendix C and would fall significantly short in hydrogen/methane production.

5.3 Selection of Beryllium Carbide as the Most Probable Contributor to CH_4 Generation

The consideration of the historical origins of the waste material, combined with knowledge of the reactivity of beryllium carbide provide a strong circumstantial case for the hydrolysis of Be_2C being the reactant responsible for the production of CH_4 . Significant Be was on occasion used at the Rocky Flats facilities that are known to have generated the waste material in the event drum. In twelve samples collected from the event drum (eight from ejected material, four from material that remained in the drum), Be concentrations ranged from ~ 4 to 18 moles/kg.

Beryllium in the metallic form is stable, however processes at Rocky Flats would have resulted in formation of Be_2C , which is generated from the reaction of molten Be and graphite used in the molds.^{34,40} In addition, Be_2C was deliberately formed from Be and BeSO_4 as a protective film covering the interior surfaces of the molds. Be_2C displays significant stability, which would be consistent with its survival in the waste for several decades, but Be_2C is also reactive with H_2O , acids and bases, especially when heated⁴¹⁻⁴⁴ (see reactions in Section 5.2).

Subsequent to the emergence of these considerations, a series of analyses and experiments were performed at SwRI that were designed to provide speciation information on the metals that were present in the waste material, and to evaluate the properties of the waste when it was subjected to heating. Of specific interest was the evolution of gas upon heating. The results of the analyses and experiments were consistent with the production of significant CH_4 upon sample heating, and further implicated beryllium species, specifically carbide, as the CH_4 precursor. These results are described in sections 5.4 and 5.5.

In addition, experiments performed on ejected samples subjected to density separations showed that Be_2C was present in the low-density fractions, and that these fractions were responsible for CH_4 production. These results are described in Section 5.4.3.

5.4 Bench Test Demonstrating Methane Production and Pressure Generation

A series of experiments were conducted in which small quantities (up to ~ 3g) of samples collected from the event were placed in a modest pressure vessel and heated. The pressure vessel had a volume of approximately 15 cm^3 , and was equipped with a resistance heater, an interior thermocouple and a pressure transducer (Figure 24). Experiments were conducted by ramping the temperature of the pressure vessel, which was done by a programmed increase in current through the heater that caused the heater temperature to increase in a roughly linear fashion versus time. What was observed during the experiments was an increase in temperature recorded on the internal thermocouple, and an increase in pressure. The head-space of the pressure vessels could be sampled by withdrawing a gas sample via a

sampling port, and samples were generally collected after the pressure generation event and analyzed for CH₄, CO₂, and other gases.

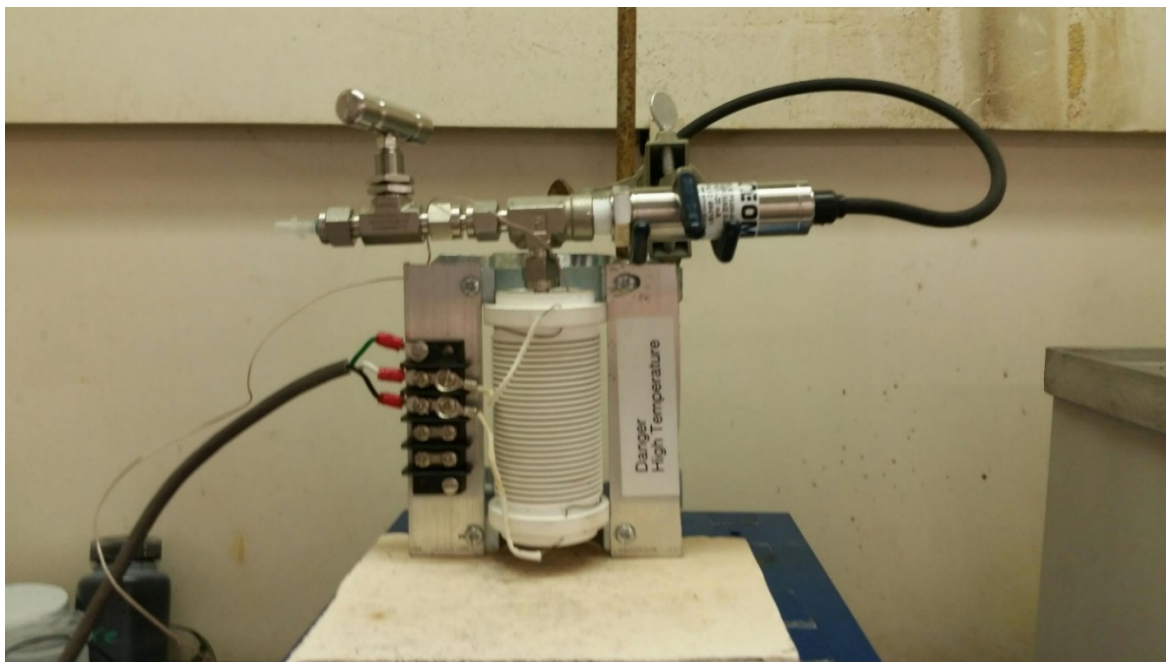


Figure 24. Pressure vessel used for pressure vs. temperature profiles of samples of waste materials.

The pressure temperature vs. time experiments are affected by the rate of heating, the sample mass, and the headspace atmosphere. Understanding the effects of these parameters was required to correctly interpret the CH₄ production experiments. However, the results of these parameter investigations comment more directly on the experiment process and less directly on the CH₄ production chemistry. Accordingly, the parameter investigations are reported in Appendix D.

5.4.1 Pressure and CH₄ Production: Comparison of Ejected vs. Drum Material

Small samples of waste materials that were heated in the pressure vessel to 250°C all showed increased pressure, signaling generation of gaseous products. The most important conclusion derived from these experiments is that when samples of the solid, dry waste material that had been ejected from the drum were heated, a large pressure increase was observed. For example, ejected sample 1013 started to generate pressure at about 110°C (Figure 25, red trace); pressure increased at a slow rate until about 200°C, and then displayed a nearly vertical increase at ~ 210°C, achieving a pressure of 460 psig. By about 210°C the dramatic pressure increase had stopped, however, pressure still increased at a slower rate. In this experiment, the temperature was then held at 220°C and during this time, pressure continued to slowly increase. Since the temperature was not increasing, the slow increases appear as vertical lines on the right-hand side of the plot. Analysis of the head-space gas produced by heating the ejected sample 1013 showed that it consisted of about 60% CH₄ (Figure 26, tan-colored bars).

In contrast, three of the four samples collected from within the drum showed much smaller increases, to 40 – 50 psig at 250°C (samples 10013, 11013, and 14013, Figure 25). Pressure continued to increase to the 110 – 130 psig range when the temperature was held at 250°C. The lower pressure increases are hypothesized to be due to higher temperatures experienced by the samples collected from within the drum, after the initial lid ejection event. Recall that the drum lids were ejected prior to internal heating that accelerated when the contents of the drum were stirred after the drum was ruptured, which accelerated the rate of oxidation, and resulted in charred paint on the external drum surface. The higher

temperature would have functioned to accelerate the rate of the methane-producing reactions, and consequently the drum samples have decreased capacity for producing CH₄.

In spite of the reduced CH₄ production capacity, the fraction of CH₄ in the headspace of the heated drum samples remained high. The head-space from drum sample 10013 contained ~ 26% CH₄, and the other three drum samples ranged from ~ 62 to 78% (Figure 26, green data points). It is worthwhile emphasizing that if the samples were not heated, CH₄ was not produced: in a series of experiments in which ejected and drum samples were heated to a mere 60°C, little or no CH₄ was generated (Figure 26, center).

The pressure trace for drum sample 13013 exhibited a pressure generation profile that was intermediate between ejected sample and that of the other three drum samples. It achieved a pressure of ~ 170 psig at 250°C and rose to 300 psig as the experiment was maintained at that temperature. This indicates that not all of the waste material in the event drum was exposed to high temperature upon stirring. Uneven temperatures would be expected if the heat produced were not uniformly generated throughout the drum. This would account for a drum sample with high CH₄-production capacity.

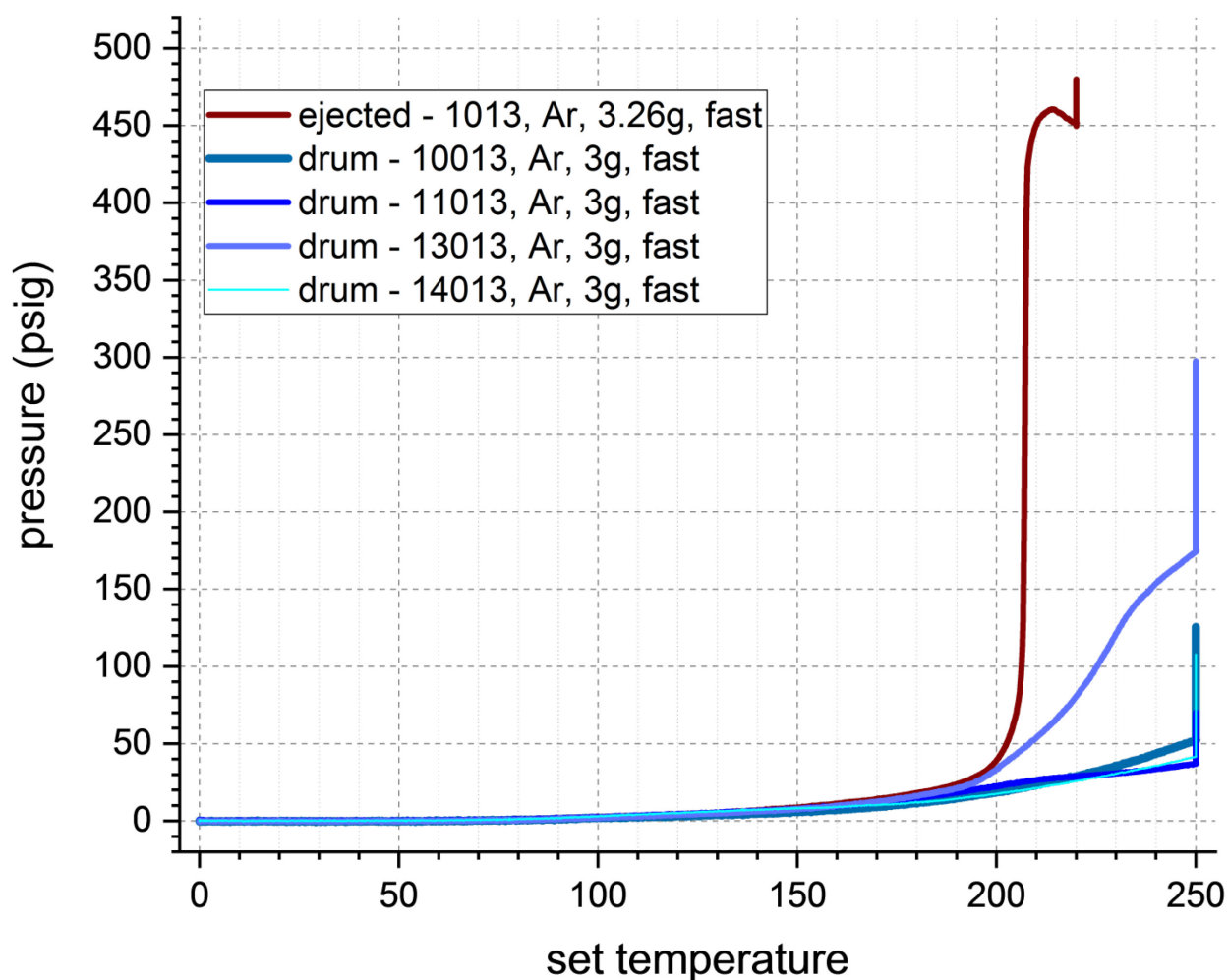


Figure 25. Pressure vs. temperature profile for ejected sample 1013, compared with samples collected from the drum.

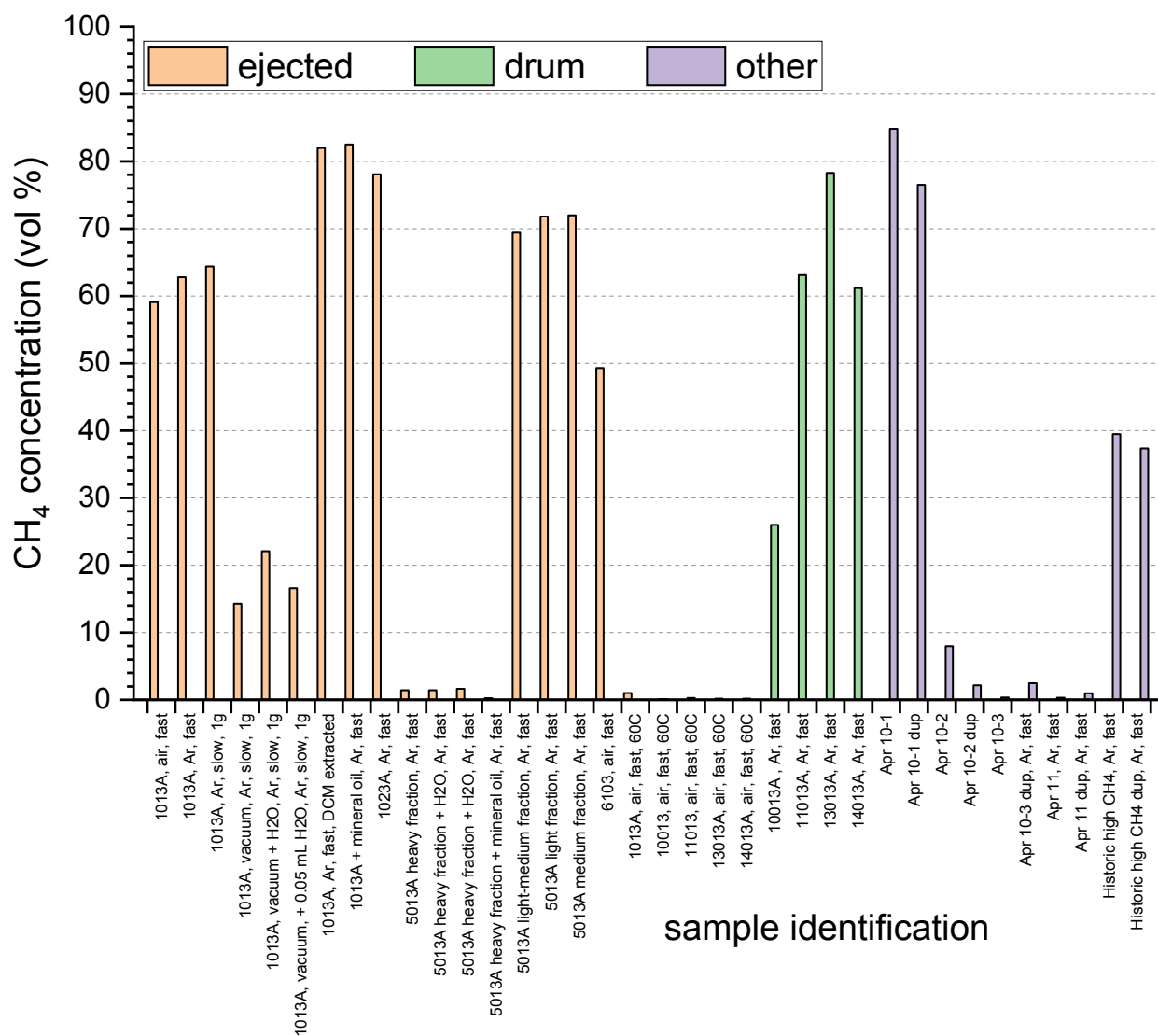


Figure 26. CH₄ concentrations (volume %) in the head-space of the pressure vs. temperature experiments. All samples were approximately 3g, except for tan columns 3-6, which were 1g.

5.4.2 Effect of Pre-Evacuation, H₂O on Gas Production

Water existing in the sample appears to facilitate production of CH₄. In a benchmark experiment, the pressure vs. temperature profile for 1 g of ejected sample 1013 shows an intermediate maximum at 42 psig at 136°C, followed by a steady rise to 165 psig at 250°C (Figure 28, red trace). The pressure rise in these experiments was smaller because the sample mass was lower (1 g compared to 3 g in preceding experiments). The CH₄ percentage in this experiment was ~ 65% (see Figure 26, tan columns 3-6). A subsequent sample was then evacuated and heated: the intermediate maximum, and low-temperature increase were not observed, and instead a steady increase to 40 psig at 250°C was observed. The maximum pressure observed in the evacuated experiment was about 4 times lower than the non-evacuated benchmark, as was CH₄ (~ 15%) The effect of the pre-evacuation was hypothesized to remove reactive constituents (specifically H₂O) from the sample, reducing the quantity of gas produced. Water was hypothesized to be the source of H atoms needed to generate CH₄.

The effect of the evacuation could be reversed by addition of H₂O. A 0.1 mL aliquot of H₂O was added to the evacuated sample, and the sample was re-heated to a temperature of 150°C. This resulted in an increase in the pressure at 150°C, from 7 psig in the evacuated sample, up to 32 psig in the ‘H₂O added’ experiment (Figure 27, teal trace) It also increased the CH₄ in the headspace to ~ 22% The experiment was again stopped, and an additional 0.05 mL H₂O was added. At 150°C, the pressure in this experiment was 23 psig, and continuing to increase the temperature to 250°C resulted in a pressure of about 102 psig (light blue trace). Methane produced in this experiment was 17% (Figure 26, tan column 6).

These results clearly indicate that a small quantity of H₂O significantly facilitates production of CH₄, and that the pre-evacuation treatment depressed gas generation by removing H₂O. This conclusion is consistent with the explanation that CH₄ is produced by the reaction of H₂O with Be₂C.

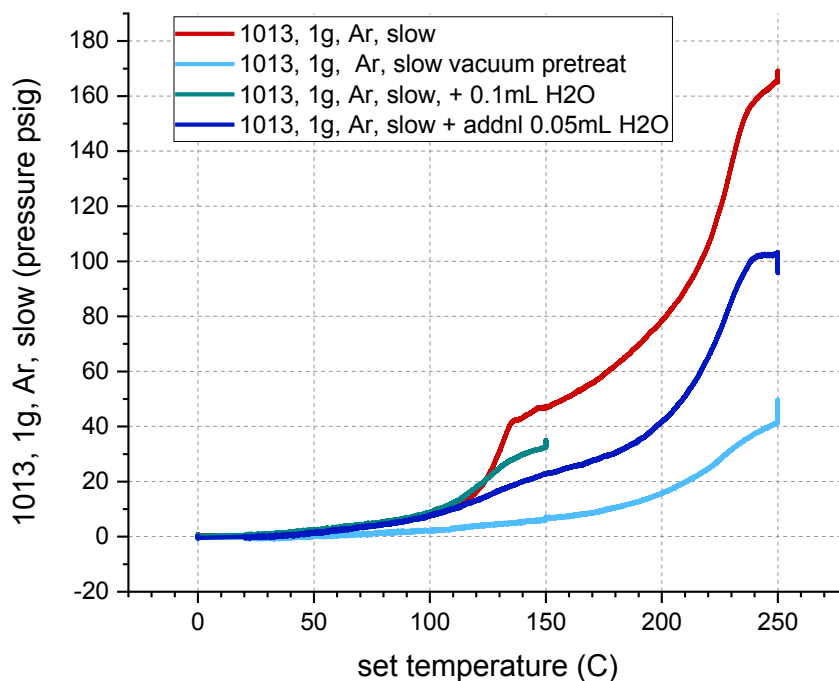


Figure 27. Pressure vs. temperature (set value) for ejected sample 1013, 1g. atmosphere, pretreatment and H₂O availability compared.

5.4.3 Evaluation of the Effect of Regal Oil: DCM Extraction and Mineral Oil Addition

An alternative hypothesis for the CH₄ generation was that Regal oil was undergoing catalytic cracking to form CH₄. Regal oil is a long-chain paraffinic hydrocarbon mixture that was known to be present in most of the Rocky Flats waste. Two types of experiments were conducted to evaluate this possibility:

1. Extraction of the waste material with dichloromethane (DCM)
2. Addition of mineral oil to the waste.

Pressure vs. temperature measurements were performed after both experiments.

DCM extraction exerted very little influence over the production of CH₄ compared to the untreated sample. Comparison of the pressure trace for ejected sample 1013 extracted with DCM showed identical behavior up to 170°C when compared to an untreated 1013 benchmark, and an untreated ejected sample 6013 (Figure 28). The temperature corresponding to the rapid rise was about 8°C higher in the DCM sample compared to the untreated 1013 benchmark and was nearly identical with the 6013 benchmark. The headspace from the pressure vs. temperature study of the DCM-extracted sample contained ~ 82% CH₄ (Figure 26), which was 17% higher than the untreated benchmark, and ~ 30% greater than the 6013 benchmark.

The DCM experiment showed that CH₄ production was in no way affected by the extraction, which strongly suggests that the hydrocarbons (Regal oil) are not the chemical precursor of CH₄.

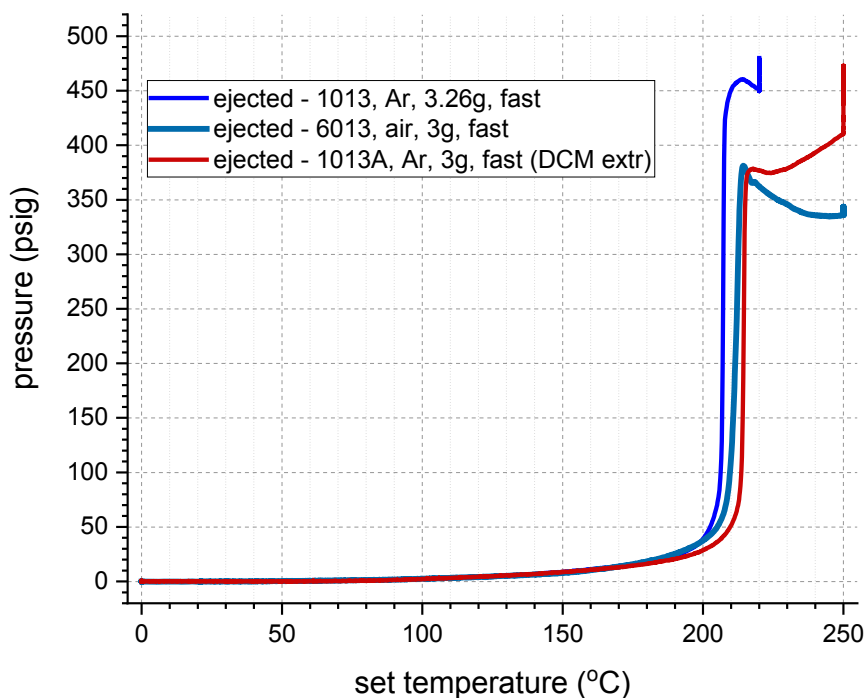


Figure 28 Pressure vs. set temperature profiles of extracted samples 1013 and 6013. Comparison of the effect of methylene chloride (DCM) extraction (red) with un-extracted samples (blue).

Subsequent experiments involved adding mineral oil (Regal oil) to the ejected waste samples, on the expectation that if the Regal oil were responsible for CH₄ generation, then addition of another paraffinic oil should result in increased pressure and CH₄ generation. A 2.20 g ejected waste sample was dosed with a small quantity of mineral oil, and then subjected to the pressure vs. temperature testing protocol. A sharp pressure rise to ~ 290 psig was recorded at 190°C (Figure 29, red trace), a value about 30% lower compared to an unmodified 2.88 g sample, which showed a sharp pressure rise to ~ 390 psig at 205°C. Scaled for the greater mass in the benchmark, the two experiments produced about the same pressure rise. The mineral oil-modified experiment also produced a high CH₄ percentage in the headspace gas, ~ 83%, but again, this was comparable to the percentage measured in the unmodified benchmark (78%, see Figure 26, tan columns 8, 9). These results demonstrate that the CH₄ concentration is not impacted by the addition of Regal oil.

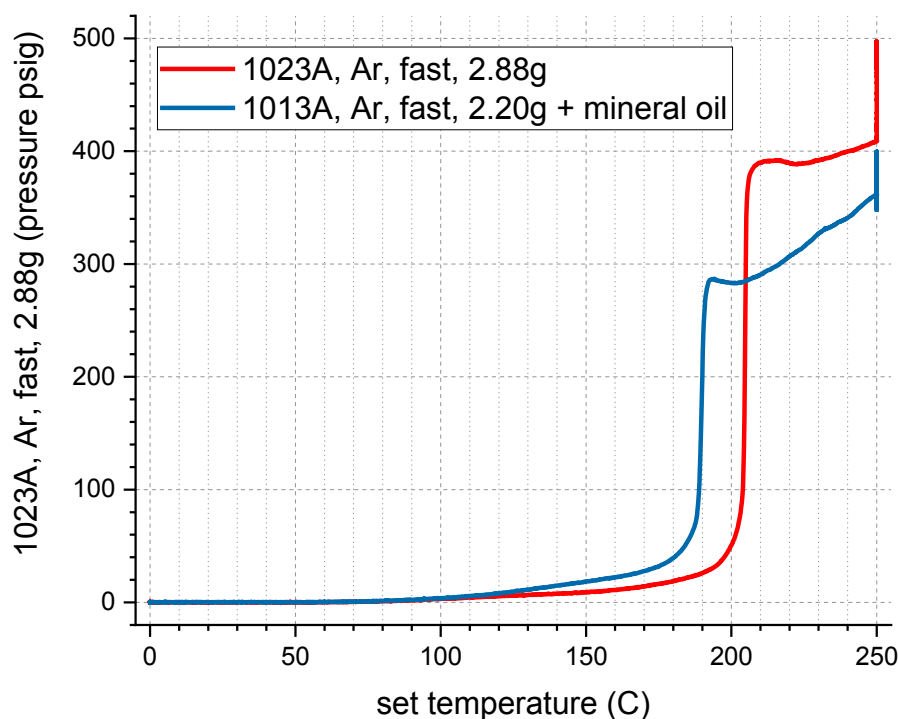


Figure 29. Pressure vs. temperature traces for 2 g aliquots of ejected sample 1013, unmodified, and amended with a small quantity of mineral oil.

5.4.4 CH₄ Production Differentiated by Waste Sample Density

5.4.4.1 Density Separation and Spectroscopy of Ejected Sample 5013. If CH₄ were generated from beryllium-bearing solids, these would be expected to be characterized by low particle density; in contrast, if CH₄ originated from uranium-containing solids, these would be expected to have high particle densities. To evaluate this possibility, ejected sample 5013 (SWR005013A (SWRI #631477)) was subjected to particle separations that were conducted by floating the solid particles in dense liquids, viz., diiodo-, and then dibromo-methane (Figure 30). Flotation in diiodomethane, with a density (ρ) = 3.3 g/mL, will enable separation of dense particles ('heavy' fraction, $\rho > 3.3$) from less dense particles ('light-medium' fraction, $\rho < 3.3$). The light-medium fraction was then further separated by flotation in dibromomethane ($\rho = 2.17$ g/mL), producing a 'medium' fraction with ρ between 3.3 and 2.17 g/mL, and a 'light' fraction, with $\rho < 2.17$ g/mL.

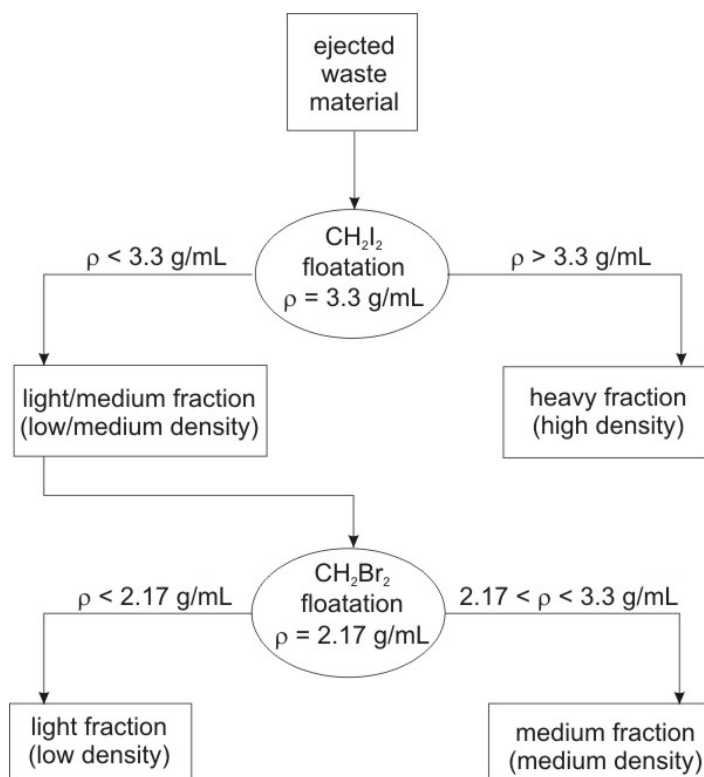
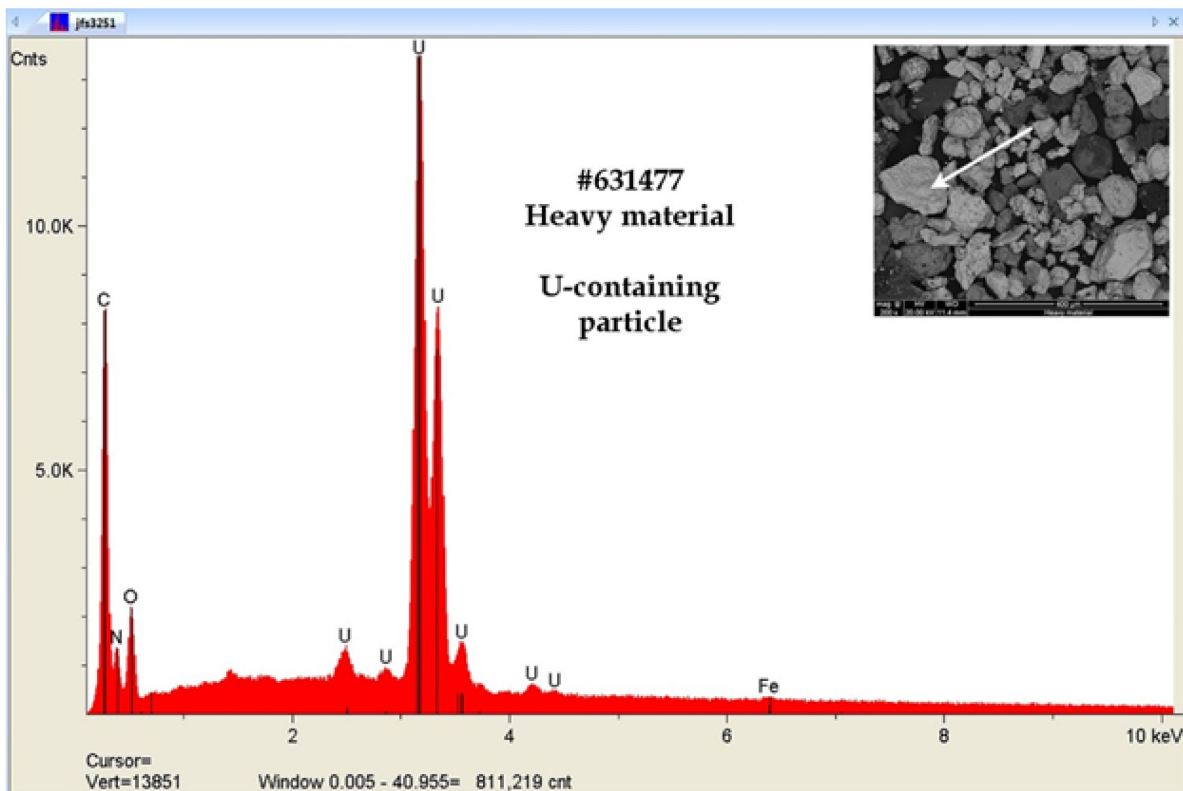


Figure 30. Schematic diagram for serial density separation using diiodomethane, then dibromomethane.

The heavy fraction accounted for ~8% of the total mass and was analyzed using SEM and EDS. The EDS spectral analysis showed intense peaks corresponding to uranium, and also significant carbon (Figure 31). The presence of significant uranium in the heavy fraction is consistent with the high density of the material. The bright particles seen in the back-scattered electron image suggest the presence of heavy metals in the sample, and uranium accounts for 35% of the weight of this sample, with carbon and nitrogen accounting for 46 and 11% respectively. However, concentrations expressed as atom percentages show that uranium only represents 2.77% of the sample, with carbon, nitrogen and oxygen accounting for the remainder. The EDS concentrations should be viewed as rough estimates, since this type of analysis does not detect lighter elements like Be. In fact, the heavy fraction did contain 3140 mg/Kg Be (~0.3%) as measured by ICP/OES.

One particle on the left-hand side of the microscopic image is particularly bright, and in fact likely corresponds to uranium carbide. This assignment is supported by the elemental maps, which show bright images for carbon and uranium for the large particle on the left (Figure 32). Many of the other particles in the image also display bright uranium registration, but not carbon, which indicates that these have a different composition, with different uranium speciation, perhaps uranium metal with a thin oxide coating.



<u>Elt.</u>	<u>Line</u>	<u>Intensity</u> (c/s)	<u>Atomic</u> %	<u>Conc</u>	<u>Units</u>	
C	<u>Ka</u>	179.30	72.61	45.92	wt.%	
N	<u>Ka</u>	26.05	14.77	10.89	wt.%	
O	<u>Ka</u>	41.97	9.79	8.25	wt.%	
Fe	<u>Ka</u>	3.34	0.05	0.16	wt.%	
U	<u>Ma</u>	459.63	2.77	34.78	wt.%	
			100.00	100.00	wt.%	Total

Figure 31. EDS spectral data for heavy fraction of sample SWR005013A. The atom percent and weight percent concentrations are provided in the table below the spectrum. The back-scattered electron microscopic image is shown in the inset. The x-dimension is ~ 160 μm .

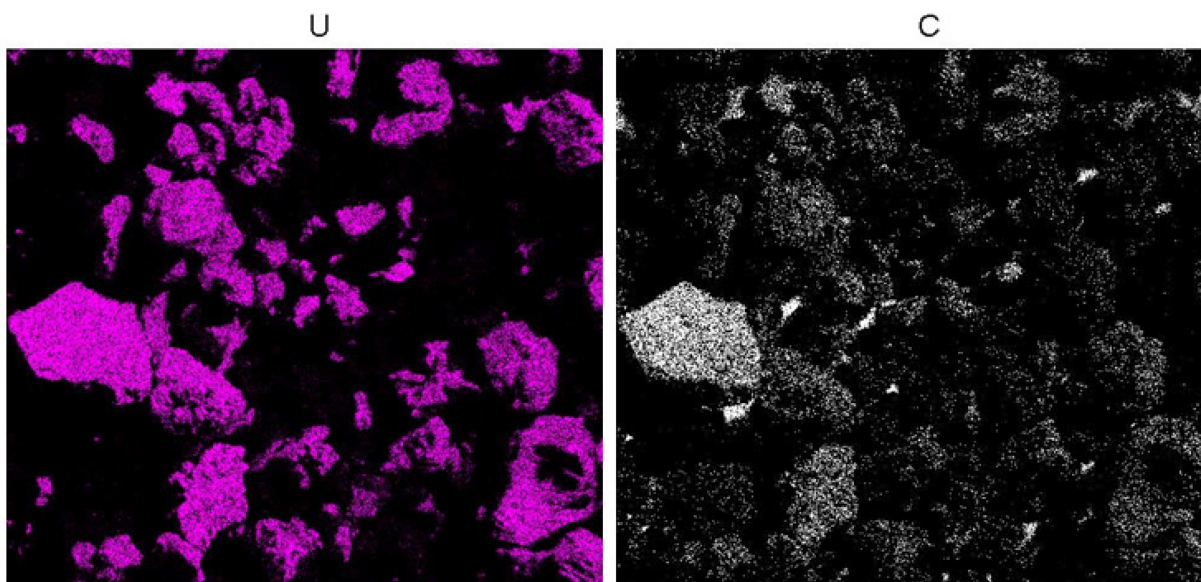
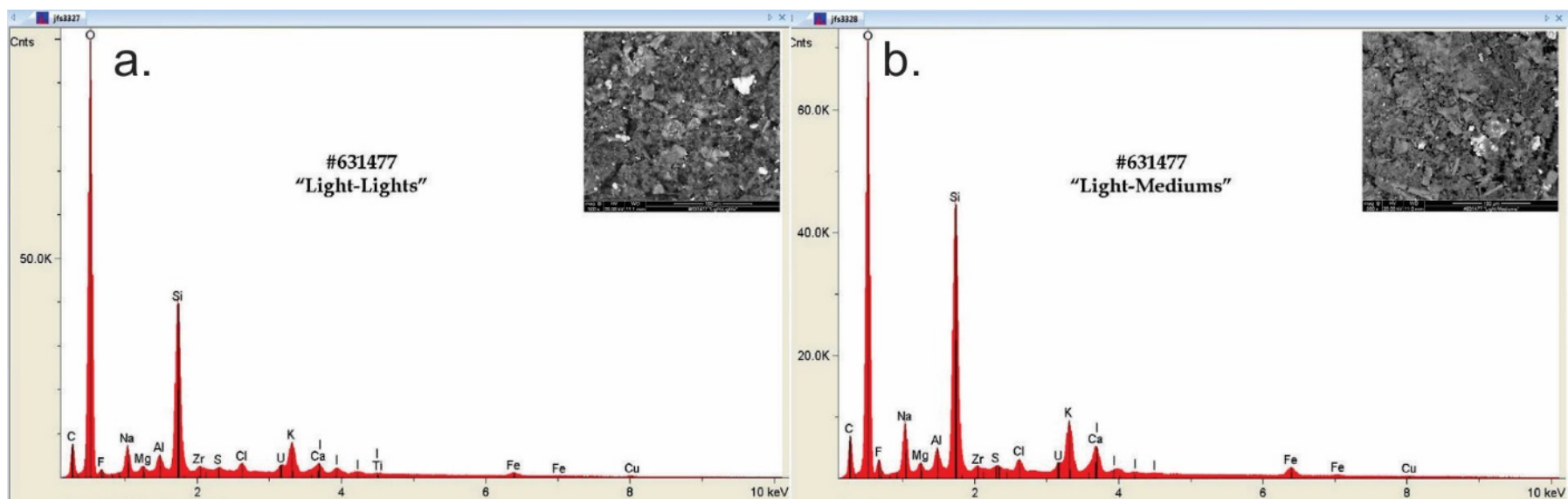


Figure 32. Uranium (left) and carbon (right) elemental maps of the heavy fraction of Sample SWR005013A.

The light-medium fraction, which accounted for about 90% of the mass of the original sample, was again subjected to density separation by flotation, this time using dibromomethane. This separation furnished the light, and medium fractions, which accounted for 30% and 60% of the original sample mass. The EDS spectra of the light and medium fractions displayed very little uranium, and instead were dominated by intense signals from oxygen and silicon (Figure 33), suggesting that they principally consist of silicate absorbent. The light fraction contained Na^+ and K^+ as counter cations; this was also true for the medium fraction, however Ca^{2+} and Fe were more prominent in this fraction, consistent with its higher density.

A limitation of the EDS analyses was that it is insensitive to Be, and hence the samples were further compared using XRD. This provided additional, convincing evidence for the presence of Be_2C , BeO and metallic Be, all three of which were found in the XRD spectrum of the light fraction. (Figure 34a). The spectrum has abundant SiO_2 phases, but in addition contains the highly diagnostic peak at 30° for Be_2C , three peaks at 38.5° , 41.5° and 44° for bromelite (BeO), and 53° for Be metal. The XRD spectrum of the medium fraction also contained peaks consistent with Be_2C and BeO (Figure 34b) but did not contain evidence for Be metal. These data are in accord with the presence of significant Be_2C in both of the lower-density fractions of the sample. Subsequent ICP measurements performed on the light and medium fractions showed large quantities of Be: the medium fraction contained 70,000 mg/Kg (7% by mass), while the light fraction contained 248,000 mg/Kg (24.8%).

5.4.4.2 Pressure-Temperature Studies of Density Fractions. The lighter density constituents of the ejected waste samples were found to be responsible for the majority of the CH_4 generation. Since both Be_2C and UC were hypothesized to be present in the samples, either could be responsible for CH_4 generation, since both are known to undergo hydrolytic production of CH_4 . Methane production originating from the low-density material (light fraction) was differentiated from the high-density material (heavy fraction) by conducting pressure-temperature experiments.



74 Figure 33. Energy dispersive X-ray spectroscopy analyses of density separated fractions of ejected sample 5013. a. Light fraction (density < 2.17 g/mL). b. Medium fraction (2.17 < density < 3.3 g/mL). Insets are backscattered electron photomicrographs of the separated particulate samples, 240 μm on a side.

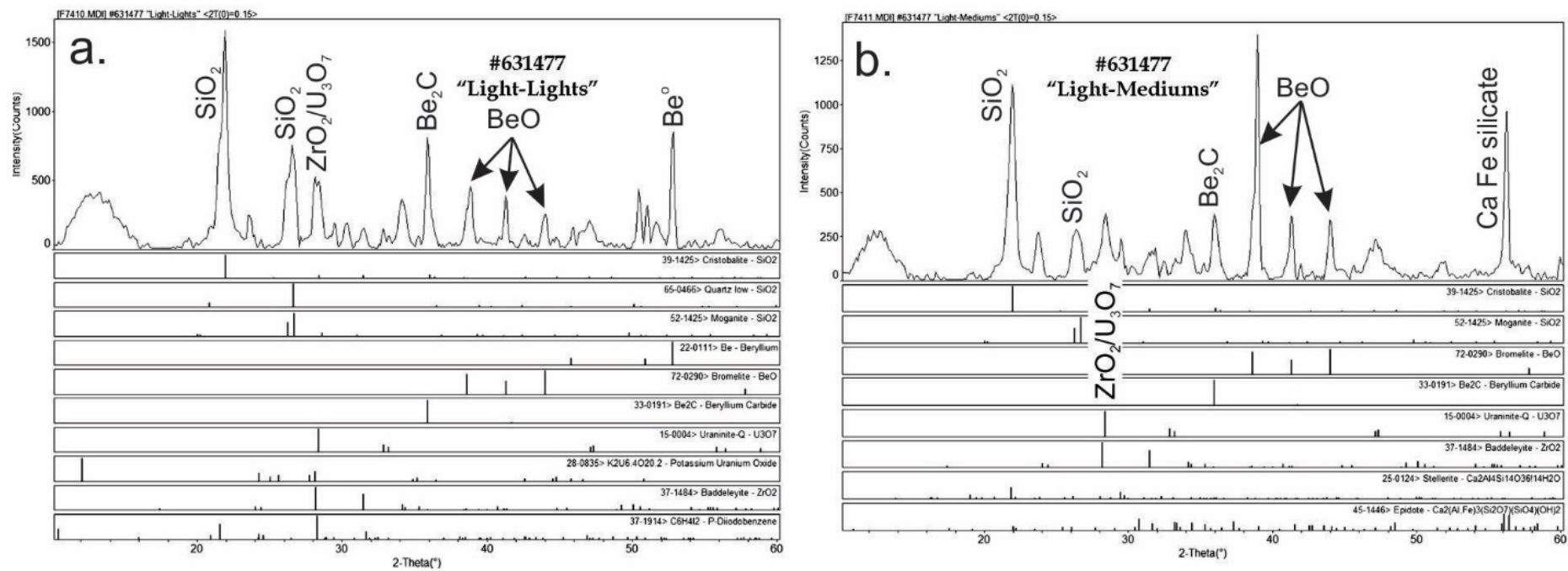


Figure 34. X-ray diffraction (XRD) analyses of density separated fractions of ejected sample 5013. a. Light fraction (density < 2.17 g/mL). b. Medium fraction (2.17 < density < 3.3 g/mL).

The heavy fraction displayed a very modest pressure increase, to about 11 psig by the time the temperature reached 250°C (Figure 35). The very low-pressure change was thought to be due to the absence of any sources of hydrogen atoms, and so the experiment was repeated, however this time dosing the sample with 0.1 mL H₂O. The water changed the pressure profile, which rose to 47 psi by 205°C; this is felt to be principally due to the volatilization of the water. The pressure continued to rise as the temperature increased to 250°C, but only to 50 psi. Analysis of the headspace in these experiments showed very low percentages of CH₄, on the order of 2% (Figure 26, Column 10).

Pressure-temperature experiments performed on the light-medium fraction produced a much different pressure profile. Pressure generation was not observed until about 150°C, however the pressure then exponentially increased to 284 psi, with the profile becoming nearly vertical at 230°C. After this point, as temperature continued to increase, the pressure dropped to ~ 230 psi. The CH₄ concentration in the headspace of this experiment was high, at 69%.

These results provide strong evidence that the lower density, light-medium fraction is responsible for the majority of the pressure rise and CH₄ production. It could be argued that the lower pressure rise observed in the testing of the heavy fraction is the result of the lower mass, however, if the gas generation was in fact mainly derived from the heavy fraction, then a pressure rise comparable to the unseparated sample should have been observed, and it was not. In addition, the absence of CH₄ in the headspace of the heavy fraction experiment also strongly indicates that the denser material, i.e., UC, is not responsible for the gas generation.

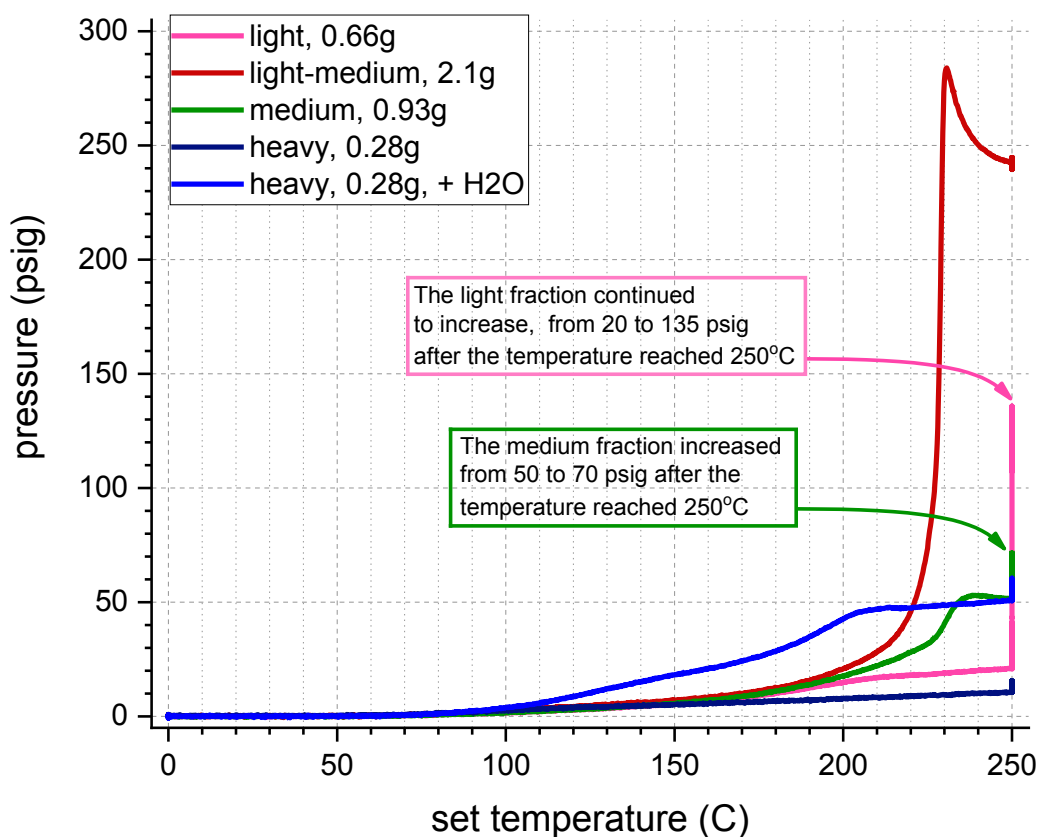


Figure 35. Pressure vs. temperature (set point) profiles for light and heavy fractions of ejected sample 5013. All experiments were conducted using an Ar headspace, and a fast temperature ramp (10°C/min), which shifts the observed pressure rise to higher values.

Both the light-light and medium fractions displayed significant pressure generation when heated, although much of the pressure rise was not observed until after the temperature reached the ceiling value of 250°C; this appears as a straight vertical line in the pressure vs. temperature plots.

Better clarity could be seen by plotting pressure and temperature vs. time. The pressure in the light sample increased to ~ 135 psig, which is within the range expected for a 0.66 g sample (Figure 36a). The temperature corresponding to the sharp pressure rise was 250°C, maintained for ~ 7 minutes. This is somewhat higher compared to earlier measurements, the difference being in part attributable to the fast ramp rate (10°C/min).

The pressure in the medium fraction increased to ~ 71 psig, with the sharpest pressure rise occurring at a temperature of about 225°C (Figure 36b). These results demonstrate that CH₄ is originating from both fractions, consistent with the observation of Be₂C in the XRD spectra of both samples (see Figure 34).

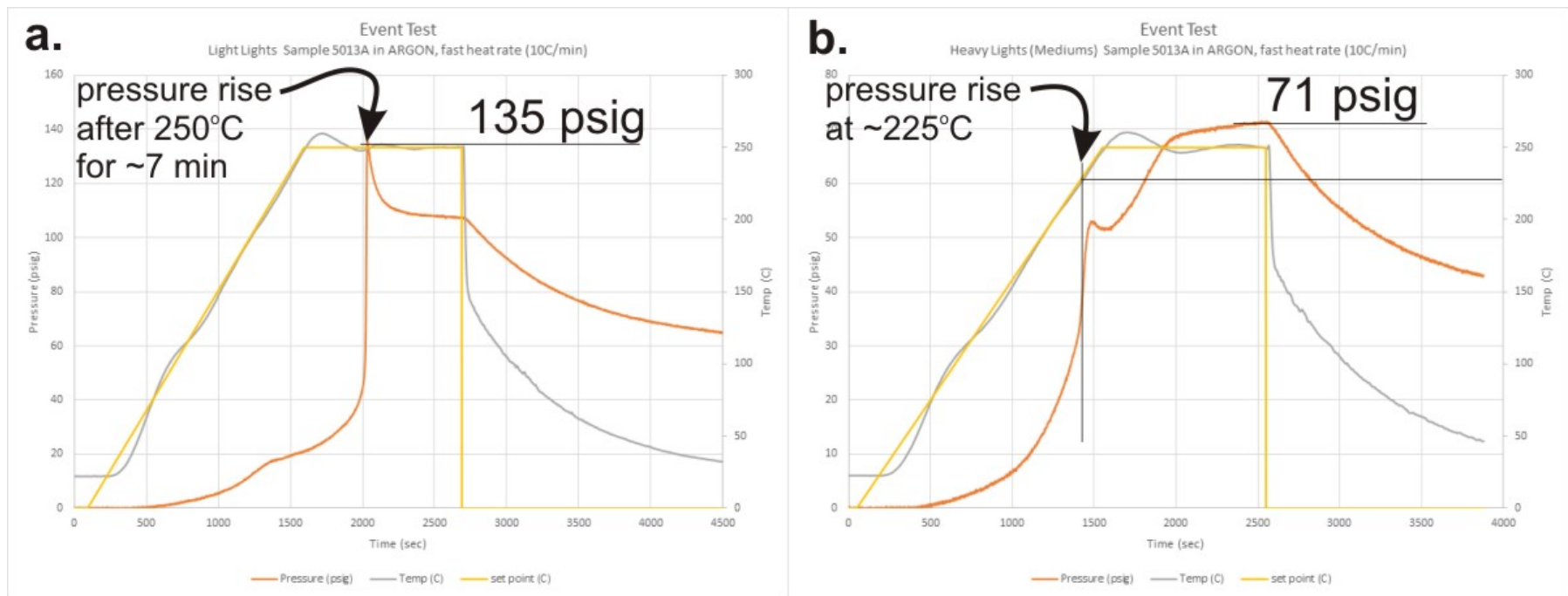


Figure 36. Pressure, temperature vs. time plots. **a.** Light fraction **b.** Medium fraction. The temperature ramp rate was 10°C/min.

5.4.5 Impact of Acid/Base

If CH₄ is indeed produced by hydrolysis of Be₂C, then the effect should be observable upon addition of acids or bases, equations 5 and 6, since in aqueous solutions these are known to accelerate the reaction



This is what was observed: addition of H₂SO₄ to ejected sample 1023 resulted in an immediate pressure rise to 23 psig, which was accompanied by a temperature increase to 85°C (Figure 37c). Since this experiment was not heated, the temperature rise is assumed to originate from the exothermic hydrolysis reaction. In comparison, addition of water only resulted in a 0.9 psig pressure increase, and essentially no change in temperature (Figure 37a), and the system was not affected by heating to 35°C. Addition of NaOH (Figure 37d) to the sample resulted in an immediate pressure increase of 1.6 psig, and was accompanied by an increase in temperature to 25.5°C. This is a much more modest effect compared to H₂SO₄, but the pressure and temperature profiles are consistent with hydrolysis.

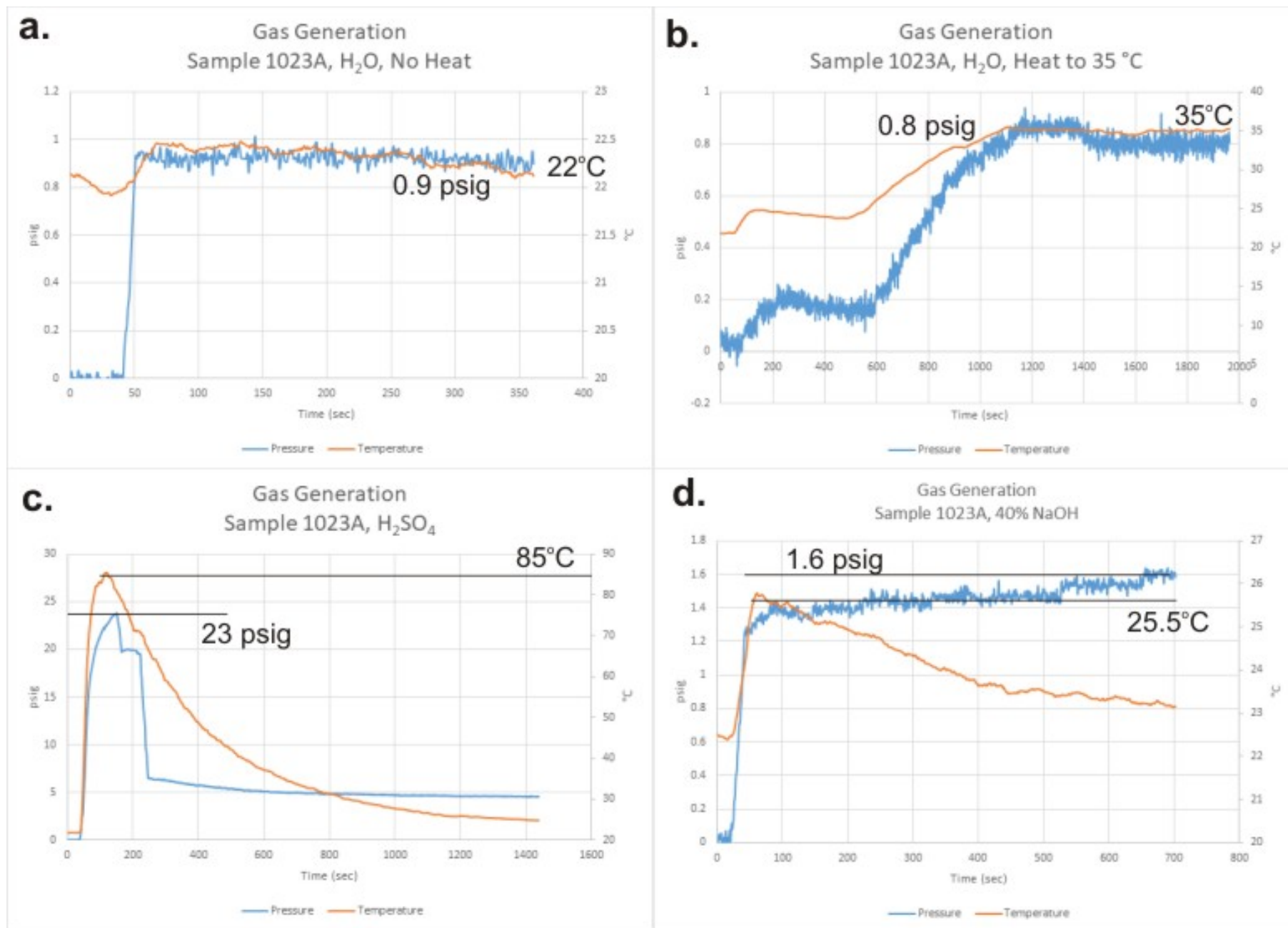


Figure 37. Pressure, temperature vs. time plots for ejected sample 1023. **a.** H₂O addition, 22°C (no heating). **b.** H₂O addition, heating to 35°C. **c.** H₂SO₄ addition, no heating. **d.** NaOH addition, no heating.

Addition of KOH to the sample resulted in an immediate pressure rise to ~ 3 psig at 22°C. This experiment was then heated in a stepwise fashion, which resulted in increasing pressure (Figure 38c). At 90°C, a pressure of 14 psig was achieved. These experiments clearly indicate that addition of acid and base will result in augmented production of CH₄, a conclusion in accord with the notion that Be₂C is present in the waste materials. The fact that base will speed CH₄ production may be particularly relevant since the pH of water exposed to the waste material is basic, in the 10 – 11 range.

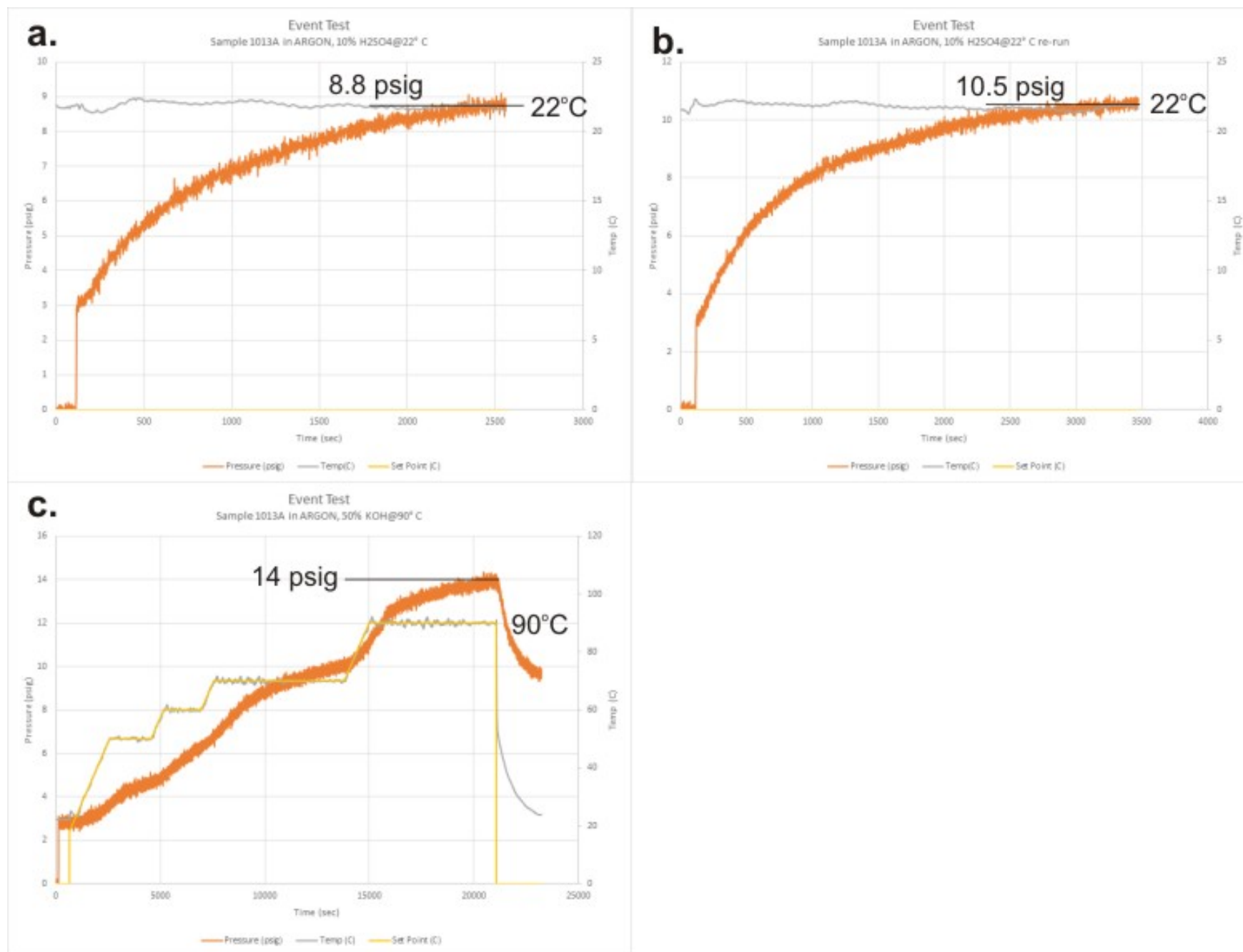


Figure 38. Pressure, temperature vs. time plots for ejected sample 1013 **a.** H₂SO₄ addition, 22°C (no heating) **b.** H₂SO₄ addition, no heating (replicate experiment) **c.** KOH addition, stepwise heating to 90°C.

Pressure, temperature vs. time experiments were conducted using the density-separated fractions, with the expectation that the light-density fraction, which contains Be_2C , would produce significant CH_4 when exposed to H_2SO_4 and KOH . This is what was observed: at ambient temperature, addition of H_2SO_4 to the light density fraction of ejected sample 5013 resulted in a pressure rise to 17.5 psig (Figure 39b), a value significantly higher compared to the measurement for unseparated ejected sample 1013 (Figure 39a). In contrast, H_2SO_4 addition to the medium and heavy fractions generated pressure increases of 3.7 and 2.7 psig, respectively.

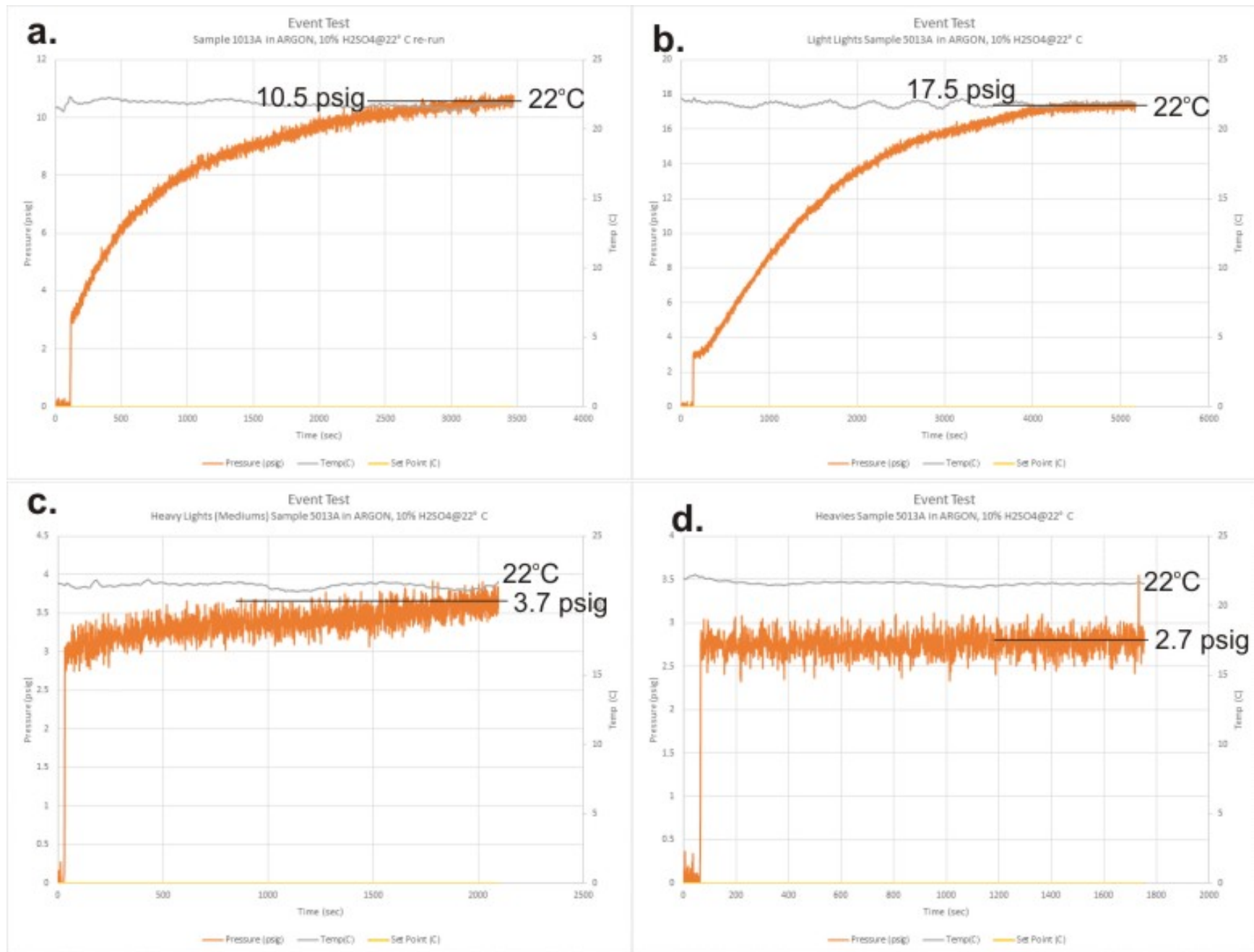


Figure 39. Pressure, temperature vs. time plots for H₂SO₄ addition to density-separated fractions of ejected sample 5013 **a.** H₂SO₄ addition to benchmark sample 1013 **b.** H₂SO₄ addition to the light fraction, 22°C (no heating) **c.** H₂SO₄ addition to the medium fraction, 22°C (no heating) **d.** H₂SO₄ addition to the heavy fraction, 22°C (no heating).

Addition of KOH to the light-light fraction generated a pressure rise of 19 psig upon heating to 90°C (Figure 40b). This was slightly in excess of the pressure rise measured for the unseparated sample of ejected 5013, suggesting that the light density fraction was responsible for the pressure generation. By way of contrast, the medium and heavy fractions treated with KOH experienced pressure increases of 8.8 and 6.5 psig, respectively. This reactivity with acid and base to produce a gaseous product with an accompanying pressure rise is consistent with the presence of carbide and suggests that Be₂C predominantly resides in the light density fraction of ejected sample 5013.

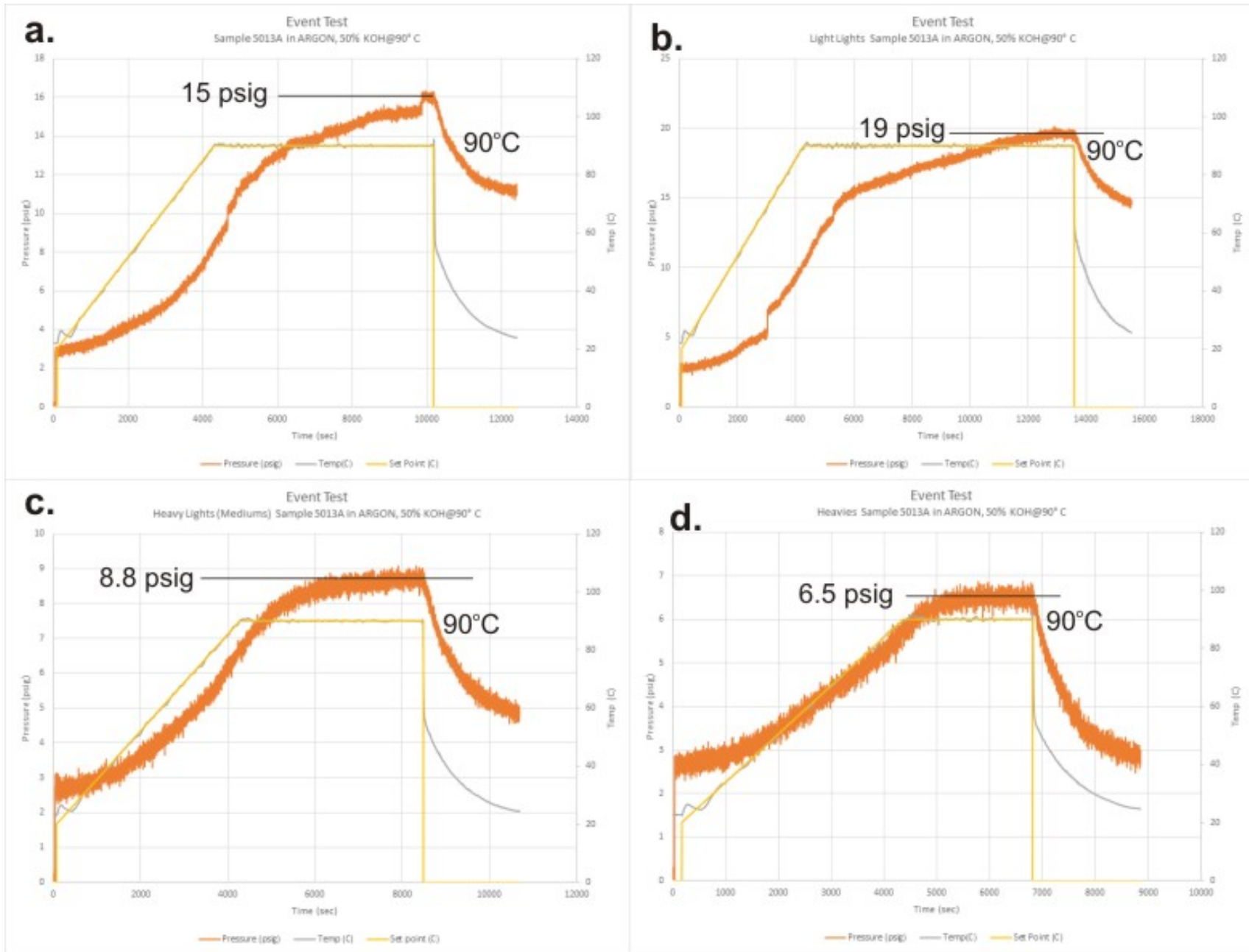


Figure 40. Pressure, temperature vs. time plots for KOH addition to density-separated fractions of ejected sample 5013 All experiments were externally heated to 90°C **a.** KOH addition to unseparated 5013 **b.** KOH addition to the light density fraction **c.** KOH addition to the medium fraction **d.** KOH addition to the heavy fraction.

5.4.6 Reaction Temperature Dependence

A series of experiments were conducted in which ejected sample 1013 was repeatedly heated to a defined, intermediate temperature, allowed to cool, and then heated to 250°C. The objective was to gain a better understanding of the relationship between increasing temperature and the observed pressure rise. The experiments showed that neither 40°C nor 80°C were sufficient to cause the very dramatic pressure rise and CH₄ generation seen in the ejected samples. However, both the extreme pressure rise and CH₄ generation could be observed by initial heating to 160°C. This result is consistent with the earlier conclusion from the slow temperature ramp experiments that indicated that the temperature required for CH₄ generation was on the order of 140°C, and not >200°C as indicated by the fast ramp experiments.

In the first series of experiments (Figure 41a), a 3.00 g sample was ramped to 40°C at a rate of 1°C/min, which resulted in a very modest increase in pressure, to ~ 0.9 psig and when the heat was removed, pressure dropped back to near ambient. Analysis of the headspace gas of this experiment did not identify CH₄. The sample was then heated to 40°C a second and a third time (Figure 41b, c). The pressure increase was very similar in both of the subsequent experiments –increases of ~ 1 psi were observed. CH₄ was not observed in the second replicate (and the headspace was not analyzed in the third).

The sample was then heated at 1°C/min to 250°C (see Figure 41d). Pressure began increasing around 110°C, and the profile became nearly vertical at ~130°C, spiking to 320 psig at 135°C before falling to ~ 280 psig. As the temperature continued its linear increase, the pressure resumed its increase, reaching a maximum (P_{\max}) at 404 psig at $T_{\max} = 250^\circ\text{C}$. When the heat was removed, the pressure fell to $P_{\text{final}} = 239$ psig at $T_{\text{final}} = 35^\circ\text{C}$. Analysis of the headspace gas showed that it was ~79% CH₄.

After cooling, the ejected sample 1013 was again reheated to 250°C (Figure 41e). The remarkably sharp rise in pressure was not observed in this experiment, instead the pressure began rising at ~65°C, and followed a much less steep, exponential-like increase to ~ 69 psi, which was achieved at ~ 230°C. As the temperature continued to increase, pressure actually decreased. This experiment produced only ~ 7% CH₄ in the headspace; instead, ~10% CO₂ was produced. The origin of the CO₂ is not known. The apparatus was then cooled and 50 µL of H₂O was added, and the experiment was then repeated (Figure 41f). In terms of pressure rise, the results were very similar to those for the 250°C re-heat, although the concentration of CH₄ was only ~ 2% while the CO₂ concentration was 9.2%. The addition of H₂O had no significant effect on the pressure rise in this experiment.

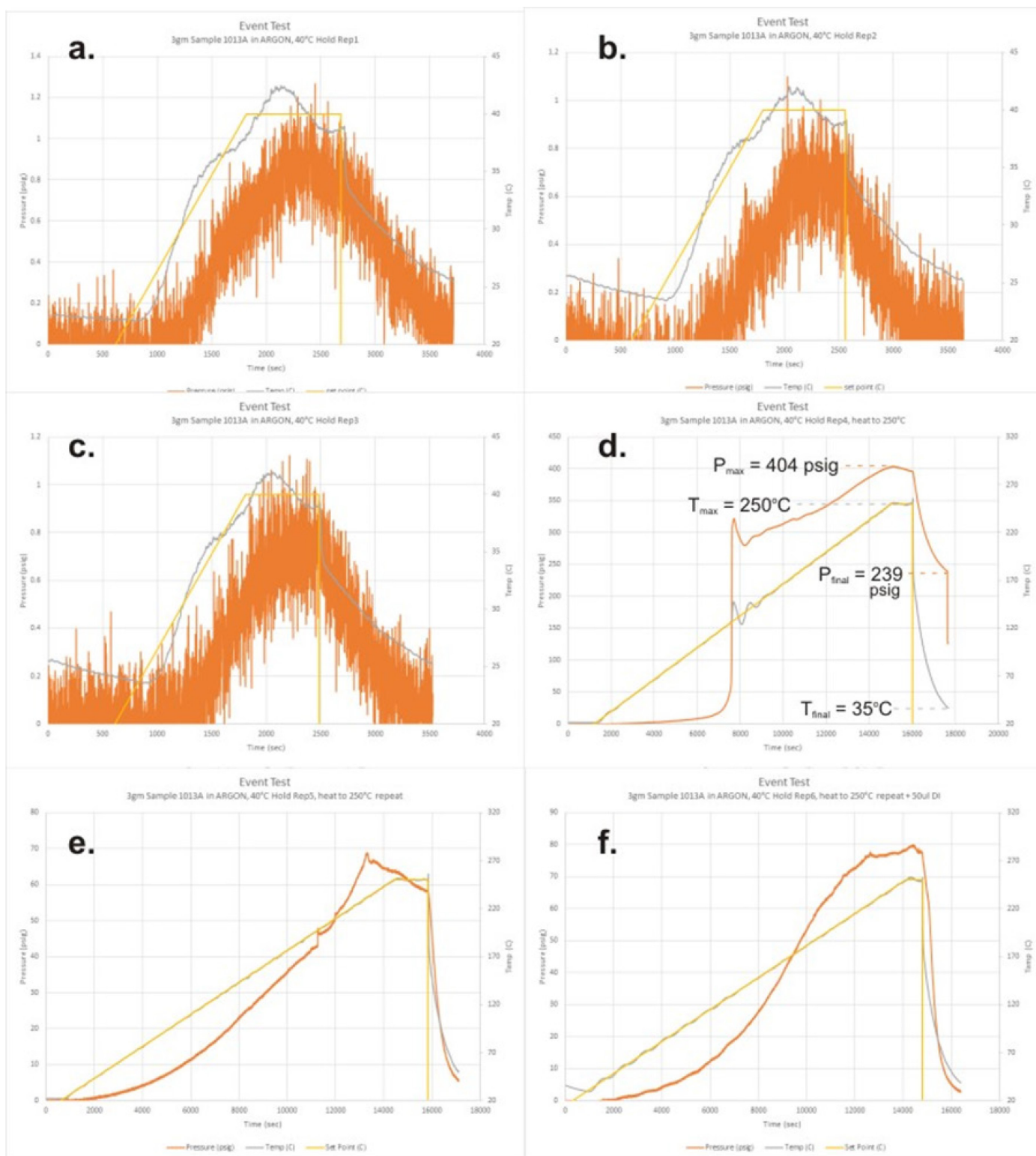


Figure 41. Serial pressure, temperature vs. time plots for ejected sample 1013. The initial headspace atmosphere was Ar, and the heating rate was $1^{\circ}\text{C}/\text{m}$ in all experiments. **a, b, c:** Sample heated to 40°C . **d, e:** Sample heated to 250°C . **f:** Sample heated to 250°C after addition of $50\ \mu\text{L H}_2\text{O}$.

A second set of serial experiments were performed using another 3.0 g aliquot of ejected sample 1013, only in this case the temperature in the first three replicates was 80°C (Figure 42). A temperature of 80°C resulted in a gradual pressure rise to between 4 and 6 psig in the first three serial experiments, more than what was observed in the 40°C experiments, but nevertheless very modest values. The gas analyses did not show significant CH₄, CO₂, CO or H₂, which suggests volatilization of condensable compounds like H₂O. The fourth heating experiment raised the temperature to 250°C, and produced results that were very similar to those in the first set of serial experiments (in which the initial target temperature was 40°C): a nearly vertical pressure increase to 300 psig occurring at 130 - 140°C, followed by a slower increase to 400 psig as the temperature continued to increase to 250°C. Consistent with the sharp pressure rise, the CH₄ concentration in the headspace gas was measured at 75.5%.

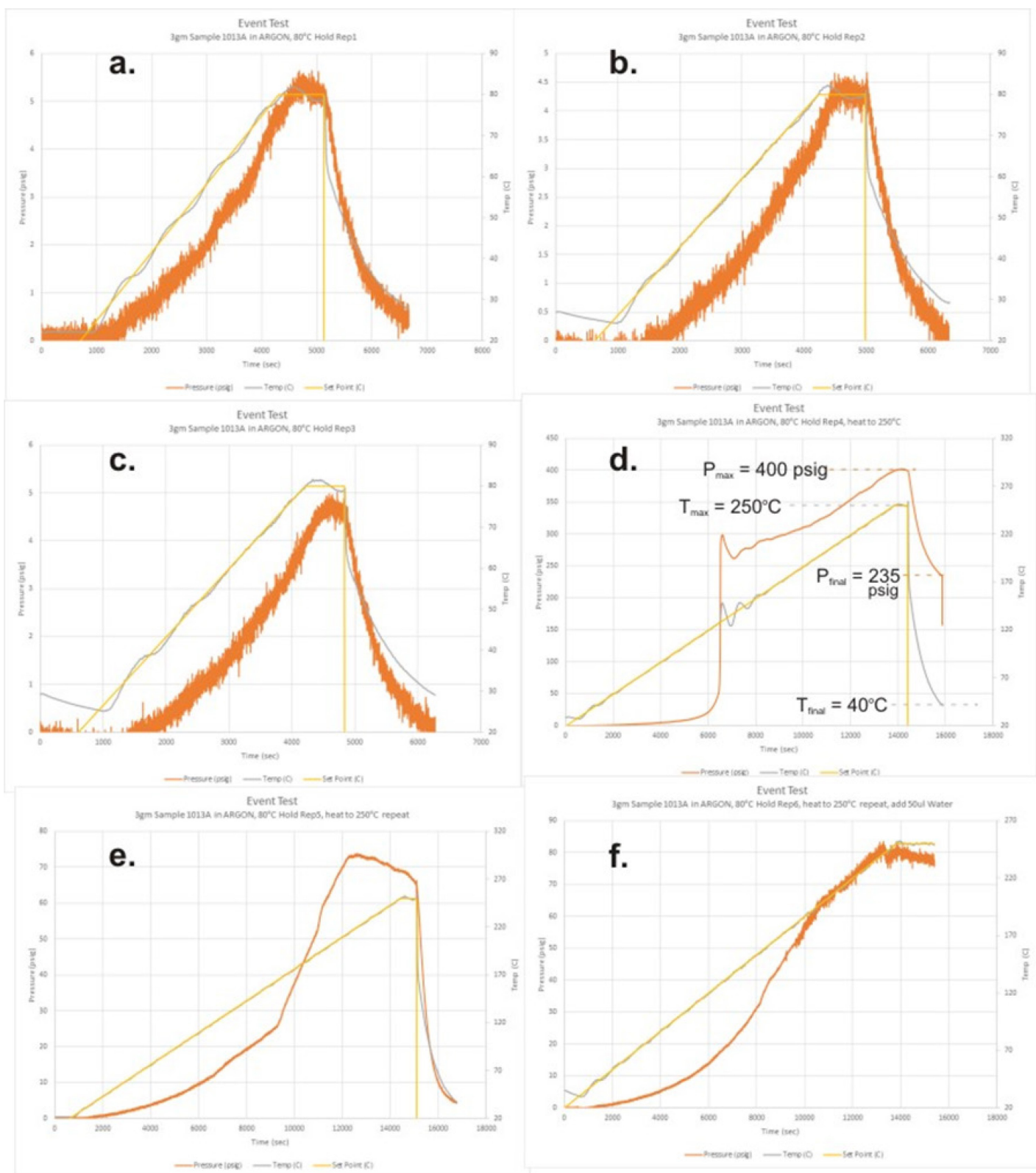


Figure 42. Serial pressure, temperature vs. time plots for ejected sample 1013. The initial headspace atmosphere was Ar, and the heating rate was 1°C/m in all experiments. **a, b, c:** Sample heated to 80°C. **d, e:** Sample heated to 250°C. **f:** Sample heated to 250°C after addition of 50 μ L H₂O.

A third set of serial experiments were conducted in which the temperature of ejected sample 1013 (3.02 g) was initially raised to 160°C. This resulted in a sharp pressure increase to 286 psig, which occurred at ~ 135°C (Figure 43a). The CH₄ concentration in the headspace of this experiment was 74.4%. Upon cooling to 39°C, the pressure decreased to 195 psig. As before, the fact that it did not return to near ambient indicates that CH₄ is produced. After cooling, this experiment was repeated twice more using the same sample, which resulted in P_{max} values of 27 and 32 psig, following a slow apparently exponential profile. When the sample was cooled, the pressure dropped to near ambient, suggesting that the gas that responsible for the pressure increase was a condensable fluid. This is consistent with the CH₄ concentrations, which were only 17.3 and 14.6%, and indicated that the majority of the CH₄ was liberated the first time the sample temperature was raised to 160°C.

In the fourth replicate experiment conducted on the 3.02 g sample, temperature was raised to 250°C, which resulted in slow pressure increase to 104 psig, producing a CH₄ concentration in the headspace of 22.8% (Figure 43d). When the sample was cooled, most of the pressure dissipated, however a residual pressure of about 19 psig remained when the temperature was ambient. This showed that the CH₄-precursor was still present, but that the majority of CH₄ was liberated in the first replicate where the temperature was raised to 160°C. The fifth replicate experiment was a repeat of the fourth, but the temperature ramp only extended to ~ 200°C and so the results cannot be used for comparison. The sixth replicate repeated the temperature increase to 250°C subsequent to addition of 50 µL of H₂O. The addition of H₂O had no discernable effect on the pressure vs. time profile, which maximized at P_{max} = 108 psig. The CH₄ concentration was not measured in the fifth and sixth experiments.

5.4.7 Estimating the Amount of Beryllium Carbide

About one third of the beryllium in the ejected samples was in the form of Be₂C. This conclusion was derived from a consideration of the increase in methane measured in the serial reaction temperature dependence experiments described in Section 5.4.6 and substantiated by the XRD spectrum given in Figure 27. The quantity of CH₄ produced can be related to the Be₂C concentration as follows.

The moles of CH₄ produced can be calculated from the P_{max}, T_{max} values measured in the serial pressure-temperature experiments where the initial hold was 40°C, specifically in the fourth replicate where the temperature was raised to 250°C for the first time (Figure 43d). Given that the sample mass is 3.00 g, and the volume of the headspace is constant at 0.0117 L (sample chamber volume of 0.015 L corrected for the sample mass (3 g) / density (0.9 g/cm³)), a pressure rise to P_{max} = 404 psig at T_{max} = 250°C would correlate to the production of 0.0075 moles of gas:

$$\left(\frac{404 \text{ psi}}{523 \text{ K}}\right) \left(\frac{1 \text{ atm}}{14.7 \text{ psi}}\right) (0.0117 \text{ L}) \left(\frac{\text{mol K}}{0.082 \text{ L atm}}\right) = 0.0075 \text{ moles gas} \quad (7)$$

Assuming that the gas is 78.5% CH₄ (per the gas analysis), and that one mole CH₄ consumes two moles Be:



The Be concentration would thus be 3.9 moles Be/kg as Be₂C (2.0 moles Be₂C/kg):

$$(0.0075 \text{ mol gas})(0.785) \left(\frac{2 \text{ mol Be}}{\text{mol CH}_4}\right) \left(\frac{1}{3.00 \text{ g}}\right) \left(\frac{1000 \text{ g}}{\text{kg}}\right) = \frac{3.9 \text{ mol Be}}{\text{kg}} \quad (9)$$

This value is lower than the Be concentration in the ejected 1013 sample, which was measured at 11 mole/kg by ICP (Figure 14). However, this is expected because multiple Be species are present in the waste material: the XRD analysis of the light-light fraction of a sample of ejected waste showed prominent peaks corresponding to Be^o and BeO in addition to Be₂C, that were about equal in intensity as shown in Figure 34.

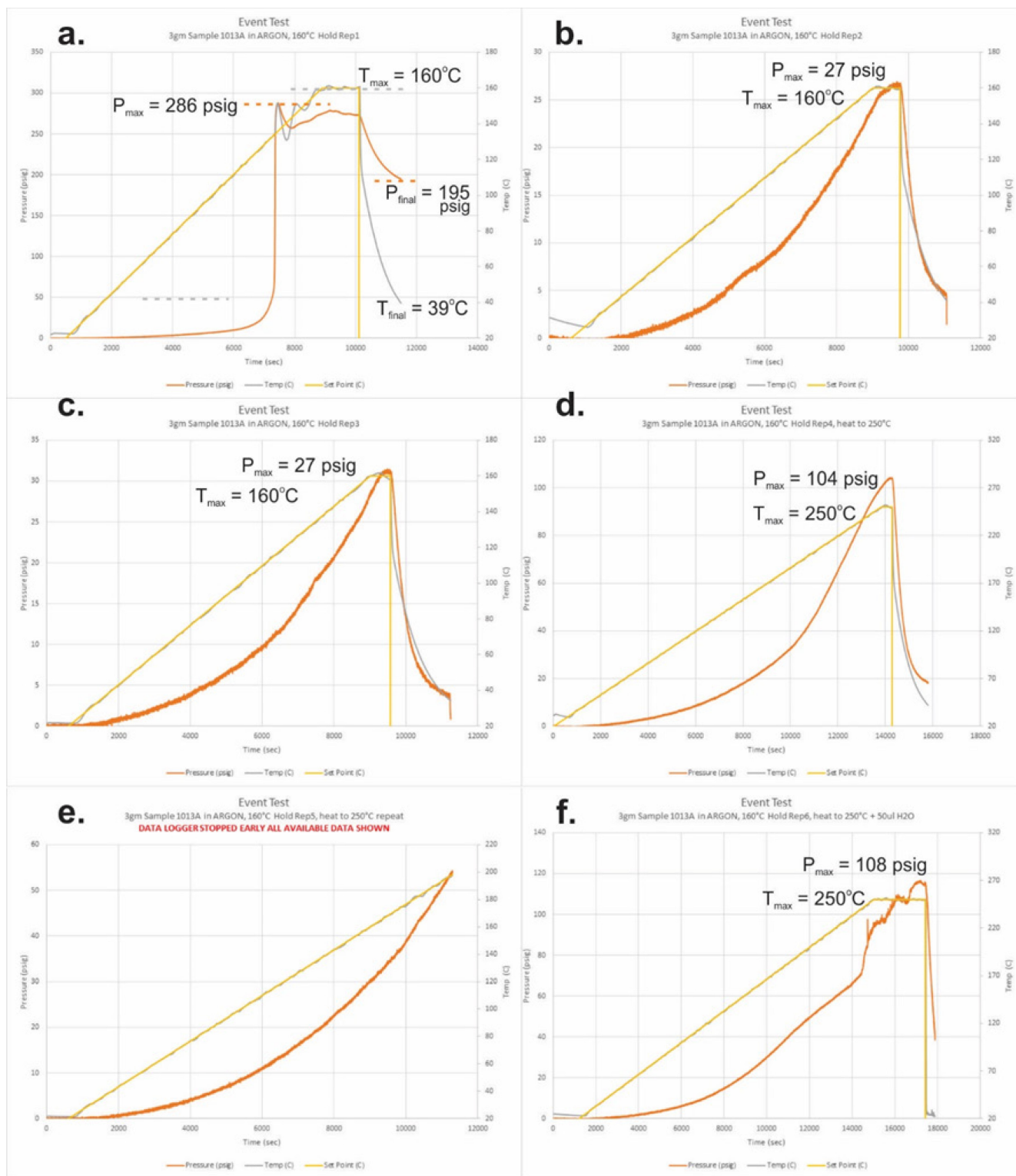


Figure 43. Serial pressure, temperature vs. time plots for ejected sample 1013. The initial headspace atmosphere was Ar, and the heating rate was $1^{\circ}\text{C}/\text{m}$ in all experiments. **a.** Sample heated to 160°C , held, then cooled. **b, c:** Sample heated to 160°C (second and third replicates, same sample aliquot). **d, e:** Sample heated to 250°C . Rep e was inadvertently truncated. **f:** Sample heated to 250°C after addition of $50\ \mu\text{L}$ H₂O.

The same analysis was performed using the P_{final} , T_{final} values of 239 psig and 35°C seen in Figure 44: this calculation generated an identical quantity of CH₄ and identical Be concentration in the ejected sample.

The quantity of CH₄ produced was also calculated from the serial experiments in which the intermediate temperature was 80°C, specifically from the fourth replicate in which the temperature was raised to 250°C for the first time. The moles of CH₄ calculated using the P_{max} , T_{max} and P_{final} , T_{final} values (see Figure 43d) produced values of 0.0112 and 0.011 moles, respectively, both correlating to a Be concentration of 3.7 moles Be/kg (as Be₂C). These values are very close to those calculated for the serial experiments in which the target temperature was 40°C.

The calculation for the experiments in which the initial target temperature was held at 160°C resulted in 3.1 and 3.0 moles Be/kg (as Be₂C), values somewhat lower than those in which the initial target temperatures were 40°C and 80°C. The difference is reconciled by the fact that pressures measured in the 40°C and 80°C experiments were determined in the fourth replicate, where the temperature was ramped all the way to 250°C. The lower values in the experiments where the initial target was held at 160°C were generated from data measured in the first replicate, i.e., where the temperature was only ramped to 160°C (Figure 43a). When the temperature was increased all the way to 250°C, another 104 psig was recorded, which is sufficient to achieve good agreement between the three sets of experiments.

The same calculations were performed for the sample collected from the mechanistic drum sample processed on April 10 (Drum 10648022). The pressure-rise resulted in a Be₂C concentration of 1.2 mol/kg, or 2.5 mol/kg Be as Be₂C. Using the P_{final} , and T_{final} values from the end of the experiment, concentrations of Be₂C and Be as Be₂C were 1.3 and 2.6 mol/kg. The ICP/MS analysis of this sample generated Be concentrations of about 3×10^5 mg/kg, equivalent to 10 mol Be/kg. Thus, the gas analysis data indicates that about 25-26% of the Be in the mechanistic sample processed on Apr 10 exists as Be₂C.

5.4.8 Elimination of Be metal as a potential source of gas pressure

Be metal was considered as a potential source of CH₄, because it can undergo oxidation, and as indicated by XRD spectra and by the comparison of estimated Be₂C with measured total Be concentrations, it is very likely present in significant quantities in the waste material. A small mass (0.28 g) of Be powder was placed in the pressure apparatus, which was then back-filled with Ar, and heated using the fast temperature ramp (10°C/min). A slow, linear pressure rise was measured that maximized at 12 psig after about 20 min at 250°C (Figure 44a). After the heating was terminated at 3300 sec, the temperature fell to 42°C, accompanied by the pressure falling to $P_{\text{final}} = 1$ psig. Thus, the pressure rise was attributable to residual condensable fluids in the reaction chamber or adsorbed to the Be metal (e.g. residual H₂O). No CH₄ was measured in the headspace. In a second experiment, 50 µL H₂O was added to 0.24 g of Be powder, and the experimental protocol was repeated. The H₂O volatilized, resulting in a steady pressure increase to a maximum of 56 psig at 250°C. Upon cooling to 46°C, a residual $P_{\text{final}} = 4$ psig was measured, which was in part attributable to H₂. The gas analysis for this sample showed only 0.6% CH₄, and 3.3% H₂, the latter probably the result of H₂O oxidation of Be°. These results show that Be° is not the reactive precursor for CH₄ or the pressure generation that is observed in the waste samples.

5.5 Evaluating the Thermodynamic Favorability of Beryllium Carbide Hydrolysis

The HSC calculation outputs described in Table 25 and Figure 22 were redone with the addition of a small amount of beryllium carbide (0.2 mols). The beryllium carbide was consumed producing methane demonstrating that the generation of methane in the mix of components is a thermodynamically favored product.

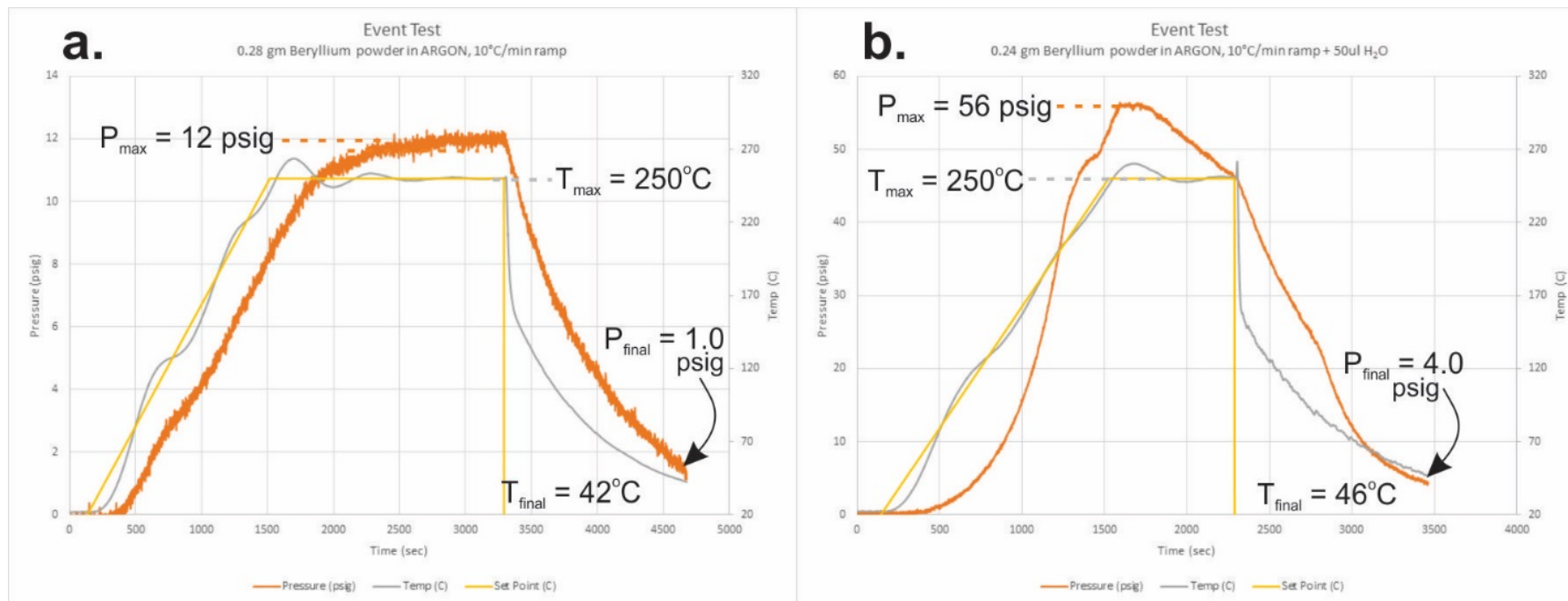


Figure 44. Pressure, temperature vs. time experiments for samples of Be metal powder. **a.** Unmodified Be powder. **b.** Be powder dosed with 50 μL H₂O.

6. COMPARISON WITH WASTE FROM DRUMS LOCATED PROXIMATE TO THE EVENT DRUM, THE SORTING TABLE, TRANSFER TRAY, AND A HISTORICALLY HIGH CH₄ DRUM

In an effort to further elucidate chemical characteristics responsible for the rupture of the event drum, several additional samples were evaluated in order to compare their composition with that of the event drum. These comparisons are noteworthy for two reasons. First, they showed that the atomic compositions of neighboring, non-rupturing drums were significantly different than the composition of the event drum. Secondly, they showed that high Be concentrations did not necessarily indicate a potential for gas generation. The additional samples included:

- Waste from three drums that were processed on April 10 (drums 10648022, 10647908, and 10647928), the day before the rupture event
- Waste from one drum that was processed on April 11 (Drum 10647909) (the day of the rupture event), but before the event drum waste was processed
- Waste from a historically high CH₄ drum.

6.1 Composition and Speciation in Un-Ruptured Drums

The metal concentrations of the neighboring samples processed on April 10 and 11 showed significant differences compared to the waste from the event drum (either ejected or remaining in the drum) (Figure 28). Further, the sample from the first un-ruptured drum sampled from April 10 (Drum 10648022) was much different than the other un-ruptured drum samples (drums 10647908, 10647928, and 10647909): it contained nearly 300,000 ppm Be, and notable Pb, U, and Zr. These values were all significantly higher compared to the event drum samples Be by about a factor of two. In addition, Ca, K, Na and Si were significantly lower. This indicates that the sample was predominately Be plus the heavy metals, and contained little Micro-Cel E. In contrast, samples from the other two drums collected on April 10, and the sample from the un-ruptured drum collected on April 11 contained essentially no Be, U, Zr and very little Pb, but had significant Ca, K, Na and Si.

The speciation of the un-ruptured drum that contained high beryllium was consistent with the presence of a significant quantity of Be₂C, which was identified by XRD. The XRD spectrum of the un-ruptured, high-Be waste sample contained peaks attributed to Be₂C, BeO, ZrO₂, UO₂ and Be^o, together with minor peaks assigned to SiO₂ and calcium silicate phases (Figure 29). In contrast, the spectrum of the second un-ruptured drum sample collected on April 10 showed only calcite, SiO₂ and calcium silicate phases.

Gas generation from the proximate waste drums (drums 10648022, 10647908, 10647928, and 10647909) were subjected to pressure-temperature experiments, which showed that the high-Be waste sample from Drum 10648022 produced the highest CH₄ concentrations seen in these studies, at around 80%. However, the pressure generated was significantly lower compared to samples from the event drum – a sharp pressure rise was seen about 2 min after the temperature reached 250°C, and finally maximized at about 122 psig about 25 min after the temperature reached 250°C (see Figure 46a). The duplicate from this sample required 10 min at 250°C, and only maximized at 102 psig. When the temperature was dropped to near ambient, the reaction vessel remained significantly pressurized, indicating that a non-condensable gas (CH₄) was now present.

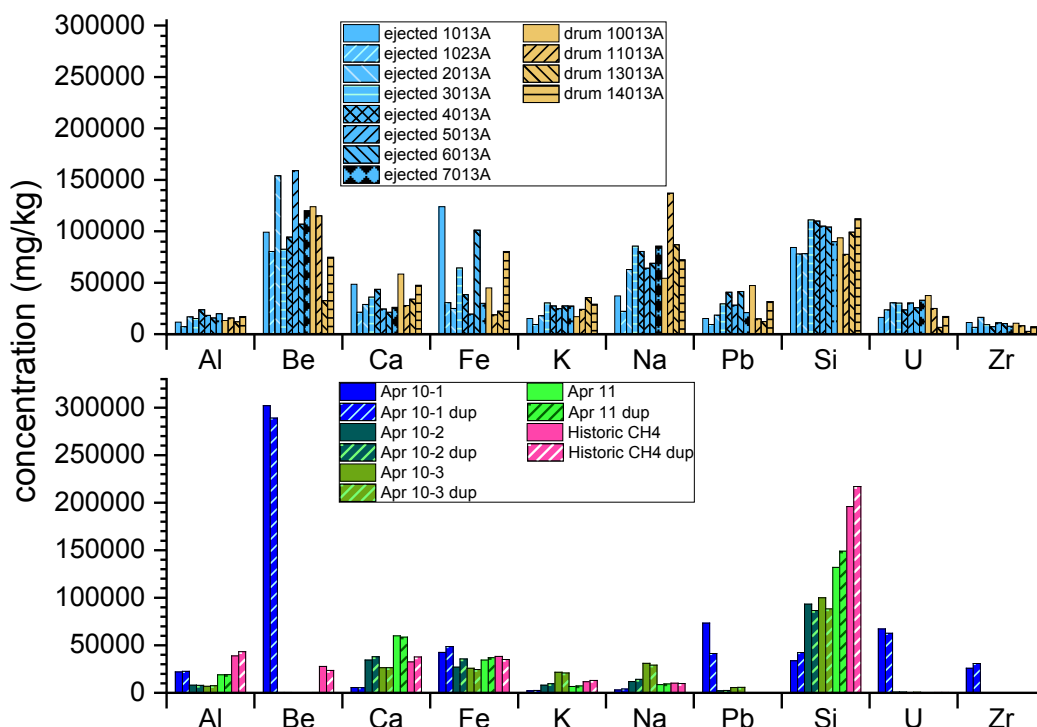


Figure 45. Metal concentrations measured by ICP. Top, samples from the event drum, ejected (blue) and remaining in the drum (gold). Data is the same as that in Figure 14, re-plotted here for comparison with un-ruptured drum samples. Bottom, sample from the high-Be, unruptured drum (blue), low-Be, unruptured drums (green), a historic high CH₄ waste (pink), the sorting table (red), and the transfer tray (purple).

A low Be sample (Drum 10647908) also displayed a pressure increase, albeit somewhat lower than the high Be sample. The two duplicates generated P_{\max} values of 80 and 70 psig, and the CH₄ concentrations were 8% and 2% for these two experiments. When the temperature was decreased back to ambient, the pressure fell to very nearly its original value, indicating that the pressure was due to condensable gases, likely H₂O. These observations indicate the pressure generated is not derived from CH₄.

The lower-than-anticipated pressure rise for the high Be sample (Drum 10648022) is rationalized in terms of limited H₂O present in the sample. It is likely that H₂O principally absorbs into the Micro-Cel E, which is mainly calcium silicate. The elemental analysis of sample from Drum 10648022 has the lowest concentrations Ca and Si of any sample that was analyzed (Figure 46) and thus probably has the lowest capacity for H₂O absorption. The conclusion that H₂O is in sufficient quantity is required for rapid production of CH₄ is in accord with the evacuation, and H₂O addition experiments involving the waste from the event drum, see Section 5.4.2. By way of contrast, sample from Drum 10647908 has Ca and Si concentrations that are on par with the other samples from un-ruptured drums, and with the samples from the event drum. This would enable this sample to absorb H₂O and other fluids, but they do not react because they contain insufficient Be.

The hypothesis that lower-than-anticipated water content might be responsible for the lower pressure increase in the high Be sample from Drum 10648022 was supported by a subsequent experiment in which 50 μ L H₂O was added to a 3 g aliquot, and then subjected to a fast heating ramp. What was observed was a near-vertical pressure rise at 135°C to a $T_{\max} = 275$ psig, more than double the pressure rise that was observed in the experiment conducted without H₂O (see Figure 47). When the heat was stopped, the temperature dropped back to ambient (22°C), but the pressure only fell to 165 psig, signaling that non-condensable gases, i.e. CH₄, had been formed. The analysis of the headspace revealed that it consisted of 73% CH₄.

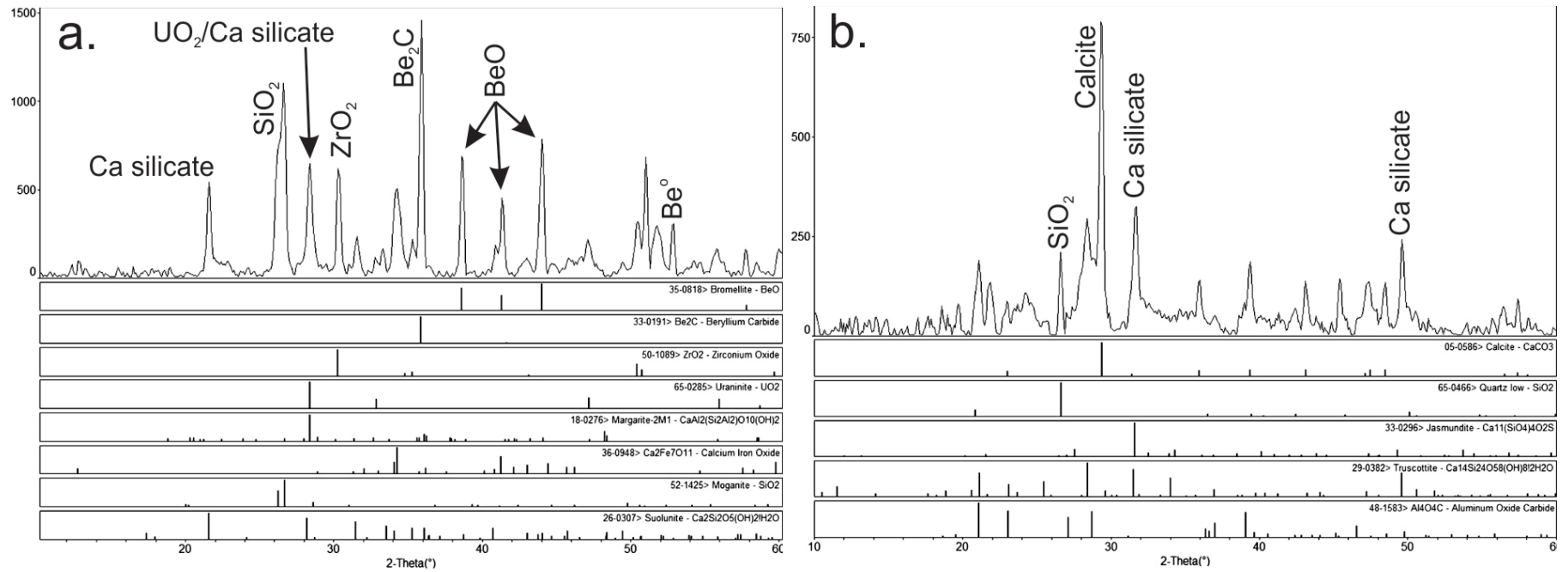


Figure 46. XRD spectra of waste samples from un-ruptured drums that were proximate to the event drum. **a.** April 10 sample from Drum 1. **b.** April 10 sample from Drum 2.

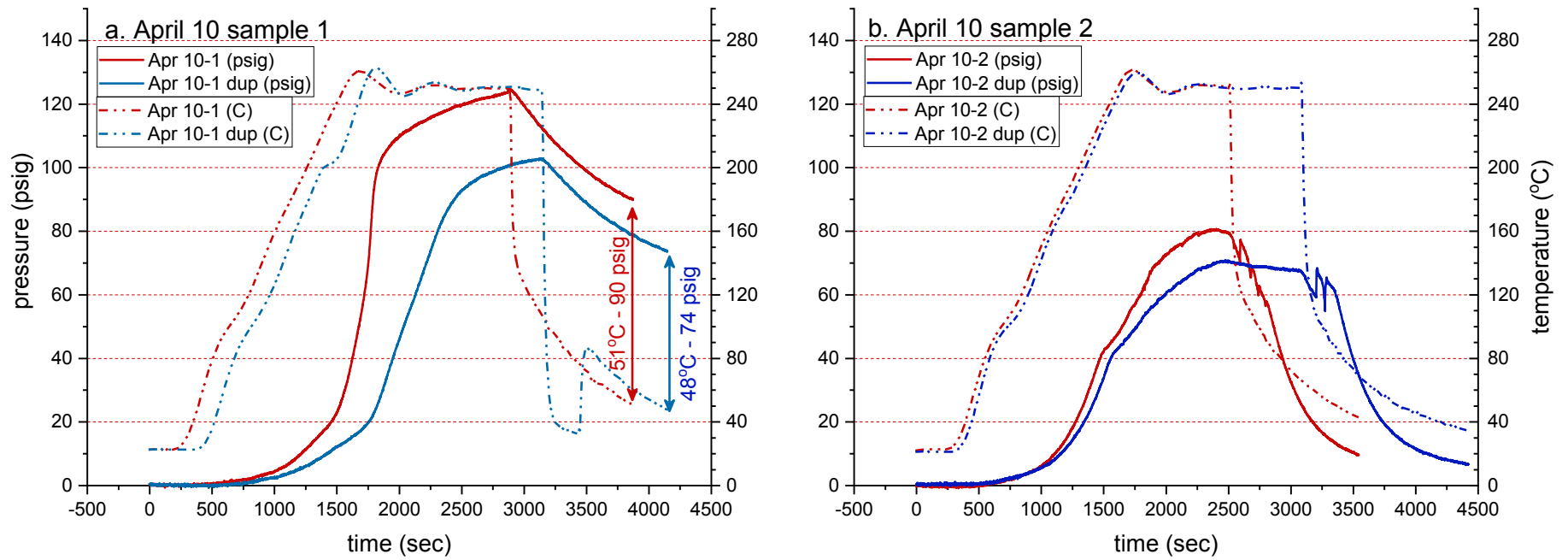


Figure 47. Pressure, temperature vs. time experiments conducted for waste samples from un-ruptured drums processed on April 10.
a. Sample from Drum 10648022, high Be. **b.** Sample from Drum 10647908, low Be.

The quantity of CH₄ generated from heating the sample collected from the first un-ruptured drum processed on April 10 (Drum 10648022) suggested that a significant percentage of the Be was in the form of Be₂C. The pressure-rise of 275 psig (Figure 48) resulted in a Be₂C concentration of 1.2 mol/kg, or 2.5 mol/kg Be as Be₂C. Using the P_{final}, and T_{final} values from the end of the experiment, concentrations of Be₂C and Be as Be₂C were 1.3 and 2.6 mol/kg. The ICP/MS analysis of this sample generated Be concentrations of about 300,000 mg/kg, equivalent to 10 mol Be /kg. Thus, the gas analysis data indicates that about 25-26% of the Be in sample from Drum 10648022 exists as Be₂C.

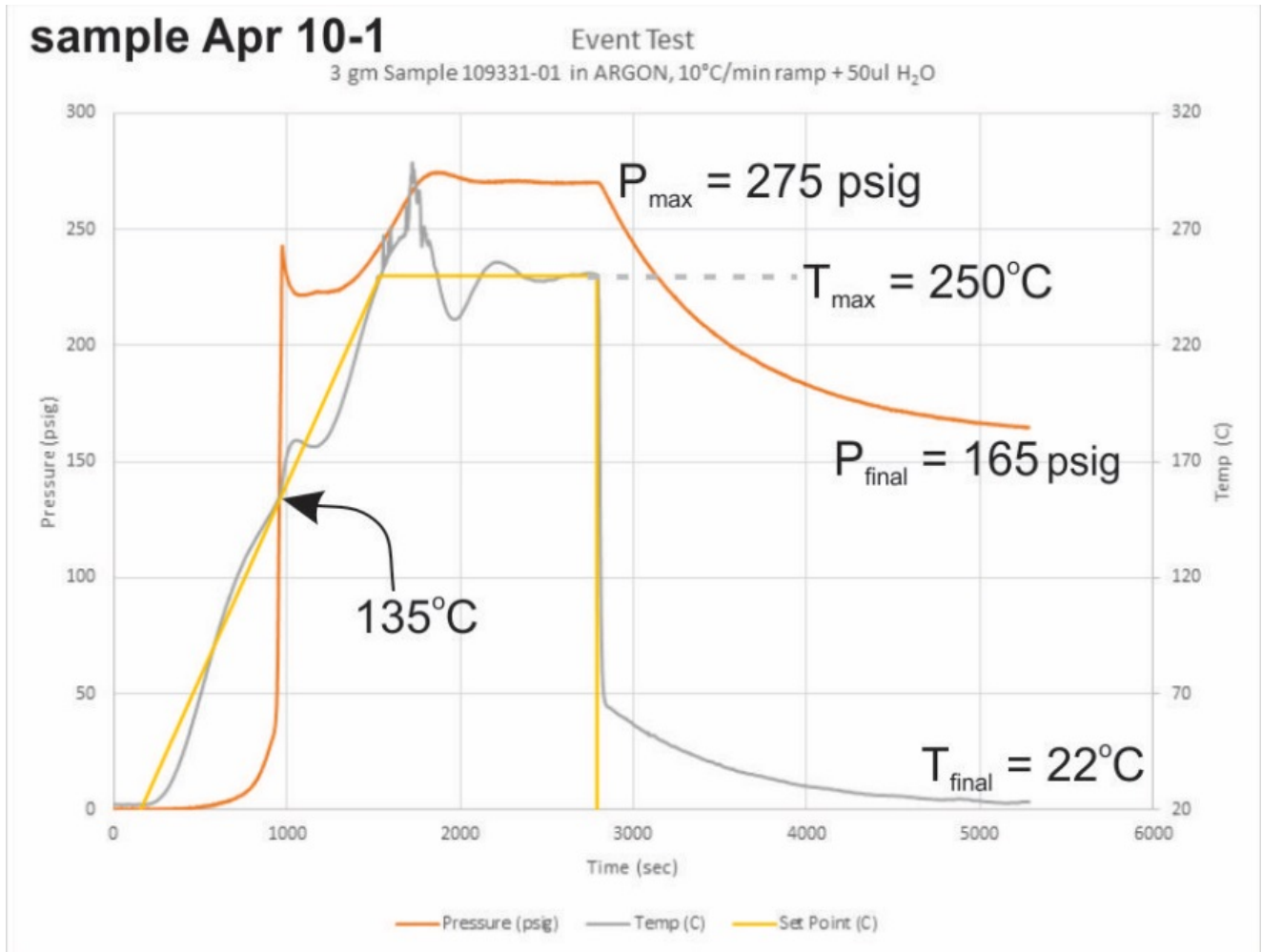


Figure 48. Pressure, temperature vs. time experiment conducted for a 3 g sample of the first un-ruptured drum sampled April 10 (sample from Drum 10648022), subsequent to addition of 50 μL H₂O.

7. LID EJECTION PRESSURES

7.1 Objective and Summary

The objectives and summary of Section 7.0 Lid Ejections Pressures are as follows:

- Determine the pressure required to eject lids given Fluor Idaho's drums and torquing criteria.
 - Empirically determined to be 38-48 psig (Section 5).
- Demonstrate that the reaction mechanism results in pressure exceeding 38-48 psig.
 - Pressure/temperature experiments and modeling demonstrate that pressures can greatly exceed 38-48 psig (Section 5 and Section 6.2.2).
- Determine if methane combustion could have resulted in lid ejections.
 - There is insufficient oxygen to support combustion (Section 6.3).
 - Furthermore, the volatile organic and water content when the drums were originally closed and torque could not generate sufficient pressure due to thermal heating alone.
 - An additional source of gas (i.e. Be_2C hydrolysis) from reactions is required to achieve the pressure mentioned above.

7.2 Fluor Idaho Mechanical Pressurization Testing

7.2.1 Empirical Lid Ejection Pressures

To determine the pressures required to eject the lid and material a test was created to pneumatically pressurize several drums until the drum either vented or the lid ejected. Ten-E Packaging Services was subcontracted to perform the testing at their facility in Minnesota. Sixteen drums were sent equipped with rigid liners, PVC transfer bags, Nucfil filters, lids, and lock rings. Enough Micro-Cel E absorbent was also sent to fill two drums 50% full. All materials came out of the inventory from RWMC. A test matrix was developed with 13 tests each with varying flow rates and the condition that the tests parameters could be changed by engineers depending on the results of previous tests. The tests were performed, and the drum would start to bulge, deform, and then would eventually self-vent at the bolted connection on the lock ring. Venting also occurred at the Nucfil filter on the tests that the filters remained unplugged. If the flow rate entering the drum was greater than the flow rate venting the pressure would increase, the drum would stop self-venting, and shortly thereafter the lid would eject. It is unknown why the drum stops to self-vent before ejecting the lid. Orientation of bung filter and lock ring, torque values, rigid liners and transfer bags, Nucfil filter plugged or unplugged, moisture on gasket and lock ring, and pressurization rate were all parameters that were adjusted during testing.

The empirical pressure testing results are provided in Table 28 As the drums were pressurized, the lids and bottoms of the drums were deformed at pressures between 25 and 30 psig. The lids were ejected from the drums at pressures between 35 and 45 psig.

Table 28. Empirical drum pressure temperature results.

Test	Bung Filter and Lock Ring Orientation	Torque Value	Rigid Liner and PVC Transfer Bag	NucFil Filter Plugged	50% full of surrogate material	Moisture on Gasket and Lock Ring	Did the Drum Burst	Pressurization Rate (SCFM)	Time to Rupture (Min:Sec)	Maximum Pressure Prior to Lid Ejection (psi)	Comments:
1	In-line	55	No	No	No	No	No	20	3:38	36	Vented on Bottom
2	In-line	55	No	No	No	No	No	20	3:53	32	Vented at Ring
3	In-line	55	Yes	No	No	No	No	20	1:29	22	Vented at Ring
4	Offset	55	Yes	Yes	No	No	No	20	1:15	30	Vented at Ring
5	Offset	55	Yes	Yes	No	No	No	25	1:10	42	Vented on Bottom
6	Offset	55	Yes	Yes	No	No	No	No Flow Meter	1:09	44	Vented on Bottom
7	Offset	10	Yes	Yes	No	No	No	No Flow Meter	0:53	33	Vented on Bottom
8	Offset	55	Yes	Yes	Yes	No	No	No Flow Meter	1:06	45	Vented on Bottom
9	Offset	10	Yes	Yes	Yes	No	No	No Flow Meter	0:51	35	
10	Offset	10	Yes	Yes	Yes	Yes	Yes	No Flow Meter	0:37	32	
11	Offset	10	Yes	Yes	No	Yes	Yes	No Flow Meter	2:10	40	
12	Offset	55	Yes	Yes	No	Yes	Yes	No Flow Meter	3:08	52	
13	Offset	55	Yes	Yes	No	No	Yes	No Flow Meter	2:56	46	
14	Offset	55	Yes	No	No	No	No	No Flow Meter	4:30	40	

7.2.2 Waste Mass needed to Eject Drum Lid

Empirical measurements demonstrate that lid ejection occurs at nominally 35 psig. When this pressure is coupled with the empirically determined gas production efficiency, moles gas produced divided by mass tested, (ejected sample material results) the waste mass needed to achieve lid ejection can be estimated. Table 29 shows the results. These estimates are based on a drum fill factor of 45%.

Table 29. Estimated kilograms of waste needed to eject drum lid.

Sample Mass, g	psi	Test °C	Void volume, mL	Moles CH ₄ produced	Production efficiency, moles / g sample	Empirically derived drum target pressure, psi	Required moles to achieve target drum pressure	kg needed to achieve target drum pressure
0.5	22	150	14.4	6.2E-04	1.2E-03	35	7.6	6.1
1	40	150	13.9	1.1E-03	1.1E-03	35	7.6	7.0
2	202	150	12.8	5.1E-03	2.5E-03	35	7.6	3
2	185	165	12.8	4.5E-03	2.2E-03	35	7.6	3.4
3	280	140	11.7	6.6E-03	2.2E-03	35	7.6	3.5
0.5	202	250	14.4	4.6E-03	9.3E-03	35	7.6	0.82
1	128	250	13.9	2.8E-03	2.8E-03	35	7.6	2.7
2	290	250	12.8	5.9E-03	2.9E-03	35	7.6	2.6

The amounts range from < 1kg to 7 kg. As shown in Figure 22, DU can produce sufficient heat to exceed the temperature required to initiate rapid methane generation, 150 to 250°C, and the mass of waste matrix needed, < 1 to 7 kilograms, to eject a drum lid. The thermodynamic modeling supports the empirical observations of localized heating and that localized heating is sufficient to eject a drum lid.

7.3 Combustion versus Over-pressurization

7.3.1 Bulging Lids

The first responders reported bulged lids in addition to a lid that was ejected. Based on the empirical testing lid bulging occurred at approximately 25-30 psig.

7.3.2 Combustion and Limiting Oxygen Concentration

The increased pressure in the drums causing the drums lids and bottoms to bulge was due to methane generation from beryllium carbide hydrolysis. The generation of methane would have diluted the concentrations of the head-space gases (oxygen) initially in the drum after it was closed by the operators. The oxygen concentration in the drums at the point the lids and bottoms began to bulge can be estimated by applying ideal gas pressure relations to the initial concentration.

Using the low end of the deformation range (25 psig), the pressure in the drum increased by a conservative factor of,

$$(14.7 + 25) / 14.7 = 2.7 \quad (10)$$

The initial oxygen concentration in the drum is assumed to be equal to the typical atmospheric concentration, 21%. As the pressure in the drum increased, the concentration of the oxygen decreased due to the accumulation of the generated methane. The decrease would be inversely proportional to the pressure increase. Thus, the concentration at the point of bulging would have been,

$$21\% / 2.7 = 7.8 \% \quad (11)$$

This is a conservative (high) estimate. Analysis of the head-space gas samples taken from the methane producing drums yielded oxygen contents in the drums ranged from 16.1 to 20.6%. These values are below the atmospheric concentration of 21%. In addition, this provides no credit for displacement of the oxygen through the filter vent.

The limiting oxygen concentration (also known as the minimum oxygen concentration) required to support methane combustion is 12%. Below this concentration, methane combustion is not possible. The oxygen concentration in the bulged drum was conservatively estimated to be 7.8%, well below that required to support combustion. Thus, the lids were ejected from the drum strictly due to methane generation and subsequent over-pressurization, not combustion of the accumulated methane.

7.3.3 Sympathetic Deflagration

Sympathetic deflagration was discussed and dismissed. Drum 10648033, the only drum which experienced a significant thermal event, was physically pulled away from the adjacent drums. The distance was too great to result in a sympathetic deflagration of the other three event drums.

8. ACCEPTABLE KNOWLEDGE EVALUATION OF BERYLLIUM CARBIDE AND DEPLETED URANIUM

The acceptable knowledge (cumulative technical information derived from process knowledge and historical records) record was evaluated to identify the source of the beryllium carbide and DU

8.1 Beryllium Carbide

It is believed that the beryllium carbide was generated at the Rocky Flats Plant. The Rocky Flats Plant converted commercial grade, scrap beryllium, originally made by powder-metallurgy techniques, into ingot sheets and usable shapes using vacuum-induction casting in graphite molds and crucibles. The following is reproduced from Acceptable Knowledge document RF-P244 concerning Ingot-Sheet Beryllium Fabrication at Rocky Flats: "Graphite molds and crucibles were used. Because molten beryllium reacts with carbon, all graphite surfaces that contacted the beryllium received a protective coating. Crucibles and molds were given a hand-rubbed coating of a beryllium-beryllium sulfate (Be-BeSO_4) wash and baked at 1450°C for 30 minutes. The crucible received a spray coating of the wash on the internal surfaces, the pour-hole mold crucible interface, and stopper rod. Molds were not spray-coated because a protective film of Be_2C is formed during the initial baking, which prevents further reaction. After use, both the mold and crucible should be cleaned thoroughly and the crucible recoated, as described earlier"³⁴. This process is the most likely source of the beryllium carbide.

8.2 Depleted Uranium-Building 444

It is believed that the DU was also generated at the Rocky Flats Plant. As discussed, Drum 10595963 appeared to contain floor sweepings with dense specks throughout the drum. It is now known that the reacted drums material contained numerous and varied metal turnings and fines. This is consistent with floor sweepings. It is believed that Rocky Flats Building 444 was the source. B44 or B444 was built in 1953 and was a beryllium and depleted uranium manufacturing foundry and assembly facility. The building purpose was beryllium and uranium component assembly; assembly/disassembly area for non-fissile parts; machining of DU and beryllium; component coating facility; support for Building 707 and 460; and support for tooling; grinding, and carbon molds.

8.2.1 Trough Processing/Mixing

Based on the chemical analysis results for DU in the reacted drums and radioassay results from the parent drums, additional waste co-mingling occurred more than that represented above in Figure 13. It is believed that the DU contained in Drum 10595963 was dispersed into each of the four reacted drums.

9. CONCLUSION

9.1 Reaction Summary

An oxidation reaction, initiated during repackaging, involving DU generated sufficient heat to accelerate the hydrolysis of beryllium carbide yielding methane gas and internal pressure sufficient to eject the drum lids and expel a portion of the drum contents.

This is shown graphically in Figure 49.

ARP-V Drum Event - 4/11/18

106

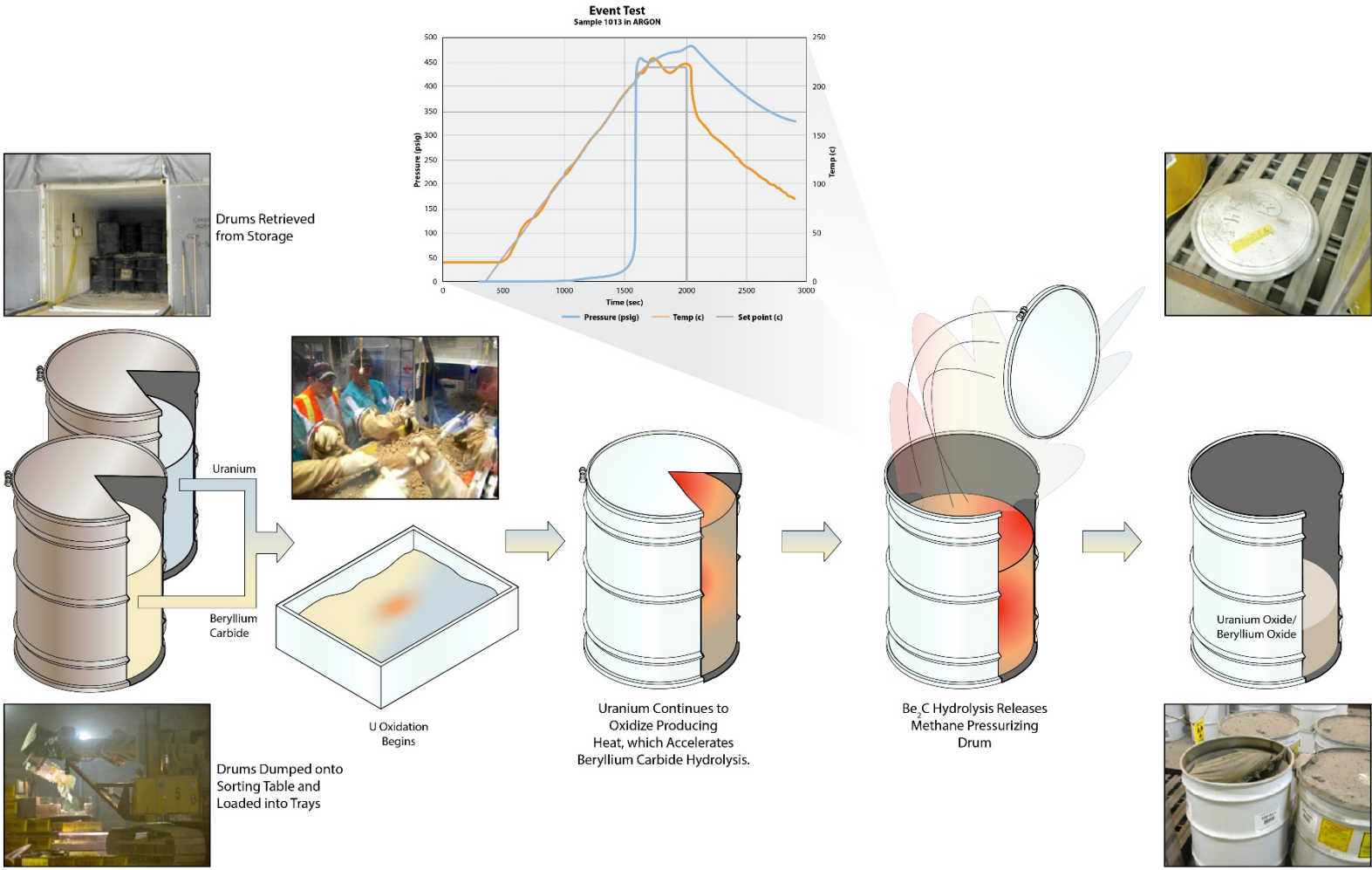


Figure 49. ARP V drum event reaction summary.

10. RECOMMENDATIONS

In many cases, determining when conditions exist for an adverse chemical reaction (i.e. undesirable or uncontrolled reaction) requires an understanding beyond the knowledge that two potentially reactive chemicals co-exist within the same drum. For example, given the conclusions reached in this report, DU accelerated the hydrolysis of beryllium carbide, consider the analytical results for beryllium and uranium reported in Table 30 from the repackaged drums.

Table 30. Measured beryllium and DU.

55-gallon Drum	DU (mg/kg)	Beryllium (mg/kg)
Drum 1	37,500	124,000
Drum 2	67,300	302,000
Drum 3	24,900	115,000
Drum 4	6,520	32,600
Drum 5	17,100	74,700

After repackaging, four of the drums in Table 27 experienced adverse chemical reactions and ejected their lids while one did not. Drum 2 did not react even though it had both the highest concentration of beryllium and DU. Predicting which drums will or will not react is not achievable with the information provided in Table 30. However, ensuring engineered controls described in the paragraph below can ensure that DU has been oxidized prior to packaging.

Readers familiar with working electrical systems know that prior to handling potentially live wires, even after a lockout/tagout has been performed, a zero-energy verification is required. In an analogous fashion, prior to physical handling/packaging of uranium or other potentially reactive metals, a “zero energy verification” is recommended. When choosing between an administrative control or an engineered control the preferred choice is an engineered control. The practice recently instituted at Fluor Idaho to remotely thoroughly rake, hold for 24 hours, and thermally monitor prior to packaging uranium-bearing waste and other reactive metal-bearing waste provides an engineered control to allow an oxidation-state check, i.e., a zero-energy verification. It is recommended that an analogous practice be implemented in all locations in which waste that contains potentially-reactive metals are processed.

11. REFERENCES

1. RPT-TRUW-91, *Acceptable Knowledge Document for Pre-1980 INL Exhumed Waste*
2. RPT-TRUW-05, *Waste Matrix Code Reference Manual*
3. SPR-252, *Sampling and Analysis Protocol for Investigation fo the ARP V Drum Incident.*
4. EFP-MISC-1386, *ARP-V Drum Incident Bulk Sampling, Transportation, and Analysis Plan.*
5. EFP-MISC-1388, *ARP-V Drum Incident Cleanup Monitoring Plan.*
6. EPA-600/2-80-076, *A Method for Determining the Compatibility of Hazardous Wastes.*
7. Epstein, M., Luangdilok, W., Plys, M. G., Fauske, H. K., On Prediction of the Ignition Potential of Uranium Metal and Hydride, *Nuclear Safety*, 37, 12-25 (1996).
8. Baker, M. McD, Less, L. N., Orman, S., Uranium + water reaction. Part 1.—Kinetics, products and mechanism, *Transactions of the Faraday Society*, 62, 2513-2524 (1966).
9. Baker, M. McD, Less, L. N., Orman, S., Uranium + water reaction. Part 2.—Effect of oxygen and other gases, *Transactions of the Faraday Society*, 62, 2525-2530 (1966).
10. McGillivray, G. W., Geeson, D. A., Greenwood, R. C., Studies of the kinetics and mechanism of the oxidation of uranium by dry and moist air A model for determining the oxidation rate over a wide range of temperatures and water vapour pressures, *Journal of Nuclear Materials*, 208, 81-97 (1994).
11. Totemeier, Terry C., A Review of the Corrosion and Pyrophoricity Behavior of Uranium and Plutonium, Argonne National Laboratory-West, Idaho Falls, ID 83402, ANL/ED/95-2, 1995.
12. Ritchie, A. G., A review of the rates of reaction of uranium with oxygen and water vapour at temperatures up to 300°C, *Journal of Nuclear Materials*, 102, 170-182 (1981).
13. Ritchie, A. G., The kinetics of the initial stages of the reaction of uranium with oxygen, *Journal of the Less Common Metals*, 98, 193-214 (1984).
14. Sladky, R. E., An Ellipsometric Study of the Corrosion of Uranium and Uranium-7.5 Weight Percent Niobium-2.5 Weight Percent Zirconium Alloy, Union Carbide Corporation Nuclear Division, Oak Ridge Y-12 Plant, Oak Ridge, TN, Y-1829, 1972.
15. Larson, D. T., Taylor, N. W., Ellipsometer Studies on the Cleaning and Oxidation of Uranium, The Dow Chemical Company, Rocky Flats Division, Golden, CO, RFP-674, 1966.
16. Haycock, E. W., Transitions from Parabolic to Linear Kinetics in Scaling of Metals, *Journal of The Electrochemical Society*, 106, 771-775 (1959).
17. Lories, J., *C. R. Acad. Sci., Ser. A*, 234, 91 (1952).
18. Baker, L., Bingle, J. D., The kinetics of oxidation of uranium between 300 and 625°C, *Journal of Nuclear Materials*, 20, 11-21 (1966).

19. Schnizlein, J.G., Pizzolato, P.L., Porte, H.A., Bingle, J.D., Fischer, D.F., Mishler, L.W., Vogel, and R.C., Ignition Behaviour and Kinetics of Oxidation of the Reactor Metals, Uranium, Zirconium, Plutonium, and Thorium, and Binary Alloys of Each, Argonne National Laboratory, Chicago, IL, Technical Report ANL-5974, 1959.
20. Baker, L., Schnizlein, G., Bingle, J. D., The Ignition of Uranium, *Journal of Nuclear Materials*, 20, 22-38 (1966).
21. Abrefah, J., Huang, F. H., Gerry, W. M., Gray, W. J., Marschman, S. C., Thornton, T. A., Analysis of Ignition Testing on K-West Basin Fuel, Pacific Northwest National Laboratory, Richland, WA, PNNL-11816, UC-602, 1999.
22. Plys, M. G., Epstein, M., Malinovic, B., Uranium Pyrophoricity Phenomena and Prediction, Hanford Spent Nuclear Fuel Project, Burr Ridge, IL, Inc. Fauske & Associates, SNF-6192-FP, 2000.
23. Tetenbaum, Marvin, Mishler, Larry, Schnizlein, Glenn, Uranium Powder Ignition Studies, *Nuclear Science and Engineering*, 14, 230-238 (1962).
24. Weakley, E. A., Interim Report on Concreted Uranium Fines and Chips Billet Curing Tests -- A Basis for Resuming Shipment of Concreted Uranium Scrap Billets, United Nuclear Industries, Inc, Hanford, WA, UNI-1454, 1980.
25. Wood, David H., Snowden, Sharon A., Howe, Harry J., Lee Thomas, L., Moon, Donald W., Gregg, Hugh R., Miller, Philip E., Regarding the chemistry of metallic uranium stored in steel drums, *Journal of Nuclear Materials*, 209, 113-115 (1994).
26. Taylor, Christopher D., Lookman, Turab, Lillard, R. Scott, Ab initio calculations of the uranium–hydrogen system: Thermodynamics, hydrogen saturation of α -U and phase-transformation to UH₃, *Acta Materialia*, 58, 1045-1055 (2010).
27. Winer, K., Colmenares, C. A., Smith, R. L., Wooten, F., Interaction of Water-Vapor with Clean and Oxygen-Covered Uranium Surfaces, *Surface Science*, 183, 67-99 (1987).
28. Ritchie, A. G., The kinetics and mechanism of the uranium-water vapour reaction — an evaluation of some published work, *Journal of Nuclear Materials*, 120, 143-153 (1984).
29. Wilkinson, Walter D., *Uranium Metallurgy*, Interscience Publishers, New York (1962).
30. Solbrig, C. W., Krsul, J. R., Olsen, D. N., Pyrophoricity of Uranium in Long-Term Storage Environments, Argonne National Laboratory, Idaho Falls, ID, 1994.
31. 18-MN10228, *Pneumatic Rupture Test, 55 Gallon Open Head Skolnik Drum*, TEN-E Packaging Services, Inc., Newport, MN, contracted by Fluor Idaho (2018).
32. Murbach, E.W., The Chemical Reactivity of Uranium Carbide, Atomic International, NAA-SR-11235, June 30, 1965.
33. Bradley, M. J., and Ferris L. M., Hydrolysis of Uranium Carbides between 25 and 100° I. Uranium Monocarbide, *Inorganic Chemistry*, Vol. 1, No. 3, August, 1962, pp683-7; S. Evered, F.H. Pollard and G.Nickless, Part II: The Hydrolysis of Uranium Carbides, *J.Chromatography*, 15 (1964) 223-227; L.J.Colby,JR, Kinetics of the Reaction of Uranium Monocarbide with Water, *J. Less-Common Metals*, 10 (1966) 425-431; A. Schürenkämper, Uranium Monocarbide in the temperature Range 30°C -90°C, *J.inorg. nucl. Chem.*, 1970 Vol 32 pp 417 to 429.

34. Frankeny, J. L., and Floyd, D.R., RF-P244 Ingot-Sheet Beryllium Fabrication, Document Number RFP-901 Revision NA, February 9, 1968.
35. Hartman, I., Nagy, J., and Jacobson, M., "The Explosive Characteristics of Titanium, Zirconium, Thorium, Uranium, and their Hydrides," U.S. Bureau of Mines, Report of Investigation 4835, U.S. Department of the Interior, December 1951.
36. Frost, B. R. T., The Carbides of Uranium, *Journal of Nuclear Materials*, 10, 265-300 (1963).
37. Gasparinni, Claudia, Podor, Renaud, Horlait, Denis, Rushton, Michale J. D., Fiquet, Olivier, Lee, William Edward, Oxidation of UC: An in situ high temperature environmental scanning electron microscopy study, *Journal of Nuclear Materials*, 494, 127-137 (2017).
38. Le Guyadec, F., Genin, X., Bayle, J. P., Dugne, O., Duhart-Barone, A., Ablitzer, C., Pyrophoric behaviour of uranium hydride and uranium powders, *Journal of Nuclear Materials*, 396, 294-302 (2010).
39. Berthinier, C., Coullomb, S., Rado, C., Blanquet, E., Boichot, R., Chatillon, C., Experimental study of uranium carbide pyrophoricity, *Powder Technology*, 208, 312-317 (2011).
40. Storms, E. K., Beryllium Carbide, in J.J. Zuckerman and Hagen, A. P., *Inorganic Reactions and Methods*, Ed., 1991, 302.
41. Kosolapova, T. Y., Chapter VIII, Chemical Properties of Carbides, in *Carbides: Properties, Production, and Applications*, Ed., Springer-Verlag, New York, 1971.
42. Reed, S. A., Funston, E. S., Bridges, W. L., Analysis of Beryllium Carbide, *Analytica Chimica Acta*, 10, 429-442 (1954).
43. Bridges, W. L., Funston, E. S., Reed, S. A. , Methods for the Analysis of Beryllium Carbide, Fairchild Engine and Airplane Corporation, NEPA Division, Oak Ridge, TN, Fairchild Engine and Airplane Corporation, NEPA-940-SCR-40, 1949.
44. Neely, J. J., Teeter, Jr., C. E., Trice, J. B., Thermal Conductivity and Heat Capacity of Beryllium Carbide, *Journal of the American Ceramic Society*, 33, 363-364, (1950).

Appendix A
Chemical Compatibility

Appendix A

Chemical Compatibility

A-1 Metals

Most chemical evaluations consider components of the waste less than 1% to be trace or insignificant. However, for this evaluation metals with a mass percentage equal to or greater than 0.1% by mass are evaluated. Metals with a mass concentration of less than 0.1% are assumed to be insignificant and are not evaluated due to their low percentage in the waste. Non-detects are not discussed.

The metals assigned to be insignificant based on a mass concentration of less than 0.1% are:

Antimony	Lanthanum	Silver	Vanadium
Arsenic	Lithium	Strontium	Yttrium
Barium	Manganese	Thallium	
Bismuth	Molybdenum	Thorium	
Cadmium	Nickel	Tin	
Cobalt	Selenium	Titanium	

The remaining elements were assigned a RGN.

To perform a bounding evaluation, the analytical results are reported as if the metal constituents are in an elemental form. In the vast majority of instances, the elements are in a compound form and not elemental. Table A-1 lists elements, their various uses, the average percentages found in analysis, assigned RGNs, and a chemical/reactivity evaluation. The evaluation in Table A-1 is not intended to be a final representation of the constituents involved in the lid ejection event but provides background and basis for a final compatibility evaluation. Table A-3 aligns the assigned RGNs to demonstrate possible incompatible materials and potential reactions. Note that the concentration column distinguishes values measured for samples that were ejected from the drums and from samples that were collected from within the drums. Table A-2 lists incompatible RGNs and evaluates the possible incompatibility.

A-1.1 Organics

The data from the organic analysis of the incident drums and ejected material were also measured following approved laboratory protocols at both Southwest Research Institute Laboratories and Savannah River National Laboratory. The results are listed in the following table as a weight percent of the waste. Consideration must be given to the interpretation of the organic analysis results. The original organic chemical concentration in the waste matrix is unknown. It is assumed the original organic concentration would have been greater prior to lid ejection than that found during analysis, i.e., post reaction. To facilitate the review, sample concentrations are reported for both the ejected material and from the drum samples as appropriate. The organic compounds concentrations are well below 1% and are normally considered trace insignificant. Since this evaluation is to assess possible problem constituents, all measured analytes are reported. After analysis, the compounds were assigned RGNs based on the same protocols used for the metals analysis.

The data for the tentatively identified compounds (TIC) contains numerous alkanes, alkenes, alcohols, and unknown phthalates. Phthalates, alcohols and alkanes are considered due to their presence as identified compounds. An additional class, identified as alkenes, was added. The estimated concentrations demonstrated by the TICs are similar to the concentrations of the known analytes with the exception of alkanes and alkenes. The alkanes and alkenes could be present in greater concentrations (a hydrocarbon hump observed in the semi volatile chromatogram). Even if not uniquely identified, TIC compounds may have participated in the WMF-1617 (ARP V) drum incident.

After the tables, the results will be discussed and an evaluation made.

A-1.2 Chemical Material of Concern Evaluation

Table A-1. Chemicals/Materials of Concern.

Chemical/ Material	Use/Description/Location (AK Source)	Concentration (% by mass)	RGN	Chemical/Material Evaluation
1-butanol	Also known as n-butyl alcohol. Found in drum incident analysis.	Ejected 2.03E-4%	4	With a sufficient quantity, this compound could have participated in the WMF-1617 (ARP V) drum incident.
2,4-dimethylphenol	Found in drum incident analysis.	Ejected 6.68E-5%	31	With a sufficient quantity, this compound could have participated in the WMF-1617 (ARP V) drum incident.
4-methy-2-pentanone	Also known as methyl isobutyl ketone (MIK). Found in drum incident analysis.	Ejected 9.10E-6%	19	With a sufficient quantity, this compound could have participated in the WMF-1617 (ARP V) drum incident.

Table A-1. (continued).

Chemical/ Material	Use/Description/Location (AK Source)	Concentration (% by mass)	RGN	Chemical/Material Evaluation
acetone	<p>Found in drum incident analysis.</p> <p>Plutonium fabrication.</p> <p>Beryllium fabrication.</p> <p>Research and development including plating, inertial confinement fusion microshaping.</p> <p>Analytical laboratory extractant, cleaning agent, scintillation cocktail component, and solvent.</p> <p>Mixed with oils used in depleted uranium machining.</p> <p>Component of Aquastar Coulometric Titrator.</p> <p>Homogeneous solids sampling and analysis of organic setups was previously conducted by both the Rocky Flats and INL 3,100 M3 TRU Waste Programs. Based on the analytical data from both programs, the maximum concentration measured was less than 10 ppm.</p>	<p>Ejected 2.2E-4%</p> <p>Drum 3.3E-5%</p>	19	<p>With a sufficient quantity, this compound could have participated in the WMF-1617 (ARP V) drum incident.</p>
acetophenone	<p>Found in drum incident analysis.</p>	<p>Ejected 1.26E-4%</p>	19	<p>With a sufficient quantity, this compound could have participated in the WMF-1617 (ARP V) drum incident.</p>

Table A-1. (continued).

Chemical/ Material	Use/Description/Location (AK Source)	Concentration (% by mass)	RGN	Chemical/Material Evaluation
alkanes and alkenes	TICs found in drum incident analysis	Volatile Ejected 5.23E-5% Volatile Drum 1.91E-5% Semi-VOA Ejected 3.39E-4% Semi-VOA Drum 1.90E-4%	28, 29	With a sufficient quantity, these compounds could have participated in the WMF-1617 (ARP V) drum incident.
aluminum	Scrap, machined parts, turnings, and reagents	Ejected 1.5% Drum 1.4%	22, 23	<p>Aluminum does not exist in the native form in nature. Exposure to oxygen forms a passivation layer making aluminum chemically resistant to further corrosion or chemical interactions. It is rapidly oxidized by water above 180°C, generating hydrogen gas. Finely divided powder can ignite violently. Due to the expected passivation layer, aluminum most likely did not initiate the incompatible reaction in the WMF-1617 (ARP V) drum incident.</p> <p>Aluminum hydride is not in this waste because synthesis would require unstable chemicals or extreme conditions. Aluminum hydride would also react with moisture in the air, preventing it from persisting during waste storage conditions.</p>

Table A-1. (continued).

Chemical/ Material	Use/Description/Location (AK Source)	Concentration (% by mass)	RGN	Chemical/Material Evaluation
benzene	<p>Found in drum incident analysis.</p> <p>Plutonium fabrication including ultrasonic testing.</p> <p>Analytical laboratory solvent for depleted uranium and beryllium analyses, standards.</p> <p>Present in oils used in the Vacuum Accumulators in Building 776.</p> <p>Homogeneous solids sampling and analysis of organic setups was previously conducted by both the Rocky Flats and INL 3,100 M3 TRU Waste Programs. Based on the analytical data from both programs, the maximum concentration measured was 5 ppm.</p>	Drum 1.95E-5%	16	With a sufficient quantity, this compound could have participated in the WMF-1617 (ARP V) drum incident.
benzoic acid	Found in drum incident analysis.	Ejected 3.31E-4%	3	With a sufficient quantity, this compound could have participated in the WMF-1617 (ARP V) drum incident.

Table A-1. (continued).

Chemical/ Material	Use/Description/Location (AK Source)	Concentration (% by mass)	RGN	Chemical/Material Evaluation
beryllium	Alloys, machined parts, turnings, and reagents	Ejected 10.3% Drum 9.3%	24	<p>Passivation layer makes beryllium chemically resistant below 1000°C. Once ignited, beryllium will combust to form beryllium oxide and beryllium nitride. Beryllium is also non-sparking. Mechanical agitation of the waste would not produce a spark and lead to an incompatible reaction. Due to the elevated temperature required for ignition, it is unlikely beryllium initiated the incompatible reaction in the WMF-1617 (ARP V) drum incident.</p> <p>Beryllium hydride is not in this waste because synthesis would require unstable chemicals or extreme conditions. Beryllium hydride could persist in the waste if already present. Since the only documented use is as an experimental rocket fuel, it is very unlikely beryllium hydride is in the waste.</p>
bis(2-ethylhexyl) phthalate	Found in drum incident analysis.	Ejected 2.56E-3% Drum 3.26E-4%	13	With a sufficient quantity, this compound could have participated in the WMF-1617 (ARP V) drum incident.
butylbenzylphthalate	Found in drum incident analysis.	Ejected 7.67E-5%	13	With a sufficient quantity, this compound could have participated in the WMF-1617 (ARP V) drum incident.

Table A-1. (continued).

Chemical/ Material	Use/Description/Location (AK Source)	Concentration (% by mass)	RGN	Chemical/Material Evaluation
calcium	Used in the plutonium purification process.	Ejected 3.6% Drum 4.37%	21, 105, 107	<p>Calcium reacts with air to form a passivation oxide-nitride layer. It will react with moisture to form calcium hydroxide and hydrogen gas. Finely divided powder will ignite in air. It may combust or explode upon heating. Calcium may be stored at room temperature in dry air (less than 30% relative humidity). Depending on storage conditions, it is unlikely but possible that calcium metal could have survived in the waste until recent activities with the WMF-1617 (ARP V) drum incident. Even though the exact source of the waste is unknown, the processes that employed calcium metal used it as a reducing agent for plutonium salts. This reaction consumed the calcium, leaving oxidized calcium slag. If any survived the process, the slag was leached to reclaim any plutonium. The leaching process would then consume the remaining calcium.</p> <p>After analysis of the waste, it appears that the ratio of fluoride ions to calcium ion is consistent enough to determine the source of calcium is calcium fluoride and did not contribute to the WMF-1617 (ARP V) drum incident.</p> <p>Calcium hydride is not in this waste because synthesis would require elemental calcium, hydrogen gas, and high temperatures. Calcium hydride would also react with moisture in the air, preventing it from persisting during waste storage conditions.</p>

Table A-1. (continued).

Chemical/ Material	Use/Description/Location (AK Source)	Concentration (% by mass)	RGN	Chemical/Material Evaluation
carbon dioxide	Found in drum incident analysis.	Ejected (22°C) 0.40% Ejected (50°C) 4.44% Drum (22°C) 0.08% Drum (50°C) 0.68%	N/A	All values measured are > the atmospheric concentration of 0.04%. The source of the carbon dioxide is currently under investigation. Under most circumstances, carbon dioxide behaves as an inert gas. It may not have initiated a chemical reaction, but can be the end product of many reactions. Heating it may cause pressurization. In this specific incidence, percentages are given by volume.
carbon tetrachloride	Found in drum incident analysis. Used in lathe coolant and for large scale cleaning and degreasing of parts Used as a laboratory solvent, titration component, and present in solutions analyzed, and present in waste standards in the analytical laboratories.	Ejected 1.4E-5%	17	With a sufficient quantity, this compound could have participated in the WMF-1617 (ARP V) drum incident.
chloride anion	Found in drum incident analysis	Ejected 0.52% Drum 3.1%	N/A	The source of the chloride anion in the analysis could be due to halogenated organics or inorganic chloride salts. Halogenated organics are discussed elsewhere in this document. The chloride anion formed simple salts in the waste and are covered in the discussion of RGN 24, for toxic metals. Any reactions involving the chloride anion have already occurred, and the anion will not contribute to any further reactions.

Table A-1. (continued).

Chemical/ Material	Use/Description/Location (AK Source)	Concentration (% by mass)	RGN	Chemical/Material Evaluation
chloroform	<p>Found in drum incident analysis.</p> <p>Coulometric titration and uranium and beryllium analysis and present in samples and standards used in the analytical laboratories.</p> <p>Used for cleaning samples and parts.</p> <p>Present in oils used in the Vacuum Accumulators in Building 776.</p> <p>Component of Karl Fischer reagent.</p> <p>Homogeneous solids sampling and analysis of organic setups was previously conducted by both the Rocky Flats and INL 3,100 M3 TRU Waste Programs. Based on the analytical data from one or both programs, the UCL90 exceeded the RTL.</p>	Ejected 5.56E-5%	17	<p>With a sufficient quantity, this compound could have participated in the WMF-1617 (ARP V) drum incident.</p>
copper	Scrap, machined parts, turnings, and reagents	Ejected 0.36% Drum 0.38%	23, 24	<p>Copper reacts with atmospheric oxygen to form a passivation layer. Finely divided powder is combustible. It is unlikely that copper initiated the incompatible reaction in the WMF-1617 (ARP V) drum incident.</p> <p>Copper hydride will not persist in the waste because it decomposes at temperatures above -60oC.</p>

Table A-1. (continued).

Chemical/ Material	Use/Description/Location (AK Source)	Concentration (% by mass)	RGN	Chemical/Material Evaluation
diethylphthalate	Found in drum incident analysis.	Ejected 3.78E-4%	13	With a sufficient quantity, this compound could have participated in the WMF-1617 (ARP V) drum incident.
di-n-butylphthalate	Found in drum incident analysis.	Ejected 5.36E-5%	13	With a sufficient quantity, this compound could have participated in the WMF-1617 (ARP V) drum incident.
di-n-octylphthalate	Found in drum incident analysis.	Ejected 8.06E-4% Drum 1.86E-4%	13	With a sufficient quantity, this compound could have participated in the WMF-1617 (ARP V) drum incident.
fluoranthene	Found in drum incident analysis.	Ejected 5.06E-5%	16	With a sufficient quantity, this compound could have participated in the WMF-1617 (ARP V) drum incident.
fluoride anion	Found in drum incident analysis.	Ejected 3.0% Drum 3.7%	15	The presence of the fluoride anion corresponds to the inorganic salt, calcium fluoride. The fluoride anion will be unavailable for further reactions and would not have initiated the WMF-1617 (ARP V) drum incident.
iron	Scrap, machined parts, turnings, and reagents	Ejected 5.6% Drum 4.4%	23	Reacts with air to oxidize. It will not form a passivation layer, and will eventually be consumed. Finely divided powder is pyrophoric. Materials that spark do so when the particle size is small enough to react with pyrophoricity, or when the particle of material has absorbed enough energy through mechanical means, most likely friction, to combust. Particles created during the process of grinding or machining that do not spark, are large enough to not demonstrate the characteristics of pyrophoric fines. Fines may still be combustible. Iron hydride will not persist in the waste because it decomposes at ambient conditions.

Table A-1. (continued).

Chemical/ Material	Use/Description/Location (AK Source)	Concentration (% by mass)	RGN	Chemical/Material Evaluation
lead	Shielding, scrap, machined parts, turnings, and reagents	Ejected 2.4% Drum 2.4%	23, 24	Lead reacts with air to form a passivating oxide layer, preventing further reactions. Finely divided lead is pyrophoric and will react immediately. The passivation layer, formed on other lead particle sizes, make it unlikely that lead initiated the WMF-1617 (ARP V) drum incident. Lead hydride is an unstable colorless gas that will not be in the waste because of the difficulty of synthesis and ease of decomposition.
magnesium	Used in metal purification.	Ejected 0.57% Drum 0.63%	21, 22	Reacts with air to form a passivating oxide layer. In water, magnesium reacts to form hydrogen gas. This reaction occurs faster at higher temperatures. Finely divided powder is pyrophoric. It is unlikely that magnesium initiated the WMF-1617 (ARP V) drum incident, because of the passivation layer and the possibility of reacting with atmospheric moisture over the years of storage. If magnesium survived storage, it could have contributed to the reaction after initiation. Magnesium hydride is not in this waste because synthesis would require unstable chemicals or extreme conditions. It will also react with moisture and decompose into hydrogen gas and magnesium hydroxide, preventing magnesium hydride from persisting in storage conditions.
m-cresol and p-cresol	Found in drum incident analysis.	Ejected 1.52E-4%	31	With a sufficient quantity, this compound could have participated in the WMF-1617 (ARP V) drum incident.

Table A-1. (continued).

Chemical/ Material	Use/Description/Location (AK Source)	Concentration (% by mass)	RGN	Chemical/Material Evaluation
methane	Found in drum incident analysis.	Ejected (22°C) 0.35% Ejected (20°C) 4.92% Drum (22°C) 0.06% Drum (50°C) 0.69%	29	The source of the methane is currently under investigation. It has a severe fire and explosion hazard, and form an explosive mixture with air (5-15% by volume). The autoignition temperature is 537°C. Methane can be the byproduct of some chemical reactions. Heating it may cause pressurization, fire, and explosion. In this specific incidence, percentages are given by volume.
methyl ethyl ketone	Also known as MEK. Found in drum incident analysis. Research and development. Analytical laboratory solvent and present in samples. Present in waste organic liquids and sludges generated in Building 881. Homogeneous solids sampling and analysis of organic setups was previously conducted by both the Rocky Flats and INL 3,100 M3 TRU Waste Programs. Based on the analytical data from both programs, the maximum concentration measured was 274 ppm.	Ejected 3.66E-5% Drum 2.03E-5%	19	With a sufficient quantity, this compound could have participated in the WMF-1617 (ARP V) drum incident.

Table A-1. (continued).

Chemical/ Material	Use/Description/Location (AK Source)	Concentration (% by mass)	RGN	Chemical/Material Evaluation
methyl methacrylate	Found in drum incident analysis.	Ejected 5.38E-4% Drum 1.00E-4%	13, 103	With a sufficient quantity, this compound could have participated in the WMF-1617 (ARP V) drum incident.
nitrate anion	Found in drum incident analysis.	Ejected 0.70% Drum 0.62%	104	With a sufficient quantity, this compound could have participated in the WMF-1617 (ARP V) drum incident.
n-nitroso-di-n-propylamine	Found in drum incident analysis.	Ejected 1.14E-4%	7	With a sufficient quantity, this compound could have participated in the WMF-1617 (ARP V) drum incident.
o-cresol	Found in drum incident analysis.	Ejected 6.52E-5%	31	With a sufficient quantity, this compound could have participated in the WMF-1617 (ARP V) drum incident.
pentachlorophenol	Found in drum incident analysis.	Drum 2.64E-4%	17, 31	With a sufficient quantity, this compound could have participated in the WMF-1617 (ARP V) drum incident.
phenanthrene	Found in drum incident analysis.	Ejected 6.36E-5%	16	With a sufficient quantity, this compound could have participated in the WMF-1617 (ARP V) drum incident.
phenol	Found in drum incident analysis.	Ejected 1.24E-3% Drum 2.68E-4%	31	With a sufficient quantity, this compound could have participated in the WMF-1617 (ARP V) drum incident.

Table A-1. (continued).

Chemical/ Material	Use/Description/Location (AK Source)	Concentration (% by mass)	RGN	Chemical/Material Evaluation
phosphorus	Various chemical processes	Ejected 0.16% Drum 0.30%	105, 107	<p>Phosphorous metal, white or red, was not used in processes at Rocky Flats. It is likely that most of the phosphorous identified in the waste is in the form of phosphates. White phosphorus is the most reactive form of phosphorus. Over time, white phosphorus changes to the more stable red phosphorus. White phosphorus is pyrophoric with oxygen, and will ignite at about 30°C. Red phosphorus will ignite at about 260°C. Large quantities will ignite spontaneously and with exposure to oxidizing materials. Red phosphorus will also react with oxygen and water vapor to create phosphine gas. The waste storage conditions are not conducive to maintaining white phosphorus without reacting. Any white phosphorus, over time, would have become red phosphorus. Red phosphorus could have remained in the waste to react at a later time in a different waste configuration.</p> <p>Phosphorus hydride is a colorless gas that will not be in the incident WMF-1617 (ARP V) drums because opening the drums and sorting the waste would dissipate the gas and expose it to oxygen, causing a pyrophoric reaction.</p>
plutonium (Pu239)	Fines and machine turnings	Ejected 3.26E-3% Drum 3.05E-3%	22, 23, 101, 107	<p>Plutonium as fines and turnings is pyrophoric. Since plutonium was the material recovered during the processes, the concentration in the waste would be negligible, and unable to initiate the WMF-1617 (ARP V) drum incident.</p> <p>Plutonium hydride acts as a catalyst for the oxidation of the metal, consuming both oxygen and nitrogen gases. This reaction and the recovery of plutonium from the waste make it unlikely that plutonium survived in the waste to react later.</p>

Table A-1. (continued).

Chemical/ Material	Use/Description/Location (AK Source)	Concentration (% by mass)	RGN	Chemical/Material Evaluation
potassium	Bulk chemical processes	Ejected 2.3% Drum 2.5%	21, 107	<p>Potassium readily reacts with oxygen and water, and requires special storage conditions to maintain the metal. Reactions with water produce hydrogen gas at temperatures that will ignite the hydrogen. Storage conditions of the waste were not conducive to maintaining metallic potassium and it will not persist in the waste.</p> <p>Potassium hydride reacts violently with air and with the contact of oxidizers. It will react with moisture in the air to liberate hydrogen gas. It is unlikely that potassium hydride formed or persisted in the waste.</p>
pyrene	Found in drum incident analysis.	Ejected 5.40E-5	16	With a sufficient quantity, this compound could have participated in the WMF-1617 (ARP V) drum incident.
sodium	Bulk chemical processes	Ejected 6.8% Drum 8.1%	21, 105, 107	<p>Sodium readily reacts with oxygen and water and requires special storage conditions to maintain the metal. Reactions with water produce hydrogen gas at temperatures that will ignite the hydrogen. It will spontaneously ignite in air when heated. Storage conditions of the waste were not conducive to maintaining metallic sodium and it will not persist in the waste.</p> <p>Sodium hydride reacts violently with air and with moisture in the air to liberate hydrogen gas. It is unlikely that sodium hydride formed or persisted in the waste.</p>
sulfate anion	Found in drum incident analysis	Ejected 0.19% Drum 0.41%	24	The sulfates found in the analysis are most likely from metal sulfate salts. These salts have previously reacted and are unlikely to participate in the WMF-1617 (ARP V) drum incident.

Table A-1. (continued).

Chemical/ Material	Use/Description/Location (AK Source)	Concentration (% by mass)	RGN	Chemical/Material Evaluation
sulfur	Bulk chemical processes in the form of sulfates	Ejected 0.17% Drum 0.20%	101	Elemental sulfur was not used in any production processes. In the waste, the sulfur will most likely exist as a sulfate, and be unavailable for further reactions. Hydrogen sulfide (sulfur hydride) is frequently the byproduct of anaerobic microbial breakdown of organic matter. The dumping of the waste and sorting it would dissipate most of the gas, but it may persist.
tetrachloroethylene (perchloroethylene, perc)	Also known as tetrachloroethene. Found in drum incident analysis. Used for parts cleaning and degreasing. Stainless-steel fabrication, parts cleaning and degreasing. Analytical laboratory reagent, used in standards and present in samples analyzed.	Ejected 5.36E-4% Drum 3.40E-5%	17	With a sufficient quantity, this compound could have participated in the WMF-1617 (ARP V) drum incident.
toluene	Found in drum incident analysis. Toluene is a component of other chemical products.	Ejected 4.66E-5% Drum 2.50E-5%	16	With a sufficient quantity, this compound could have participated in the WMF-1617 (ARP V) drum incident.

Table A-1. (continued).

Chemical/ Material	Use/Description/Location (AK Source)	Concentration (% by mass)	RGN	Chemical/Material Evaluation
trichloroethylene (Alk-Tri)	<p>Also known as trichloroethene.</p> <p>Found in drum incident analysis.</p> <p>Plutonium fabrication including ultrasonic parts cleaning.</p> <p>Beryllium and uranium fabrication including ultrasonic cleaning and degreasing.</p> <p>Stainless-steel fabrication including cleaning and degreasing.</p> <p>Analytical laboratory solvent and present in samples analyzed in the laboratories.</p> <p>Alk-Tri and Neu-Tri consists of ~99 percent trichloroethylene and <1 percent 1,2-butylene oxide (stabilizer).</p>	<p>Ejected 1.94E-3%</p> <p>Drum 6.80E-5%</p>	17	<p>With a sufficient quantity, this compound could have participated in the WMF-1617 (ARP V) drum incident.</p>

Table A-1. (continued).

Chemical/ Material	Use/Description/Location (AK Source)	Concentration (% by mass)	RGN	Chemical/Material Evaluation
uranium	Scrap, machined parts, turnings, and reagents in the form of DU	Ejected 3.0% Drum 3.7%	22, 23, 24, 101, 107	<p>Finely divided, shavings, and turnings of uranium are pyrophoric, and will react with air and water. Oxide coatings will passivate metallic uranium, but also can significantly lower the ignition temperature. Under storage conditions prior to repackaging coarse uranium fines could have remained in the waste for further reaction.</p> <p>Uranium hydride may form when uranium is exposed to moisture. Depending on the size and distribution of the uranium hydride particles, self-ignition can occur after an indeterminate length of exposure to air. Several reports indicate that UH₃ ignition is immediate upon exposure to ambient atmosphere.</p> <p>Uranium oxide has a spalling black oxide coat which would permit continued oxidation of encapsulated metal by oxygen. Uranium metal is also known to abstract the oxygen atoms from water and CO₂ to form the oxide as well. Uranium may be able to abstract the oxygen atoms from oxygenates such as butanols as well as abstract the chloride atoms from the chloro-hydrocarbons, leaving unsaturated hydrocarbons,</p>
zinc	Alloys, machined parts, turnings, and reagents	Ejected 0.13% Drum 0.18%	22, 23, 24	<p>Zinc forms a passivation layer in air, preventing further chemical reactions. Finely divided powder and a metallic sponge are made by electrodeposition and are flammable. Bulk fines when damp, may heat and ignite spontaneously on exposure to air. Bulk fines that became moistened and then dried could have caused the WMF-1617 (ARP V) drum incident.</p> <p>Zinc hydride will not persist in the waste because it breaks down into the constituent materials at room temperature.</p>

Table A-1. (continued).

Chemical/ Material	Use/Description/Location (AK Source)	Concentration (% by mass)	RGN	Chemical/Material Evaluation
zirconium	Scrap, machined parts, turnings, and reagents	Ejected 0.94% Drum 0.83%	22, 23, 24	<p>Zirconium is resistant to corrosion in most instances. Finely divided, and turnings (1 to 10 micrometers) of zirconium are pyrophoric. Materials that spark do so when the particle size is small enough to react with pyrophoricity, or when the particle of material has absorbed enough energy through mechanical means, most likely friction, to combust. Particles created during the process of grinding or machining that do not spark, are large enough to not demonstrate the characteristics of pyrophoric fines. Fines may still be combustible.</p> <p>Zirconium hydride can form at ambient conditions, but is not chemically favorable. Zirconium hydride will oxidize readily in air and reacts violently with water, acids, oxidizers, or halogenated compounds. If zirconium hydride persisted in the waste, it could cause an incompatible reaction.</p>

Table A-2. EPA Hazardous Waste Compatibility Chart.

3	Acids, Organic	3																																							
4	Alcohols and Glycols	H, P	4																																						
7	Amines, Aliphatic and Aromatic	H		7																																					
13	Esters				13																																				
15	Fluorides, Inorganic	GT				15																																			
16	Hydrocarbons, Aromatic						16																																		
17	Halogenated Organics			H, GT				17																																	
19	Ketones								19																																
21	Metals, Alkali and Alkaline Earth, Elemental	GF, H, F	GF, H, F										H, E	GF, H	21																										
22	Metals, Other Elemental and Alloys as Powders, Vapors, or Sponges	GF											H, E		22																										
23	Metals, Other Elemental and Alloys as Sheets, Rods, Drops, Moldings, etc.												H, F			23																									
24	Metal and Metal Compounds, Toxic	S		S													24																								
28	Hydrocarbons, Aliphatic, Unsaturated												H, E					28																							
29	Hydrocarbons, Aliphatic, Saturated																																								
31	Phenols and Cresols																																								
101	Combustible and Flammable Materials, Miscellaneous																																								
103	Polymerizable Compounds	P, H																																							
104	Oxidizing Agents, Strong	H, GT	H, F	H, F, GT	H, F		H, F	H, GT	H, F	H, F, E	H, F, E	H, F		H, F	H, F	H, F																									
105	Reducing Agents, Strong	H, GF	H, GF, F	H, GF	H, F			H, E	GF, H																																
107	Water Reactive Substances	Do Not Mix with Wet Chemicals or Waste Material																		107																					
		3	4	7	13	15	16	17	19	21	22	23	24	28	29	31	101	103	104	105	107																				

Reaction Codes:

- H Heat Generation
- F Fire
- G Innocuous and Non-Flammable Gas Generation
- GT Toxic Gas Generation
- GF Flammable Gas Generation
- E Explosion
- S Solubilization of Toxic Substances

A-1.3 Reactivity Group Number

Table A-3. Reactivity Group Number Compatibility Evaluation.

RGN	Group Name	RGNs of Concern (Reaction Codes)	Evaluation of Potential Incompatibility
3	Acids, Organic	4 (H, P) 7 (H) 15 (GT) 21 (GF, H, F) 22 (GF) 24 (S) 103 (P, H) 104 (H,GT) 105 (H, GT) 107 (Extremely Reactive)	In the analysis of the waste, the only RGN 3 constituent was benzoic acid. The benzoic acid concentration in the ejected material is well below trace levels, and was not detected in the material in the drums. It is unlikely the concentration was ever high enough to cause an incompatible reaction with any of the other waste constituents.
4	Alcohols and Glycols	3 (H, P) 21 (GF, H, F) 104 (H, F) 105 (H, GF, F) 107 (Extremely Reactive)	In the analysis of the waste, the only RGN 4 constituent was 1-butanol. The butanol concentration in the ejected material is well below trace levels, and was not detected in the material in the drums. It is unlikely the concentration was ever high enough to cause an incompatible reaction with any of the other waste constituents.
7	Amines, Aliphatic and Aromatic	3 (H) 17 (H, GT) 21 (GF, H) 24 (S) 104 (H, F, GT) 105 (H, GF) 107 (Extremely Reactive)	In the analysis of the waste, the only RGN 7 constituent was n-nitroso-di-n-propylamine. The n-nitroso-di-n-propylamine concentration in the ejected material is well below trace levels, and was not detected in the material in the drums. It is unlikely the concentration was ever high enough to cause an incompatible reaction with any of the other waste constituents.

Table A-3. (continued).

RGN	Group Name	RGNs of Concern (Reaction Codes)	Evaluation of Potential Incompatibility
13	Esters	21 (GF, H) 104 (H, F) 105 (H, F) 107 (Extremely Reactive)	In the analysis of the waste, the RGN 13 constituents in the waste were various phthalate compounds and methyl acrylate. The sum of the concentrations of the RGN 13 in the ejected material and the drums is well below trace levels. It is unlikely the sum of the concentrations was ever high enough to cause an incompatible reaction with any of the other waste constituents.
15	Fluorides, Inorganic	3 (GT) 107 (Extremely Reactive)	In the analysis of the waste, the only RGN 15 constituent was the fluoride anion. The lack of any visible liquid precludes the possibility of hydrofluoric acid. The ratio of the fluoride ion to the calcium ion seems to correlate to the salt calcium fluoride. Calcium fluoride is innocuous in the waste and would not start or perpetuate a reaction in the waste. It is compatible with the other waste constituents.
16	Hydrocarbons, Aromatic	104 (H, F) 107 (Extremely Reactive)	In the analysis of the waste, the RGN 16 constituents in the waste were various organic carbon ringed compounds. The sum of the concentrations of the RGN 16 in the ejected material and the drums is well below trace levels. It is unlikely the sum of the concentrations was ever high enough to cause an incompatible reaction with any of the other waste constituents.
17	Halogenated Organics	7 (H, GT) 21 (H, E) 22 (H, E) 23 (H, F) 104 (H, GT) 105 (H, E) 107 (Extremely Reactive)	The constituents of RGN 17 were varied. The sum of the concentrations of the RGN 17 in the ejected material and the drums is well below trace levels. It is unlikely the sum of the concentrations was ever high enough to cause an incompatible reaction with any of the other waste constituents.
19	Ketones	21 (GF, H) 104 (H, F) 105 (GF, H)	In the analysis of the waste, the RGN 19 constituents in the waste were various ketone compounds. The sum of the concentrations of the RGN 19 in the ejected material and the drums is well below trace levels. It is unlikely the sum of the concentrations was ever high enough to cause an incompatible reaction with any of the other waste constituents.

Table A-3. (continued).

21	Metals, Alkali and Alkaline Earth, Elemental	<p>3 (GF, H, F) 4 (GF, H, F) 7 (GF, H) 13 (GF, H) 17 (H, E) 19 (GF, H) 31 (GF, H) 101 (H, G, F) 103 (P, H) 104 (H, F, E) 107 (Extremely Reactive)</p>	<p>Even though the exact source of the waste is unknown, the processes that generated the waste at Rocky Flats did not employ the use of sodium or potassium metals (RGN 21). These metals readily react with oxygen and water, and require special storage conditions to maintain the metals. Reactions with water produce hydrogen gas at temperatures that may ignite the hydrogen. Storage conditions of the waste were not conducive to maintaining metallic sodium or potassium and they will not persist in the waste.</p> <p>Magnesium (RGN 21) reacts with air to form a passivating oxide layer. In water, magnesium reacts to form hydrogen gas. Finely divided magnesium powder is pyrophoric. It is unlikely that magnesium started the WMF-1617 (ARP V) drum incident, because of the passivation layer and the possibility of reacting with atmospheric moisture over the years of storage. If magnesium survived storage, it could have contributed to the reaction after initiation.</p> <p>In the analysis of the waste, the only RGN 3 constituent was benzoic acid. The benzoic acid concentration in the ejected material is well below trace levels, and was not detected in the material in the drums. It is unlikely the concentration was ever high enough to cause an incompatible reaction with any of the other waste constituents.</p> <p>In the analysis of the waste, the only RGN 4 constituent was 1-butanol. The butanol concentration in the ejected material is well below trace levels, and was not detected in the material in the drums. It is unlikely the concentration was ever high enough to cause an incompatible reaction with any of the other waste constituents.</p> <p>In the analysis of the waste, the only RGN 7 constituent was n-nitroso-di-n-propylamine. The n-nitroso-di-n-propylamine concentration in the ejected material is well below trace levels, and was not detected in the material in the drums. It is unlikely the concentration was ever high enough to cause an incompatible reaction with any of the other waste constituents.</p> <p>In the analysis of the waste, the RGN 13 constituents in the waste were various phthalate compounds and methyl acrylate. The sum of the concentrations of the RGN 13 in the ejected material and the drums is well below trace levels. It is unlikely the sum of the concentrations was ever high enough to cause an incompatible reaction with any of the other waste constituents.</p> <p>The constituents of RGN 17 were varied. The sum of the concentrations of the RGN 17 in the ejected material and the drums is well below trace levels. It is unlikely the sum of the concentrations was ever high enough to cause an incompatible reaction with any of the other waste constituents.</p> <p>In the analysis of the waste, the RGN 19 constituents in the waste were various ketone compounds. The sum of the concentrations of the RGN 19 in the ejected material and the drums is well below trace levels. It is unlikely the sum of the concentrations was ever high enough to cause an incompatible reaction with any of the other waste constituents.</p> <p>The RGN 31 constituents in the waste were various phenol and cresol compounds. The sum of the concentrations of the RGN 31 in the ejected material and the drums is well below trace levels. It is unlikely the sum of the concentrations was ever high enough to cause an incompatible reaction with any of the other waste constituents.</p>
----	--	---	---

Table A-3. (continued).

RGN	Group Name	RGNs of Concern (Reaction Codes)	Evaluation of Potential Incompatibility
			<p>In this instance, RGN 101 is being applied to the pyrophoric metals uranium and plutonium. Both of these metals are pyrophoric even when not finely divided. Plutonium metal was the end product of most chemical separations processes, and was also recovered from waste manufacturing processes. The recovery efforts for plutonium will limit the amount that could be in the waste, and will not be present to initiate a reaction. Uranium was frequently part of the waste. Various sizes and shapes of uranium metal could be available for later reaction, and initiate an incompatible reaction.</p> <p>Sulfur is also an RGN 101. Elemental sulfur was not used in any production processes. In the waste, the sulfur will most likely exist as a sulfate, and be unavailable for further reactions.</p> <p>In the analysis of the waste, the only RGN 103 constituent was methyl methacrylate. The methyl methacrylate concentration in the ejected material and in the drum is well below trace levels. It is unlikely the concentration was ever high enough to cause an incompatible reaction with any of the other waste constituents.</p> <p>The RGN 104 component in the waste is the nitrate anion. Nitrate was found in the ejected material and in the drums from the WMF-1617 (ARP V) drum incident. With a sufficient quantity, this compound could have participated in the WMF-1617 (ARP V) drum incident. Test results show that the amount of nitrate present is low enough to not deem the bulk properties of the waste an oxidizer. It would take over twenty-eight times more nitrates to require treatment as an oxidizer.</p> <p>For this analysis, RGN 107 refers to sodium, potassium, plutonium, and uranium. Sodium and potassium would not be able to persist in the waste because; these metals readily react with oxygen and water, and require special storage conditions to maintain the metals. Reactions with water produce hydrogen gas at temperatures that may ignite the hydrogen. Storage conditions of the waste were not conducive to maintaining metallic sodium or potassium.</p> <p>Both plutonium and uranium are water reactive. Multiple reports in the chemical literature indicate a strong exothermic reaction with the ambient atmosphere at relative humidity values as low as 2%. The waste material was exposed to higher humidity when the parent drum was opened for repackaging. Plutonium metal was the end product of most chemical separations processes, and was also recovered from waste manufacturing processes. The recovery efforts for plutonium will limit the amount that could be in the waste, and will not be present in a large enough quantity to initiate a reaction. Uranium was frequently part of the waste. Various sizes and shapes of uranium metal could be available for later reaction, and initiate an incompatible reaction.</p> <p>The waste was visually examined and determined to be dry. The absence of liquid will prevent a reaction by a water reactive substance (RGN 107) in the waste.</p>

Table A-3. (continued).

RGN	Group Name	RGNs of Concern (Reaction Codes)	Evaluation of Potential Incompatibility
22	Metals, Other Elemental and Alloys as Powders, Vapors, or Sponges	3 (GF) 17 (H, E) 28 (H, E) 102 (H, E) 103 (P, H) 104 (H, F, E) 107 (Extremely Reactive)	<p>In the analysis of the waste, the only RGN 3 constituent was benzoic acid. The benzoic acid concentration in the ejected material is well below trace levels, and was not detected in the material in the drums. It is unlikely the concentration was ever high enough to cause an incompatible reaction with any of the other waste constituents.</p> <p>The constituents of RGN 17 were varied. The sum of the concentrations of the RGN 17 in the ejected material and the drums is well below trace levels. It is unlikely the sum of the concentrations was ever high enough to cause an incompatible reaction with any of the other waste constituents.</p> <p>Alkenes (RGN 28) The alkenes eluded to in the semi-volatile chromatogram have the possibility of reacting with metal fines in the waste. The concentrations of the alkene compounds are well below 1% and are considered trace insignificant. If the concentration in the original waste was greater, they could have caused an incompatible reaction.</p> <p>Calcium (RGN 102) and calcium compounds were used for various plutonium purification processes. The ratio of the calcium ion to the fluoride ion seems to correlate to the salt calcium fluoride. Calcium fluoride is innocuous in the waste and would not start or perpetuate a reaction in the waste. It is compatible with the other waste constituents. Analysis of the waste also seems to indicate that the calcium in the waste is from calcium fluoride, and is not available for further reactions.</p> <p>In the analysis of the waste, the only RGN 103 constituent was methyl methacrylate. The methyl methacrylate concentration in the ejected material and in the drum is well below trace levels. It is unlikely the concentration was ever high enough to cause an incompatible reaction with any of the other waste constituents.</p> <p>The RGN 104 component in the waste is the nitrate anion. Nitrate was found in the ejected material and in the drums from the WMF-1617 (ARP V) drum incident. With a sufficient quantity, this compound could have participated in the WMF-1617 (ARP V) drum incident. Test results show that the amount of nitrate present is low enough to not deem the bulk properties of the waste an oxidizer. It would take over twenty-eight times more nitrate to require treatment as an oxidizer.</p> <p>RGN 22 materials existing as fines, turnings, or scrapings may be pyrophoric, for example uranium, and plutonium.</p> <p>The waste was visually examined and determined to be dry. The absence of liquid will prevent a reaction by a water reactive substance (RGN 107) in the waste.</p>

Table A-3. (continued).

RGN	Group Name	RGNs of Concern (Reaction Codes)	Evaluation of Potential Incompatibility
23	Metals, Other Elemental and Alloys as Sheets, Rods, Drops, Moldings, etc.	17 (H, F) 103 (P, H) 104 (H,F) 107 (Extremely Reactive)	<p>The constituents of RGN 17 were varied. The sum of the concentrations of the RGN 17 in the ejected material and the drums is well below trace levels. It is unlikely the sum of the concentrations was ever high enough to cause an incompatible reaction with any of the other waste constituents.</p> <p>In the analysis of the waste, the only RGN 103 constituent was methyl methacrylate. The methyl methacrylate concentration in the ejected material and in the drum is well below trace levels. It is unlikely the concentration was ever high enough to cause an incompatible reaction with any of the other waste constituents.</p> <p>The RGN 104 component in the waste is the nitrate anion. Nitrate was found in the ejected material and in the drums from the WMF-1617 (ARP V) drum incident. With a sufficient quantity, this compound could have participated in the WMF-1617 (ARP V) drum incident. Test results show that the amount of nitrate present is low enough to not deem the bulk properties of the waste an oxidizer. It would take over twenty-eight times more nitrate to require treatment as an oxidizer.</p> <p>Many of the RGN 23 materials could exist as debris in the waste. The waste was visually examined and determined to be dry. The absence of liquid will prevent a reaction by a water reactive substance (RGN 107) in the waste.</p>
24	Metal and Metal Compounds, Toxic	3 (S) 7 (S) 103 (P, H) 107 (Extremely Reactive)	<p>In the analysis of the waste, the only RGN 3 constituent was benzoic acid. The benzoic acid concentration in the ejected material is well below trace levels, and was not detected in the material in the drums. It is unlikely the concentration was ever high enough to cause an incompatible reaction with any of the other waste constituents.</p> <p>In the analysis of the waste, the only RGN 7 constituent was n-nitroso-di-n-propylamine. The n-nitroso-di-n-propylamine concentration in the ejected material is well below trace levels, and was not detected in the material in the drums. It is unlikely the concentration was ever high enough to cause an incompatible reaction with any of the other waste constituents.</p> <p>In the analysis of the waste, the only RGN 103 constituent was methyl methacrylate. The methyl methacrylate concentration in the ejected material and in the drum is well below trace levels. It is unlikely the concentration was ever high enough to cause an incompatible reaction with any of the other waste constituents.</p> <p>Many of the RGN 24 materials could exist as debris in the waste. The waste was visually examined and determined to be dry. The absence of liquid will prevent the leaching of toxic metals and a reaction by a water reactive substance (RGN 107) in the waste.</p>

Table A-3. (continued).

RGN	Group Name	RGNs of Concern (Reaction Codes)	Evaluation of Potential Incompatibility
28		22 (H, E) 104 (H, F)	<p>Alkenes (RGN 28) The alkenes eluded to in the semi-volatile chromatogram have the possibility of reacting with metal fines in the waste. The concentrations of the alkene compounds are well below 1% and are considered trace insignificant. If the concentration in the original waste was greater, they could have caused an incompatible reaction.</p> <p>The RGN 104 component in the waste is the nitrate anion. Nitrate was found in the ejected material and in the drums from the WMF-1617 (ARP V) drum incident. With a sufficient quantity, this compound could have participated in the WMF-1617 (ARP V) drum incident. Test results show that the amount of nitrate present is low enough to not deem the bulk properties of the waste an oxidizer. It would take over twenty-eight times more nitrates to require treatment as an oxidizer.</p>
29	Hydrocarbons, Aliphatic, Saturated	104 (H, F)	<p>The RGN 104 component in the waste is the nitrate anion. Nitrate was found in the ejected material and in the drums from the WMF-1617 (ARP V) drum incident. With a sufficient quantity, this compound could have participated in the WMF-1617 (ARP V) drum incident. Test results show that the amount of nitrate present is low enough to not deem the bulk properties of the waste an oxidizer. It would take over twenty-eight times more nitrates to require treatment as an oxidizer.</p>
31	Phenols and Cresols	21 (GF, H) 103 (P, H) 104 (H, F) 105 (GF, H) 107 (Extremely Reactive)	<p>The RGN 31 constituents in the waste were various phenol and cresol compounds. The sum of the concentrations of the RGN 31 in the ejected material and the drums is well below trace levels. It is unlikely the sum of the concentrations was ever high enough to cause an incompatible reaction with any of the other waste constituents.</p>

Table A-3. (continued).

<p style="text-align: center;">101</p>	<p style="text-align: center;">Combustible and Flammable Materials, Miscellaneous</p>	<p style="text-align: center;">21 (H, G, F) 104 (H, F, G) 105 (GF, H) 107 (Extremely Reactive)</p>	<p>Even though the exact source of the waste is unknown, the processes that generated the waste at Rocky Flats did not employ the use of sodium or potassium metals (RGN 21). These metals readily react with oxygen and water, and require special storage conditions to maintain the metals. Reactions with water produce hydrogen gas at temperatures that may ignite the hydrogen. Storage conditions of the waste were not conducive to maintaining metallic sodium or potassium and they will not persist in the waste.</p> <p>Magnesium (RGN 21) reacts with air to form a passivating oxide layer. In water, magnesium reacts to form hydrogen gas. Finely divided magnesium powder is pyrophoric. It is unlikely that magnesium started the WMF-1617 (ARP V) drum incident, because of the passivation layer and the possibility of reacting with atmospheric moisture over the years of storage. If magnesium survived storage, it could have contributed to the reaction after initiation.</p> <p>In this instance, RGN 101 is being applied to the pyrophoric metals uranium and plutonium. Both of these metals are pyrophoric even when not finely divided. Plutonium metal was the end product of most chemical separations processes, and was also recovered from waste manufacturing processes. The recovery efforts for plutonium will limit the amount that could be in the waste, and will not be present to initiate a reaction. Uranium was frequently part of the waste. Various sizes and shapes of uranium metal could be available for later reaction, and initiate an incompatible reaction.</p> <p>Sulfur is also an RGN 101. Elemental sulfur was not used in any production processes. In the waste, the sulfur will most likely exist as a sulfate, and be unavailable for further reactions.</p> <p>The RGN 104 component in the waste is the nitrate anion. Nitrate was found in the ejected material and in the drums from the WMF-1617 (ARP V) drum incident. With a sufficient quantity, this compound could have participated in the WMF-1617 (ARP V) drum incident. Test results show that the amount of nitrate present is low enough to not deem the bulk properties of the waste an oxidizer. It would take over twenty-eight times more nitrates to require treatment as an oxidizer.</p> <p>Rocky Flats did not employ the use of sodium metal (RGN 105). It readily reacts with oxygen and water and requires special storage conditions to maintain the metal. Reactions with water produce hydrogen gas at temperatures that will ignite the hydrogen. It will spontaneously ignite in air when heated. Storage conditions of the waste were not conducive to maintaining metallic sodium and it will not persist in the waste.</p> <p>Documentation from Rocky Flats does not show the use of elemental phosphorus (RGN 105). White phosphorus is the most reactive form of phosphorus. Over time, white phosphorus changes to the more stable red phosphorus. White phosphorus is pyrophoric with oxygen, and will ignite at about 30°C. Red phosphorus will ignite at about 260°C. Large quantities will ignite spontaneously and with exposure to oxidizing materials. Red phosphorus will also react with oxygen and water vapor to create phosphine gas. The waste storage conditions are not conducive to maintaining white or red phosphorus without reacting. Any white phosphorus, over time, would have become red phosphorus. Red phosphorus, with atmospheric water and oxygen, would react to form phosphine gas. It is unlikely but, red phosphorus could have remained in the waste to react at a later time in a different waste configuration.</p> <p>Various metal hydrides (RGN 105) may persist in the waste and pose the possibility of an incompatible reaction in the waste.</p>
--	---	--	--

Table A-3. (continued).

RGN	Group Name	RGNs of Concern (Reaction Codes)	Evaluation of Potential Incompatibility
			The waste was visually examined and determined to be dry. The absence of liquid will prevent a reaction by a water reactive substance (RGN 107) in the waste.
103	Polymerizable Compounds	3 (P, H) 21 (P, H) 22 (P, H) 23 (P, H) 24 (P,H) 31 (P, H) 104 (H, F, GT) 105 (H, P, GF) 107 (Extremely Reactive)	In the analysis of the waste, the only RGN 103 constituent was methyl methacrylate. The methyl methacrylate concentration in the ejected material and in the drum is well below trace levels. It is unlikely the concentration was ever high enough to cause an incompatible reaction with any of the other waste constituents.
104	Oxidizing Agents, Strong	3 (H, GT) 4 (H, F) 7 (H, F, GT) 13 (H, F) 16 (H, F) 17 (H, GT) 19 (H, F) 21 (H, F, E) 22 (H, F, E) 23 (H, F) 28 (H, F) 29 (H, F) 31 (H, F) 101 (H, F, G) 103 (H, F, GT) 105 (H, F, E)	The RGN 104 component in the waste is the nitrate anion. Nitrate was found in the ejected material and in the drums from the WMF-1617 (ARP V) drum incident. With a sufficient quantity, this compound could have participated in the WMF-1617 (ARP V) drum incident. Test results show that the amount of nitrate present is low enough to not deem the bulk properties of the waste an oxidizer. It would take over twenty-eight times more nitrates to require treatment as an oxidizer.

Table A-3. (continued).

RGN	Group Name	RGNs of Concern (Reaction Codes)	Evaluation of Potential Incompatibility
		107 (Extremely Reactive)	
105	Reducing Agents, Strong	3 (H, GF) 4 (H, GF, F) 7 (H, GF) 13 (H, F) 17 (H, E) 19 (GF, H) 31 (GF, H) 101 (GF, H) 103 (H, P, GF) 104 (H, F, E) 107 (Extremely Reactive)	<p>Rocky Flats did not employ the use of sodium metal (RGN 105). It readily reacts with oxygen and water and requires special storage conditions to maintain the metal. Reactions with water produce hydrogen gas at temperatures that will ignite the hydrogen. It will spontaneously ignite in air when heated. Storage conditions of the waste were not conducive to maintaining metallic sodium and it will not persist in the waste.</p> <p>Documentation from Rocky Flats does not show the use of elemental phosphorus (RGN 105). White phosphorus is the most reactive form of phosphorus. Over time, white phosphorus changes to the more stable red phosphorus. White phosphorus is pyrophoric with oxygen, and will ignite at about 30°C. Red phosphorus will ignite at about 260°C. Large quantities will ignite spontaneously and with exposure to oxidizing materials. Red phosphorus will also react with oxygen and water vapor to create phosphine gas. The waste storage conditions are not conducive to maintaining white or red phosphorus without reacting. Any white phosphorus, over time, would have become red phosphorus. Red phosphorus, with atmospheric water and oxygen, would react to form phosphine gas. It is unlikely but, red phosphorus could have remained in the waste to react at a later time in a different waste configuration.</p> <p>Various metal hydrides (RGN 105) may persist in the waste and pose the possibility of an incompatible reaction in the waste.</p>
107	Water Reactive Substances	All	The waste was visually examined and determined to be dry. The absence of liquid will prevent a reaction by a water reactive substance (RGN 107) in the waste.

Appendix B

Literature Review of Uranium Oxidation

Appendix B

Literature Review of Uranium Oxidation

B-1 Uranium Oxidation Literature Review

In general, isothermal rates of uranium oxidation (eq.B-1) could be rationalized following an Arrhenius-type equation (eq.B-2), which describes the effects of both time and temperature on the reaction rate⁷,



$$m_{ox} = At^{(1-n)/n} e^{(-\frac{E}{RT})} \quad (\text{B-2})$$

where m_{ox} is the rate of oxidation in $\text{mg U/cm}^2\text{h}$, A is the pre-exponential factor, E is the activation energy, t is time, R is the gas constant, 1.987 cal/mol K, and T is absolute temperature. The reaction order is set by the exponent $(1-n)/n$, which reflects the influence of the oxide layer. It should be stated that except for high vacuum environments, uranium metal will have an oxide layer. In general, Epstein noted that oxide layer is non-protective if its volume is smaller than that of the metal, in which case values for n are < 1 and the rate law accelerating (Figure B-1)⁷. A model constructed using $n = 0.9$, and Ritchie's values for dry air¹² for the pre-exponential factor ($6.9 \times 10^8 \text{ mgU/cm}^2/\text{H}$) and activation energy (-18300 cal/mol) at 300K shows that the rate is very slow but accelerates by about a factor of two over the course of 1000 hours. The same acceleration is seen at 400K, but the oxidation rates are $>$ three orders of magnitude higher. At 500K, using a value for $n = 1.1$ results in a decelerating rate of oxidation, by nearly two orders of magnitude over the same period of time. This was interpreted in terms of the volume of oxide exceeding that of U metal, slowing the diffusion of ions in the oxide layer, and the rate of oxidation.

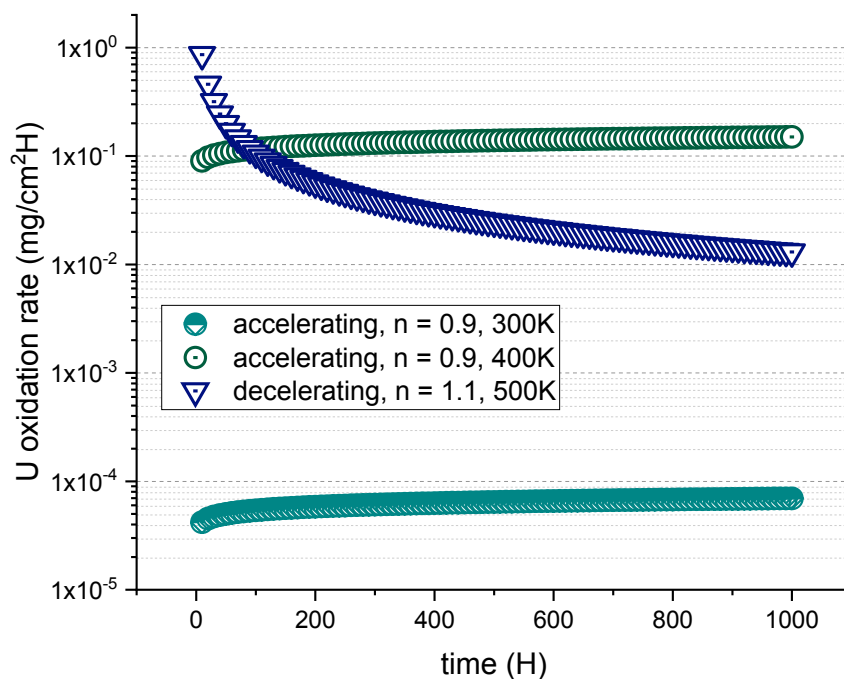


Figure B-1. Oxidation rates plotted v time (H), modeled using Epstein's equation (2).

B-2 U Oxidation Rates by O₂ and Dry Air

B-2.1 Time Dependence

Baker and Bingle studied U oxidation in pure O₂, which showed that at lower temperatures (< 450°C) the oxidation reaction was self-accelerating, that is, the rate increased as the reaction progressed under isothermal conditions¹⁸. While an oxide layer was being formed, it was not protective. At temperatures > 450°C, the reaction was decelerating, which was indicative of formation of an oxide layer that was protective. These early results were consistent with the Epstein's general expression published three decades later⁷.

The rate laws were initially parabolic, becoming linear as the reaction proceeds, which suggested that the rate limiting step of the oxidation is the diffusion of O⁻ through the growing coherent oxide lattice^{11,28}. Below 100°C the process is governed by the electric field of the oxide, and the rate equation has an inverse log form (eq. B-3)²⁸,

$$1/y = 1/y_0 - K' \ln(1+a(t-t_0)) \quad (\text{B-3})$$

where y and t are the oxide thickness and time y₀ thickness at time zero (t₀), and a and K' are constants (parameters found in table 2 of Reference 27). The equation was applied to data from uranium oxidation, with air reported by Sladky¹⁴, and with oxygen reported by Larson¹⁵. The kinetic model shows a rapidly increasing extent of reaction at short times (Figure B-2). These samples had been sputter cleaned in vacuum at time zero, and the rapid increase at short times results from formation of a protective oxide layer of UO₂. As time proceeds the reaction continues at slower rates following linear kinetics and may continue in this fashion for months or years.

Ritchie felt that the similarity between the data sets of Sladky and Larson, which differed in oxygen content (Sladky air, Larson O₂), showed that the rates were controlled by diffusion through the initially formed oxide layer and not by the oxygen concentration. The model also clearly indicates a strong temperature dependence on further oxidation – note the very sharp increase in oxide thickness for the models of experiments run at 93°C, compared to the modest increases measured near room temperature.

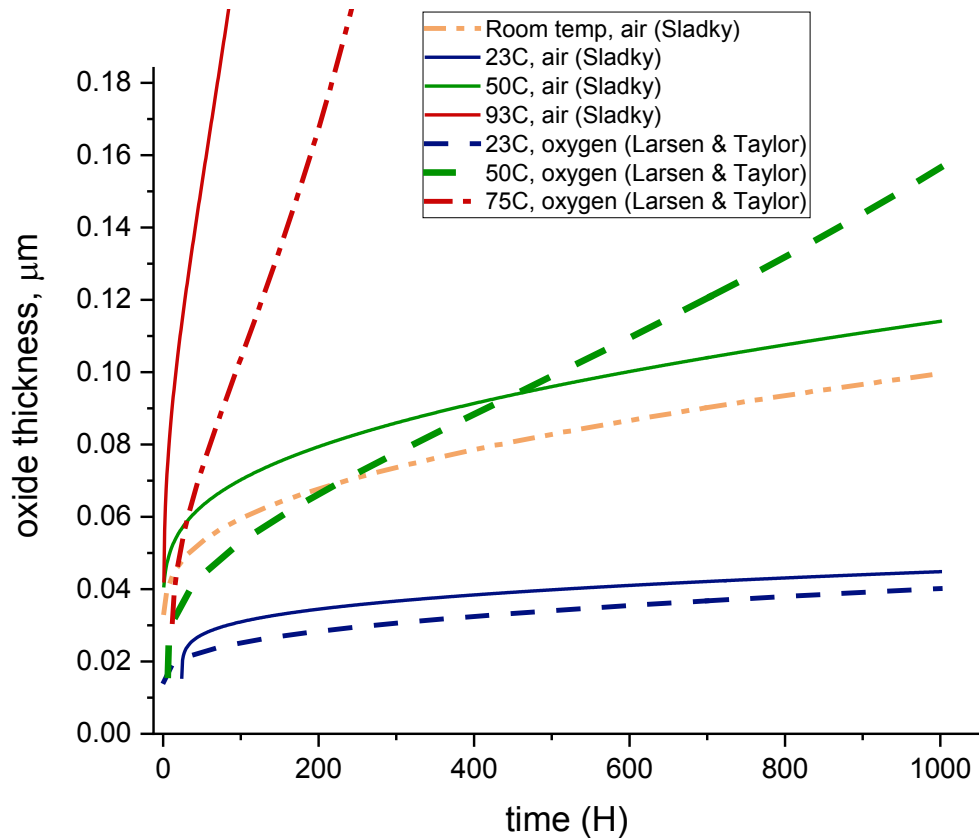


Figure B-2. Plot of extent of uranium oxidation by O₂ measured as the oxide thickness, versus time. Plots were generated using the inverse log model of Ritchie²⁸, fitted to ellipsometry data acquired for the reaction of uranium in air¹⁴ and oxygen¹⁵.

For the case where an initially protective oxide exists, oxidation still occurs at low temperatures. The reaction is modeled using combined parabolic – linear models that reflect the existence of an oxide layer that was initially protective but became un-protective as oxidation proceeded²⁸. In particular, the kinetic model of Haycock was able to fit data to an expression that utilized both parabolic and linear rates, according to eq. B-4¹⁶,

$$X = K_p/K_l(\ln(K_p/(K_p - K_l(X-K_l t))) \quad (\text{B-4})$$

where X is the extent of oxidation, t is time, K_p is the parabolic rate constant and K_l is the linear rate constant. Data modeled at 100°C showed an initial rapid rise following a parabolic profile (Figure B-4, time < 40 H), followed by a more linear regime at longer times. The good fit supported the general mechanism in which the oxidation rate is controlled diffusion of oxygen ions through a thin protective oxide, which is converted to an un-protective layer as oxidation proceeds past formation of UO₂. Oxidation was independent of the oxygen pressure, which was consistent with the notion that rate is controlled by diffusion through the oxide layer, and not an equilibrium condition. The same basic profile was generated for experiments conducted at higher temperatures, although the rates of reaction were much greater (c.f. the plot for the 240°C data, Figure B-3).

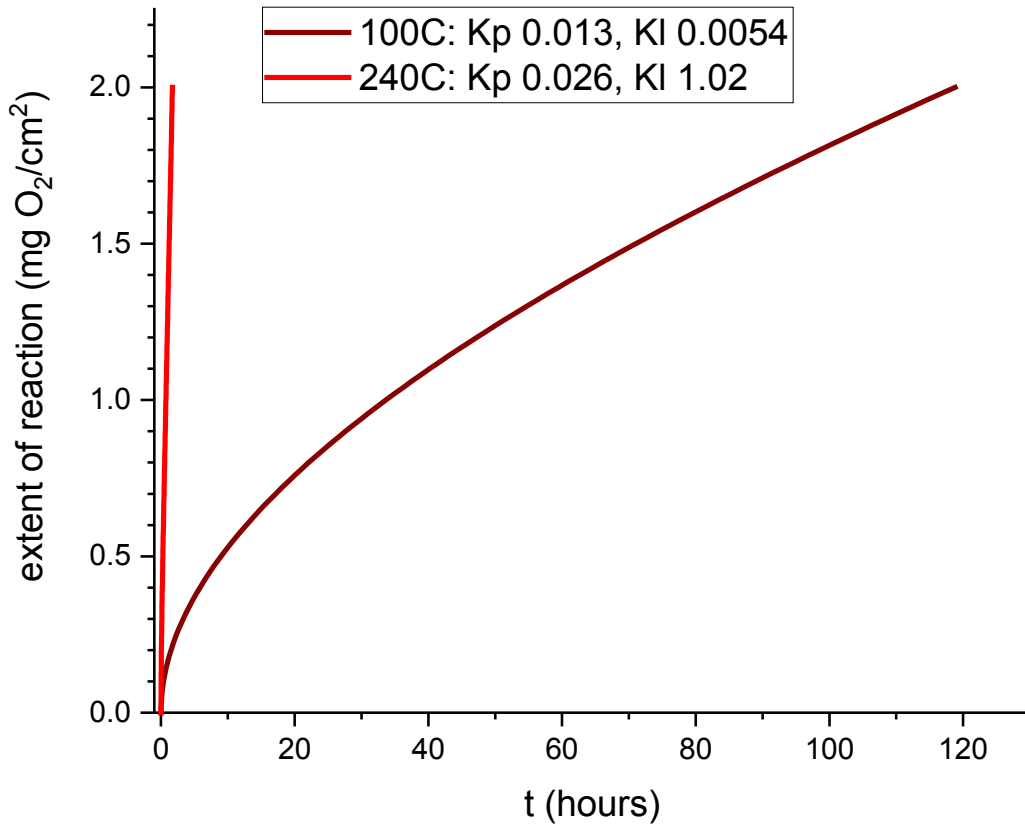


Figure B-3. Parabolic – linear kinetic model for oxidation of metal surfaces, developed by Haycock¹⁶, and applied by Ritchie²⁸ to the uranium oxidation of Loriers¹⁷. Rate constant values are from Ritchie’s manuscript²⁸.

B-2.2 Temperature Dependence

The oxidation of uranium in oxygen over temperatures from 125°C to 295°C occurred in two stages¹⁹. At the lowest temperatures, first stage oxidation follows a parabolic rate law. The first stage is significantly slower compared to the second stage.

Ritchie reviewed reaction rates of uranium oxygen and water in 1981¹³, and noted that the temperature dependence of uranium oxidation by O₂ were described by the general reaction in eq. B-5, and the Arrhenius expression in eq. B-6,



$$k = A e^{\left(\frac{-E}{RT}\right)} \quad (B-6)$$

where the units for the pre-exponential factor A are mg U cm⁻²H⁻¹, R = 1.987 cal mol⁻¹ K⁻¹, T is degrees K, and the units for k are mg U cm⁻² H⁻¹. Values fitted for data collected U oxidation in 200 mm of pure O₂ were depicted by the red trace in Figure B-4²⁸, which shows the exponential dependence of rate on temperature. Extremely small, but continually increasing values are observed until about 470K, at which point the rate exceeds 0.1 mg cm⁻²H⁻¹. The rate continues to increase exponentially above this temperature. The model for dry air shows the same profile, only the rates are about 50x faster¹³; a priori, one would expect similar values, however we hypothesize that the “dry air” experiment may actually have

contained traces of H₂O vapor. This would make the measured reaction rates, and subsequent fitted model, much faster (Figure B-4).

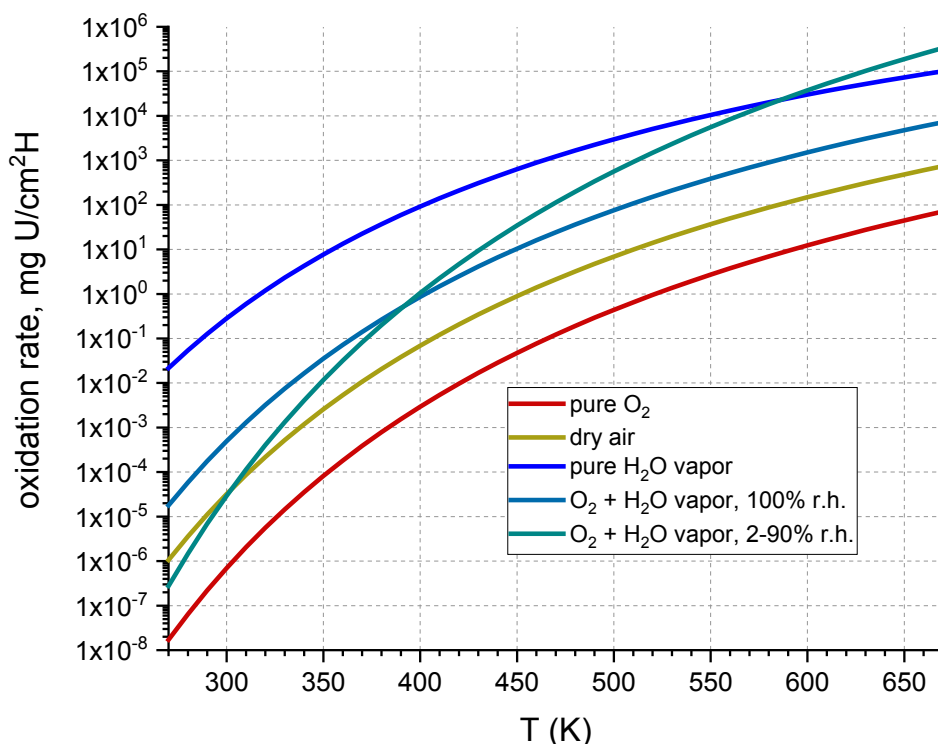


Figure B-4. Oxidation rates vs. temperature, from Arrhenius expressions of Ritchie^{13,28}.

A consideration of the measured activation energies also indicated that the diffusion of O₂ through the oxide layer was the rate limiting step. A value of 27 kcal mol⁻¹ was modeled for oxidation of uranium below 100°C, and at higher temperatures, the value decreased to 20 kcal mol⁻¹. These values are close to the activation energy for the diffusion of O₂ through UO₂ (22 kcal mol⁻¹). Marker experiments showed that oxygen diffuses through the UO₂ layer, and not uranium¹⁹.

B-2.2.1 Heat Build-Up

The oxidation of uranium by O₂, and H₂O is exothermic. If heat generated cannot be dissipated, then temperature will increase, resulting in a much faster rate of oxidation, as shown above. The fact that the oxide layer is insulating will slow heat dissipation, and so as the oxide layer thickens, the rate of heat dissipation decreases. Sites of heating have been correlated to metal irregularities that can become sites of accelerated oxidation or ignition if the rate of liberation of heat due to metal oxidation is greater than the rate of loss of heat¹⁹.

B-2.2.2 Implications to Event Drum

The phenomenon of accelerating oxidation rates in dry air or O₂ under isothermal conditions may be responsible for phenomena occurring in the ARP V event drums, specifically the time delay observed between the initial exposure to atmosphere (when the parent drum was opened, and contents moved to the sorting tray), and the lid ejections. The very rapid rates seen at very short times in experiments reported in the literature may not be applicable, since some of these started with a uranium surface maintained in an un-oxidized state in vacuum. However, the continued acceleration seen at longer times, when the oxide coating had already formed, may be partially analogous to behavior of material present in the parent drum. It is emphasized that these rate accelerations described in section 4.4.1 were observed in

experiments conducted isothermally. It is likely that oxidation occurring in the drum material were also accompanied by a temperature increase, which will drastically increase oxidation rates.

B-2.2.3 Uranium Reaction with H₂O and H₂O Vapor

All available literature reports indicate that the rate of uranium oxidation with H₂O is significantly faster compared to O₂ over what are the relevant temperature ranges. The reaction initially generates UO₂ and H₂ (eq. 7), but can proceed further to form hyperstoichiometric UO_{2+x}. H₂ can diffuse away, or will react to form UH₃ if it contacts zero-valent uranium (eq. 8). Formation of U(OH)₃ or hydrated oxide, UO_{2+x}·nH₂O.¹¹



Early studies (1959) indicated that the effect of H₂O vapor was negligible up to about 3% relative humidity¹⁹, but then increased with increasing moisture content, consistent with Epstein's conclusion that the oxidation rate was dependent on the water vapor partial pressure, which in turn was directly proportional to the fraction of the reacting surface covered by adsorbed H₂O.¹

The reaction of uranium (swarf, rods and foil) with H₂O in the absence of O₂ were reported in 1966^{8,9,18}, which showed that a less-than-stoichiometric quantity of H₂ is formed, which was attributed to formation of a protective layer of UO₂ that stops the reaction from proceeding to completion. The reaction progress as measured by H₂ evolved was linear with time, which indicated that the reaction rate was dependent on the surface area. Reaction rates were independent of H₂ pressure, but strongly dependent on temperature. It was concluded that oxidation by water was ~ 5000X faster than O₂ oxidation over the temperature range studied^{8,9,18}. Activation energies ranged from 12 to 17 kcal/mol, significantly lower compared to oxidation reactions with O₂. The reaction of the foil sample occurred at lower relative humidity compared that of the rod samples. Reaction profiles measured in 100% relative humidity (RH) were identical to those immersed in H₂O.

Oxygen slowed the rate of reaction by a factor of 30 to 100X^{8,9,18}. The kinetic profiles of these experiments showed an initially slow period where the kinetics were parabolic, increasing in a linear fashion until all the O₂ is consumed. At that point, the reaction rate increased to that of pure H₂O. As before, the kinetic behavior suggested that the oxidation was diffusion controlled. These phenomena were echoed by McGillivray in 1994, who noted when water was re-introduced subsequent to a previous exposure that strongly exothermic reactions could occur¹⁰. Oxidation rate data was correlated with water vapor pressure to derive a semiempirical relationship between the oxidation rate and temperature that incorporated water vapor pressure (eq. 9). The equation was considered valid from 0 to 350°C, and water vapor pressures from 0 to 100 kPa:

$$m_{ox} = \frac{0.4197 P_{\text{H}_2\text{O}} e^{\left(\frac{-6432}{T}\right)}}{1 + 2.48 \times 10^{-7} P_{\text{H}_2\text{O}} e^{\left(\frac{5372}{T}\right)}} + 10.95 e^{\left(\frac{-8077}{T}\right)} \quad (\text{B-9})$$

Using this model, a linear plot of oxidation rate versus temperature with a H₂O partial pressure of 2 kPa shows little change prior to about 450K (177°C), followed by accelerating rates up to the upper temperature limit of the model at 623K (Figure B-5a). However, the semi-log plot (Figure B-5b) shows that the overall oxidation rate increases by more than an order of magnitude between 298K and 323K (25°C and 50°C), and that this rapid increase in rate with increasing temperature continues throughout the relevant temperature range. A second notable feature of the model is that it enables separation of relative contributions of H₂O and O₂. At the lowest temperature, oxidation by O₂ is ~ 40% faster than H₂O oxidation, however two oxidants are equal at 303K (30°C), and H₂O is more reactive over the remainder of the valid temperature range. For example, H₂O oxidation is about four times faster than O₂ oxidation at

373K (100°C). The model also indicates that the system is sensitive to increasing H₂O partial pressure: at 373K, the rate increases by about 40x on going from 0 to 1 kPa, and by another factor of 2 on going from 1 to 4 kPa (Figure B-6).

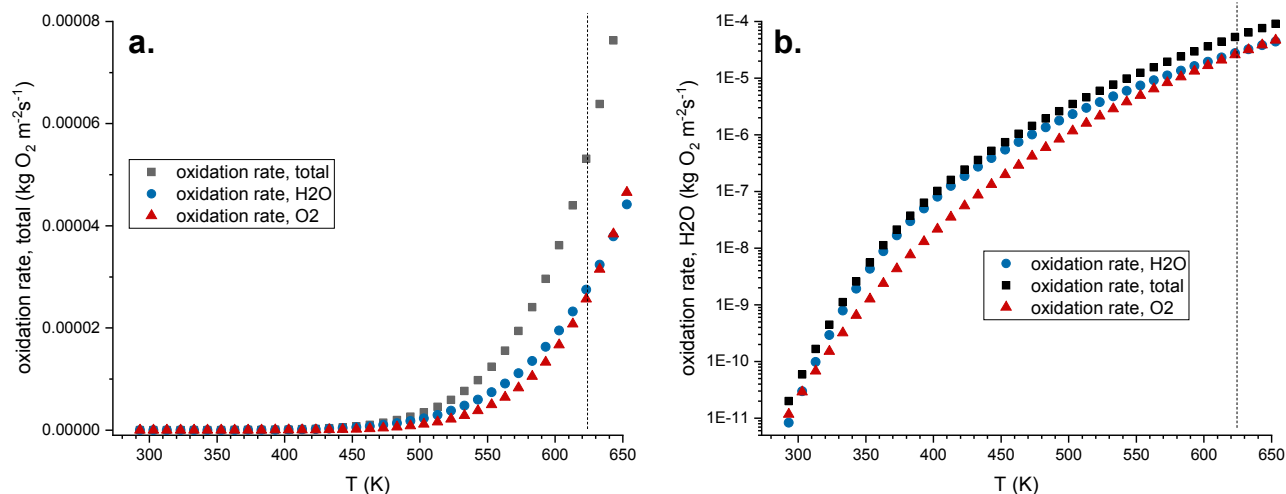


Figure B-5. Oxidation rate versus temperature modeled using the semi-empirical rate law developed by McGillivray^{10,1}. **a.** Linear plot. **b.** Semi-log plot. The model is valid from 273K to 623K (marked by a vertical dashed line). Models were generated using a H₂O partial pressure of 2 kPa.

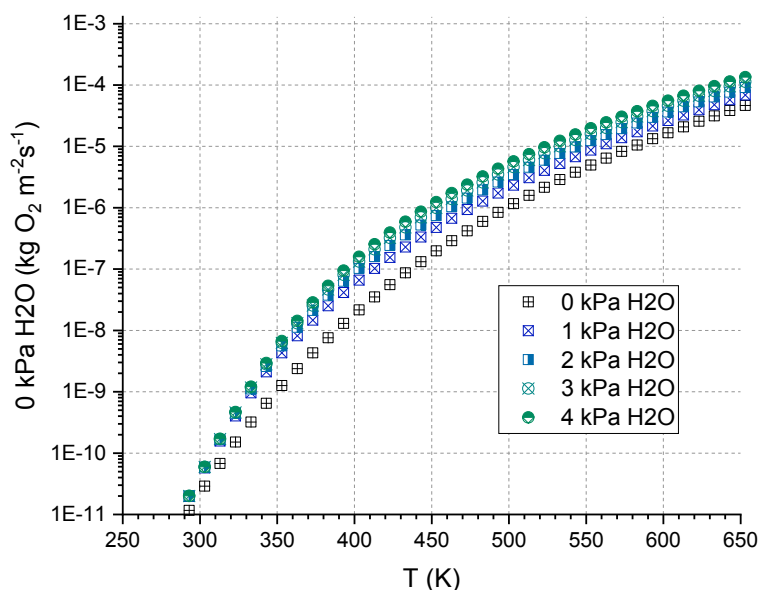


Figure B-6. Overall oxidation rates modeled at varying H₂O partial pressures, using the expression of McGillivray^{10,1}.

Water vapor greatly accelerates reaction rates across the temperature range of interest. Ritchie reviewed rates using Arrhenius expressions derived from fitting data from experiments collected under different atmospheric conditions^{12,28}. By far the fastest rate was for pure water vapor, and that humid oxygen was also considerably faster compared to dry air and oxygen (Figure 16). The presence of O₂ in water vapor slowed the rate of reaction by at least two orders of magnitude. Conversely, the presence of H₂O in pure O₂ speeded up the reaction by 1 – 3 orders, depending on the temperature and relative humidity.

The Arrhenius expressions were modified to account for relative humidity (RH) according to Equation B-10¹³:

$$k = (3.5 \times 10^8)(RH)^{1/2} \exp(-14,100/RT) \quad (\text{B-10})$$

At 25°C, increasing the RH from 0.1 to 1.0 will increase the rates by a factor of 4 (Figure B-7), and similar increases are seen for models at 50°C, 75°C and 100°C. As noted previously, the models also show the effect of increasing temperature on reaction rates.

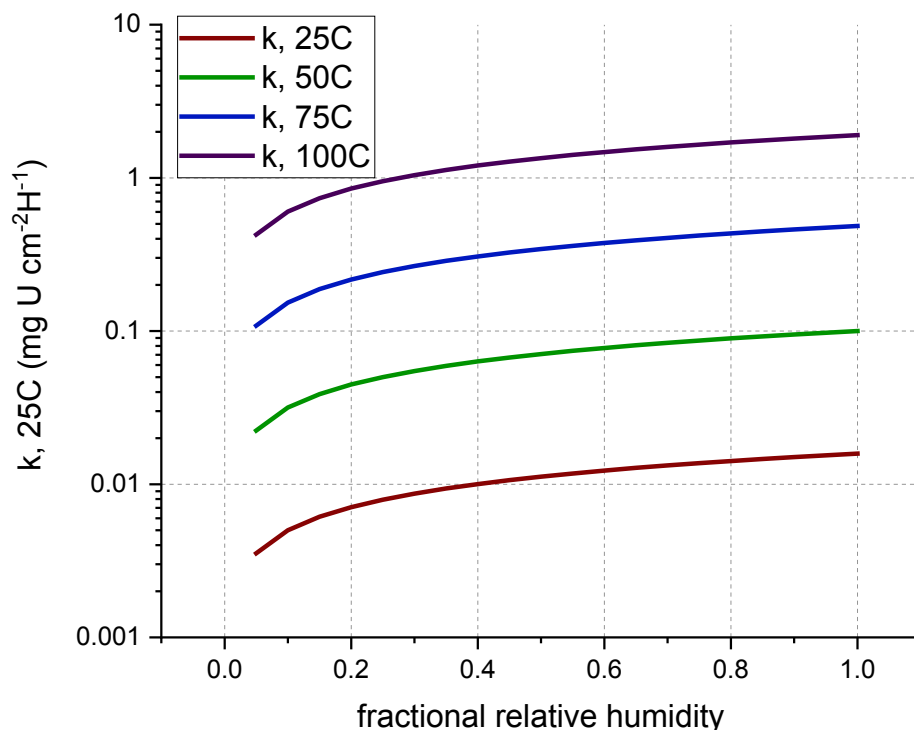


Figure B-7. Rate constant for U + H₂O modeled at 25°C, 50°C, 75°C and 100°C, versus fractional relative humidity¹³.

Significantly as the rate increases, so does the rate of heat generation. Epstein notes that ignition will occur if the rate of heat generation by the oxidation reaction exceeds the rate of heat dissipation¹.

B-2.2.4 Implications to Event Drums

The sharp differences in reaction rates seen in comparisons of dry conditions with those in which H₂O is present indicate that upon opening the parent drum, fast reactions with O₂ and H₂O began occurring immediately. According to the modeled oxidation rates, H₂O oxidation will be competitive with O₂ oxidation at 50% relative humidity and 50°C, and as temperature increases, reaction with H₂O will be significantly faster compared to O₂. This suggests that oxidation rates can be moderated by limiting or eliminating H₂O vapor from the atmosphere to which the drum contents are exposed when they are removed from the parent drum. This observation is in accord with those previously made by Solbrig and coworkers³⁰.

The fact that the initially formed oxide layer formed below 450°C is non-protective may have implications for the reaction of H₂O, which under these conditions has a dramatic effect on the uranium oxidation rate¹. The humidity, estimated to be 50% or greater to which the waste was exposed when the parent drum was opened, spread out, and repackaged, is sufficient to support this reaction sequence, and is consistent with the latency period.

B-2.2.5 U Oxidation in a Mixed H₂O/O₂ Atmosphere

Generally, the presence of O₂ retards the uranium-water vapor reaction, as a result of formation of a monolayer of adsorbed or chemisorbed oxygen atoms on the oxide surface, which block adsorption of H₂O. Ritchie¹² compared the effects of H₂O vapor on oxidation rates. As noted, at lower temperatures saturated H₂O vapor reacts substantially faster compared to O₂, and O₂ with H₂O vapor (Figure 20., eq. 3, 6, 10, 11). The presence of O₂ results in a slower overall oxidation rate for uranium metal. However, at higher temperatures Ritchie's expression predicts rates that are much faster when O₂ is present.

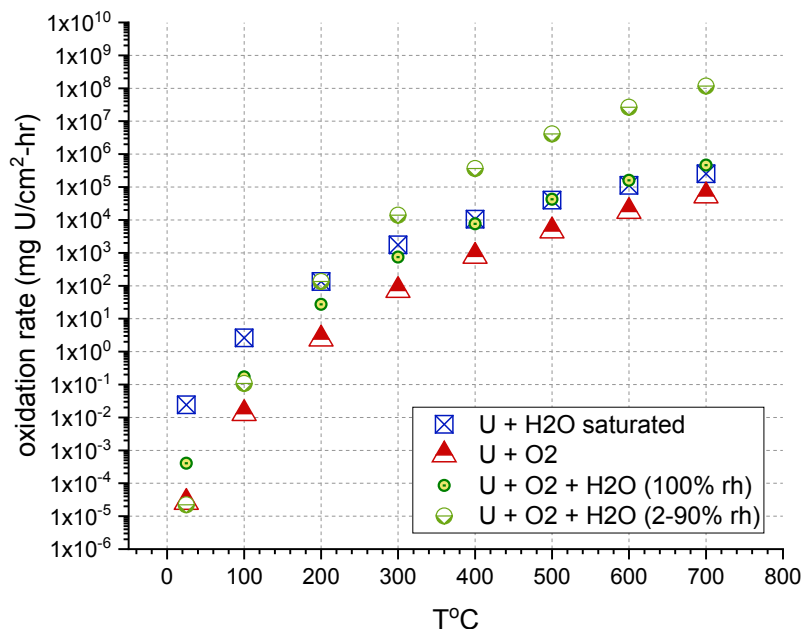


Figure B-8. Comparison of rates versus temperature, using phenomenological models of Ritchie.

$$\text{saturated H}_2\text{O} \quad k = 3.2e8 \exp(-13800/RT) \quad (\text{B-11})$$

$$\text{O}_2 \quad k = 6.9e8 \exp(-18300/RT) \quad (\text{B-12})$$

$$\text{O}_2 + \text{H}_2\text{O } 100 \% \text{ r.h.} \quad k = 4.6e9 \exp(-17800/RT) \quad (\text{B-13})$$

$$\text{O}_2 + \text{H}_2\text{O, } 2 - 90\% \text{ r.h.} \quad k = 4.8e13 \exp(-25000/RT) \quad (\text{B-14})$$

B-2.2.6 Implications to Event Drums-Effect of Irradiation.

The effect of prior irradiation on oxidation of uranium in dry and moist air was to increase oxidation by a factor of two at a minimum, per the articles of Bennett, 1975, 1981, 1985, and Pearce 1988.

B-2.2.7 Implications to Event Drums-Uranium Ignition.

If unchecked, the ignition temperatures can be exceeded. Small increases in oxidation rate could make the difference between slow corrosion and spontaneous ignition. For uranium, small sample sizes with high surface area, and that were thin resulted in lower ignition temperatures, dropping from the 600 - 640°C range to as low as 315°C¹⁹. Metallurgical variations also cause variation in the ignition temperature¹⁹.

Regarding ignition, the most important variable leading to lower ignition temperatures was found to be specific area¹⁹. A linear relationship was determined between the reciprocal of the absolute temperature and the specific area of the sample:

$$\log(ssa) = 4190/T - 5.23 \quad (B-15)$$

where ssa is the specific surface area in g/cm². It was further shown that the ignition of a foil with a high specific area at a low temperature in oxygen could cause ignition of a much larger piece of uranium. Schnizlein noted that “the fact that the smallest particle may cause ignition of the entire sample of powder makes the specific area of the smallest particle the determining factor instead of the specific area of the entire sample.”

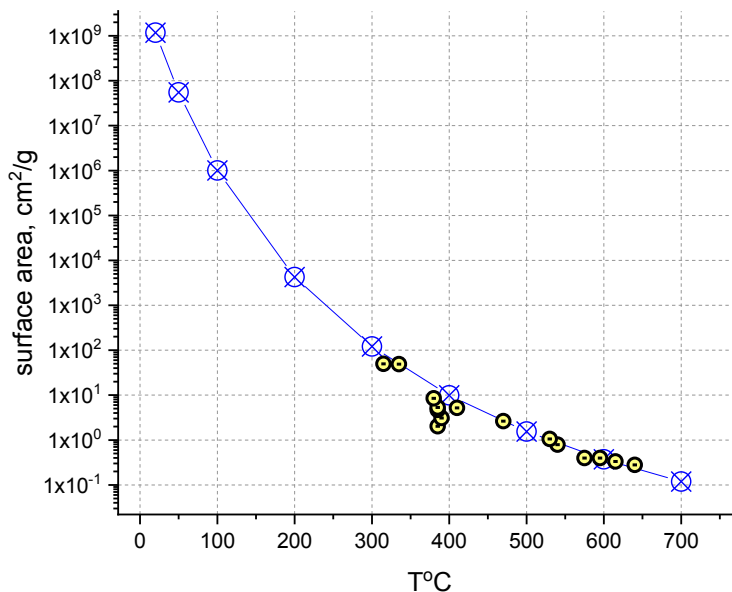


Figure B-9. Relationship between ignition temperature and surface area reported by Schnizlein in 1959. Blue trace generated using model, yellow data extracted from events in the literature.

B-2.2.8 Implications to Event Drums-Uranium Pyrophoricity

Pyrophoricity is the tendency of metals to ignite and burn in a self-sustaining oxidation reaction. A critical figure of merit is the ignition temperature, which is strongly affected by a number of factors. Once ignited, burning temperatures can be extremely high. Pyrophoric metals in powdered form are an explosion hazard due to high surface area and thus reaction rates.

The ignition temperature is related to rates of heat generated by oxidation and rate of heat lost through transfer to the surroundings. “As temperature increases, the oxidation rate and heat production rates dramatically increase. At some point the production of heat exceeds the rate of heat lost to the surroundings, and the reaction becomes self-sustaining, and ignition occurs. Factors influencing heat generation or heat loss include:

- specific area (most important)
- gas composition
- oxidation rate.

It was noted that prior oxidation and or pyrophoric reaction products can influence ignition temperature.

The ignition temperature was a strong function of surface area, modeled using the Arrhenius type relationship (equation 9)¹¹. The pronounced decrease in ignition temperature with increasing surface area was not reproduced by Tetenbaum (1962, see Totemeier Figure 5): they observed a decrease from ~ 340°C to 240°C as the surface area went from 2 to 100 cm²/g. Nevertheless, both studies clearly indicated that ignition temperature was acutely affected by surface area. Curiously, saturated H₂O vapor did not affect ignition temperatures.

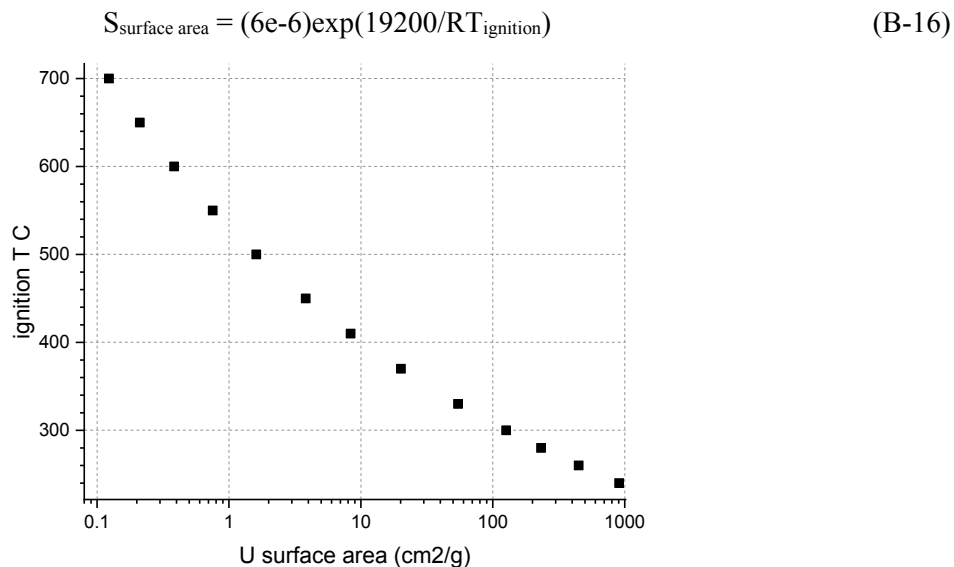


Figure B-10. Ignition temperature of uranium vs. log material surface area.

B-2.2.9 Cubes and Foils

Baker, Schnizlein and Bingle used a heat balance equation, in which uranium self-heating by oxidation was balanced by the sum of convective heat loss, and radiative heat loss²⁰. They tested ignition of cubes of uranium metal in air, which was measured at temperatures ranging from 650 to 700°C, and once ignited, achieved peak burning temperatures of about 1500°C in air²⁰. Ignition temperatures for two wire samples were measured at 475 and 525°C, and bundles of wires could have ignition temperatures 200°C lower than these values. Other surprising results were three foils that had thicknesses of 130, 30 and 10 μm, which ignited at 380, 335 and 315°C, respectively. A small piece of a 250 μm foil placed on top of a uranium cube ignited at 400°C, and once burning caused ignition of the cube²⁰.

The ignition temperature was found to be strongly affected by the physical size of the uranium, for example, foils and wires ignited at much lower temperatures compared to the cubes²⁰. The lower ignition temperatures were correlated with objects having large “specific surface area”, which is here defined as the macroscopic ratio of surface area to mass. Foils were observed to ignite in air at temperatures as low as 315°C. In comparing the oxide layer in these samples, it was found to be protective at higher temperatures, but incomplete at lower temperatures.

B-2.2.10 Powders and Finely Divided Uranium

A study by Tetenbaum, Mishler and Schnizlein in 1962 examined the ignition temperature of powder samples and noted that they were *much lower* compared to cubes of uranium metal. For the fine particles (63-74 μm) ignition temperature decreased with increasing sample weight, from ~ 330°C at 0.1 g, to ~ 250°C at 2 g; no further change was seen at higher masses. The fine particles showed a surprising dependence on sample *height*, (i.e., height of the powder bed), which caused ignition temperature to drop from about 330°C to ~ 260°C as the powder bed depth increased from ~ 0.1 to 1 mm.

The same experiment conducted for the coarse particles (841 – 1,000 μm) showed a decrease in ignition temperature from $\sim 400^\circ\text{C}$ to $\sim 320^\circ\text{C}$. They concluded that ignition was occurring in the center of a shallow zone in the upper layers of the powder bed. This latter experiment highlighted their conclusion that uranium ignition temperatures decrease with increasing specific surface area, and further that small quantities of fines in coarse uranium powder can significantly lower the ignition temperature. Surprisingly, they noted that pre-oxidation of the powders served to *decrease* the ignition temperature, an effect that was particularly pronounced in the smaller sized particles.

Plys and coworkers compiled a review of uranium pyrophoricity, emphasizing equations that relate particle size, object form factors to ignition temperature²². They predicted that 50 gal drums with particle sizes as low as 100 μm could ignite at temperatures $< 30^\circ\text{C}$ for an isolated drum, and that side-by-side drums would ignite about 10°C lower.

Epstein predicted that mm sized particles would be prone to spontaneous ignition, using an equation in which the rate of chemical heat generation is balanced by the heat loss by natural convection¹. The results were expressed in a plot of ambient ignition temperature versus the characteristic dimension of the powder, defined as the ratio of volume to area for the powder bed. The modeling showed two surprising results: (1) it predicted ambient ignition temperatures in the $20 - 80^\circ\text{C}$ range for small powdered deposits of uranium metal, and (2) it showed that the ambient ignition temperatures were higher in instances where the characteristic dimension was *higher*, i.e., in cases where the area was lower relative to the volume. This implies that lower ignition temperatures are realized for uranium powders that are piled deeper, which may suggest that the insulation of piled U powder is what is needed for ignition.

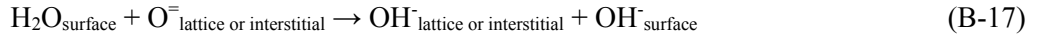
Hartman³⁵ showed that layers of small quantities of uranium and UH_3 powders would ignite at about 100°C and spontaneously at room temperature, respectively; these uranium powders had particle diameters of about 10 μm .

B-2.2.11 Effect of Depth of Uranium Material on Ignition Temperature

The height of the uranium powder influences the ignition powder. Tetenbaum measured ignition temperatures of $\sim 350^\circ\text{C}$ for 60 μm uranium at very shallow powder heights²³, however these values dropped to $\sim 260^\circ\text{C}$ when the powder height was $\geq \sim 1$ mm. Similar trends were seen for 840 μm uranium powder, although temperatures ranged from 400°C at zero powder height to $\sim 320^\circ\text{C}$ for powder heights $\geq \sim 2$ mm. However, Epstein concluded that particle size was unimportant, as Tetenbaum's size-dependence correlations showed only very weak dependence¹. Epstein notes that Tetenbaum's results have been interpreted to mean that the most important variable affecting the ignition temperature of uranium powder is the specific surface area and noted that in fact Schnizlein generated a correlation between ignition temperature and surface area expressed in terms of cm^2/g ¹⁹. Nevertheless, Epstein does conclude that ignition is caused by a condition in which heat is not lost through the top of the material, an assumption he notes is consistent with the observation that onset of ignition occurred at the radial center of the powder just below the surface¹. In his final modeling, he shows that drums situated side-by-side are prone to spontaneous ignition, dropping the ambient ignition temperature by 30°C . Isolated drums were not likely to spontaneously ignite, however those that were close packed will, and this phenomena accounts for many fires in the 1940s and 1950s.

B-2.2.12 The Mechanism of Oxidation and Influence of the Oxide Layer

The mechanism of uranium oxidation by water is hypothesized to involve dissociation of H₂O at the oxide surface:



Once formed, OH⁻ is thought to diffuse through the oxide faster compared to O⁻, accounting for the faster reaction rate of H₂O compared to O₂. Reaction of OH⁻ with U then generates UO₂ and H₂, which can go on to react with U to form UH₃. H₂ may also react with OH⁻ to form H₂O, which would result in no net production of H₂ or consumption of H₂O when both H₂O and O₂ were present.

At the U-UO₂ interface, OH⁻ will react with uranium to form UO₂ and H₂, the latter then further reacting with U metal:



Ritchie assumed that the electrons released will flow to the UO₂ surface, balancing the inward flow of OH⁻, which should be facile since UO₂ is a semiconductor. At the surface, the combination of electrons with additional OH⁻ may re-form O_o⁻ and create more H₂:



where O_o⁻ and OH_o⁻ are oxide and hydroxide on oxygen sites in UO₂.²⁷

If the OH⁻ concentration is controlling, then the relevant equation is derived from eq. B-20 (above):

$$K = [\text{OH}_o^-][\text{OH}_i^-]/[\text{O}_o^-]\text{P}_{\text{H}_2\text{O}} \quad (\text{B-21})$$

which implies that the rate is proportional to the square of the OH⁻ concentration, indicated by the modified Arrhenius equation 4.

Based on the modeling results, McGillivray assessed the mechanism, which initially involved H₂O adsorption onto the oxide surface and reaction with oxide ions (eq. 27). This reaction was previously identified by Winer and Colemares for H₂O adsorbed to the surface of the oxide layer²⁷.



The resulting hydroxyl ions then diffuse through the oxide lattice to the oxide/metal interface²⁷ where the uranium oxidation occurs.



An alternative H₂ formation mechanism involves combination of H at the surface and is supported by observations of complete stoppage of H₂ production on uranium oxide surfaces when O₂ was introduced²⁷.

Colmenares noted that in moist air, O₂ is preferentially chemisorbed onto surface sites occupied by H₂O in a pure water vapor environment²⁷. H₂O would then be bound to O atoms on the surface rather than reacting, which is consistent with the observation that addition of 100 v ppm of O₂ to the U / H₂O system

caused a large and rapid decrease in rate. It is thought that the O^{\ominus} ions block passage of OH^- through the lattice. Reaction is then perhaps limited by the rate of O^{\ominus} diffusion. Note that in a dry system, O^{\ominus} is thought to diffuse through the oxide layer to the metal-oxide interface²⁷. However, some of the oxygen remains on the surface as chemisorbed O_2^- , O^- or in the near-surface as interstitial O^- . This process is how the hyperstoichiometric UO_{2+x} is formed; this layer grows into the UO_2 , until the entire layer is interstitial-rich UO_{2+x} .²⁷ Comenares suggested that O_2 on uranium oxide blocks adsorption sites normally available for H_2O hydrolysis, which interrupts formation of the OH^- intermediates²⁷.

Ritchie hypothesized an oxidation mechanism for the reaction of $H_2O + U$ metal that was highly dependent on diffusion of oxygen species through an oxide layer¹³. He noted that any uranium surface will have an oxide layer with the stoichiometry UO_{2+x} , and that the extra O atoms in the hyperstoichiometric uranium dioxide can be treated as O_o^{\ominus} , which is an oxygen ion on an oxygen site. It reacts with H_2O as following eq. 12. The rate of reaction is controlled by the quantity of OH^- formed and by its rate of diffusion through the UO_2 layer. Note that the activation energy for the uranium- H_2O reaction (9.0 kcal/mole) is much less than that for the uranium- O_2 reaction (18.3 kcal/mole), consistent with the idea that diffusion of OH^- will be more facile compared to diffusion of O^{\ominus} .

The mechanism of uranium is oxidation by O_2 is similar, and has been summarized by Wilkinson^{29,11}:

- Transport of O_2 to the oxide
- Adsorption of O_2 to the surface
- Dissociation of O_2 into O atoms
- Ionization of O atoms at the oxide, and oxide-metal surfaces
- Diffusion of O^- through the oxide driven by an ion concentration gradient in the oxide
- Reaction of O^- with U ions at the oxide-metal interface.

In all of the mechanistic hypotheses in the literature, a key step in the reaction is the diffusion of OH^- or O^{\ominus} through the oxide layer. Consequently, the nature of the oxide, specifically its diffusivity, is an important factor in determining the overall rate of oxidation, either by H_2O or O_2 . The initially formed oxide layer, UO_2 , can be protective with respect to further oxidation. However, as the oxidation progresses, forming UO_{2+x} , compressive stresses are generated in the oxide, due to a mismatch of lattice parameters and densities between the oxide and the metal. The stresses are relieved by cracking and spallation in the outer layers of the oxide, forming micro-fissures, a phenomenon thought to be exacerbated by H_2 evolution^{8,9,18}. These cracks in the oxide layer may influence or control the overall rate of oxidation, because it has been thought that the rate-determining step may be the diffusion of OH^- and O^{\ominus} through the oxide layer to the oxide-metal interface, leading to further oxidation to UO_{2+x} . This is consistent with the observation that while increasing water vapor pressure will accelerate the oxidation rate, it will maximize at modest relative humidity values, with the rate being largely insensitive to changes in the relative humidity (from ~ 2% to 90%)¹³. The onset of cracking can be correlated with the transition to linear kinetics, with the rate controlled by O^{\ominus} and or OH^- diffusion through the oxide layer.

Appendix C
Radiolysis Incident Timeframe

Appendix C

Radiolysis Incident Timeframe

Radiolysis and Lid Ejection

To explain the ejection of the drum lids, a deflagration event invoking radiolytically generated hydrogen was evaluated. This is demonstrated by the following extreme bounding hydrogen gas generation calculation.

The rate of radiolytic gas generation (n) in moles per second from a material is given by:

$$n = W \times \sum_i (F_i \times G_i) \times C \quad (\text{C-1})$$

where

- W = total decay heat (watts),
- F_i = fraction of energy emitted that is of radiation type i and is absorbed by the material (range 0 to 1),
- G_i = number of molecules of gas produced (or consumed) per 100 eV of energy absorbed from radiation type i , and
- C = conversion constant
- = $(1 \text{ joule/W-sec}) \times (1\text{E}7 \text{ erg/joule}) \times (1 \text{ eV}/1.6\text{E-}12 \text{ erg}) \times (1 \text{ g-mole}/6.02\text{E}23 \text{ molecules})$
- = $1.04\text{E-}5 \text{ (g-mole)(eV)/(molecule)(W-s)}$
- = $1.04\text{E-}7 \text{ (g-mole)(100 eV)/(molecule)(W-s)}$.

To calculate a worst case radiolytic hydrogen gas generation scenario the bounding inputs were determined as follows:

Watts (Parent drum assay performed by Fluor Idaho)

Considering that the four daughter drums involved do not have validated individual assay data, the worst case scenario was determined using the suspect parent drums.

Parent Drum 10595963 (event drum parent) – 1.10×10^{-04} Watts

Parent Drum 10630243 – 4.68×10^{-02} Watts

Parent Drum 10630238 – 1.78×10^{-03} Watts

The largest wattage, Parent Drum 10630243, was used in calculating hydrogen gas generation.

Conservatism:

- *Largest wattage observed.*
- *Takes no credit for splitting the waste within trays.*

Fi-Fraction of Energy Emitted and Absorbed

The fraction of energy (F) depends on the nature of the emitted energy and the materials being irradiated. In the case of short-range radiation, F also will depend on the spatial distribution of radioactivity, especially when several different materials are present, such as in waste. F is the product of FP, the fraction of energy emerging from the particles (P), and FM is the fraction of energy absorbed by material (M)¹. Calculating a bounding value for the ARP V incident is based on the assumption that radionuclides are well dispersed throughout the waste forms, and that all radiation is emitted from the particle of origin and is available for gas generation. These assumptions result in an FP (i.e., the fraction of energy emerging from the particles) value of 1.

Conservatism:

- *Assumes no energy interaction with the base material.*

Gi -Number of Gas Molecules produced per 100 eV

For most materials, bond dissociation energies can be used to estimate an extreme upper bound to the number of gas molecules produced by radiolysis per unit energy absorbed. Dissociation energies of chemical bonds in common polymers range from about 65 kcal/g-mol (C-Cl) to 108 kcal/g-mol (C-F), with carbon-carbon bonds in the middle of the range (75–85 kcal/g-mol)¹. The carbon-hydrogen bond dissociation energy is about 90-100 kcal/g-mole (3.9–4.4 eV/molecule).

Based on volatile and semi-volatile data from the reacted ARP V drums numerous hydrogen bearing organics are present. Hydrogen (H₂) is the major gaseous product from radiolysis of most organic liquids and polymers that contain hydrogen. In the simplest case, a hydrogen molecule conceptually could be formed by breaking two C-H bonds and recombining the two hydrogen atoms. If all the radiation energy went into breaking bonds, then the energy needed to form one hydrogen molecule is given by twice the bond dissociation energy, or $2 \times (3.9\text{-}4.4 \text{ eV})/\text{molecule}$. This required energy results in an extreme upper bound G value estimated to be about 12 molecules generated per 100 eV of energy absorbed.

Visually the waste appeared to be dry, however, it is worth noting that water may have been present or sorbed as humidity. A G value of 12 is still conservative. The G value reported in CH-TRU Payload Appendices describing an analogous waste material, Type II.³ Solid Inorganic Material with unbound absorbed ambient moisture (≤ 6 percent by weight) or organic materials as 1.71.

To illustrate hydrogen generation for this evaluation a G value of 12 will be used.

Conservatism:

- *This is an extreme upper bound because it ignores the H atoms that recombine with the parent molecule and the energy that is dissipated as heat.*
- *Assumes only C-H bonds are broken.*

Impact of Temperature

Chemical reaction rates depend on temperature. The G (H₂) values reported in the literature are typically reported at a temperature of 298 K. It was assumed that the bounding G (H₂) values were determined at a reference temperature of 298 K. One of the ARP incidents occurred at an elevated temperature. A bounding temperature can be obtained from the visual appearance of the drums and data collected by the WIPP Technical Assistance Team (TAT)². The TAT noted that paint peeling begins at 400°C (673 K). Visually one of the drums in ARP V lid ejections looks similar. This is bounding, only one of the four drums involved in lid ejection experienced paint peeling.

An elevated temperature will increase the hydrogen gas-generation G value in accordance with the Arrhenius rate law. The ratio of the temperature-corrected G (H₂) value to the reference G (H₂) value was determined using the equation below.

$$\ln (k_1/k_2) = E_a/R*[(T_1-T_2)/T_1*T_2] \quad (C-2)$$

where

- T₂ = elevated temperature (K)
- T₁ = reference temperature (K)
- E_a = activation energy (cal/g-mole)

The activation energy was assumed equal to 3 kcal/g-mole (12560 J/mol), a value that the Contact Handled Transuranic (CH TRU) Payload document appendices indicate is not exceeded for most materials¹. The ideal gas constant is equal to 1.99 cal/g-mole K (8.314 J/mol*K).

The G value temperature correction equation predicted a G (T₂ = 673 K)/G (T₁ = 298 K) ratio of 16.8. Therefore, G (H₂) values were corrected to account for the elevated temperature predicted based on peeling paint which resulted in a bounding temperature corrected G (H₂) value of 202.

Conservatism:

- The first responder (Firefighter) measured the temperature of the drum using a thermal imaging camera as 190°F and the lid was already ejected.
- Only one of the drums experienced paint peeling.

Hydrogen Generation Rate

Using the above values and equation 1, the extreme bounding hydrogen generation rate for the ARP V incident is 9.83 x 10⁻⁷ mols H₂ per second.

Conservatism:

- Using more realistic G value (1.7) and temperature (T₂ = 361K) corrected ratio of 2.42 yields a hydrogen generation rate of 2.13 x 10⁻⁸ mols H₂ per second.

Hydrogen Concentration to Achieve Lower Flammability Limit (LFL)

Based on visual examination data, an average fill factor of 55% can be used to calculate the void volume in a 55-gallon drum and results in a void volume of 30 gallons. The LFL for hydrogen is reported to be 4% (v/v). Although testing by Savannah River suggests that for total integrity failure i.e. drum lid removal will not occur below 15% (v/v)². In addition, LFLs are reported for normal oxygen atmospheric concentrations at sea level. When organics are present, the same radiolysis reaction that produces hydrogen gas, also converts atmospheric oxygen into carbon dioxide gas, diminishing the overall atmospheric oxygen concentration within the waste drum and narrowing the flammable range of most gases [raising the LFL and lowering the upper flammability limit (UFL)], including hydrogen. To be conservative, a 4% (v/v) will be used to calculate the time needed to achieve an LFL condition and equates to 1.2 gallons of hydrogen. Therefore, the total number of mols of hydrogen required for deflagration would be 0.20 mols.

Conservatism:

- *The LFL value used to achieve deflagration is likely low.*
- *This assumes no diffusion through the drum filter.*
- *Oxygen depletion from radiolysis of organics is not accounted for.*

Conclusion

In the reaction timeframe involved, the hydrogen gas generation rate due to radiolysis is insufficient. To generate 0.20 mols of hydrogen, using the bounding radiolysis assumptions, would require 57 hours. Radiolytic generation cannot result in exceeding a LFL values for hydrogen in the timeframe observed.

Conservatism:

- *Using a more realistic G value and temperature [G (H₂)4.11] would require 2608 hours for radiolysis to exceed the LFL for hydrogen.*

References:

1. CH-TRAMPAC, 2003, "Contact Handled Transuranic Waste Authorized Methods for Payload Control," Rev. 1, URL: <http://www.wipp.ws/library/CHsar/DOCUMENTS/CH-TRAMPAC.pdf>, Webpage.
2. Mechanical Response of Drum: Modeling Of Drum Behavior When Pressurized Final Technical Assessment Team Report
3. TRU Drum Hydrogen Explosion Tests, KL Dykes, ML Meyers DOE Reports Number WSRC-TR-90-165.

Appendix D

Parameter Investigations Supporting the Pressure, Temperature vs. Time Experiments

Appendix D

Parameter Investigations Supporting the Pressure, Temperature vs. Time Experiments

D-1 PRESSURE AND CH₄ PRODUCTION: EFFECT OF THE RATE OF HEATING

From an operational and a laboratory perspective, the rate at which heat was delivered to the waste material was hypothesized to be a factor that could influence the pressure buildup in the headspace. To evaluate this factor, 3 g aliquots of three ejected material samples (two from ejected sample 1013 and one from ejected sample 6013) were compared, varying the heating rate, and also the headspace atmosphere. Note that the beryllium content of both of these samples was very similar, at 9.9% and 11.8% for 1013 and 6013, respectively. The pressure vs. set temperature profile for 1013 heated in Ar with a fast temperature ramp (10°C/min) displayed a sharp pressure increase at ~205°C, that peaked at about 460 psig (Figure D-1). Consistently, sample 6013 heated at the same rate in air showed extremely similar behavior, with the pressure increase at ~210°C, and a maximum pressure at ~380 psig. In contrast, the ejected sample 1013 heated with a slow temperature ramp (1°C/min) showed the same profile, but with the sharp rise occurring at 140°C/min. The variation is explained in terms of an equilibration time for the pressure vessel, which can maintain a more uniform temperature distribution across its interior when a slow heating ramp was used. In contrast, when a fast heating ramp is used, the interior temperature of the vessel lags the set temperature because there is insufficient time for temperature equilibration. The percentage CH₄ values in the headspace was similar for ejected sample 1013 heated at fast and slow rates (Figure 32, left three columns) suggesting that the fundamental chemical process was the same using both temperature ramp rates. Since the experiments using the slow temperature ramp are not as affected by equilibration time, the slow experiments more accurately reflect the true temperature of the rapid pressure rise. However, since the slow ramp experiments were time intensive, fast ramp experiments were predominantly used for comparing samples and experimental parameters.

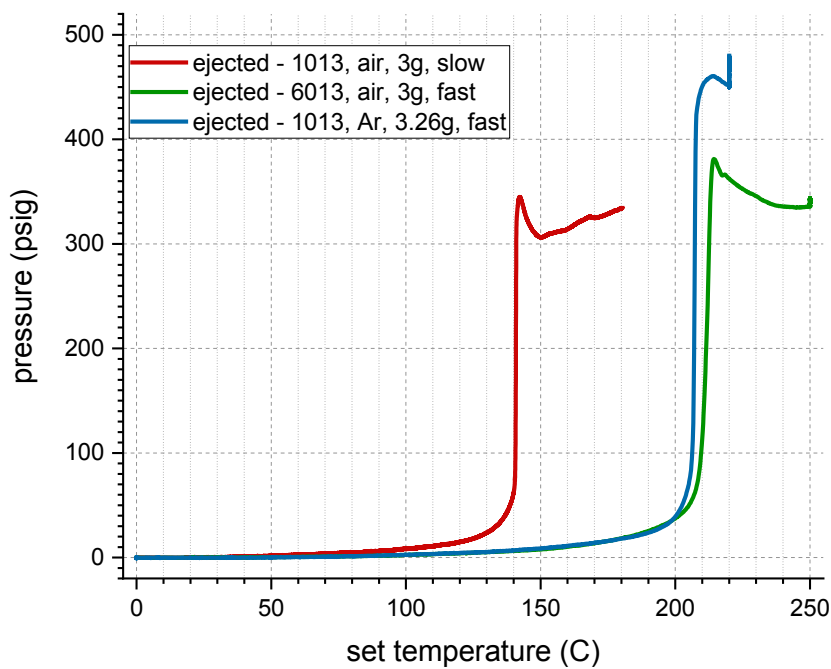


Figure D-1. Pressure vs. temperature profiles for floor (ejected) samples 1013 and 6013, acquired at heating rates of 1°C/min and 10°C/min, respectively.

D-2 EFFECT OF SAMPLE MASS ON GAS PRODUCTION

The quantity of gas generated is related to the mass of the waste material in a linear fashion. Aliquots of ejected sample 1013 with varying masses were tested using a slow, 1°C/min temperature ramp, to evaluate the effect of sample mass on the gas pressure. As the set temperature increases to about 110°C, curves from experiments using four different sample masses were superimposable (Figure D-2) indicating that the modest pressure rise over this range was likely due to outgassing of the chamber. Above 110°C, the pressure profiles diverge, with the profile for the 3.0 g sample rising the most quickly to an intermediate maximum at 340 psig, and the profile for the 0.5 g sample rising very slowly to an intermediate maximum of about 25 psig. The experiments conducted using 1.0 and 2.0 g samples produced profiles identical with that of the 3 g sample. The very sharp rise in pressure at 140 - 150°C is a dramatic departure from the slowly increasing pressure at lower temperatures, an observation consistent with the idea that an activation energy has been exceeded for a gas-producing reaction. When the intermediate maximum pressure is plotted versus the sample mass, an approximately linear relationship is seen (Figure D-2, right).

The slow pressure rise above the intermediate maxima cannot be attributed to temperature rise: for example, the 2 g experiment increases from ~ 180 to 280 psi over a temperature change of 160 to 250°C, or 433 to 523K, which would account for a pressure increase to only 217 psi. Therefore, the slower pressure rise at temperatures above the intermediate maxima are the result of production of additional gas.

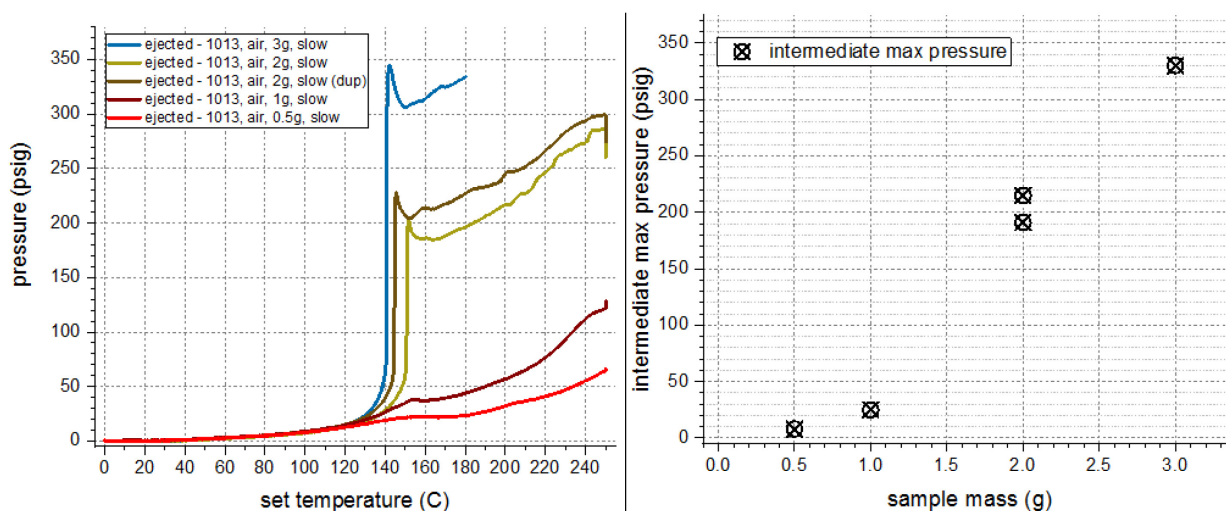


Figure D-2. Left, pressure vs. set temperature profiles for varying sample sizes of ejected sample 1013. The 2.0 g experiment was conducted in duplicate. Right, P_{\max} v. sample mass.

D-3 EFFECT OF HEAD-SPACE ATMOSPHERE

The bench-scale experiments suggested that the ambient atmosphere was not directly responsible for the gas generation. Two sets of comparisons were conducted to evaluate the effect of the ambient atmosphere on the gas evolution. In a comparison of 1 g samples of ejected sample 1013, heating in air resulted in an intermediate maximum of 39 psig at 152°C, followed by a slower pressure rise to ~ 120 psi at 250°C (see Figure D-3). When the sample was purged with Ar, the intermediate maximum was about the same at 41 psig, but at lower temperature, 130°C. A similar comparison of 3 g samples of drum material (sample 10013) showed very similar behavior for the air and Ar experiments. The air experiment displayed a slow pressure increase to 46 psig at 250°C, while the Ar experiment showed a slow increase to 52 psig at the same temperature (given the experimental error, these values are considered the same).

For the drum sample, the same trend is seen, although the Ar and air experiments are very similar. The plot of these experiments shows that pressure continues to increase for a long period of time at the end of the experiment when the temperature was held at 250°C (accounting for the vertical lines at the right-hand side of the plots).

If the gas production is the result of the reaction of Be_2C with two moles of H_2O , the fact that the head-space does not appear to affect gas generation indicates that the required H_2O must be residual in the samples. To achieve a pressure rise of 350 psig at 150°C (423K) in a volume of 11.7 cm^3 , 8.0 millimol or 145 mg H_2O would be required. This would constitute about 1.9% of the 3 g sample, which is conceivable, and may explain why the evacuated samples displayed mitigated gas generation. (See Section 5.5.1). Finally, atmospheric oxygen does not impact pressure production.

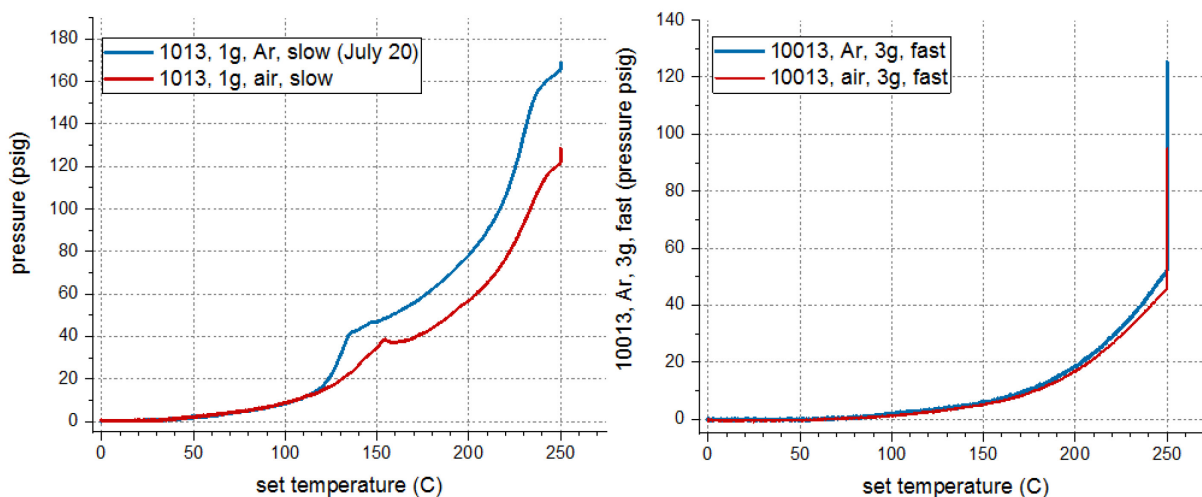


Figure D-3. Pressure v temperature profiles. Left, sample 1013 (ejected material), 1 g, heated in air and Ar. Right, sample 10013 (drum material), 3 g, heated in air and Argon.

Appendix E

SwRI Particle Size Distribution Data Sheets

Appendix E

SwRI Particle Size Distribution Data Sheets

Sample ID

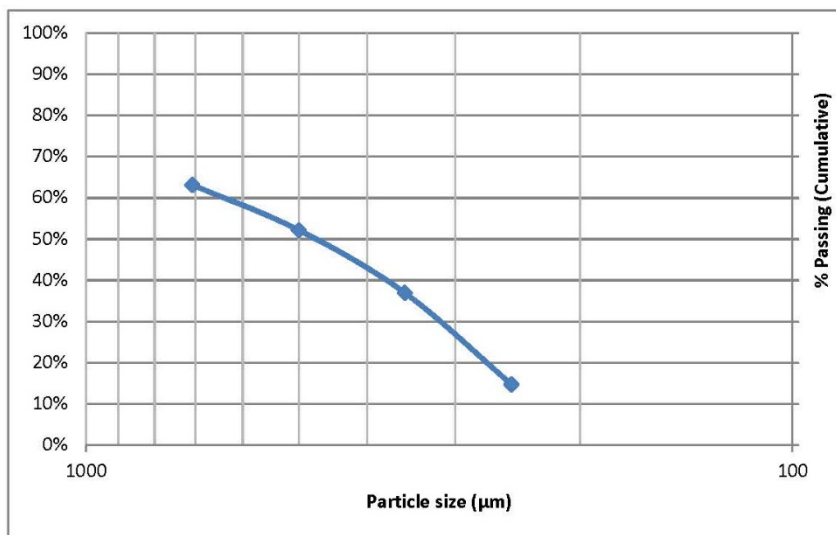
SWR001013A

Lab Name: Southwest Research Institute
Lab Code: SwRI
Matrix: Solid
SDG: SWR001013A
Lab System ID: 631472

Client: Fluor Idaho
Project No.: 22165.24.001
SRR #: 61623
TO#:
Method:

Sample wgt used for sieving (g): 11.2451

Sieve	Micron Size	Wt on sieve (g)	Cumulative	
			% pass	% retained
25	707	4.1477	63.1%	36.9%
35	500	1.2334	52.1%	47.9%
45	354	1.7129	36.9%	63.1%
60	250	2.4964	14.7%	85.3%
< 60	< 250	1.6547	0.0%	100.0%



Sample ID

SWR001023A

Lab Name: Southwest Research Institute

Lab Code: SwRI

Matrix: Solid

SDG: SWR001013A

Lab System ID: 631473

Client: Fluor Idaho

Project No.: 22165.24.001

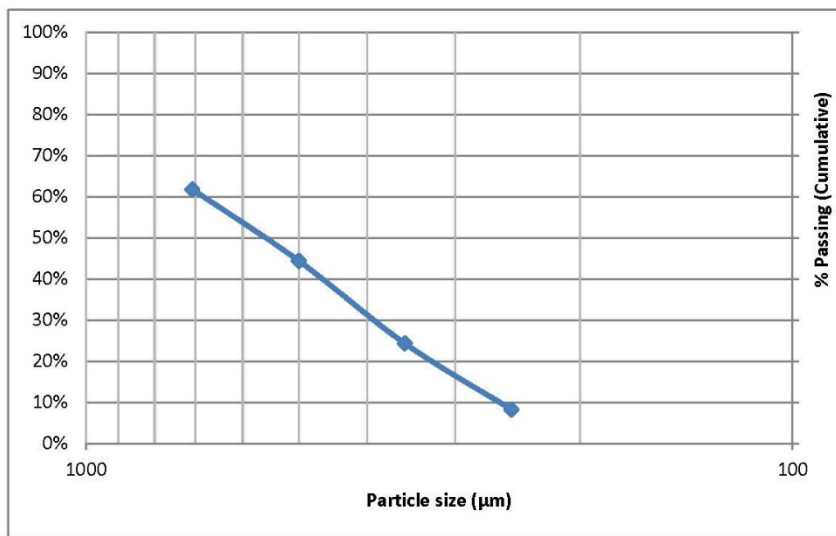
SRR #: 61623

TO#:

Method:

Sample wgt used for sieving (g): 10.5577

Sieve	Micron Size	Wt on sieve (g)	Cumulative	
			% pass	% retained
25	707	4.0344	61.8%	38.2%
35	500	1.8372	44.4%	55.6%
45	354	2.1193	24.3%	75.7%
60	250	1.6973	8.2%	91.8%
< 60	< 250	0.8695	0.0%	100.0%



Sample ID

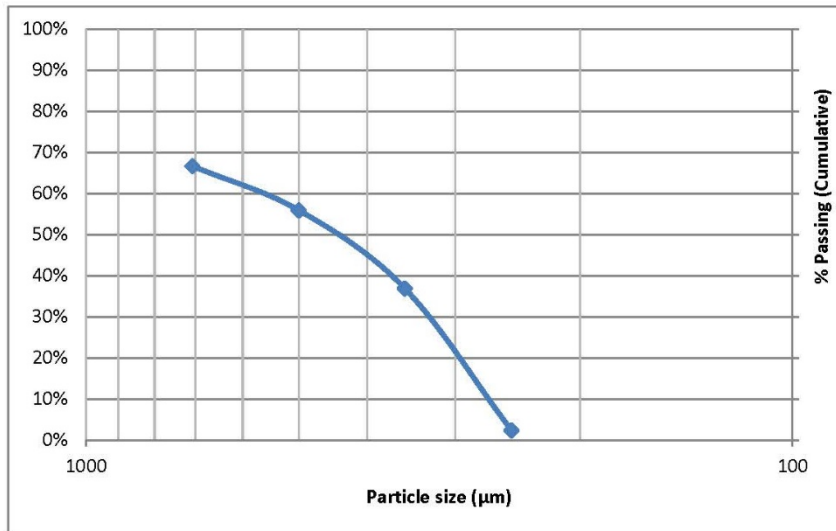
SWR002013A

Lab Name: Southwest Research Institute
Lab Code: SwRI
Matrix: Solid
SDG: SWR001013A
Lab System ID: 631474

Client: Fluor Idaho
Project No.: 22165.24.001
SRR #: 61623
TO#:
Method:

Sample wgt used for sieving (g): 11.8579

Sieve	Micron Size	Wt on sieve (g)	Cumulative	
			% pass	% retained
25	707	3.9547	66.6%	33.4%
35	500	1.2736	55.9%	44.1%
45	354	2.2547	36.9%	63.1%
60	250	4.0974	2.3%	97.7%
< 60	< 250	0.2775	0.0%	100.0%



Sample ID

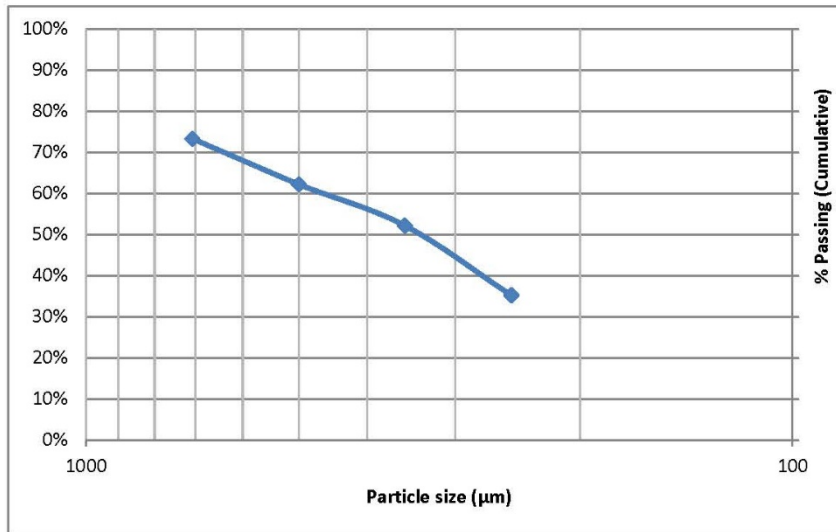
SWR003013A

Lab Name: Southwest Research Institute
Lab Code: SwRI
Matrix: Solid
SDG: SWR001013A
Lab System ID: 631475

Client: Fluor Idaho
Project No.: 22165.24.001
SRR #: 61623
TO#:
Method:

Sample wgt used for sieving (g): 10.5744

Sieve	Micron Size	Wt on sieve (g)	Cumulative	
			% pass	% retained
25	707	2.8264	73.3%	26.7%
35	500	1.1713	62.2%	37.8%
45	354	1.0605	52.2%	47.8%
60	250	1.7987	35.2%	64.8%
< 60	< 250	3.7175	0.0%	100.0%



Sample ID

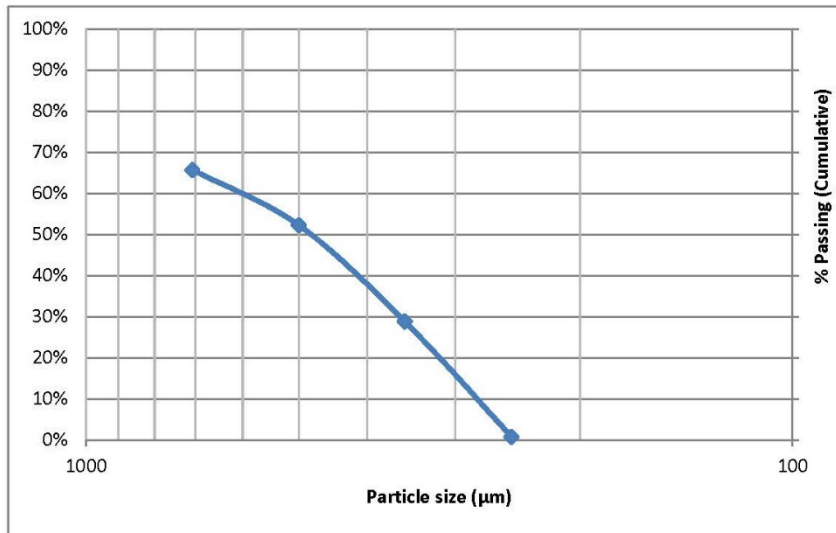
SWR004013A

Lab Name: Southwest Research Institute
Lab Code: SwRI
Matrix: Solid
SDG: SWR001013A
Lab System ID: 631476

Client: Fluor Idaho
Project No.: 22165.24.001
SRR #: 61623
TO#:
Method:

Sample wgt used for sieving (g): 11.8075

Sieve	Micron Size	Wt on sieve (g)	Cumulative	
			% pass	% retained
25	707	4.0442	65.7%	34.3%
35	500	1.5941	52.2%	47.8%
45	354	2.7628	28.8%	71.2%
60	250	3.3156	0.8%	99.2%
< 60	< 250	0.0908	0.0%	100.0%



Sample ID

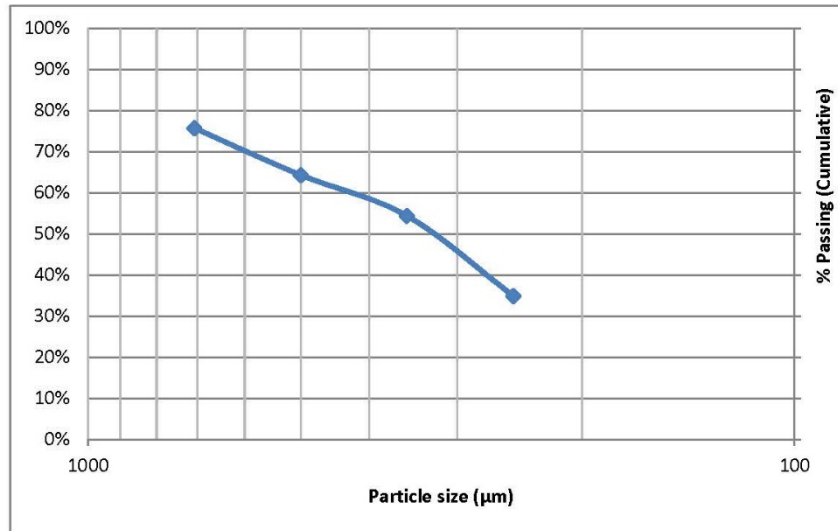
SWR005013A

Lab Name: Southwest Research Institute
Lab Code: SwRI
Matrix: Solid
SDG: SWR001013A
Lab System ID: 631477

Client: Fluor Idaho
Project No.: 22165.24.001
SRR #: 61623
TO#:
Method:

Sample wgt used for sieving (g): 10.7834

Sieve	Micron Size	Wt on sieve (g)	Cumulative	
			% pass	% retained
25	707	2.6189	75.7%	24.3%
35	500	1.2295	64.3%	35.7%
45	354	1.0683	54.4%	45.6%
60	250	2.1030	34.9%	65.1%
< 60	< 250	3.7637	0.0%	100.0%



Sample ID

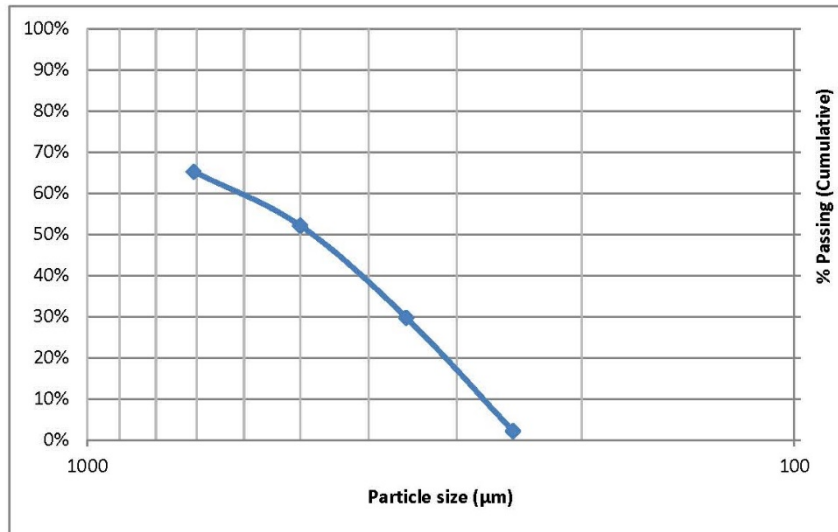
SWR006013A

Lab Name: Southwest Research Institute
Lab Code: SwRI
Matrix: Solid
SDG: SWR001013A
Lab System ID: 631478

Client: Fluor Idaho
Project No.: 22165.24.001
SRR #: 61623
TO#:
Method:

Sample wgt used for sieving (g): 6.3772

Sieve	Micron Size	Wt on sieve (g)	Cumulative	
			% pass	% retained
25	707	2.2155	65.3%	34.7%
35	500	0.8369	52.1%	47.9%
45	354	1.4271	29.8%	70.2%
60	250	1.762	2.1%	97.9%
< 60	< 250	0.1357	0.0%	100.0%



Sample ID

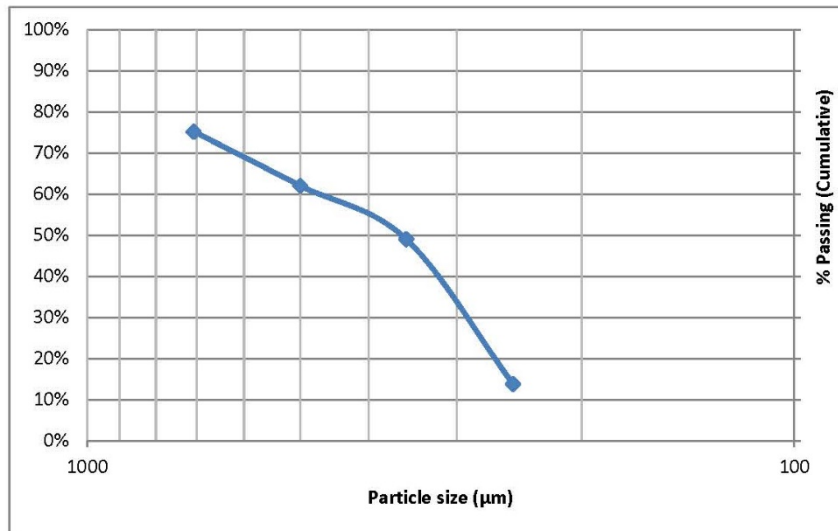
SWR007013A

Lab Name: Southwest Research Institute
Lab Code: SwRI
Matrix: Solid
SDG: SWR001013A
Lab System ID: 631479

Client: Fluor Idaho
Project No.: 22165.24.001
SRR #: 61623
TO#:
Method:

Sample wgt used for sieving (g): 11.5876

Sieve	Micron Size	Wt on sieve (g)	Cumulative	
			% pass	% retained
25	707	2.8725	75.2%	24.8%
35	500	1.5239	62.1%	37.9%
45	354	1.5092	49.0%	51.0%
60	250	4.0867	13.8%	86.2%
< 60	< 250	1.5953	0.0%	100.0%



Sample ID

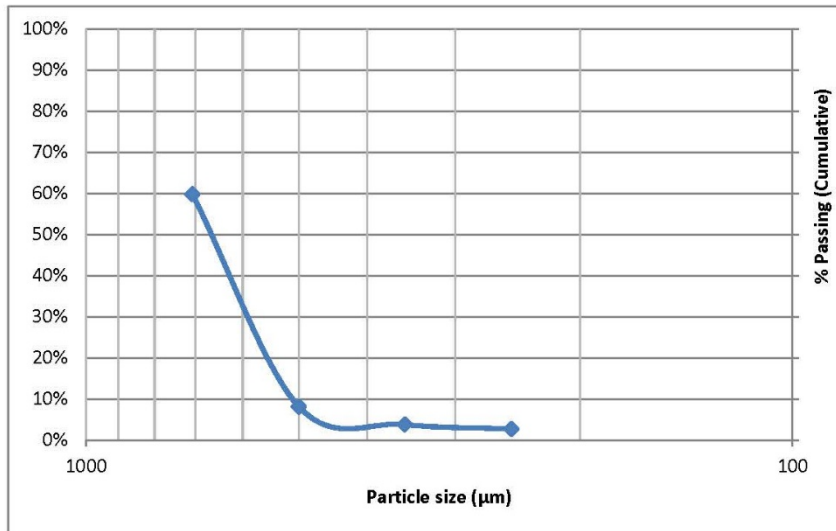
SWR010013A

Lab Name: Southwest Research Institute
Lab Code: SwRI
Matrix: Solid
SDG: SWR010013A
Lab System ID: 632268

Client: Fluor Idaho
Project No.: 22165.25.001
SRR #: 61699
TO#:
Method:

Sample wgt used for sieving (g): 10.9512

Sieve	Micron Size	Wt on sieve (g)	Cumulative	
			% pass	% retained
25	707	4.3972	59.8%	40.2%
35	500	5.6636	8.1%	91.9%
45	354	0.4786	3.8%	96.2%
60	250	0.1187	2.7%	97.3%
< 60	< 250	0.2931	0.0%	100.0%



Sample ID

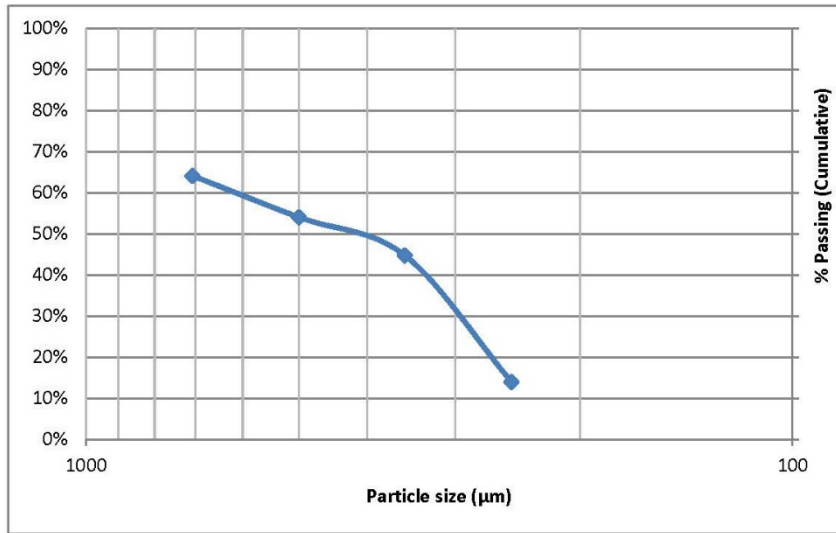
SWR011013A

Lab Name: Southwest Research Institute
Lab Code: SwRI
Matrix: Solid
SDG:SWR010013A
Lab System ID: 632269

Client: Fluor Idaho
Project No.: 22165.25.001
SRR #: 61699
TO#:
Method:

Sample wgt used for sieving (g): 11.0593

Sieve	Micron Size	Wt on sieve (g)	Cumulative	
			% pass	% retained
25	707	3.9681	64.1%	35.9%
35	500	1.1149	54.0%	46.0%
45	354	1.0288	44.7%	55.3%
60	250	3.4021	14.0%	86.0%
< 60	< 250	1.5454	0.0%	100.0%



Sample ID

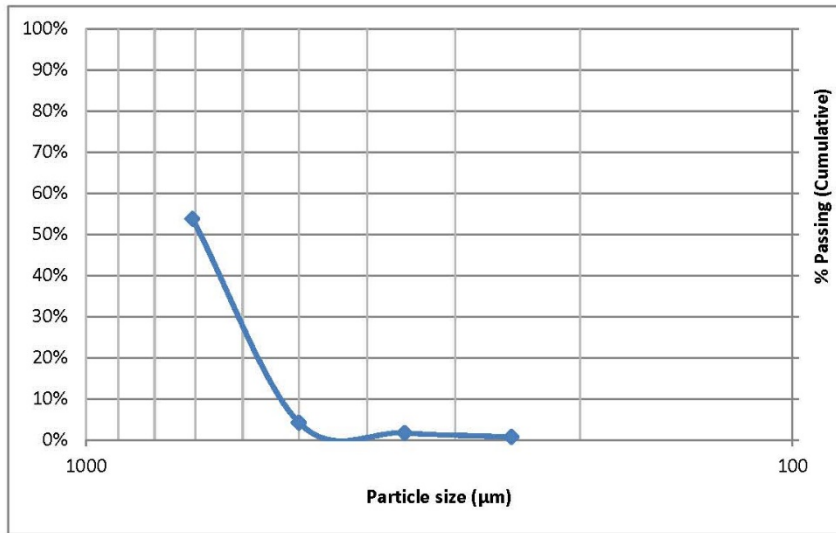
SWR013013A

Lab Name: Southwest Research Institute
Lab Code: SwRI
Matrix: Solid
SDG: SWR010013A
Lab System ID: 632270

Client: Fluor Idaho
Project No.: 22165.25.001
SRR #: 61699
TO#:
Method:

Sample wgt used for sieving (g): 12.3760

Sieve	Micron Size	Wt on sieve (g)	Cumulative	
			% pass	% retained
25	707	5.7126	53.8%	46.2%
35	500	6.1400	4.2%	95.8%
45	354	0.3162	1.7%	98.3%
60	250	0.1199	0.7%	99.3%
< 60	< 250	0.0873	0.0%	100.0%



Sample ID

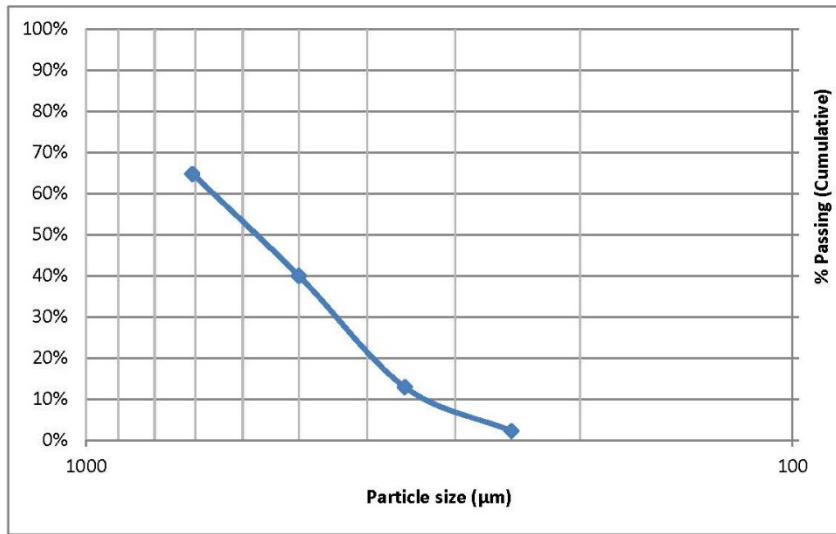
SWR014013A

Lab Name: Southwest Research Institute
Lab Code: SwRI
Matrix: Solid
SDG: SWR010013A
Lab System ID: 632271

Client: Fluor Idaho
Project No.: 22165.25.001
SRR #: 61699
TO#:
Method:

Sample wgt used for sieving (g): 12.1399

Sieve	Micron Size	Wt on sieve (g)	Cumulative	
			% pass	% retained
25	707	4.2739	64.8%	35.2%
35	500	3.0128	40.0%	60.0%
45	354	3.2845	12.9%	87.1%
60	250	1.2996	2.2%	97.8%
< 60	< 250	0.2691	0.0%	100.0%



Appendix F
Pneumatic Rupture Test

Appendix F

Pneumatic Rupture Test



PNEUMATIC RUPTURE TEST



55 Gallon Open Head Skolnik Drum

TEST REPORT #: 18-MN10228

TESTING PERFORMED FOR:

FLUOR IDAHO
1580 Sawtelle Street
Idaho Falls, ID 83402

ATTN: Jason Wilding

TESTING PERFORMED BY:

TEN-E PACKAGING SERVICES, INC.
1666 County Road 74
Newport, MN 55055
Phone: 651-459-0671
Fax: 651-459-1430

October 4, 2018

TABLE OF CONTENTS

NOTES2
OBJECTIVE2
INDUSTRY STANDARD REFERENCES2
COMPONENT INFORMATION3
TEST PROCEDURES AND RESULTS5
DISCLAIMER OF WARRANTIES19

NOTES

Each drum test was video recorded and given to Fluor Idaho for further evaluation. Testing was in accordance with Statement of Work – 871 and subcontractor number 18-7279.

OBJECTIVE

To conduct Pneumatic Rupture testing on the 55 Gallon Open Head Skolnik Steel Drum with Bolt Locking Ring.

INDUSTRY STANDARD REFERENCES

Pressure	ASTM ^③ D7660:	Standard Guide for Conducting Internal Pressure Tests on United Nations (UN) Packagings
-----------------	-----------------------------	---

③ American Society for Testing and Materials (ASTM)

EQUIPMENT

All inspection, measuring and test equipment that can affect product quality is calibrated and adjusted at prescribed intervals, or prior to use, and is traceable to NIST, using ANSI Z540 as an overall guide for calibration certification.

COMPONENT INFORMATION

55 Gallon Open Head Skolnik Steel Drum with Bolt Locking Ring		DRAWING
Container Description:	Skolnik 55 Gallon Open Head Steel Drum	
Closure Description	Bolt Locking Ring and Filter Plug	
Bag Description:	ARP FF-Gallon Transfer Bag Rigid Plastic Liner	
Sample Size:	(14) Samples	
Photos		

PNEUMATIC RUPTURE TESTING OF 55-GALLON DRUMS

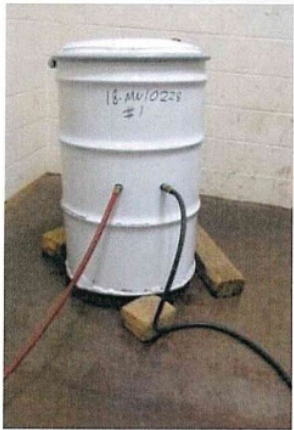
Drum #	Drum Lot #	Bung Filter & Lock Ring Orientation	Torque Value	Rigid Liner & PVC Transfer Bag	NucFil Filter Plugged	50% Full of Surrogate Material	Moisture on Gasket & Lock Ring	Lid Ejection
1	1	In-Line	55	No	No	No	No	No
2	1	In-Line	55	No	No	No	No	No
3	1	In-Line	55	Yes	No	No	No	No
4	1	Offset	55	Yes	Yes	No	No	No
5	1	Offset	55	Yes	Yes	No	No	No
6	1	Offset	55	Yes	Yes	No	No	No
7	1	Offset	10	Yes	Yes	No	No	No
8	1	Offset	55	Yes	Yes	Yes	No	No
9	1	Offset	10	Yes	Yes	Yes	No	No
10	1	Offset	10	Yes	Yes	Yes	Yes	Yes
11	1	Offset	10	Yes	Yes	No	Yes	Yes
12	1	Offset	55	Yes	Yes	No	Yes	Yes
13	1	Offset	55	Yes	Yes	No	No	Yes
14	1	Offset	55	Yes	No	No	No	No





PNEUMATIC RUPTURE TESTING OF 55-GALLON DRUMS


Drum #	Pressure Rate (SCFM)	Time to Rupture (Min:Sec)	Max Pressure (PSI)	Height of Lid Ejection (Feet)	Deformation to Bottom of Drum (Inches)	Concentricity of Top Opening (Inches)
1	20	3:38	36	0	2.0625	23.5
2	20	3:53	32	0	2.2500	23.5
3	20	1:29	22	0	1.4375	23.5
4	20	1:15	30	0	1.7500	23.5
5	25	1:10	42	0	2.3750	23.5
6	*No Flow Meter	1:09	44	0	2.9375	23.5
7	*No Flow Meter	0:53	33	0	1.7500	23.5
8	*No Flow Meter	1:06	45	0	2.5000	23.5
9	*No Flow Meter	0:51	35	0	2.3750	23.5
10	*No Flow Meter	0:37	32	35	2.5000	23.5
11	*No Flow Meter	2:10	40	75	1.7500	23.5
12	*No Flow Meter	3:08	52	100	2.0000	23.5
13	*No Flow Meter	2:56	46	100	1.7500	23.5
14	*No Flow Meter	4:30	40	0	2.2500	23.5

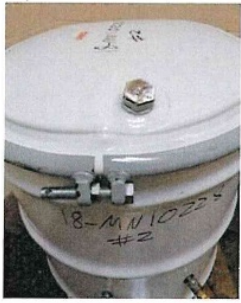



* Note: Maximum inlet pressure was around 100 PSI when there was no flow meter being used.


TEST PROCEDURES AND RESULTS





SAMPLE #1 TEST INFORMATION		Test Set Up Photo
TEST CONTENTS:	Empty	
FILTER PLUGGED:	No	
TORQUE VALUE:	55 Ft-Lbs.	
PRESSURIZATION RATE:	20 SCFM	
MOISTURE ON GASKET AND RING:	No	
TEST DURATION:	3 Minutes and 38 Seconds	
MAXIMUM PRESSURE:	36 PSI	
AREA OF PRESSURIZATION:	Through the Sidewall	
TEST EQUIPMENT:		
Regulated Air Source #: 2	Flow Meter #: 644	
Digital Pressure Gauge #: 643	Stop Watch #: 154	


Photos			
			
Comments			
<p>There was damage to the gasket prior to receiving the drum sample. During the test, leakage occurred on the bottom seam with deformation to the top and bottom heads of the drum.</p>			


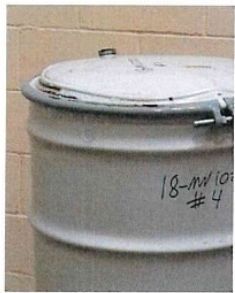
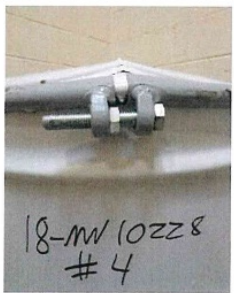

SAMPLE #2 TEST INFORMATION		Test Set Up Photo
TEST CONTENTS:	Empty	
FILTER PLUGGED:	No	
TORQUE VALUE:	55 Ft-Lbs.	
PRESSURIZATION RATE:	20 SCFM	
MOISTURE ON GASKET AND RING:	No	
TEST DURATION:	3 Minutes and 53 Seconds	
MAXIMUM PRESSURE:	32 PSI	
AREA OF PRESSURIZATION:	Through the Sidewall	
TEST EQUIPMENT:		
Regulated Air Source #: 2	Flow Meter #: 644	
Digital Pressure Gauge #: 643	Stop Watch #: 154	


Photos			
			
Comments			
<p>There was damage to the gasket prior to receiving the drum sample. During the test leakage occurred through the filter, at the joint of the bolt ring, and one spot on the bottom seam. There was deformation to the top and bottom heads of the drum.</p>			

SAMPLE #3 TEST INFORMATION		Test Set Up Photo
TEST CONTENTS:	Rigid Liner and Transfer Bag	
FILTER PLUGGED:	No	
TORQUE VALUE:	55 Ft-Lbs.	
PRESSURIZATION RATE:	20 SCFM	
MOISTURE ON GASKET AND RING:	No	
TEST DURATION:	1 Minutes and 29 Seconds	
MAXIMUM PRESSURE:	22 PSI	
AREA OF PRESSURIZATION:	Through the Sidewall	
TEST EQUIPMENT:		
Regulated Air Source #: 2	Flow Meter #: 644	
Digital Pressure Gauge #: 643	Stop Watch #: 154	


Photos			
			
Comments			
<p>There was damage to the gasket prior to receiving the drum sample. During the test, leakage occurred through the filter at 38 seconds and at the joint of the bolt ring. There was deformation to the top and bottom heads of the drum.</p>			

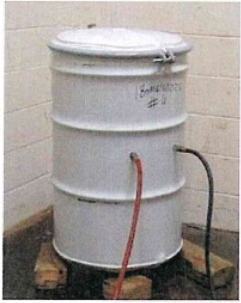



SAMPLE #4 TEST INFORMATION		Test Set Up Photo
TEST CONTENTS:	Rigid Liner and Transfer Bag	
FILTER PLUGGED:	Yes	
TORQUE VALUE:	55 Ft-Lbs.	
PRESSURIZATION RATE:	20 SCFM	
MOISTURE ON GASKET AND RING:	No	
TEST DURATION:	1 Minutes and 15 Seconds	
MAXIMUM PRESSURE:	30 PSI	
AREA OF PRESSURIZATION:	Through the Sidewall	
TEST EQUIPMENT:		
Regulated Air Source #: 2	Flow Meter #: 644	
Digital Pressure Gauge #: 643	Stop Watch #: 154	


Photos			
			
Comments			
<p>There was damage to the gasket prior to receiving the drum sample. During the test, leakage occurred 90 degrees to the left of the joint of the bolt ring and at the joint of the bolt ring. There was deformation to the top and bottom heads of the drum.</p>			

SAMPLE #5 TEST INFORMATION		Test Set Up Photo
TEST CONTENTS:	Rigid Liner and Transfer Bag	
FILTER PLUGGED:	Yes	
TORQUE VALUE:	55 Ft-Lbs.	
PRESSURIZATION RATE:	25 SCFM	
MOISTURE ON GASKET AND RING:	No	
TEST DURATION:	1 Minutes and 10 Seconds	
MAXIMUM PRESSURE:	42 PSI	
AREA OF PRESSURIZATION:	Through the Sidewall	
TEST EQUIPMENT:		
Regulated Air Source #: 2	Flow Meter #: 644	
Digital Pressure Gauge #: 643	Stop Watch #: 154	


Photos			
			
Comments			
<p>There was damage to the gasket prior to receiving the drum sample. During the test, leakage occurred at the bottom seam of the drum and at the joint of the locking ring. There was deformation to the top and bottom heads of the drum.</p>			

SAMPLE #6 TEST INFORMATION		Test Set Up Photo
TEST CONTENTS:	Rigid Liner and Transfer Bag	
FILTER PLUGGED:	Yes	
TORQUE VALUE:	55 Ft-Lbs.	
PRESSURIZATION RATE:	No Flow Meter (Max Air)	
MOISTURE ON GASKET AND RING:	No	
TEST DURATION:	1 Minutes and 09 Seconds	
MAXIMUM PRESSURE:	44 PSI	
AREA OF PRESSURIZATION:	Through the Sidewall	
TEST EQUIPMENT:		
Regulated Air Source #: 2	Stop Watch #: 154	
Digital Pressure Gauge #: 643		


Photos			
			
Comments			
<p>There was damage to the gasket prior to receiving the drum sample. During the test, leakage occurred at the bottom seam of the drum and under the locking ring. There was deformation to the top and bottom heads of the drum.</p>			

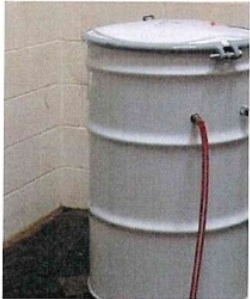


SAMPLE #7 TEST INFORMATION		Test Set Up Photo
TEST CONTENTS:	Rigid Liner and Transfer Bag	
FILTER PLUGGED:	Yes	
TORQUE VALUE:	10 Ft-Lbs.	
PRESSURIZATION RATE:	No Flow Meter (Max Air)	
MOISTURE ON GASKET AND RING:	No	
TEST DURATION:	53 Seconds	
MAXIMUM PRESSURE:	33 PSI	
AREA OF PRESSURIZATION:	Through the Sidewall	
TEST EQUIPMENT:		
Regulated Air Source #: 2	Stop Watch #: 154	
Digital Pressure Gauge #: 643		


Photos			
			
Comments			
<p>There was damage to the gasket prior to receiving the drum sample. During the test, leakage occurred at the bottom seam of the drum and at the joint of the locking ring. There was deformation to the top and bottom heads of the drum.</p>			





SAMPLE #8 TEST INFORMATION		Test Set Up Photo
TEST CONTENTS:	Rigid Liner, Transfer Bag, 55% Filled with Oil Dry Absorbent Material	
FILTER PLUGGED:	Yes	
TORQUE VALUE:	55 Ft-Lbs.	
PRESSURIZATION RATE:	No Flow Meter (Max Air)	
MOISTURE ON GASKET AND RING:	No	
TEST DURATION:	1 Minute and 06 Seconds	
MAXIMUM PRESSURE:	45 PSI	
AREA OF PRESSURIZATION:	Through the Sidewall	
TEST EQUIPMENT:		
Regulated Air Source #: 2	Stop Watch #: 154	
Digital Pressure Gauge #: 643		


Photos			
			
Comments			
<p>There was damage to the gasket prior to receiving the drum sample. During the test, leakage occurred at the bottom seam of the drum, at the joint of the locking ring, and 90 degrees to the left. There was deformation to the top and bottom heads of the drum.</p>			





SAMPLE #9 TEST INFORMATION		Test Set Up Photo
TEST CONTENTS:	Rigid Liner, Transfer Bag, 55% Filled with Oil Dry Absorbent Material	
FILTER PLUGGED:	Yes	
TORQUE VALUE:	10 Ft-Lbs.	
PRESSURIZATION RATE:	No Flow Meter (Max Air)	
MOISTURE ON GASKET AND RING:	No	
TEST DURATION:	51 Seconds	
MAXIMUM PRESSURE:	35 PSI	
AREA OF PRESSURIZATION:	Through the Sidewall	
TEST EQUIPMENT:		
Regulated Air Source #: 2	Stop Watch #: 154	
Digital Pressure Gauge #: 643		


Photos		
		
Comments		
<p>There was damage to the gasket prior to receiving the drum sample. During the test, leakage occurred at 22 seconds into the test 90 degrees to the left of the joint of the locking ring. There was deformation to the top and bottom heads of the drum.</p>		





SAMPLE #10 TEST INFORMATION		Test Set Up Photo
TEST CONTENTS:	Rigid Liner, Transfer Bag, 55% Filled with Oil Dry Absorbent Material	
FILTER PLUGGED:	Yes	
TORQUE VALUE:	10 Ft-Lbs.	
PRESSURIZATION RATE:	No Flow Meter (Max Air)	
MOISTURE ON GASKET AND RING:	Yes	
TEST DURATION:	37 Seconds	
MAXIMUM PRESSURE:	32 PSI	
AREA OF PRESSURIZATION:	Through the Sidewall	
TEST EQUIPMENT:		
Regulated Air Source #: 2 Digital Pressure Gauge #: 643	Stop Watch #: 154	


Photos			
			
Comments			
There was damage to the gasket prior to receiving the drum sample. During the test, the lid ruptured 35 feet into the air and half of the oil dry absorbent material exploded out of the drum.			





SAMPLE #11 TEST INFORMATION		Test Set Up Photo
TEST CONTENTS:	Rigid Liner and Transfer Bag	
FILTER PLUGGED:	Yes	
TORQUE VALUE:	10 Ft-Lbs.	
PRESSURIZATION RATE:	No Flow Meter (Max Air)	
MOISTURE ON GASKET AND RING:	Yes	
TEST DURATION:	2 Minutes and 10 Seconds	
MAXIMUM PRESSURE:	40 PSI	
AREA OF PRESSURIZATION:	Through the Sidewall	
TEST EQUIPMENT:		
Regulated Air Source #: 2	Stop Watch #: 154	
Digital Pressure Gauge #: 643		


Photos			
			
Comments			
<p>There was damage to the gasket prior to receiving the drum sample. During the test, the lid ruptured 75 feet into the air and landed 120 feet away.</p>			



SAMPLE #12 TEST INFORMATION		Test Set Up Photo
TEST CONTENTS:	Rigid Liner and Transfer Bag	
FILTER PLUGGED:	Yes	
TORQUE VALUE:	55 Ft-Lbs.	
PRESSURIZATION RATE:	No Flow Meter (Max Air)	
MOISTURE ON GASKET AND RING:	Yes	
TEST DURATION:	3 Minutes and 08 Seconds	
MAXIMUM PRESSURE:	52 PSI	
AREA OF PRESSURIZATION:	Through the Sidewall	
TEST EQUIPMENT:		
Regulated Air Source #: 2	Stop Watch #: 154	
Digital Pressure Gauge #: 643		

Photos			
			
Comments			
<p>There was damage to the gasket prior to receiving the drum sample. During the test, the lid ruptured 100 feet into the air and landed 135 feet away.</p>			

SAMPLE #13 TEST INFORMATION		Test Set Up Photo
TEST CONTENTS:	Rigid Liner and Transfer Bag	
FILTER PLUGGED:	Yes	
TORQUE VALUE:	55 Ft-Lbs.	
PRESSURIZATION RATE:	No Flow Meter (Max Air)	
MOISTURE ON GASKET AND RING:	No	
TEST DURATION:	2 Minutes and 56 Seconds	
MAXIMUM PRESSURE:	46 PSI	
AREA OF PRESSURIZATION:	Through the Sidewall	
TEST EQUIPMENT:		
Regulated Air Source #: 2	Stop Watch #: 154	
Digital Pressure Gauge #: 643		

Photos			
			
Comments			
<p>There was damage to the gasket prior to receiving the drum sample. During the test, the lid ruptured 100 feet into the air and landed 110 feet away.</p>			

SAMPLE #14 TEST INFORMATION		Test Set Up Photo
TEST CONTENTS:	Rigid Liner and Transfer Bag	
FILTER PLUGGED:	No	
TORQUE VALUE:	55 Ft-Lbs.	
PRESSURIZATION RATE:	No Flow Meter (Max Air)	
MOISTURE ON GASKET AND RING:	No	
TEST DURATION:	4 Minutes and 30 Seconds	
MAXIMUM PRESSURE:	40 PSI	
AREA OF PRESSURIZATION:	Through the Sidewall	
TEST EQUIPMENT:		
Regulated Air Source #: 2	Stop Watch #: 154	
Digital Pressure Gauge #: 643		

Photos		
		
Comments		
<p>There was damage to the gasket prior to receiving the drum sample. During the test, leakage occurred through the filter and there was deformation to the top and bottom heads of the drum.</p>		

DISCLAIMER OF WARRANTIES

TEN-E PACKAGING SERVICES, INC. certifies that the previously described testing services have been performed in accordance with standard good laboratory practices. The results included within this test report relate only to the items tested. **ALL OTHER WARRANTIES, EXPRESSED OR IMPLIED, INCLUDING ANY WARRANTY THAT THE PACKAGING TESTED IS MERCHANTABLE OR FIT FOR A PARTICULAR PURPOSE, ARE DISCLAIMED.** In no event shall TEN-E Packaging Services, Inc. liability exceed the total amount paid by Fluor Idaho for services rendered.

In the event of future changes to the above referenced test standard, it is the responsibility of **Fluor Idaho** to determine whether additional testing or updating of past testing is necessary to verify that the packaging we have tested remains in compliance with those standards.



Tyler Kinderman
Packaging Engineer
TEN-E Packaging Services, Inc.
1666 County Road 74
Newport, MN 55055